THERMODYNAMICS AND KINETICS OF SLIP

U. F. KOCKS
Argonne National Laboratory

A. S. ARGON
Massachusetts Institute of Technology

M. F. ASHBY*
Harvard University

* Now at: University of Cambridge, University Engineering Laboratories, Trumpington Street, Cambridge, England

including ERRATA to Dec. 2003
U.F. Kocks

PROGRESS IN MATERIALS SCIENCE

Volume 19

Edited by

BRUCE CHALMERS

Division of Engineering and Applied Physics, Harvard University, Cambridge, Mass., U.S.A.

J. W. CHRISTIAN

Department of Metallurgy, University of Oxford

and

T. B. MASSALSKI

Mellon Institute of Science, Carnegie-Mellon University, Pittsburgh, Pa., U.S.A.

Pergamon Press Ltd., Headington Hill Hall, Oxford, England
Pergamon Press Inc., Maxwell House, Fairview Park, Elmsford,
New York 10523, U.S.A.
Pergamon of Canada Ltd., 207 Queen's Quay West, Toronto 1, Canada
Pergamon Press (Aust.) Pty. Ltd., 19a Boundary Street,
Rushcutters Bay, N.S.W. 2011, Australia
Pergamon Press GmbH, 3300 Braunschweig,
Burgplatz 1, West Germany

First edition 1975

Library of Congress Catalog Card No. 72-85096

* Basic Reading

CONTENTS

OBSOLETE (1983)

ACKNOWLEDGMENTS

THIS work has been generously supported by the Materials Science Division at Argonne National Laboratory, under the auspices of the U.S. Atomic Energy Commission; we are grateful to P. G. SHEWMON and N. L. PETERSON for their sustained encouragement. We have greatly benefited from discussions with many colleagues; especially significant contributions were made by A. V. GRANATO, J. P. HIRTH, R. LABUSCH, and P. D. NEUMANN, and by our co-workers E. S. P. DAS, H. J. FROST and R. O. SCATTERGOOD. V. HEITSCH and S. JONES coped admirably with the difficult typing.

LIST OF SYMBOLS

Accents

$\dot{}$	total derivative with respect to time
$'$	current value in integral or general variable whose critical value is to be found
$\hat{}$	maximum value
$\tilde{}$	amplitude

Prefixes

d	total differential
∂	in partial derivative (all other variables held constant)
δ	virtual variation (other hidden variables in equilibrium)
Δ	usually difference between values at stable and unstable equilibrium configuration, for thermal activation

Roman (and italic) letters		*See eq., Fig., Table*
A	constant in phenomenological relations	34h, 61f
	also: general area, e.g. of surface	21i
a	area swept by dislocation	22-1, 22c, 45-2
a_{BOW}	— bowing between two discrete obstacles	25t
a_{RUN}	— after release in jerky glide	33a
a_{SWEPT}	— after activation event at flow stress	25-11
Δa	activation area	41e, 44c′, q
$\Delta a'$	apparent activation area	43g, h, l″, 44h
B	drag coefficient per unit length of dislocation	31a
b	amount of Burgers vector for full disl.	22c, 27a
b_{P}	— for partial dislocation	27a
$\vec{b},b_1,b_1^\circ$	Burgers vector, components, unit v.	22b
C	normalized obstacle stiffness	42h, i, 63g
c	concentration (atomic or vol. fraction)	25ee, 25-16, 52l′
c_{ij}	elastic stiffness referred to crystal axes	2-I
c_v	specific heat per atom at const. vol.	31y
D	(diffusion coefficient)	
d	jog height, dipole spacing	26-1, 32x
	also: slip plane spacing	33y, z, cc
	also: activation distance (when $\neq y$)	52n, o

NUMBERING CONVENTIONS

Equations have the number of the section and a letter: 21a, 21b, 21b′, . . ., 21z, 21aa, . . .

Figures have the number of the section and a number: 21-1, 21-2, 21-2a, . . .

Tables have the number of the Chapter and a roman number: 2-I 2-II, . . .

	also: parameter in particle resistance laws	52-7 through 14
k_P	Hall-Petch parameter	24i
L	distance between especially strong obstacles	24i, 24-6, 33y, z
	also: specimen length	64a
$\mathscr{L}$	any length of dislocation	23f, 24h, 42r, 51-6
l	average inter-obstacle spacing	25aa
l_e	center-to-center spacing of two obstacles along dislocation, also average of same	25-1, 25jj, 44i
l_n	length of dislocation touching n obstacles ($\sigma = 0$)	25-17
$\mathscr{M}$	mass per unit length of dislocation	31a, k, l, n
$\mathscr{M}_{KINK}$	mass per unit length of kink	31m, o
M_{KINK}	total mass of kink	42u
m	relative stress sensitivity of the strain rate	34r, 43c, 61b
	(exponent in pheno. relation)	34h
m_o, m_G	contributions to m	45a, b, 62c, 63g
N	number of vibrational modes of dislocation	42o
N	number of dislocation segments per unit volume	
N_{WAIT}, N_m	waiting and mobile segment density	33a, c, s
$\dot{N}_{NUCL}$	nucleation rate per unit volume	51ee
n	exponent in phenomenological relation $\dot{\gamma}(\sigma)$	61f
	also: negative exponent in obstacle profile law $\tau(\Delta a)$	43v
n	number: e.g., dislocations in pile-up	24j, p
n_j	unit vector: perpendicular to surface	21i
	perpendicular to slip plane	22b
P	fraction of peaks in τ_{LINE}-map below σ	25-12
δP, P	fraction of segments released (per unit time)	33a, p
P_t, P_σ, P_τ	partial derivatives of P	33e, f, g, h, j
$\vec{P}_t, \overleftarrow{P}_t$	forward and reverse activation rate	45f
p	exponent in pheno. relation $\Delta G(\sigma)$	43w
p′	— same for $\Delta G(K)$	44l
p	hydrostatic pressure	43d
Q	operationally defined activation energy	61a, u
δQ	heat flowing into body	21a
q	exponent in pheno. relation $\Delta G(\sigma)$	43w

E	effective line tension	25n, o, q, r, 25-8
$\mathscr{E}$	line tension (self force per curvature)	23j, k, 25-8
E_{THERM}	thermal energy density	31t
F	(Helmholtz) free energy	21c, e
ΔF	activation free energy (at given stress)	41-1, 41c
F_o	total free energy to overcome one obstacle	25b, 34o, 41h, 45o, q, 62g
F_{BIND}	binding energy of one solute atom to dislocation	25mm
F_{KINK}	free energy of one kink	51n
F_{NUCL}	free energy to nucleate double kink or bulge	51d′, l
F_{STOR}	free energy stored during deformation	22g
$\mathscr{F}_{\text{DIS}}$	free energy per unit length of dislocation ("line energy")	23g, h′, l, m
$\mathscr{F}_{\text{SCREW}}$, $\mathscr{F}_{\text{EDGE}}$:	line energy of screw, edge	23h, i, 25-8
$\Delta\mathscr{F}_{\text{DIS}}$	— difference between high and low energy position	24-3, 51-1
$\mathscr{F}_{\text{BIND}}$	binding energy per unit length of dislocation	24-2
f	cosine of breaking angle	25v, w′, 52m
G	free enthalpy, Gibbs free energy	41g+
ΔG	activation free enthalpy (also "activation energy")	41-1, 41a, f, g, 43a′, w, 61n
$\overrightarrow{\Delta G}$, $\overleftarrow{\Delta G}$	— for forward and reverse jump	45c
ΔG_{NUCL}	activation energy for nucleation of bulge or double kink	51d′, i, p″
$\Delta\mathscr{G}_{\text{DIS}}$	free enthalpy per unit length of dislocation	51-6, 51g″
$g(\sigma/\mu)$	normalized activation free enthalpy	43l′
H	enthalpy	
ΔH	activation enthalpy (also "activation energy")	41-4b, 41l, m, 43t
h	partial strain hardening rate	33ee
	also: height of partial kink	51-6
i, j	vector and tensor subscripts	
K	effective resisting force of discrete obstacle	25a, g′, 52j
K_x, K_y, K_θ	— components of elemental force	52g″, h, 5-I
K_i	force exerted on body at surface	21h, i
k	Boltzmann's constant, $k = 1.38 \times 10^{-23}$ J/K	21e

$\bar{v}_{RUN}$	velocity averaged over running disl.	33k
$v_S \equiv v_{SOUND}$	terminal velocity of screw dislocations	31e, 34i
v_t, v_l	transverse and longitudinal speed of sound	31l
W	work done on body (only in virtual variation: δW)	21a, h, j
ΔW	activation work	41-1, 41d, 44e
$\Delta W'$	apparent activation work	43k, 61b′
w	width of discrete obstacle	25-1, 25ff
	also: interaction range	25-15
	also: width of kink	51-6
	also: width of Lüders front	64b
X	outer cut-off radius in disl. line energy	23h
	also: any distance along quasi-straight disl.	23-4, 23q, 25-4
x	coordinate along avg. disl. direction	23-2, 23q
x_{KINK}	average spacing of kinks	32r
Y	distance perpendicular to quasi-straight dislocation	25-4, 25f
	also: normalized coordinate	51j, k
y	coordinate, direction of average dislocation motion	23a, 31a, 51-1
Δy	activation distance	44c
y_{BACK}	distance moved by emitted dislocation before source can operate again	32t, v, 33z, aa
y_m	distance moved by dislocation before it is trapped	32t, 33y
y_{RUN}	"forward" distance moved after release	33c
y_{STOP}	distance moved coasting under inertia	31-2, 31dd
y_o	average depth of obstacle	25-1, 31ff
Z	partition function	21e
z	coordinate perpendicular to slip plane	

Greek letters

α	angle between line direction and Burgers vector	23k
β	bow-out angle	24f′, 25-7, 51g
γ	"shear" or "glide": amount of engineering shear strain produced by dislocation glide	22c
γ_o	macroscopic shear produced in waiting time	33d
$\dot{\gamma}_o, \dot{\gamma}_H$	constants in pheno. relations	34k, 61e′, 61g′, s
δ	depth of linear barrier	24-3, 24-5, 27b

R	radius of curvature of dislocation (avg. or local)	23-5, 24-2, 25s
	also: phonon scattering radius	31u, v
r	exponent in pheno. relation $\Delta G(\sigma)$	43x′
r	radius of spherical particle	25ff
	also: partial recovery rate	33ff
r_o	inner cut-off radius in disl. energy	23h
r_P	inner cut-off radius in phonon scattering	31w
S	symbol for the stable equilibrium state	41-1, 41a, 42-1
S	entropy	21b, f
S_1, S_2, S_3	structure parameters	1a, b
S_o	total entropy of activation	41i
ΔS	activation entropy	41k, o′, o″, 42n, 43s
ΔS_{DIS}	entropy associated with dislocation vibrations	42l
s	normalized plane glide resistance (discrete obstacles)	25ii
T	temperature	21b
T_o	characteristic temperature $T_o(F_o, \dot{\gamma})$	45o, 51ll
T_{DEBYE}	Debye temperature	31-1
T_v	temperature below which quantum effects may occur	42k
t	time	31cc
t_{ACC}	time constant in equation of motion	31aa
t_{RUN}	running time between obstacles in jerky glide	33n
t_{WAIT}	inverse of total release rate $\dot{P}$	33r
U	symbol for the unstable equilibrium state	41-1, 41a, 42-1
U	internal energy	21a, g
U_o	total internal energy of activation	41j, 61f
$\mathscr{U}$	internal line energy of disl. at rest	31j
$\mathscr{U}_v$	internal line energy of moving disl.	31j
u_l	displacement (of surface element)	21h
V	total volume of body	21j, 22c
V_o	constant in phenomenological relation	34u
ΔV	activation volume (pressure effects)	43d, e′
v	velocity of dislocation	31j, r, 31cc
v_o	— initial value	31dd
$\bar{v}$	avg. disl. velocity in time, space	32b, f, k, o, q
$\bar{v}_m$	velocity averaged over mobile dislocations only	33u
v_L	Lüders front velocity	64a

σ_{ij}^{LOC}	total local stress tensor	21n, o, w
σ_{eff}	"effective stress" in continuous glide	32g, i
σ_0	constant in phenomenological relation	34k, v
σ_{LIM}	stress at which terminal velocity is reached	31z
τ	glide resistance	22e
$\bar{\tau}$	mechanical threshold (abbrev. for $\hat{\tau}_{PLANE}$)	22i, 43w″, 52
$\hat{\tau}$	amplitude of element glide resistance	32d
τ_{ij}	deformation resistance	21u
τ_{ij}^{INT}	deformation resistance due to internal stresses	21y
τ_{BACK}	back stress in pile-up	24m,n
τ_{DYN}	dynamic threshold	31-4
τ_{ELEM}	element glide resistance	23-2, 23b, 25-10
τ_{FLOW}	flow stress (also abbreviated τ)	44o
τ_{IDEAL}	ideal (or "theoretical") shear strength	34j, 51c
τ_{INT}	internal stress from mobile disl.	32e, l, bb
τ_u	athermal glide resistance plateau	43-6
τ_{LINE}	line glide resistance	23c, 25-10, 31a, 41a
τ_P	Peierls stress	51a, b
τ_{PLANE}	plane glide resistance	24i, 25-10, 25dd, ww, 44a, b
τ_{SELF}	dislocation self stress	23e, f, j
τ_{STOR}	average element glide resistance	22g, 45j
$\bar{\tau}_{THERM}$	thermal shear stress amplitude	31t
τ_1, τ_2	line or plane resistance due to one mechanism	24-6, 24i, 33i′, 43w‴ 44-9, 10, 11
$\Delta\tau$	difference in glide resistance from two mechanisms	24-6
ϕ	half the cusp angle at a discrete obstacle	25g, v, 25-4, 52-5
χ	free energy per unit area:	
χ_{APB}	— of antiphase-boundary	52b
χ_{FAULT}, χ_{SF}	— of (stacking) fault	27c, 2-III
χ_{INT}	— of interface (precipitate-matrix)	52f, g
ψ	complement of bow-out angle β	23-4, 5, 25-7
Ψ	dissipation function ($\delta\Psi$ only)	21r, s, t, v, 22f
$\omega_A \equiv \omega_{AT}\phi_M$	an atomic frequency	31f
Ω	atomic volume	31i, q, 34l

10

ϵ, ϵ_{ij}	macroscopic strain tensor	21k, l, m, 64c
$\lvert\epsilon\rvert$	amount of unconstrained misfit strain	52d
ϵ_L	Lüders strain	64a
$\Delta\epsilon_{ij}$	activation strain	43e
η	separation of partials in extended dislocation	27b, 2-III
θ	angle betw. disl. and particle interface	52-5, 6, 52h
	also: work-hardening rate $d\tau/d\gamma$ at standard T and $\dot{\gamma}$	44n′
θ'	— same at zero temperature	44n
Θ	work-hardening rate $d\sigma/d\epsilon$	64c
κ	local curvature of dislocation line	23g, j, 25l
λ	wavelength of periodic linear barrier	31-3, 4, 32d, 51-1
Λ	mean-free-path (of kinks)	51aa
Λ_{pp}	phonon-phonon mean-free-path	31w
μ	shear modulus in line energy of screw dislocation	23h, 2-I
μ°	— same extrapolated to T = 0 K	41-5
μ'	shear modulus in slip plane and slip direction	31e, 3-I, 42h, 51c
ν	Poisson's ratio	23i
ν_{eff}	— effective value in edge energy, incl. elastic anisotropy	2-I
ν_D	Debye frequency	31i
ν_E	Einstein frequency	31h
$\nu_{FRIEDEL}$	dislocation attempt frequency according to Friedel	42f
ν_G, ν_H	frequency factors in disl. activation	42a, b, g, j
ν_{NUCL}	freq. factor for bulge nucleation	51w′
ν_0	ground frequency of vibrating dislocation segment	42d
ξ	running coordinate along disl. line	23a, 23-4, 25-7
ρ	mass density of material	31e
	dislocation length per unit volume:	
ρ_m	mobile dislocation density	32m, aa, 33q, 63g
ρ_{RUN}	density of running dislocations	33k
ρ_{SOURCE}	density of linear dislocation sources	32t, u, 33y
ρ_{WAIT}	density of waiting dislocations	33b, c
$\dot{\rho}^+$	*generation rate* of running dislocation (not net change)	33x
σ	applied stress *resolved in slip plane and direction*	22d
σ_{ij}	applied stress tensor in arbitrary coordinate system	21i, o, p
σ_{ij}^{INT},qz	internal stress (see τ_{IJ}^{INT})	21w,y

1. INTRODUCTION

IT IS now almost 50 years since BECKER (1925) and OROWAN (1934) first suggested that the *non-linear resistance to deformation* of solids (in distinction to the linear-viscous resistance of most liquids) derives from the much-larger-than-atomic-size flow units in the solid. In the language of BECKER and OROWAN, the larger-size flow units in plastic deformation produce large internal concentrations of the applied stress where thermally activated production of new flow units becomes easy. In contemporary language, the rate process in plastic deformation derives from the thermally activated motion of crystal dislocations over local slip plane obstacles at which the bowing of a single dislocation or the cooperative motion of many dislocations can strongly concentrate the applied stress.

The ideas of BECKER and OROWAN were developed and extended by OROWAN (1940), KAUZMANN (1941), SEEGER (1954) and FRIEDEL (1956); since then, a rapidly expanding body of literature has appeared on the subject. Much of this has focused on the experimental and theoretical investigation of the thermally activated motion of single dislocations past obstacles that obstruct their glide motion in a single slip plane. As a result it is now possible to characterize experimentally, at least in broad outline, the various slip plane obstacles governing the rate process. In this treatise we present a comprehensive and self-consistent approach to thermal analysis of plastic slip, starting from basic principles of the motion of a single dislocation through a given topography of slip plane obstacles and concluding with a detailed discussion of the macroscopic properties of a crystal containing a given distribution of microscopic obstacles to flow.

The total mechanical behavior of a material is described by a *constitutive law*: a set of equations relating strain rate $\dot{\epsilon}_{ij}$ to stresses σ_{ij}, rates of change of stress $\dot{\sigma}_{ij}$, temperature T, and—through a number of structure parameters S_1, S_2, S_3, etc., such as dislocation density (or various moments of it), grain size, and so on—to the thermo-mechanical history of the material. In differential form, a constitutive law may be written as a set of coupled differential equations:

$$\dot{\epsilon}_{ij} = f(\sigma_{ij}, \dot{\sigma}_{ij}, T, S_1, S_2, S_3, \ldots), \qquad [1a]$$

$$\left.\begin{aligned} dS_1 &= f_1(\sigma_{ij}, \dot{\sigma}_{ij}, T, S_1, S_2, S_3, \ldots)\, dt, \\ dS_2 &= f_2(\sigma_{ij}, \dot{\sigma}_{ij}, T, S_1, S_2, S_3, \ldots)\, dt, \\ dS_3 &= f_3(\sigma_{ij}, \dot{\sigma}_{ij}, T, S_1, S_2, S_3, \ldots)\, dt \end{aligned}\right\} \qquad [1b]$$

where dt is an increment of time. The law is made up of a rate-of-flow equation (or simply: *rate-equation*), eq. [1a], and a set of *structure-change equations*, eqs.

LIST OF TABLES

The tensorial rate equation [1a] for general stress states follows from this by a set of geometrical and kinematic relations with which we are not concerned in this treatise; they have been reviewed elsewhere (KOCKS, 1970a).

For the case of single crystals deforming, under simple boundary conditions, by slip on a single slip system, eq. [1c] already represents the entire constitutive law. Under more complicated boundary conditions, and for polycrystalline specimens, additional relations are needed. These are well established for some materials, such as face-centered cubic and body-centered cubic metals deforming in a quasi-homogeneous manner (KOCKS, 1970a). For other materials, the problem of relating macroscopic flow to slip on a single slip system may yet have to be solved; but, so long as slip is the underlying process, eq. [1c] will describe the *kinetic law* for all materials. In this sense, thermally activated flow of non-metallic elements, of inorganic compounds, and of molecular crystals, as well as metals and alloys, can all be treated in the manner set out below; we have further found a modification of it to be helpful in understanding flow in polymers and glassy solids.

In Chapter 2, we start by considering *equilibrium* conditions for dislocations in a slip plane; these lead to the definition of various forces on dislocations (per unit length). The force opposing the motion of a straight test element of dislocation at any position in the slip plane is called the *element glide resistance*; its contour reflects all relevant properties of the *obstacles to dislocation motion*. When a flexible dislocation is placed in the slip plane and pressed against the contour of the element glide resistance, by an applied stress, the dislocation will be locally held up at the high points of the element glide resistance profile, and bow out in areas where the applied stress exceeds the local glide resistance, until, primarily through its curvature, it develops enough *self stress* to equal the difference between the applied stress and the local element resistance. This process of smoothing the high points of the element resistance by the bowing dislocation gives rise to the dislocation *line glide resistance* which is the sum of the element resistance and the self stress. In equilibrium, it must equal the applied stress along the entire length of the bowed-out dislocation. Conversely, any *difference* between the applied stress and the line glide resistance at any point along the length of the dislocation is the *driving force* for dislocation motion. A continuous sequence of equilibrium configurations of a dislocation line in a slip plane may be derived by demanding that, in every configuration, the line glide resistance be constant along the dislocation, but allowing that the applied stress with which this line glide resistance is in equilibrium be different from one configuration to the next; the resulting contour is the line resistance profile. It has peaks and valleys which, however, are much less pronounced than those of the element resistance contour. Finally, even the line resistance contour may be smoothed out to some extent by dislocations forming groups or following special paths; we have called this the *plane glide resistance*. There is an upper limit to the applied stresses under which equilibrium is possible: it is the maximum plane glide resistance or *mechanical threshold*. Chapter 2 ends with the discussion

[1b]. This is not the only form in which a constitutive law can be written. But it is one with particular advantages for use as a basis for microscopic modeling because—in principle, at any rate—it is possible to devise experiments to investigate each of the functions, $f, f_1, f_2, f_3 \ldots$ by studying the microstructure directly (by transmission microscopy, for example) or indirectly (by studying x-ray line broadening, for example).

The quantities $S_1, S_2, S_3, \ldots$ define the *state of the material*: two samples with the same $S_1, S_2, S_3 \ldots$ are in the same state. In general, flow changes the state so that finite strain can be described only by integrating eqs. [1a] and [1b] simultaneously. There is one exception: at sufficiently large strains, materials show a steady-state flow behavior in which

$$0 = dS_1 = dS_2 = dS_3 \ldots$$

Equations [1b] then become a set of simple simultaneous equations to be solved for S_1, S_2, S_3, etc., which are then substituted into eq. [1a] to give the strain rate.

The establishment of a constitutive law for a material, or class of materials, is one of the ultimate goals of the kind of detailed analysis we review here—but we are still a long way from achieving it. *The treatise examines the principles underlying the calculation of the rate of flow at constant structure*—eq. [1a]. We do not discuss the structure-change equations, or the physics of how the structure evolves with strain, or time. Nor do we consider heterogeneous deformation (itself frequently a result of structural change) or twinning. Finally, we restrict ourselves to the range of temperatures in which diffusion, and diffusion-controlled effects, can be ignored.

Our concern here is to answer the question: given a certain set of microscopic obstacles to slip, how should the macroscopic mechanical properties be calculated? And alternatively: given a set of macroscopic measurements, what can we learn from them about the microscopic processes involved? The result of thermal analysis, done by abrupt change in the strain-rate, or load, or temperature, at various points, is a smoothed-out map of the slip plane obstacles. Of interest is the decomposition of this map into various constituent processes which in combination give rise to the experimentally measured obstacle profile. In effect, the experiments furnish the integral processes: what is desired is the solution of the integral equation. As in the somewhat parallel case of the properties of gases where, by means of the kinetic theory, one derives the macroscopic properties of a gas by integrating over the behavior of molecules, we adopt the approach of constructing the macroscopic mechanical behavior of crystals by integrating the behavior of individual dislocations under the action of the slip plane obstacles, the applied stress, and other moving dislocations.

Since the motion of individual dislocations furnishes a single component of strain rate ($\dot{\gamma}$), and is primarily controlled by a single component of stress (σ), the *kinetic law* describing such motion is a single scalar equation of the kind

$$\dot{\gamma} = f_0(\sigma, \dot{\sigma}, T, S_1, S_2, S_3 \ldots) \qquad [1c]$$

an application of the methods outlined in the following to a number of varied practical cases should produce the necessary experience.

This treatise is not a review in the simple sense of a literature survey; rather it is a reworking of the principles involved in calculating a kinetic law for plastic deformation from a general and, in some respects, new point of view. Needless to say, we have been profoundly influenced by the vast literature on this subject, and by numerous stimulating and critical discussions we have had with colleagues in the field. Although we have made a serious attempt to furnish references wherever necessary, we feel that in a work of this complexity it is impossible to always give proper credit to the original source. We are certain that we have failed more than once in this respect and wish, therefore, to tender apologies to our unintentionally slighted colleagues.

of the various smoothing processes and the mechanical threshold for several common slip plane obstacles.

In Chapter 3, we consider the *dynamics* of individual dislocations, their inertial mass, and the lattice drag processes which check their velocity. We consider the *continuous glide* of dislocations *above* the mechanical threshold against the lattice drag as the simplest of superposition problems. Next we consider kinematics and phenomenological kinetics of the *jerky glide* of dislocations at stresses *less* than the mechanical threshold where the continued motion of a dislocation requires thermal activation past local obstacles. For both types of glide, we discuss the *mobile dislocation density* and its stress dependence to arrive at expressions for the macroscopic strain rate. We end the chapter with a summary of *phenomenological and empirical kinetic relations.*

In Chapter 4, we discuss the details of the *local activation process* of a dislocation based on the theory of thermal fluctuations. To determine the *frequency factor* of activation and the activation free energy we consider the statistical mechanics of the modes of oscillation of a dislocation pressed against an obstacle. Further, we discuss the *stress dependence* of the activation free enthalpy as an obstacle-size-sensitive parameter and give a detailed application to *discrete obstacles.* Finally, we consider the limiting form of the strain-rate expression at *very low stresses.*

In Chapter 5, we discuss a number of important glide resistance *models* in detail, from the element resistance up to the macroscopic strain rate, as guides for eventual experimental thermal analysis. In this chapter, we are concerned less with the development of a detailed model for one obstacle type than with the examination of the model characteristics of certain classes of obstacles. The chapter discusses specifically the *lattice resistance*, the glide resistance due to *precipitate particles*, and (briefly) that due to dilute *solid solutions.* It ends with a short summary of the various forms of *superposition* of mechanisms.

In Chapter 6, we discuss the rational selection of *operational parameters* and the best choices for normalization of these parameters. We then consider in detail the methods of operational thermal analysis for *rate insensitive* and *rate sensitive* materials based only on some very general mechanistic assumptions. Finally, we review the principal *experimental methods* and evaluation procedures to measure the operational parameters.

In Chapter 7, we attempt to give our *assessment* of the present understanding of the field: we recount a number of problems that we consider to be essentially solved, and some that stand out as being worth solving.

The ultimate aim of the entire procedure outlined here would be the production of a *flow chart* that specifies a sequence of experiments, proceeding from easier ones to harder ones, each one of which narrows down the range of possible underlying mechanisms and, thereby, the range of possible extrapolations into other aspects of the mechanical behavior not yet measured. We feel confident that this aim will be attained in the not-too-distant future:

in the free energy of the crystal and must be taken account of. We call the combination of these self stresses with the element resistance the *line glide resistance* τ_{LINE}. It is usually substantially lower than τ_{ELEM}. Finally, dislocations moving across an entire slip *plane* may smooth out the local line glide resistances to some extent by forming groups or following special paths. The resulting *plane glide resistance* τ_{PLANE} is a material property relevant to *large-scale* dislocation movement.

After introducing these three glide resistances in sec. 23, we describe them specifically for three broad classes of obstacles: *linear barriers* (sec. 24) and *discrete obstacles* (sec. 25), both of which are fixed in the slip plane, and *dragging obstacles* (sec. 26). We conclude the chapter with a discussion of the influence of dislocation *dissociation* (sec. 27).

There have been many excellent discussions on the equilibrium properties of dislocations and basic thermodynamics of glide, which will form a useful background to our discussion in this chapter. The reader may find the following limited selection particularly useful:

ESHELBY (1951), *The Force on an Elastic Singularity;*
FRIEDEL (1964), *Dislocations;*
HIRTH and LOTHE (1968), *Theory of Dislocations;*
SEEGER (1955a), *Theorie der Gitterfehlstellen.*

21. THERMODYNAMICS OF STRESSED SOLIDS

The application of thermodynamics to the plastic deformation of solids requires special caution in a number of respects. First, this deformation is essentially *irreversible*. Equilibrium relations are of considerable interest, for example to define a reference state from which actual deviations constitute a driving force; but it is important that such relations holding only under equilibrium conditions (or for reversible changes) be carefully distinguished from other laws of general validity.

Second, plastic deformation depends sensitively on *shear* stresses, not pressure, and it leads to *shape* changes, not volume changes. While the introduction of shear stresses poses no special problems in a closed system, the introduction of "shape" does: unlike volume, it is not a "state function", in the following sense. When the temperature and all stresses are prescribed, the volume could be derived from a complete knowledge of all material properties; so could the energy and the entropy to within an additive constant; but the "shape" of the specimen could not be derived in any way. It is thus imperative that constitutive relations contain the strain only in *differential* form (see also HART, 1970).

For a derivation of equilibrium properties, and for a definition of driving forces, a *differential* formulation of the thermodynamic laws is all that is needed. *Integral* values of the extensive variables are used in conventional thermodynamics to specify the *state of the material*: if *all* macroscopic variables are known, the material parameters in the constitutive laws follow

2. EQUILIBRIUM

Summary

Plastic deformation is an essentially irreversible phenomenon. The driving force for such processes is the *deviation from* (*static*) *equilibrium*. Evidently, the reference state, thermo-mechanical equilibrium, must be well described before a treatment of irreversible deformation can be accomplished. Thermodynamic relations under the essential presence of shear stresses and strains are given in sec. 21.

Equilibrium properties take on a special importance in plastic flow since, in contradistinction to most other irreversible processes, the response to applied forces is here extremely nonlinear. In fact, at the lowest level of approximation, there is a *range* of stresses under which a solid can be in equilibrium; it is the limit of this range that is of prime interest. We call it the mechanical threshold or, in a restricted sense, the yield strength.

Plastic deformation occurs almost exclusively by the motion of dislocations (sec. 22). During such motion, the (Helmholtz) free energy of the crystal may, at least locally and at least temporarily, increase providing a *resistance* to the motion. We call the rate of change of free energy δF per unit volume V, with the shear strain $\delta\gamma$, at constant temperature, the *glide resistance*:

$$\tau = \frac{1}{V}\frac{\delta F}{\delta \gamma}.$$

If the motion takes place reversibly, exactly this rise in free energy must be supplied by the external work δW, which is being expended with strain as

$$\sigma = \frac{1}{V}\frac{\delta W}{\delta \gamma}.$$

In other words: in equilibrium, the applied stress σ and the glide resistance τ must be equal. Any excess of σ over τ provides a driving force for glide.

While the applied stress is uniform throughout any volume of interest here, the glide resistance to dislocation motion generally varies drastically from place to place. However, peaks in the resistance may be overcome by thermal fluctuations, even though $\sigma < \tau$ locally. Again, the rate of thermal release depends on the difference between τ and σ.

On a local basis, one may consider the interaction of a small, straight *element* of dislocation with obstacles in the crystal and derive the corresponding rate of change of free energy, τ_{ELEM}, the *element glide resistance*. However every dislocation element is a part of a longer dislocation *line*; its interaction with neighboring elements (and possibly even far ones) contributes to changes

uniquely if there are not more parameters than observable constitutive relations—which are, then, called "equations of state". In crystal plasticity, the number of relevant material parameters may far exceed the number of macroscopically observable relations; the use of energy, volume, etc., as "state variables" then becomes meaningless: plastic deformation is *path dependent*. The *differential formulation* called for above is thus more proper from a fundamental standpoint. (For a similar treatment, see RICE, 1973.)

Thermal Equilibrium

Among the quantities used to describe the properties of a closed system (a "body") are its (internal) energy U and its entropy S. Their variations in an interchange with the surroundings of the body, during which no particles are interchanged, but during which an increment of work δW is done on the body and an increment of heat δQ flows into it, are restricted by the first and second laws of thermodynamics:

$$\delta U = \delta Q + \delta W \qquad (\textit{First Law, closed system}), \qquad [21a]$$

$$\delta S \geq \frac{\delta Q}{T} \qquad (\textit{Second Law, closed system}). \qquad [21b]$$

The equality sign in [21b] defines thermal equilibrium (or reversible processes) at a fixed temperature T.

Throughout this article, we will be concerned with properties and variations *at constant temperature*. For this case, it is useful to define another property of the material, its (Helmholtz) free energy F whose variation is

$$\delta F = \delta U - T\,\delta S \qquad (\delta T = 0). \qquad [21c]$$

The first and second laws then combine to give

$$\delta F \leq \delta W \qquad (\delta T = 0) \qquad [21d]$$

where again the equality sign defines thermal equilibrium or reversible processes at a fixed temperature.

Equations [21b] and [21d] can be used to *measure* changes in the material properties S and F through their interactions with the surroundings (work and heat flow), when these interactions are reversible. In phenomenological thermodynamics, it is then common to operationally *define* the entropy change by the reversible heat flow divided by the temperature, and *define* the free energy change by the reversible work; changes in internal energy then follow from eq. [21c].

From a physical point of view, on the other hand, one often thinks of the material properties as given, in principle, by the positions and velocities of all the atoms comprising the "body". From their potential and kinetic energies, one can then derive the partition function Z and, from it, *define* the free energy by

$$F \equiv -kT \ln Z \qquad [21e]$$

($k \equiv$ Boltzmann constant). Similarly, the entropy and internal energy would then be defined from it by

$$S \equiv -\frac{dF}{dT}, \qquad [21f]$$

$$U \equiv F + TS. \qquad [21g]$$

In materials science problems such as slip, one is not interested in the free energy of the entire crystal. Instead, one models the body to consist of an ideal crystal and structural defects. The free energy is then that of all the defects, such as internal and external surfaces, point defects and dislocations.

Often, such models are essentially zero-temperature models (i.e. finite-temperature behavior extrapolated to zero temperature and without zero-point effects); in that case, the calculated energy is the internal energy U and, appropriately, the material properties used, such as specific surface energy, elastic constants, etc., should be the "zero-temperature" values. On the other hand, within the same model, one may often assume that the *only* contribution to the entropy comes from the temperature dependence of the specific surface free energy, the elastic constants, etc., and not, for example, from changes in dislocation core configuration; in that case, insertion of the values of these constants *at temperature* immediately gives the *free* energy F, and one may obtain S and U from eqs. [21f], [21g].

Mechanical Equilibrium

In this article, we shall only be concerned with mechanical work terms, and not with electrical or magnetic ones. The increment of work δW done on a body, reversibly or not, is then defined by the integral over the surface of the body of all the scalar products between the incremental displacement $\vec{\delta u}$ of a surface element and the locally applied force $\vec{dK}$:

$$\delta W \equiv \int_{\text{surface}} \delta u_i \, dK_i. \qquad [21h]^*$$

Mechanical equilibrium demands that all the forces dK_i (if treated as free) and all their moments balance out to zero, so that the body will not accelerate or rotate. The forces are transmitted through the body by means of a stress field σ_{ij}. In the simplest case, which we shall consider first because it is usually realized in test conditions, this stress field is uniform. The statement of mechanical equilibrium then reduces to saying that the surface tractions derived from the stress field balance the applied forces at the surface:

$$dK_i = \sigma_{ij} n_j \, dA \qquad (\textit{mechanical equilibrium}) \qquad [21i]$$

where the vector $\vec{n}$ is the surface normal and dA is the area element at a point.

The expression [21h] for the work increment then simplifies to

$$\delta W = V \sigma_{ij} \delta\epsilon_{ij} \qquad (\textit{mechanical equilibrium and } \delta\sigma_{ij} = 0) \qquad [21j]$$

if we define (HILL, 1967; RICE, 1970)

$$\delta\epsilon_{ij} \equiv \frac{1}{V} \int_{\text{surface}} \tfrac{1}{2}(\delta u_i n_j + \delta u_j n_i) \, dA. \qquad [21k]$$

* Summation is implied over repeated subscripts in this section.

(Elimination of the antisymmetric part of $\delta\vec{u}.\vec{n}$ was not necessary, but this term would not have contributed to the work, since the stress tensor is symmetric.)

Equation [21k] is an unconvential definition of the strain increment, but it is appropriate to the particular problem at hand: when the stress is uniform, the strain and the surface displacements will generally not be uniform (unless the material is homogeneous). However, only their averages enter into the work equation.

If the strain increment were instead defined, in the conventional manner, on a local basis, as

$$\delta\epsilon_{ij}^{LOC} \equiv \tfrac{1}{2}\left(\frac{\partial\delta u_i}{\partial x_j} + \frac{\partial\delta u_j}{\partial x_i}\right) \qquad [21\ell]$$

where δu_i must now be a continuous and differentiable displacement field, eq. [21k] would follow from [21ℓ] and Gauss's Theorem with

$$\delta\epsilon_{ij} = \frac{1}{V}\int \delta\epsilon_{ij}^{LOC}\,dV. \qquad [21m]$$

"The macroscopic strain is the average of the microscopic strains."

Another interesting special case is one in which the (local) strain is uniform, but the stress is not (unless the material is homogeneous). Defining the local stress by an equation of the form [21i] in terms of forces to be measured at local cuts, allows one to express the work increment (eq. [21h]) by

$$\delta W = \int \sigma_{ij}^{LOC}\,\delta\epsilon_{ij}^{LOC}\,dV. \qquad [21n]$$

This is the Principle of Virtual Work and can be derived under the assumptions of equilibrium of all forces and continuity of all displacements. If now $\delta\epsilon_{ij} = \delta\epsilon_{ij}^{LOC}$, we find immediately that eq. [21i] still holds true for the macroscopic stress and strain, if we now use

$$\sigma_{ij} = \frac{1}{V}\int \sigma_{ij}^{LOC}\,dV. \qquad [21o]$$

"The macroscopic stress is the average of the microscopic stresses."

Abstracting from these two special cases, we see that the stress, on whatever scale it is being used, is always related to the work that must be done by the applied forces to produce a given or average strain increment:

$$\sigma_{ij} \equiv \frac{1}{V}\frac{\delta W}{\delta\epsilon_{ij}}. \qquad [21p]$$

The stress used here is always an "applied" stress: it is an expression of applied forces. We shall discuss "internal" stresses further below.

Thermo-mechanical Equilibrium

We have seen that thermodynamic equilibrium requires $\delta F = \delta W$ (eq. [21d]), and that mechanical equilibrium requires $\delta W = V\sigma_{ij}\delta\epsilon_{ij}$. In thermo-

mechanical equilibrium, we can thus write

$$\delta F \leqslant V \sigma_{ij} \delta\epsilon_{ij} \qquad (\delta T = 0;\ \delta\sigma_{ij} = 0) \qquad [21q]$$

where the inequality has again been included to indicate the direction of irreversible changes (eq. [21d]).

A typical application of this equation may be illustrated by the following example. Consider an internal virtual change, such as: remove a number δn of atoms from a certain prismatic dislocation loop and place them at random positions on the outer surface. (Note that nowhere in this section have we made an assumption about any "smallness" of the change symbolized by δ.) Now calculate all changes in the free energy F of the body due to this change; for example, the change in elastic and core energies of the dislocation loop and the change in total surface free energy. If the body is under the influence of any nonzero stress, also calculate all surface displacements (or the average strain, eq. [21k]) associated with this virtual variation. All other internal, or "hidden", variables must be allowed to adjust themselves to their equilibrium values (*not be kept constant!*); for example, a glide dislocation loop near that prismatic loop may change size or shape under the influence of the changed stress field. Insertion of the calculated values of δF and $V\sigma_{ij}\delta\epsilon_{ij}$ into eq. [21q] gives the (relative) equilibrium value of n.

In practical cases, one is often not interested in *complete* equilibrium, but in equilibrium of those internal parameters that can, according to their respective kinetics, relax to equilibrium in the time spans of interest. In the above example, one may assume that the change in size or shape of the glide dislocation loop in response to the change in internal stresses occurs even faster than the main process considered, namely the change in size of the prismatic loop. On the other hand, the changed internal stress may also require an adjustment in shape of a nearby precipitate to attain complete equilibrium—but such changes may sometimes be considered to occur at negligible rate. Then, these particular hidden parameters may be kept constant during the virtual variation.

The Driving Force for Irreversible Deformation

In eqs. [21b], [21d], and [21q], we allowed for *deviations* from equilibrium, if the inequalities held, rather than the equalities. For applications to irreversible processes, it is useful to have a quantitative measure for the *degree* of deviation from equilibrium, which leads to the definition of a *driving force* for these processes. We may take the *difference* between the two quantities that must be equal in equilibrium to be such a measure. For the case of a constant temperature, in which we are only interested, we may define (using eqs. [21a], [21c])

$$\delta\Psi \equiv T\,\delta S - \delta Q = \delta W - \delta F \qquad [21r]$$

and express the Second Law as

$$\delta\Psi \geqslant 0 \qquad (\delta T = 0). \qquad [21s]$$

This quantity is the energy dissipated during the variation, or T times the "irreversible change in entropy". In Irreversible Thermodynamics (see, for

example, HAASE, 1963), one often defines the time derivatives in place of the virtual variations in eq. [21r], and then the left-hand side would be the rate of *entropy production*, times T.

For *deformations* $\delta\epsilon_{ij}$ of a body, in which again all nonmechanical work terms are neglected, eqs. [21r] and [21s] specialize to

$$\delta\Psi = V\,\sigma_{ij}\,\delta\epsilon_{ij} - \delta F \geqslant 0. \qquad [21t]$$

This equation has two applications. First, it may be used to find the equilibrium value of an "internal", "microscopic", or "hidden" parameter, as was already discussed in connection with eq. [21q]. Second, one may use the *macroscopic* strain increment $\delta\epsilon_{ij}$ itself as the quantity to be varied. With the definition

$$\tau_{ij} \equiv \frac{1}{V}\frac{\delta F}{\delta\epsilon_{ij}} \qquad [21u]$$

the quantity

$$\frac{1}{V}\frac{\delta\Psi}{\delta\epsilon_{ij}} = \sigma_{ij} - \tau_{ij} \qquad [21v]$$

may then be called the *driving-stress* for irreversible deformation, and τ_{ij} may be called the *deformation resistance*. It is seen that τ_{ij} has the same dimensions as stress and that, in fact, its definition (eq. [21u]) bears a close analogy to that of the stress σ_{ij} (eq. [21p]). However, the two are not *identical*, they are merely equal in equilibrium.

The deformation resistance τ_{ij} describes the change in free energy of the body as it is being deformed; it may be zero or non-zero depending on the physical process. For example, in elastic deformation the free energy changes due to the "stretching of atomic bonds"; this change is proportional to strain (and to an elastic constant), and when the applied stress equals the value of τ_{ij} for this strain, equilibrium is achieved and Hooke's Law is obeyed. On the other hand, in Nabarro–Herring creep, which is based on the diffusion of vacancies, the free energy does not change with deformation; thus, $\tau_{ij} = 0$ and equilibrium at a finite applied stress σ_{ij} is not possible; if the response to the resulting driving force [21v] is linear, as it is for Nabarro–Herring creep, Newtonian viscosity follows.

In dislocation glide, with which we will be exclusively concerned, an intermediate situation obtains. For example, the free energy may increase through the generation of internal surfaces when a dislocation cuts a precipitate; it may be unchanged while a dislocation travels between precipitates; and it may decrease temporarily while a dislocation is being attracted into the coherency stress field of a precipitate. For some applications, we will be interested in the *average* change in free energy during long-range dislocation motion (namely, when considering the energy stored); for some in the *instantaneous* change, whether temporary or not (namely, when defining the local glide resistance).

Internal Stresses

In the foregoing we have either assumed that the stress is prescribed and uniform, or that the strain is prescribed and uniform in which case only the *average* stress was of interest for the work done. Let us now explicitly consider variations in stress with position in the body.

These stress variations may be on a number of different scales. On one extreme, the body of interest may not be a test piece under deliberately simple boundary conditions, but a macroscopic structure subjected to various loads and displacement conditions. In this case, we assume the boundary value problem to have been solved, by the methods of solid mechanics, to the point where the stresses on various elements of the structure are known. These elements under essentially uniform stress may be many inches across; in the presence of strong stress gradients, the variations in stress may be deemed negligible over distances of a small fraction of an inch. Such elements are the "bodies" we consider in our analysis, and the stresses transmitted into them by the neighboring elements are the "applied forces" that do work.

On the other extreme, there may be microscopic variations in stress due to incompatibilities in the *material* such as dislocations or coherent precipitates. They typically vary over distances of the order of a micron or less and are often referred to as "internal stresses". If they are, for the moment, assigned the symbol σ_{ij}^{INT} (conventionally counted positive in the direction opposing the applied stress σ_{ij}), one may wish to define a truly local stress by

$$\sigma_{ij}^{LOC} = \sigma_{ij} - \sigma_{ij}^{INT}. \qquad [21w]$$

This local stress would be opposed by the local deformation resistance τ_{ij}^{LOC} so that the driving force for irreversible flow becomes

$$(\sigma_{ij} - \sigma_{ij}^{INT}) - \tau_{ij}^{LOC}. \qquad [21x]$$

Alternatively, one may realize that these internal stresses are *material* properties rather than reactions to boundary conditions. They do contribute to the free energy of the "body"—say, in an amount δF^{INT}. This free energy changes when the local element is deformed—say, by

$$\tau_{ij}^{INT} \equiv \frac{1}{V}\frac{\delta F^{INT}}{\delta \epsilon_{ij}}. \qquad [21y]$$

This quantity may be called the "deformation resistance due to internal stresses". The total driving force for irreversible deformation is, in this interpretation,

$$\sigma_{ij} - (\tau_{ij}^{INT} + \tau_{ij}^{LOC}) \equiv \sigma_{ij} - \tau_{ij}. \qquad [21z]$$

Evidently, eqs. [21x] and [21z] achieve the same purpose. Equation [21x] uses a local or "effective" stress working against a local resistance; eq. [21z] uses the applied stress and incorporates all internal stresses into the deformation resistance. HIRTH and NIX (1969) have shown in detail that a consistent

thermodynamic system can be built on either choice. We prefer the latter because it is operationally better defined: while local stresses can be measured in principle, only applied stresses can be readily measured in practice. Similarly, the total deformation resistance may be measured, essentially by measuring the applied stress in (or at the limit of) equilibrium; its various components can be separated only by the use of microscopic models.

The realization that the macroscopic effects of any microscopic internal stress are indistinguishable from those of any other deformation resistance has led some authors to call the *entire* quantity τ_{ij}, defined by eq. [21u] and called "deformation resistance" in this text, an "internal stress" or "back stress", even if it is caused, say, by incoherent inclusions without a stress field. We avoid these words, since they are used in different meanings by different authors.

There is an intermediate scale of stress variations within a body, usually referred to as "residual stresses". These arise from two common causes: either the body underwent nonuniform plastic deformation (such as bending) before being considered, in which case the scale of the variations is that of the macroscopic structure; or the body is a polycrystal which underwent heating cycles or other treatments to which the different grains respond differently, in which case the scale of the variations is that of the grain diameter. These residual stresses can sometimes be calculated on the basis of very general models, or they may be measured by the use of x-ray diffraction. In such cases, it would be appropriate to add them in with the applied stresses and consider the "body" to be of a smaller scale, for example, an individual grain in the polycrystal. The choice here depends essentially on the purposes of the investigation rather than on basic thermodynamics or operational philosophy.

22. Dislocation Glide

The most important mode of plastic deformation in solids is slip; at very high temperatures, it may be supplemented by diffusional mass transport and grain boundary sliding, at low temperatures by twinning. In slip, plastic deformation is effectively concentrated into the region between some atomic planes: in an idealized unit process, one-half of the crystal *slips* over the other half at an imaginary cut made between two neighboring atomic planes, by an amount and in the direction of the Burgers vector—generally the shortest lattice vector. After the slip has taken place, the atoms in the two halves of the crystal are again in perfect register; any evidence of the fact that slip has taken place is restricted to a change in surface shape.

Slip occurs by the generation and propagation of dislocations. The easiest definition of a dislocation loop for our purposes (although not a completely general one) is that it is the demarcation line, in one slip plane, between an area that has slipped and a surrounding area that has not. When the dislocation loop expands in the slip plane by "glide", the slipped area increases and so do the surface displacements.

On the other hand, dislocations are structural defects which contribute to the free energy of the crystal. Any change in the position of dislocation

elements may in general change the free energy. We may regard a virtual displacement of some dislocation elements as an internal variation of the kind discussed in the last section, and use as the internal parameter the area δa swept out in the process. Whether and in which direction such a variation should actually tend to take place is then determined by the "driving force" for this variation.

$$\frac{\delta \Psi}{\delta a} = V \sigma_{ij} \frac{\delta \epsilon_{ij}}{\delta a} - \frac{\delta F}{\delta a} \geqslant 0. \qquad [22a]$$

Note again that the change in free energy is not uniquely determined by the amount δa of the area swept; it may depend on the details of the prescribed variation and on all the other internal variables that adjust themselves to new equilibrium values. We shall discuss these problems in detail in the following sections.

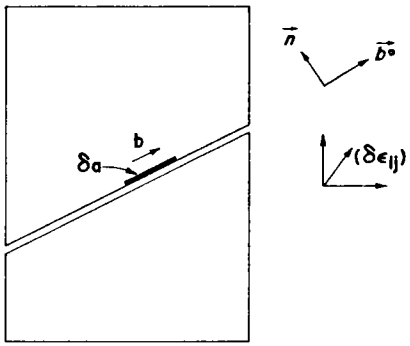

FIG. 22-1. Derivation of the macroscopic strain $\delta \epsilon_{ij}$ produced when an additional area δa is swept out by a dislocation of Burgers vector $\vec{b}$, on a slip plane with normal $\vec{n}$.

Shear

The average strain $\delta \epsilon_{ij}$ (defined in eq. [21k]) produced by an increase δa in the slipped area may be considered to consist of two parts. The first is the direct consequence of the virtual variation, without regard to any incompatibilities generated or their relaxation to equilibrium. It is easily obtained by introducing an internal surface into the body, for example along the slip plane (Fig. 22-1), but in any case containing δa as a surface element, and integrating eq. [21k] over both halves of the body. The only nonzero contribution to this integral is then from the element δa, and it is (eq. [21k])

$$\delta \epsilon_{ij} = \frac{b\, \delta a}{V} \cdot \frac{b_i^{\circ} n_j + b_j^{\circ} n_i}{2} \qquad [22b]$$

if b is the amount of the Burgers vector, $\vec{b}^\circ$ the unit vector in its direction, and $\vec{n}$ the unit vector perpendicular to the slip plane. The combination of unit vector components in eq. [22b] is the generalized Schmid factor (see, for example, KOCKS, 1970a), and the remaining factor is the "shear" or "glide" produced by dislocation motion:

$$\boxed{\delta\gamma \equiv \frac{b\,\delta a}{V}.} \qquad [22c]$$

A second contribution to the surface displacements comes from the elastic relaxation of the incompatibilities created: the strain field of the dislocation at the new position is different from that at the old position. The contribution of these relaxations to the macroscopic strain is zero so long as the material is homogeneous and linear-elastic: the local change in strain is then proportional to the local change in (internal) stress, which must average out to zero by eq. [21o] when the applied stress is constant. Equation [22c] then gives the entire strain due to dislocation movement.

When the material is not elastically homogeneous, as would be the case, for example, for a polycrystal of an elastically anisotropic material, the change in the internal stress pattern can lead to an additional contribution to the average strain. It is as "permanent" as the plastic contribution [22c], but only has the order of magnitude of elastic strains. It can be very important in the microstrain region, but not at "macroscopic" strains (larger than, say, 0.2%), as they are of concern in flow phenomena. (For an exact treatment, see KRÖNER, 1958; RICE, 1971.)

Resolved Stress and Glide Resistance

Since only one component of the strain produced by dislocation motion is nonzero (namely, that in the slip plane in the slip direction), only one component of stress contributes to the work done during slip. In analogy to the general eq. [21p], we define

$$\boxed{\sigma \equiv \frac{1}{V}\frac{\delta W}{\delta\gamma} = \frac{1}{b}\frac{\delta W}{\delta a}.} \qquad [22d]$$

This is the resolved stress, shear stress, or simply (applied) "stress", as we shall use it through the remainder of this article.

In analogy to the general definition [21u], we can also define a special deformation resistance, the "glide resistance", by

$$\boxed{\tau \equiv \frac{1}{V}\frac{\delta F}{\delta\gamma} = \frac{1}{b}\frac{\delta F}{\delta a}} \qquad [22e]$$

so that the driving force for the virtual dislocation glide under consideration is

$$\frac{\delta\Psi}{\delta a} = b\sigma - b\tau. \qquad [22f]$$

In the limiting case that δa is thought of as the differential forward displacement of a unit length of dislocation line, eq. [22f] may be said to define the *net force* per unit length on the dislocation.

Energy Stored

Any feature of a crystal which results in a nonzero value of the glide resistance τ is an *obstacle to slip*. In overcoming an obstacle, free energy may be stored *temporarily* (e.g. as the increased length of dislocation when it bows between discrete obstacles) or *permanently* (e.g. as the surface energy of new surfaces, or as jogs or point defects). The "permanently" stored energy may be removed by some independent process—recovery or annealing—either after the deformation at a higher temperature, or even during the deformation itself. In principle, it can be identified by its annealing kinetics, whereas the temporarily stored energy is inseparable from the deformation process.

Processes in which temporary energy storage occurs can, in principle, be activated by thermal fluctuations, processes which store energy at a constant *rate* cannot. (The drawing-out of a dipole is an example.) More generally, in overcoming an obstacle some energy is stored temporarily, some permanently. It is useful to know the second (permanent) component, since, ultimately, this represents the part of the flow stress which cannot be overcome with the help of thermal fluctuations.

To obtain this, we consider the virtual motion of a dislocation over an area large compared with that associated with a single obstacle. The change in free energy of the body is then given by integrating eq. [22e]:

$$F_{\text{STOR}} = V \int \tau \, \mathrm{d}\gamma \equiv V\tau_{\text{STOR}} \int \mathrm{d}\gamma. \qquad [22g]$$

We see that, whenever the *average* glide resistance τ_{STOR} defined by this equation is nonzero, the *free energy stored* is nonzero, too.

The thermodynamic conditions for macroscopic dislocation motion, or slip, now require that

$$\sigma \geqslant \tau_{\text{STOR}} \qquad (\textit{slip possible}) \qquad [22h]$$

or, in words, that the *work done, per unit volume, by the applied stress at least equal the stored free energy of deformation per unit volume*. This prescribes a lower limit to the applied stress required for flow; below this stress τ_{STOR}, no steady flow can occur even at high temperatures.

The energy stored during plastic deformation can, in principle, be measured calorimetrically during subsequent recovery or recrystallization. Note, however,

that such measured stored energies are *internal* energies U_{STOR}, which should give an upper limit to the *free* energy F_{STOR} in eq. [22g]. The method is further complicated by the fact that a very small change in the specific heat due to plastic deformation can have profound effects on the measurements (GOTTSTEIN *et al.*, 1973).

Physically, an increase in the free energy of the specimen during plastic deformation may correspond to the creation of internal surfaces when precipitate particles are cut; to disordering of an ordered structure by deformation; to the creation of point defects and jogs; to the storage of dislocations, in the form of loops, dipoles, cell walls or tangles; or to the production of cracks. When experiments (e.g. calorimetric measurements) show that a large part of the external work is stored, as in stage I of the work hardening of fcc metals, then it follows that thermal fluctuations do not have much effect on the motion of a single dislocation.

On the other hand, many types of obstacles result in no energy storage, i.e. τ_{STOR} is zero. Examples are the overcoming of internal stress fields or of Peierls hills; the conservative motion of jogs; and various diffusion controlled processes. For such mechanisms, F_{STOR} is zero, and, in principle, an infinitesimal applied stress will cause flow, although its rate may be undetectably small.

A special situation arises when the moving dislocations do not sample the entire slip plane (even though they may produce macroscopic plastic flow—see sec. 25: "statistics"). This may arise when there are impenetrable inclusions or twins in the crystal, or when localized dislocation "tangles" develop during work hardening. In these cases, the average internal stress *sampled by the moving dislocations* need not be zero and would thus lead to a finite τ_{STOR}. This is especially important when the inclusions or tangles produce a constant level of "image stresses" in the finite crystal—which they do if their stress field plus that of any previously stored dislocation loops around them decreases as $1/r^3$ or more slowly (BROWN, 1973).

The thermodynamic consideration leading to eq. [22h] holds in the average over suitably large volumes, i.e. for long-range slip. *Some* dislocation motion can occur at stresses $\sigma < \tau_{STOR}$; for example, because the non-uniform distribution of obstacles in the slip plane leads to a variation in the local glide resistance. These pre-yield effects contribute strains comparable with the elastic strain, and we shall exclude them from our discussion of general plastic flow.

Finally, at least two kinds of anelastic behavior (time-dependent, *recoverable* flow) can occur in single crystals, and must be distinguished from the *irreversible plastic flow* occurring at $\sigma \geqslant \tau_{STOR}$. First, when a stress is applied to a crystal containing obstacles, segments of dislocation bow between, or ride up on, the obstacles. This process occurs with a relaxation time controlled by the processes which dissipate energy as the dislocation moves (phonon drag, etc., see Chapter 3) and is usually very small. Second, the stress may cause some obstacles to be overcome, or cut, but in a manner which is precisely reversed when the stress is removed. The relaxation time for this process (Chapter 4) is usually longer.

The Mechanical Threshold

We have seen that, depending on the magnitude of the applied stress, dislocation motion is possible on different scales. Even at zero stress, local dislocation rearrangements can occur, but equilibrium is possible. When the stress exceeds the *average* glide resistance in any slip plane in which there are mobile dislocations, large-scale slip is possible, but it has to rely on thermal fluctuations to overcome locally higher glide resistances.

In all practical cases, there is also a *maximum* in the glide resistance on any slip plane. When the applied stress exceeds this maximum glide resistance

$\hat{\tau}$, dislocations will not be able to find any equilibrium positions and large-scale slip must, in principle occur:

$$\sigma > \hat{\tau} \qquad (\textit{equilibrium impossible}). \qquad [22i]$$

This is the *mechanical threshold*, or the *yield strength*, or the *flow stress at zero temperature*. It is the reference state for all plastic flow: at stresses above it, acceleration- and velocity-dependent forces come into play (they will be discussed in Chapter 3); at stresses below it, presuming they fulfill eq. [22h], thermal activation comes into play (as will be discussed in Chapter 4).

The variation of the glide resistance with position in the crystal, which is an equilibrium property of the material, is thus of paramount importance for its dynamic behavior. In the following sections, we will discuss various aspects of this equilibrium of dislocations within the crystal.

23. The Glide Resistance

We have established that the resistance of a material to dislocation motion is characterized by the quantity (eq. [22e])

$$\tau \equiv \frac{1}{V}\frac{\delta F}{\delta \gamma} = \frac{1}{b}\frac{\delta F}{\delta a}.$$

Here F is the (Helmholtz) free energy of the deforming crystal. The calculation of τ for a large class of obstacles is complicated because of the flexibility of the dislocation line. This ability to bend causes the free energy F, and thus τ, to depend on the *shape* of the dislocation. It is helpful, first, to calculate the quantity τ for a dislocation *element* (that is, a very short, straight segment) in spite of the fact that the dislocation may not, in reality, remain straight. This procedure allows us to isolate and describe the interaction of the element with the obstacles which oppose slip, without the complications (considered below) caused by the interaction of the dislocation with itself. The element glide resistance diagram that we obtain by this simplification describes the shape of an isolated obstacle. Later, we will take the flexibility of the dislocation into account and we will find that the glide resistance diagram for a flexible dislocation line almost always differs from that of an element; but it can be calculated if that for the element is known.

The Element Glide Resistance

Assume that the dislocation element of length $d\xi$ is located at a particular point (x, y, z) in the crystal. First identify the x-direction with the direction of this line element and the z-direction with the normal to its glide plane. Now cut from the crystal a slice of thickness $d\xi$ (and area A) perpendicular to the x-direction at position x. All necessary surface tractions and chemical potentials have to be applied over the cut faces so that the slice itself experiences no changes whatever. Conceptually the easiest way of fulfilling this

condition is to make a large number of copies of this slice and put them together into a new artificial crystal that may, in principle, be of infinite extent in the x-direction. The result of this procedure is that the dislocation element under discussion has now become an infinitely long, straight dislocation.

If this dislocation is displaced in equilibrium through the distance δy, the shear produced uniformly in each slice, of volume $A\,d\xi$, is (eq. [22c])

$$\delta\gamma = \frac{b\,\delta y\,d\xi}{A\,d\xi} = \frac{b\,\delta y}{A} \qquad [23a]$$

and the free energy of each slice will change by an amount $\delta(\mathscr{F}_{\text{ELEM}}\,d\xi)$, where $\mathscr{F}_{\text{ELEM}}$ is the free energy of the slice divided by its thickness. It is then possible to define a glide resistance (eq. [22e]) for this element: the *element glide resistance* (or, more briefly, the *element resistance*) for a straight dislocation element, by

$$\boxed{\tau_{\text{ELEM}} \equiv \frac{\delta\mathscr{F}_{\text{ELEM}}}{b\,\delta y}.} \qquad [23b]$$

Like the quantity τ defined in the last section, τ_{ELEM} has the dimensions of stress. It is a material property describing the local resistance of the crystal

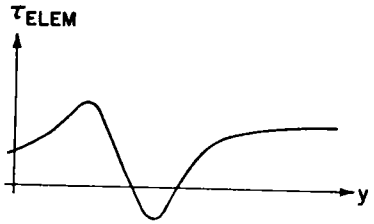

FIG. 23-1. Schematic element glide resistance for one slice of the crystal.

to the motion of a straight dislocation element. Just as $\sigma b\,d\xi$ can be regarded as the force exerted by the applied stress and urging the dislocation element forward, the quantity $\tau_{\text{ELEM}}\,b\,d\xi$ can be regarded as the force with which the crystal opposes its motion.

As the element moves forward, this resisting force may, in general, vary with position in an arbitrary fashion, an example of which is shown in Fig. 23-1. Note, however, that in each of its many positions y the dislocation is to be in equilibrium. Whether this equilibrium is stable or unstable does not interest us here. We merely consider states in which all forces on the dislocation are fully balanced and the dislocation has zero velocity.

Figure 23-1 describes a single slice through the obstacle. We must now produce further artificial crystals made up of sets of identical slices of thickness $d\xi$ and again perpendicular to the x-direction, but corresponding to

positions x, $x + d\xi$, $x + 2\,d\xi$, etc., in the real crystal. This procedure will give the information schematically shown in Fig. 23-2. Here, each slice is represented by a single curve, such as one of those contained in Fig. 23-1, located at the relevant position x.

Figure 23-2 is not yet a complete description of the interaction of the dislocation element with the crystal. The interaction may depend on the *direction* of the dislocation element, not just on its position. For example, the interaction of a screw dislocation with a particular obstacle will in general be different from that of an edge dislocation; or a particular obstacle to dislocation movement may be narrow in one direction and wide in another. In principle, we thus have to repeat the entire procedure for every direction ξ contained in the glide plane (xy). In the simplest of cases, when the cross section of the obstacle in the slip plane is circular, the largest

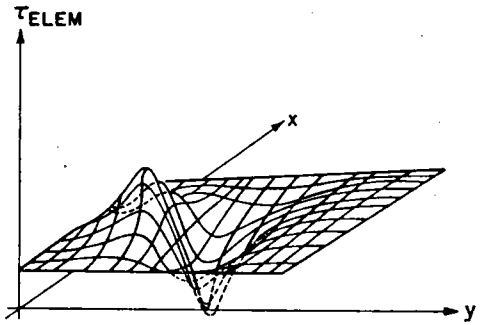

FIG. 23-2. Schematic element glide resistance for elements lying parallel to the x-direction and moving in the y-direction.

difference is that between screw and edge dislocations, and the behavior can then be adequately described by just two figures of the kind shown in Fig. 23-2. When even this difference vanishes (for example, when the resistance is to the glide shear only, no matter whether it is made by a screw or an edge dislocation), the element glide resistance is *isotropic*, and Fig. 23-2 suffices.

Of course, the element glide resistance may be different for every specific slip plane, that is for different locations z. In any application, one will only be able to deal with a "typical" element glide resistance diagram or "profile". Such a typical element glide resistance diagram, for a particular orientation of a dislocation element, may legitimately be called an (elemental) force distance diagram. However, we have reserved this term for another common (and operationally definable) meaning, namely referring to the plot of the total force exerted on a dislocation segment by a discrete obstacle versus the average forward distance moved by the segment at the obstacle (sec. 25).

The Line Glide Resistance

Figure 23-2 is a map of the glide resistance felt by a straight dislocation element of a certain direction anywhere in a certain (or a typical) slip plane. If one artificially introduced a *long straight* dislocation of the same direction

into this slip plane, its different elements would experience different forces (plotted along a line parallel to the x-direction in Fig. 23-2). Under a given applied stress σ, the driving force

$$b\sigma - b\tau_{\text{ELEM}}(\xi)$$

could then not be zero for all elements, and the condition for the virtual variation of the position of one element, namely that all other internal parameters such as the positions of all other dislocation elements be allowed to relax to their respective equilibrium values, would be violated.

If one allows such relaxations to take place, the dislocation does not remain straight, and then it exerts forces on each element of itself, which were not considered before. These forces are internal stresses of the kind more generally discussed in sec. 21 (see also BESHERS, 1971). They may be accounted for in different ways, depending on the choice of "the system" and "the surroundings": if one continues to focus on an individual dislocation element, the self stresses may be merely added to the applied stress to give a local or "effective" stress, but this implies that they are *known*; if one treats the whole crystal as "the system", or at least the entire, continuous dislocation, they are counted as a dependence of the free energy on the shape of the dislocation and contribute to the glide resistance just as the element glide resistance due to "obstacles" did. For the reasons outlined in sec. 21, we prefer the latter procedure.

Let us define, then, the stress exerted by all elements of a continuous dislocation on a particular element of itself as τ_{SELF} (to be derived in some detail below), and the total glide resistance felt by this element of a long dislocation line as

$$\boxed{\tau_{\text{LINE}} \equiv \tau_{\text{ELEM}} + \tau_{\text{SELF}}.} \qquad [23c]$$

The total driving force tending to move this element forward is then

$$b\sigma - b\tau_{\text{LINE}}. \qquad [23d]$$

It may be zero everywhere along the dislocation line, if this line adjusts its shape so as to make τ_{SELF} exactly compensate for the given variations in τ_{ELEM}: *in equilibrium, τ_{LINE} is constant along the entire length of the dislocation line*. This is a prime advantage of incorporating the self stresses into the glide resistance.

To summarize the procedure of this section:

Out of equilibrium, the expression [23d] determines the driving force on each dislocation element. Under a given applied stress, σ, each element then tends to move to a position, and to adopt a curvature, such that $\tau_{\text{ELEM}} + \tau_{\text{SELF}}$

is equal to the applied stress at every point along the dislocation. Where τ_{ELEM} has a large local value, the dislocation adopts a strong curvature such that τ_{SELF} is large and of opposite sign; the difference between the two is σ. Where τ_{ELEM} is zero (between discrete obstacles for example), the dislocation adopts a curvature such that τ_{SELF} precisely equals the applied stress. If the applied stress is raised slightly, the dislocation line advances and changes its shape, such that the line resistance, τ_{LINE} again equals σ.

Suppose that a length l of dislocation, long enough to sample a "typical" region of the element glide resistance diagram, moves forward adopting successive equilibrium shapes for which $\tau_{LINE} = \sigma$. In so doing it sweeps out

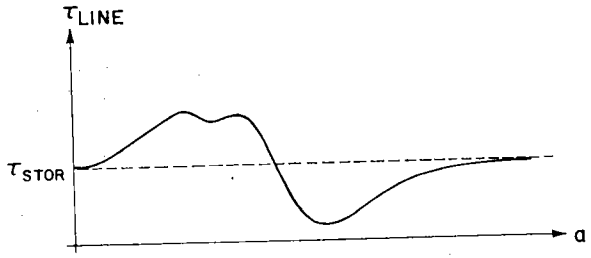

FIG. 23-3. Schematic line glide resistance diagram as a function of the area swept.

an area a, and changes its shape as it moves. The line resistance is then most conveniently represented as a plot of τ_{LINE} against glide area a:

$$\tau_{LINE} = \tau_{LINE}(a). \qquad [23e]$$

This is a one-dimensional dependence (Fig. 23-3): the x-dependence of the τ_{ELEM} diagram (Fig. 23-2) has been averaged out by the dislocation itself.

Adjustment of the dislocation line shape to a nonuniform element resistance is not the only reason for self stresses to appear. Another important class of problems consists of the nucleation of expandable shapes in front of linear barriers (sec. 24).

Dielastic Interactions

One type of glide resistance deserves special mention because its classification in the scheme developed here is somewhat arbitrary. The free energy of a crystal changes when a dislocation moves closer to a free surface or other elastic heterogeneity, such as an inclusion that has different elastic moduli. Such interactions have been termed *dielastic*, in analogy with diamagnetic and dielectric effects.

One may call such changes in free energy changes in the *self* energy of the dislocation, and their derivatives *self stresses*. There are, however, a number of differences

between these dielastic interactions and the (paraelastic) effects due to changes in *shape* of a dislocation, discussed above (and, in more detail, below). The most important difference is that the dielastic interaction of one dislocation element with all elastic heterogeneities in the body does not depend on the position of the other dislocation elements. Thus, at each position in the crystal one can state what the energy of a dislocation element (of a given orientation) would be if it were there. The gradient of that energy is a force on the dislocation element exactly like the element glide resistance. In contradistinction to other element glide resistance mechanisms, such as the generation of new interface, of point defects or jogs, or such as internal stresses, the glide resistance due to dielastic interactions is *nonlocal*: it depends on interactions with far-away parts of the body. Thus, the algorithm used to define the element glide resistance, which was based on considering only the slice of crystal perpendicular to the dislocation element, must be suitably modified if dielastic effects are to be incorporated into the element glide resistance.

The difficulty discussed above is one of nomenclature more than of physics. It illustrates the general principle that ambiguities arise when the total free energy change of a system is split up into various parts. We will treat a specific example involving dielastic interactions, in an approximate fashion, with reference to particle hardening (sec. 52).

Self Stresses and Line Tension

We have defined the self stress as a quantity which describes the variation of the free energy of a dislocation with a virtual variation in its shape, during which an incremental area δa is swept (eq. [23e]). The virtual variation may be large or small; the two equilibrium shapes to be compared depend on the details of the problem. In later sections, we will use the appropriate expressions for the self stress as we deal with specific problems. Here, we will introduce various basic models as they apply to an infinitesimal element of dislocation line.

At the lowest level of approximation, the *constant line energy model*, the free energy of a dislocation is simply proportional to its length $\mathscr{L}$, the constant of proportionality being the line energy $\mathscr{F}_{\text{DIS}}$. The self stress then becomes (eq. [23e])

$$\tau_{\text{SELF}} \equiv \frac{1}{b} \mathscr{F}_{\text{DIS}} \frac{\delta \mathscr{L}}{\delta a} \qquad \textit{(constant line energy approximation)}. \tag{23f}$$

For small variations in the radius of *circular loops*, the change in length $\delta\mathscr{L}$ divided by the change in area δa is simply the curvature κ, so that the self force per unit length becomes

$$b\tau_{\text{SELF}} = \mathscr{F}_{\text{DIS}} \cdot \kappa \qquad \textit{(constant line energy approximation)}. \tag{23g}$$

The form of this equation itself justifies that the equilibrium shape of any planar dislocation under constant stress must be one of constant curvature, in this model. Equation [23g] also holds for small variations in the curvature of circular arcs of constant secant length.

The (free) energy per unit length of a dislocation, or *line energy*, $\mathscr{F}_{\text{DIS}}$, is

then, in first order, set equal to the value appropriate for a screw dislocation:

$$\boxed{\mathscr{F}_{\text{SCREW}} = \frac{\mu b^2}{2} \cdot \frac{\ln(X/r_o)}{2\pi}} \qquad [23h]$$

where μ is the appropriate shear modulus (to be discussed below), X is a correlation distance characterizing the more distant dislocation interactions, and r_o is an effective core radius, which allows for core energy contributions. The second factor in eq. [23h] is often set equal to 1 for order-of-magnitude estimates, which corresponds to $X \simeq 500 r_o$. Then,

$$\mathscr{F}_{\text{DIS}} \simeq \frac{\mu b^2}{2}. \qquad [23h']$$

Alternatively, one might use the line energy of an edge dislocation:

$$\mathscr{F}_{\text{EDGE}} = \frac{1}{1-\nu} \mathscr{F}_{\text{SCREW}} \qquad [23i]$$

where ν is Poisson's ratio, using isotropic elasticity. We will give below (eq. [23ℓ]) a more appropriate average of the line energies [23h] and [23i] to be used with this constant line energy model.

The very admission of a difference in energies between edge and screw dislocations is inconsistent with a constant line energy model: the line energy does not only depend on length, but also on direction. Moreover, the elastic anisotropy of many crystals is not negligible; while in some cases (NaCl) it tends to decrease this difference between screw and edge energies, in most cases the difference gets accentuated (DEWIT and KOEHLER, 1959; BROWN, 1964; CHOU and SHA, 1971).

In any adjustment of dislocation shape, the free energy now changes both because of changes in length and because of changes in the angle α between the line direction and the Burgers vector. The self stress in an element, as defined by the first part of eq. [23f], is still proportional to its local curvature, but with an angle-dependent factor, the local *line tension* $\mathscr{E}$:

$$\boxed{b\tau_{\text{SELF}} = \mathscr{E}(\alpha)\,\kappa} \qquad (\textit{line tension approximation}) \qquad [23j]$$

where (DEWIT and KOEHLER, 1959; STERN and GRANATO, 1962; CHOU and ESHELBY, 1962)

$$\mathscr{E}(\alpha) \equiv \mathscr{F}_{\text{DIS}}(\alpha) + \frac{\mathrm{d}^2 \mathscr{F}_{\text{DIS}}(\alpha)}{\mathrm{d}\alpha^2}. \qquad [23k]$$

Under the governance of eq. [23j], the equilibrium shape of a dislocation loop is no longer circular, but often in a good approximation elliptical, with the ratio of major to minor axis being that of edge to screw dislocation energy.

The average line energy of a closed loop, i.e. the line energy of a circle of the same area and the same total energy, is

$$\bar{\mathscr{F}}_{\text{DIS}} = \sqrt{\mathscr{F}_{\text{SCREW}} \cdot \mathscr{F}_{\text{EDGE}}}. \qquad [23\ell]$$

This *geometric mean* is a useful value for insertion in the constant line energy model (eq. [23g]).

In *isotropic* elasticity theory, the dependence of the free energy per unit length on dislocation character is given by

$$\mathscr{F}_{\text{DIS}}(\alpha) = \mathscr{F}_{\text{SCREW}} \left(\cos^2 \alpha + \frac{1}{1-\nu} \sin^2 \alpha \right). \qquad [23m]$$

Table 2-I. Glide dislocation data for some elements at room temperature: Burgers vector b,[a] shear modulus μ for screw dislocation energy, [b],[c] and ratio of edge to screw energy.[c],[d]

	b Å	μb^3 eV (3)	μ (1) 10^{10} N m^{-2} (4)	$\frac{\mathscr{F}_{\text{EDGE}}}{\mathscr{F}_{\text{SCREW}}}$ (2)	$\nu_{\text{eff}} \equiv 1 - \mathscr{F}_S/\mathscr{F}_E$
Al	2.86	3.77	2.59	1.56	0.36
Ni	2.49	7.60	7.86	1.57	0.36
Cu	2.56	4.39	4.21	1.76	0.43
Ag	2.89	4.00	2.66	1.82	0.45
Au	2.88	3.72	2.47	1.99	0.50
Pb	3.50	1.95	0.73	2.02	0.50
Si	3.83	22.37	6.37	1.35	0.26
Ge	3.99	20.66	5.20	1.33	0.25
V	2.63	5.71	5.02	1.45	0.31
Cr	2.50	12.21	12.55	1.14	0.13
Fe	2.48	6.15	6.44	1.88	0.47
Nb	2.86	6.46	4.43	1.37	0.27
Mo	2.73	16.98	13.40	1.29	0.22
Ta	2.86	8.92	6.11	1.75	0.43
W	2.74	20.54	15.98	1.39	0.28
Mg	3.20	3.40	1.66	1.49	0.33
Zn	2.66	5.78	4.93	1.12	0.11
Cd	2.97	4.26	2.60	1.32	0.24

Notes:

(1) fcc and cph structures ($\vec{b}$ in close-packed direction): $\mu = \sqrt{c_{44}(c_{11} - c_{12})/2}$; (2) fcc and cph structures: close-packed glide plane; bcc structures: for {110} glide plane, the edge dislocation energies for other glide planes are up to 2% higher; (3) 1 eV = 1.6×10^{-12} erg $\equiv 1.6 \times 10^{-19}$ J $= 1.16 \times 10^4 . T(K)$; (4) 10^6 N m$^{-2} \equiv 10^7$ dyn cm$^{-2} \equiv 10$ bar $\simeq 102$ gf mm$^{-2} \equiv 102$ p mm$^{-2} \simeq 145$ psi.

1, bcc structures: $\frac{1}{3}(c_{11} - c_{12} + c_{44})$

References:

(*a*) *American Institute of Physics Handbook*, 2nd ed. 1963 (McGraw-Hill).
(*b*) H. B. HUNTINGTON (1958) *Solid State Physics* (SEITZ *et. al., eds.*) **7**, 213.
(*c*) Y. T. CHOU and G. T. SHA (1971) *J. Appl. Phys.* **42**, 2625.
(*d*) Y. T. CHOU and J. D. ESHELBY (1962) *J. Mech. Phys. Sol.* **10**, 27.

For the small variations in α appropriate to an infinitesimal element, one then finds from eq. [23k]:

$$\left.\begin{aligned} \mathscr{E}_{\text{SCREW}} &= \frac{1+\nu}{1-\nu}\,\mathscr{F}_{\text{SCREW}} \\ \mathscr{E}_{\text{EDGE}} &= \frac{1-2\nu}{1-\nu}\,\mathscr{F}_{\text{SCREW}} \end{aligned}\right\} \quad \textit{(local line tension)} \qquad [23n]$$

Note that the line *tension* of the screw is larger than that of the edge, while the reverse holds true for the line *energies* (eq. [23i]).

In *anisotropic* elasticity theory, the line energy of a straight dislocation can be given in terms of the anisotropic elastic constants for some combinations of line direction and Burgers vector, and has been solved numerically for others. One may then define an "appropriate shear modulus" μ so that eq. [23h] in fact gives the line energy of a screw, and an "effective Poisson's ratio" so that eq. [23i] in fact gives the line energy of an edge, even for anisotropic materials. These values are given for some elements at room temperature in Table 2-I.

Unfortunately, the line *tensions* obtained from eq. [23k] are then, in general, not well described by eqs. [23n] with the same effective value of ν; BARNETT *et al.* (1972) have derived them numerically for copper, nickel, and niobium. As an example, Table 2-II shows all values for copper, in units of $\mathscr{F}_{\text{SCREW}}$:

Table 2-II

	Anisotropic calculation	Approximation $\nu_{\text{eff}} = 0.43$	Isotropic theory $\nu = 1/3$
$\mathscr{F}_{\text{SCREW}}$	1	1	1
$\mathscr{F}_{\text{EDGE}}$	1.76	1.76	1.5
$\mathscr{F}_{\text{DIS}}$	1.33	1.33	1.22
$\mathscr{E}_{\text{SCREW}}$	3.2	2.53	2.0
$\mathscr{E}_{\text{EDGE}}$	0.61	0.24	0.5

Though a great improvement over the constant line energy approximation, this anisotropic line tension still attributes the self stress to a *local* property of the dislocation line. The self stress at (x, y) in fact depends not only on the local curvature, but on the distant shape of the dislocation also: each element interacts with *all* others, not simply with its neighbors. The form of this interaction is in fact known, even in anisotropic elasticity; the only remaining point of dispute is the correct core cut-off procedure.

For any given shape, i.e. an entire set of coordinates $\{x, y\}$,

$$\tau_{\text{SELF}} = \tau_{\text{SELF}}(\{x, y\}) \qquad [23o]$$

may then be calculated numerically. By an iterative relaxation, the equilibrium shape can be determined for any given boundary conditions (BACON, 1967; FOREMAN, 1967; BACON *et al.*, 1973). Frequently, the result can be adequately described by a judicious choice of the outer cut-off parameter X in eq. [23h]; we shall meet a case in point in eq. [25i]. In all cases so far investigated, this leads to a lower value than that used in eq. [23h']. Since, on the other hand, the anisotropic corrections tend to raise the energy, we shall retain eq. [23h'] for order-of-magnitude calculations.

Quasi-straight and Quasi-circular Dislocations

The self stress describes the tendency of a dislocation to change *shape*. It is evident that it cannot drive a dislocation forward as a rigid body (BESHERS, 1971). Any component of τ_{SELF}, say, in the y-direction, integrated along the entire length of the dislocation, must therefore vanish:

$$\int_0^\infty b\,\tau_{\text{SELF}} \sin\psi \,\mathrm{d}\xi = 0 \qquad [23p]$$

where ψ is the angle between the dislocation element (length $\mathrm{d}\xi$) and the y-axis. The integration does not have to extend over an infinitely long dislocation, but only over a length long compared with the wavelength of variations in the element glide resistance. Alternatively, it may run between any two points, x apart, along the dislocation that have a common tangent (Fig. 23-4).

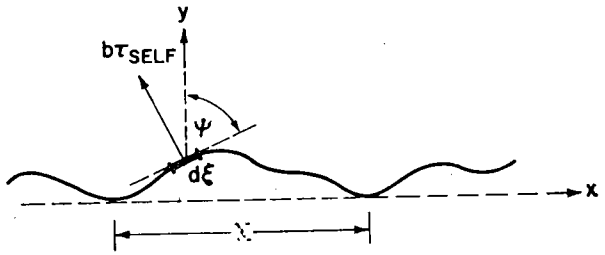

FIG. 23-4. A quasi-straight dislocation: the average forward self stress is zero.

For a quasi-straight dislocation, whose average direction is along the x-axis (perpendicular to y in the slip plane), eq. [23p] then becomes

$$\int_0^X b\,\tau_{\text{SELF}}\,\mathrm{d}x = 0, \qquad [23q]$$

or, with eq. [23c]),

$$\int_0^X \tau_{\text{LINE}}\,\mathrm{d}x = \int_0^X \tau_{\text{ELEM}}\,\mathrm{d}x. \qquad [23r]$$

In equilibrium, when τ_{LINE} is constant along the dislocation, *the line resistance is equal to the average of the element glide resistance*, averaged along the average direction of a sufficiently long, quasi-straight dislocation line. In equilibrium with an applied stress, $\sigma = \tau_{\text{LINE}}$: the total force σbX exerted on the dislocation line in the y-direction is carried by the "obstacles".

Equation [23q], multiplied by δy, expresses the postulate made above that the free energy of the crystal cannot change when the dislocation moves forward as a rigid body. It is evident that the virtual variation δy must be independent of x for eq. [23q] to hold. In most practical cases, two successive

equilibrium states do *not* correspond to such rigid-body motions; rather, the dislocation overcomes a limited region at a time, the rest of its length being unaltered. We shall treat specific cases in secs. 24 and 25.

If, instead of a quasi-straight dislocation, we consider a closed loop, say one which undulates around a circle (Fig. 23-5), we have the same rule that any one component of the self stress integrated over the loop must vanish: the self stress does not tend to move the loop as a rigid body. However, the

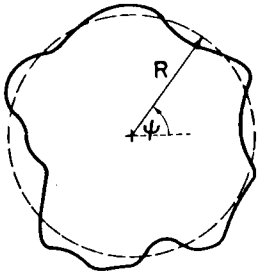

FIG. 23-5. A quasi-circular dislocation: the average radial self stress is equal to that of the exact circle (dashed).

self stress tends to effect shrinkage of the loop, a process in which motion and shape change are linked. Its average is

$$\frac{1}{2\pi}\int_0^{2\pi} \tau_{\text{SELF}}\, d\psi = \frac{\mathscr{F}_{\text{DIS}}}{bR} \qquad [23s]$$

and therefore in shape equilibrium

$$\tau_{\text{LINE}} = \frac{1}{2\pi}\int_0^{2\pi} (\tau_{\text{ELEM}})_R\, d\psi + \frac{\mathscr{F}_{\text{DIS}}}{bR} \qquad [23t]$$

where the integrand is the radial component of the element glide resistance. The last term may then be considered a *back stress* superimposed on the average element glide resistance.

The Plane Glide Resistance

Any theory of macroscopic flow is concerned with the motion of dislocations over an entire slip plane. We call the resistance to such long-range motion the *plane glide resistance*, or simply the *plane resistance*, τ_{PLANE}. In the past literature it is often assumed that the maximum plane resistance $\hat{\tau}_{\text{PLANE}}$ is simply equal to the maximum line resistance $\hat{\tau}_{\text{LINE}}$. In certain simple cases this is true; but it should never be assumed. Two important reasons why the plane glide resistance differs from the line resistance are discussed later in this chapter—we merely introduce them now.

First, the line glide resistance describes the interaction of a flexible dislocation with a single "typical" obstacle. It does not take into account the way in which obstacles are distributed in the slip plane. The plane glide resistance depends on the *statistics of the distribution*, as well as on the line glide resistance of the "typical" obstacle. This problem is discussed in sec. 25.

Second, cooperative dislocation motion is possible. A dislocation can overcome strong, widely separated obstacles with the help of other dislocations in the same slip plane, that is, by becoming part of a *dynamic pile-up*. It can be shown (sec. 24) that dynamic pile-ups can form only when obstacles to slip are separated by more than a critical distance. But when they do, they cause the plane glide resistance to be less—sometimes much less—than the line glide resistance.

Below the maximum stress a slip plane can sustain, $\hat{\tau}_{\text{PLANE}}$, the relation between the applied stress and the total area swept out by all dislocations in the slip plane may be expressed by a relation $\tau_{\text{PLANE}}(a)$. The integral under this curve contains, according to eq. [22e], the free energy temporarily stored in the rearrangement of dislocations, or in the "dynamic structure". However, it may also contain energies dissipated during this process, and in this sense τ_{PLANE} is not strictly the derivative of a free energy (eq. [22e]), as τ_{ELEM} and τ_{LINE} are (eqs. [23b] and [23f]). This becomes particularly evident at the maximum level $\hat{\tau}_{\text{PLANE}}$ where the area becomes, by definition, infinite. Nevertheless, τ_{PLANE} does represent the resistance to the motion of a dislocation (or its partners) and is a material property, derivable from equilibrium considerations; for this reason, the symbol τ is appropriate.

Reverse Glide

The element glide resistance was defined (eq. [23b]) from a virtual variation of the free energy with respect to position of a dislocation element; its sign depends on which direction is considered to be "forward" motion. If the direction of motion is reversed, the element resistance simply changes sign:

$$\tau_{\text{ELEM}}^{\text{rev}} = -\tau_{\text{ELEM}}^{\text{forw}}. \qquad [23u]$$

Thus, the parts of the element resistance diagram (Fig. 23-2) that were formerly negative are now positive, and vice versa. On the other hand, no such simple rule holds for the *line* glide resistance: the path taken by a dislocation line may well depend on the direction of motion.

The sign convention on the *applied* stress similarly relies on which direction of dislocation motion is considered positive. If reverse motions of dislocations are considered under the *same* applied stress (sec. 45), both the applied stress and the element resistance are reversed, from the point of view of the moving dislocation, and the direction of bow-out is also the same; thus, the same region of the glide resistance diagram is applicable. (For extensive discussions, see LI, 1970; NICHOLS, 1971.)

24. LINEAR BARRIERS

In the following sections, we will illustrate the concepts of element, line, and plane glide resistance with the help of some very idealized examples. We shall take this opportunity to lay the groundwork of merely geometrical or statistical nature for the more refined and more realistic treatment of glide resistance mechanism to be given in Chapter 5.

The simplest possible variation of the element glide resistance is a one-dimensional one. Imagine, for example, a long, straight Lomer–Cottrell lock with a glissile dislocation on a parallel plane trying to overcome it along its entire length; or a dislocation pinned along its entire length by a Cottrell cloud, from which it is trying to break loose. These are cases of *isolated linear barriers* (repulsive in the first case, attractive in the second). Even a *periodic* variation of the element resistance in one direction is a *linear barrier* at every position; examples are the periodic variation of the core energy of dislocations in the Peierls model, or the periodic variation of the elastic energy of dislocations, such as could occur in certain spinodally decomposed alloys or in a slip plane parallel to an array of straight parallel dislocations whose stress fields cause a periodic variation in the element glide resistance.

In all of these cases, the dislocation has an alternative to overcoming the barrier along its entire length: namely, to nucleate a "bulge" across the barrier, which may then expand along the barrier (and possibly forward). Nucleation would be necessary for this path, since the maximum stress for overcoming the barrier is not reduced; only alternative equilibrium configurations (unstable though they are) are introduced at lower stresses.

In these alternative paths, the length and shape of the dislocation is changed. This introduces *self stresses* which, according to our definitions, have to be added to the *element glide resistance* to obtain the *line glide resistance*. Thus, in the one alternative, the line resistance is identical to the element resistance, in the other it is essentially made up of the self stresses associated with the "bulge" configuration.

The *plane glide resistance* may be less than the line glide resistance, in some cases, by the formation of dynamic pile-ups. This possibility will be treated in an idealized model at the end of this section.

Isolated Linear Barriers

Figure 24-1 depicts three idealized cases of isolated linear barriers: (a) a *repulsive* barrier, in which the free energy of the dislocation shows a ridge; (b) an *attractive* barrier, in which the free energy shows a valley; and (c) an energy-storing barrier, in which the free energy shows a step. In all cases, there is an identical positive glide resistance: in our artificial example, a constant value $\hat{\tau}_{\text{ELEM}}$ over a distance δ (eq. [23b]). The cases differ in the negative portion of the glide resistance diagram, which is behind the barrier for case (a), in front for (b), and absent in case (c). Our analysis will show that, contrary to common belief, the properties of the attractive and repulsive barriers differ profoundly.

For a quantitative analysis that exhibits the principal features of the treatment, let us simplify the case of an attractive barrier even further and assume an energy valley of constant depth F_{BIND} and infinitely steep walls (Fig. 24-2a). A dislocation would then be in stable equilibrium at the bottom of the valley for all stresses. An alternative equilibrium configuration under a

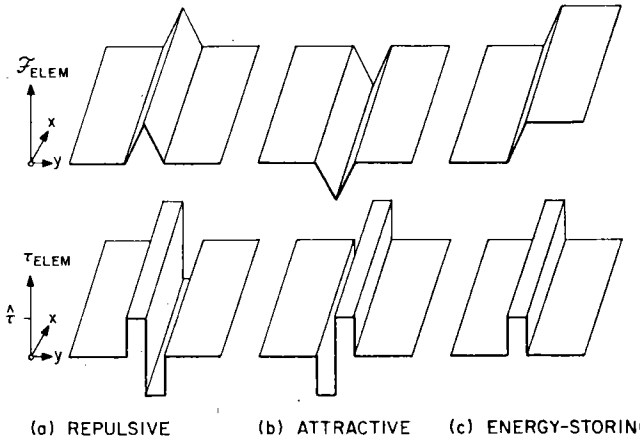

FIG. 24-1. Free energy per unit length $\mathcal{F}_{ELEM}$ and element glide resistance τ_{ELEM} as a function of forward displacement y, for three types of linear barriers: (a) repulsive, (b) attractive, (c) energy-storing.

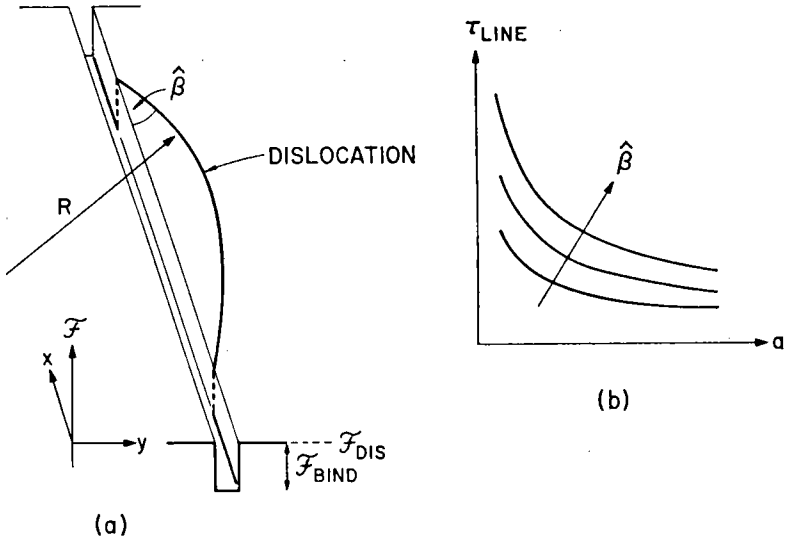

FIG. 24-2. (a) Dislocation in unstable equilibrium configuration along part of steep energy valley; (b) resulting diagram of line glide resistance τ_{LINE} vs. area a. (The element glide resistance is a δ-function.)

finite applied stress σ (although an unstable one) is also shown in Fig. 24-2a. In the "free" region ($\tau_{ELEM} = 0$), the dislocation assumes a shape so that its self stress τ_{SELF} balances the applied stress everywhere (eqs. [23c] and [23d]). For an isotropic line tension $\mathscr{E} = \mathscr{F}$ this is a circular arc of radius R given by (eqs. [23c], [23g])

$$\sigma = \tau_{\text{LINE}} = \tau_{\text{SELF}} = \frac{\mathscr{F}_{\text{DIS}}}{bR}. \qquad [24a]$$

The angle $\hat{\beta}$ between the "free" and the "bound" dislocation at the edge of the valley is given by the equilibrium between the two line tensions:

$$\mathscr{F}_{\text{DIS}} \cdot \cos\hat{\beta} = \mathscr{F}_{\text{DIS}} - \mathscr{F}_{\text{BIND}}. \qquad [24b]$$

(This condition was omitted in FISHER's treatment, 1955.) In most practical cases, the binding energy per unit length is small compared to the dislocation line energy. Then $\hat{\beta}$ is small and one may expand the cosine; eq. [24b] becomes

$$\hat{\beta} \doteq \sqrt{2\frac{\mathscr{F}_{\text{BIND}}}{\mathscr{F}_{\text{DIS}}}} \ll 1. \qquad [24b']$$

For the simple case discussed here, it is a material constant independent of stress.

The area under the circular arc is, for small angles $\hat{\beta}$,

$$a \doteq \tfrac{2}{3} R^2 \hat{\beta}^3. \qquad [24c]$$

With eqs. [24a] and [24b'], and setting $\mathscr{F}_{\text{DIS}} = \mu b^2/4$, this gives a line glide resistance diagram

$$\tau_{\text{LINE}} = \frac{1}{\sqrt{3}} \left(\frac{\mathscr{F}_{\text{BIND}}}{2\mathscr{F}_{\text{DIS}}}\right)^{3/4} \frac{\mu b}{\sqrt{a}} \qquad [24d]$$

which is plotted schematically in Fig. 24-2b.

It is useful for later applications to outline the procedure for more general free energy profiles. Without actually deriving the line glide resistance diagram, let us consider what differences there are between the triangular energy valley (Fig. 24-1b) and the square valley (Fig. 24-2a). The triangular valley has one important feature that makes it more realistic than the square valley: the dislocation can be pulled out of it mechanically at a finite stress, the maximum element glide resistance $\hat{\tau}_{\text{ELEM}}$. A second difference is that the gradual change in line energy, rather than the abrupt one, leads to a gradual "bend" in the dislocation (Fig. 24-3) rather than an abrupt kink (Fig. 24-2a).

The shape of the bulge can be treated quantitatively in a rather easy way on the line tension model. If κ is the local curvature and $d\xi$ an element of the dislocation line, we have

$$d\beta' = \kappa\, d\xi = \frac{b\tau_{\text{SELF}}}{\mathscr{E}} \frac{dy'}{\sin\beta'} \qquad [24e]$$

or

$$\int_0^{\beta} \mathscr{E} \sin\beta'\, d\beta' = \int_0^{y} (\tau_{\text{ELEM}} - \sigma)\, b\, dy'. \qquad [24e']$$

The integral over τ_{ELEM} is, by the definition [23b], the free energy change of the dislocation element. If we call $\Delta\mathscr{F}_{\text{DIS}}$ the positive difference from the

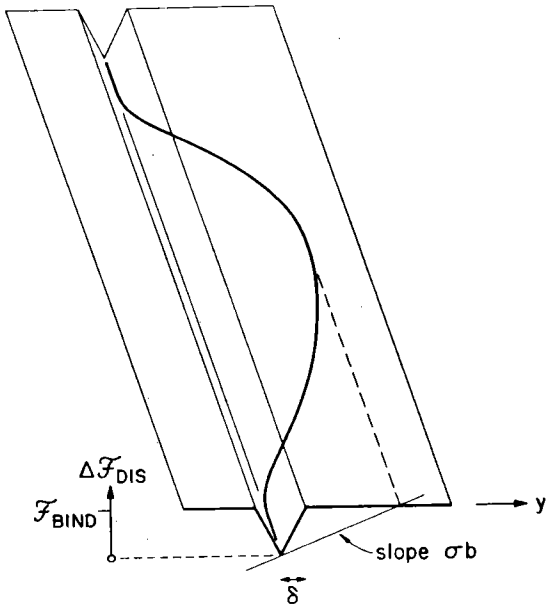

FIG. 24-3. "Triangular" valley of dislocation free energy, and an equilibrium "bulge" in the dislocation (consisting of three circular arcs), under an applied stress σ.

bound state at $y = 0$ (Fig. 24-3), integration of [24e'] for an angle-independent line tension* $\mathscr{E} = \mathscr{F}_{DIS}$ gives

$$1 - \cos\beta = \frac{\Delta\mathscr{F}_{DIS}(y) - \sigma by}{\mathscr{F}_{DIS}} \qquad [24f]$$

or, using an approximation for small angles β as before,

$$\boxed{\beta \doteq \sqrt{2\,\frac{\Delta\mathscr{F}_{DIS}(y) - \sigma by}{\mathscr{F}_{DIS}}}.} \qquad [24f']$$

This equation describes the inclination β of the dislocation as a function of its forward displacement y for any linear barrier described by $\Delta\mathscr{F}_{DIS}(y) \ll \mathscr{F}_{DIS}$. In particular, it shows that the maximum value $\hat{\beta}$, or *the inflection points of the bulge, occur where the difference between the free energy change and the work term is largest.* In our special example, this is at $y = \delta$, where

$$\beta = \sqrt{2\,\frac{\mathscr{F}_{BIND} - \sigma b\delta}{\mathscr{F}_{DIS}}} \qquad (\textit{triangular valley}). \qquad [24g]$$

Comparing this to eq. [24b'] for the square valley, we find that β now is stress

* Actually, one should use $\mathscr{E}_{EDGE}$ for a screw and $\mathscr{E}_{SCREW}$ for an edge, as can be shown by the method employed later (sec. 25) for discrete obstacles. To appreciate the importance of selecting the proper value, see Table 2–II.

dependent: at zero stress, the two cases are the same, but as the applied stress σ rises in the present case, the bulge moves back closer and closer to the edge of the plateau and more of the dislocation line "climbs up" the inclined ridges until at $\sigma = \hat{\tau}_{\text{ELEM}}$ the entire dislocation line lies parallel to the edge of the plateau.

The shape of the dislocation beyond the inflection points is identical in the two cases, since here $\tau_{\text{ELEM}} = 0$. (It is a circular arc in the constant line tension model.) On the slopes of the energy valley in the present case, we also have circular arcs (eq.[24e']), since τ_{ELEM} is here constant in this particular example. These circular arcs replace the sharp corners in the dislocation in the square valley (Fig. 24-2a).

One might then approximate the shape of the bulge by the single circular arc shown in Fig. 24-2a, using the expression [24g] instead of [24b'] for $\hat{\beta}$. Inserting this value into the expression [24c] for the area swept, and retaining eq. [24a] for the line glide resistance gives

$$\sqrt{a} = \frac{\mathcal{F}_{\text{DIS}}}{\tau_{\text{LINE}}\, b} \cdot \left(2 \cdot \frac{\mathcal{F}_{\text{BIND}} - \tau_{\text{LINE}}\, b\delta}{\mathcal{F}_{\text{DIS}}} \right)^{3/2} \cdot \sqrt{\frac{3}{2}} \qquad [24g']$$

Now, a becomes zero at a finite value of τ_{LINE}, namely $\hat{\tau}_{\text{LINE}} = \hat{\tau}_{\text{ELEM}}$.

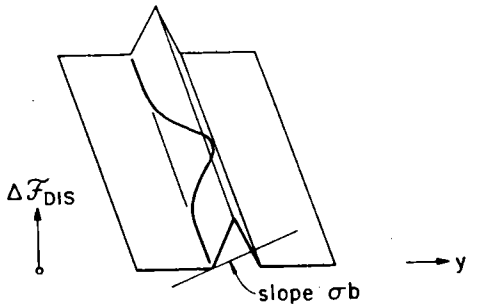

FIG. 24-4. Repulsive linear barrier with equilibrium bulge in dislocation under an applied stress σ.

Another important consequence of the general equation [24f] is the location of the turn-round point, or maximum excursion, of the bulge. It occurs where the total work done on a dislocation element precisely balances its free energy change. This is illustrated by a simple construction in Fig. 24-3. (It is independent of any assumptions on line tension, self stresses, or the smallness of β, see eq. [24e'].)

It is this observation that makes *repulsive* linear barriers profoundly different from the attractive ones discussed up to now. As may be easily seen in Fig. 24-4, the line of slope σb now always cuts the free energy diagram inside the barrier itself; thus, the maximum excursion of the bulge is the barrier width. In the attractive case, it can go far beyond, particularly at low stresses.

The *energy-storing barrier* (such as an antiphase-boundary, in which a ledge of finite additional energy is left behind if a dislocation crosses it) would show properties much like an attractive barrier. In fact, the attractive barrier *is* an energy-storing barrier from the "bound" state on forward. It is what happens *before* the dislocation reaches its initial state that makes an attractive barrier different from a repulsive one.

Periodic Linear Barriers

From the above discussion, it is evident that there is no difference at all between nucleation over repulsive isolated barriers and over periodic barriers: the equilibrium bulge never goes far enough to come into contact with the next ridge (Fig. 24-4). In sec. 51 we will treat various models of thermal activation over a Peierls barrier. One of these is, despite the atomic scale of the energy variations, based on a line tension approximation and is, therefore, exactly equivalent to the case under discussion here—and would also describe isolated repulsive barriers.

For small bulges in essentially straight dislocations, a double-kink model may be more appropriate than a continuous-bulge model. It turns out to give very similar answers (see sec. 51). In order to show some basic properties of kinks, let us here give a brief description of equilibrium configurations in a *periodic square valley* (Fig. 24-5).

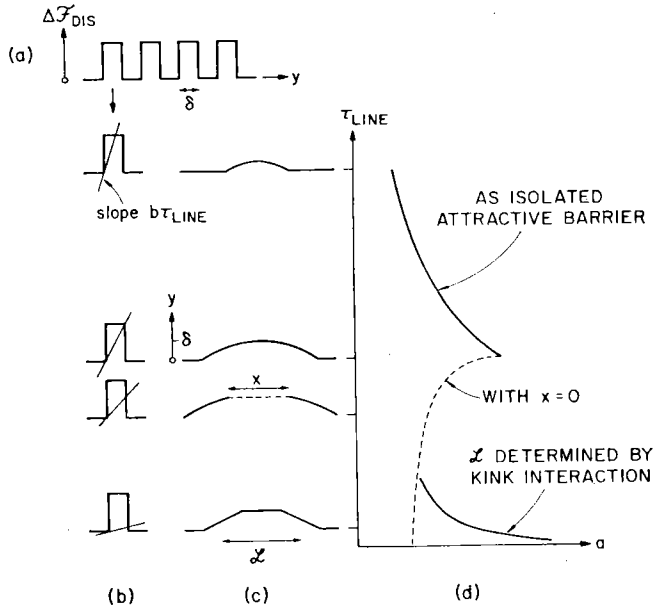

FIG. 24-5. Periodic square energy valley (a), at various stresses (b), with equilibrium dislocation configuration (c); plot of line glide resistance vs. area swept (d).

Firstly, we must observe that for high stresses this case is identical to that of an isolated attractive barrier: so long as the maximum excursion of the bulge has not reached the drop-off of the energy into the next valley. Below this critical stress, the arc that must exist on the "high plateau" in equilibrium with the stress is interrupted by the new valley. The position of the two arc pieces along the length of the ridge is now indeterminate: the extra free energy that the length of dislocation in the new valley has at finite stresses is precisely supplied by the external work done when the "kinks" are moved apart (eq. [24f], Fig. 24-5b). The line glide resistance diagram (Fig. 24-5d) shows as a dotted line in the area between the two kinks when this length x (Fig. 24-5c) is zero.

The indeterminacy is resolved by taking into account the elastic interaction between kinks. The known solution for sharp kinks should be approximately applicable when $x > 0$. For kinks in a screw dislocation, the interaction energy is (see, for example, HIRTH and LOTHE, 1968, p. 230)

$$F_{\text{KINKS}}^{\text{INT}} = \frac{\mu b^2 \delta^2}{8\pi \mathscr{L}} \cdot \frac{1+\nu}{1-\nu} \simeq \frac{\mu b^2 \delta^2}{4\pi \mathscr{L}} \qquad [24h]$$

where $\mathscr{L}$ is the average spacing of the kinks, i.e. the distance x plus the kink width w. This gives a glide resistance diagram

$$\tau_{\text{LINE}} = \tau_{\text{KINKS}}^{\text{INT}} = \frac{\mu b \delta^3}{4\pi a^2} \qquad [24h']$$

which is also plotted in Fig. 24-5d. It should be important at very low stresses, but loses its significance where the average kink spacing $\mathscr{L} = a/\delta$ becomes equal to the kink width.* This occurs at the stress where the "kink interaction" curve in Fig. 24-5d cuts the dotted line for $x = 0$.

The intermediate range of stresses cannot be treated adequately by either one of the simple models: the bulge is neither a circular arc, nor does it consist of well-separated kinks. It seems nevertheless likely, or at least possible, that the qualitative feature of the composite diagram in Fig. 24-5d is retained and the area goes through a minimum at intermediate stresses.

The Plane Glide Resistance (Dynamic Pile-ups)

The isolated linear barriers discussed above are an extreme case of a non-uniform element glide resistance: τ_{ELEM} is zero almost everywhere and has high positive (and negative) values in some isolated places. In a real crystal the resistance between the barriers would be finite, but it might be negligible. In the case of a periodic variation of the element resistance on a macroscopic scale, for example due to internal stresses, the amplitude would vary from place to place, as sketched in Fig. 24-6a, and this can have profound effects. Moreover, the peaks in the *line* glide resistance are fairly isolated even when the element resistance is periodic because of the diminishing influence of the self stresses past nucleation.

Let us idealize a crystal with a heterogeneous distribution of line glide resistances (Fig. 24-6a) by the diagram shown in Fig. 24-6b: the regions with small amplitude are smoothed out into a friction stress τ_1, but there are

* The kink width w assumed in the above comparison follows directly from the kink height δ and the angle β given in eq. [24b']; for $\mathscr{F}_{\text{BIND}}/\mathscr{F}_{\text{DIS}} \simeq 10^{-2}$, $w \simeq 7\delta$.

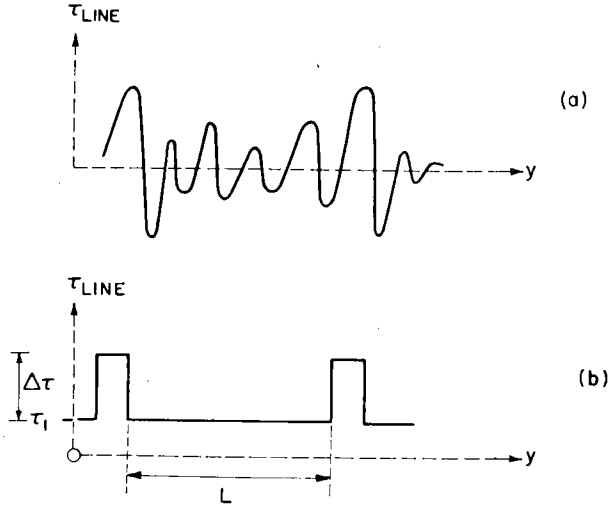

FIG. 24-6. Heterogeneous distribution of line glide resistances and their description in an idealized diagram.

isolated regions of an extra contribution $\Delta\tau$ to the line glide resistance, L apart. It is immaterial for the following whether the barriers are repulsive, attractive, or of the energy-storing kind.

Dislocations can now move in the "weak" regions at stresses, at which they will still be held up at the "strong" barriers. They will then exert back stresses on subsequent dislocations in the weak regions, but these may nevertheless move before the first dislocation can overcome a strong obstacle, provided the resistance heterogeneity $\Delta\tau$ is large enough. In this way, a pile-up is formed—although, with realistic glide resistance variations such as in Fig. 24-6a, the dislocation spacings in it may be far from those in an ideal pile-up, and although the pile-up may, in real crystals, be blunted by spread of slip into parallel planes.

The process ends at steady state when, for each dislocation that is added to the group at the rear, one leaves at the head. When this happens at all strong barriers in the slip plane, slip over the entire plane can occur. This will take place at a stress lower than $\tau_1 + \Delta\tau$ because of the stress concentration at the head of a pile-up.

From a macroscopic point of view, the dislocation joining the pile-up is indistinguishable from that leaving it: a "relay race" of many successive dislocations is like a straight-through race of a single one. The dislocations in the pile-up may, then, be viewed as a dynamic part of the obstacle structure resisting a single dislocation: their stresses serve to smooth out the heterogeneities of the glide resistance (KUHLMANN, 1951; BASINSKI, 1959).

A quantitative calculation of the slip resistance leads to the Hall–Petch relation (PETCH, 1958).

$$\tau_{\text{PLANE}} = \tau_1 + k_P L^{-\frac{1}{2}}. \qquad [24i]$$

The constant k_P will be derived for an ideal pile-up in the following, since it will be needed further on.

At an applied stress $\sigma = \tau_{\text{PLANE}}$, one dislocation can penetrate the "strong" barrier, moving forward by a distance δy_n. Let all other $(n-1)$ dislocations i move forward by δy_i into their new equilibrium positions. Equating the total work done with the total increase in free energy, both per unit length, gives (COTTRELL, 1953)

$$\sum_1^n b\,\sigma\,\delta y_i = \sum_1^n b\,\tau_1\,\delta y_i + b\,\Delta\tau\,\delta y_n. \qquad [24j]$$

If all δy_i were equal to δy_n, we would immediately have

$$\tau_{\text{PLANE}} = \tau_1 + \frac{\Delta\tau}{n}. \qquad [24k]$$

This is obviously true when $n = 1$; for larger n, and depending on the exact geometry, the second term must be multiplied by a constant such as $\pi/4$ for a double-headed, large, linear pile-up (ESHELBY *et al.*, 1951; LEIBFRIED, 1951). Equation [24k] shows the paramount feature of dynamic pile-ups: they smooth out the variation in glide resistance.

The steady-state number n is obtained by setting

$$\tau_{\text{PLANE}} = \sigma = \tau_1 + \tau_{\text{BACK}}(n) \qquad (\textit{steady state}) \qquad [24\ell]$$

where, again within a geometric multiplier of order 1,

$$\tau_{\text{BACK}}(n) = n\frac{\mu b}{L}. \qquad [24m]$$

Elimination of n gives

$$\boxed{\tau_{\text{PLANE}} = \tau_1 + \sqrt{\Delta\tau \cdot \tau_{\text{BACK}}(1)}} \qquad [24n]$$

or

$$k_P \simeq \sqrt{\mu b \Delta\tau}. \qquad [24o]$$

Equations [24n] and [24i] hold under the important proviso that $n > 1$ or

$$\Delta\tau \geqslant \tau_{\text{BACK}}(1) \simeq \frac{\mu b}{L}. \qquad [24p]$$

At and below this value, the maximum plane resistance (eq. [24n]) is equal to the maximum line resistance.

An important special application of eq. [24n] is that of dislocations moving through a field of parallel static pile-ups. Suppose these to be idealized as an array of super-dislocations of strength mb and spacing L, which we model as internal stress peaks after the manner of Fig. 24-6b. Then

$$\tau_1 = 0; \quad \Delta\tau = m\frac{\mu b}{L}. \qquad [24q]$$

The plane resistance is

$$\tau_{\text{PLANE}} = \sqrt{m}\,\frac{\mu b}{L} = \mu b \sqrt{\rho} \qquad [24r]$$

where $\rho^{-1/2}$ is the volume density of *all* dislocations. In other words, *the glide resistance does not depend on how a given number of dislocations is arranged*: if they form groups, then so do the mobile dislocations, and the effect cancels completely.

The idealization of an array of static pile-ups as a box-like internal stress pattern (Fig. 24-6b) is, of course, an over-simplification. In reality, the centers of internal stress (the pile-ups) are diffuse, and lead to an internal stress which, while it varies with position, is smoother than that assumed above. The net results must be a glide resistance which lies between the lower limit ($\mu b \rho^{\frac{1}{2}}$) calculated above by permitting dynamic pile-ups and the upper limit [$\mu b (m\rho)^{\frac{1}{2}}$] obtained if the mobile dislocations move singly.

Kink Motion

We have considered the stress necessary to *nucleate* a loop or a pair of kinks. There may also be a resistance to kink *motion*. This may be in the form of internal stresses, of a lattice resistance, or of isolated barriers like solute atoms or vacancies. Since kink motion is by its nature one-dimensional, the kink resistance diagrams (τ_{KINK} vs. x) for these three cases are identical in form to the τ_{ELEM} vs. y diagrams we have used to describe the various kinds of linear barrier to the motion of dislocations (Figs. 24-1, 24-5a).

Alternate paths of lower resistance are here not available. The possibility of lowering the critical stress for long-range motion by the formation of dynamic pile-ups, however, does exist in the case of isolated barriers or of not-strictly-periodic internal stresses. When there is a number of kinks in a kink pile-up, their *back* stresses are merely another way of describing the *self* stresses of the dislocation line in which they lie. Thus, appropriately enough, the transition from τ_{LINE} to τ_{PLANE} in the case of dislocations corresponds to the transition from τ_{ELEM} to τ_{LINE} in the case of kinks.

25. Discrete Obstacles

Linear barriers were a *one*-dimensional idealization of the general element glide resistance diagram. The two prime parameters were the *height* and the *spacing* of the energy "ridges" or "valleys" on the glide plane. A third parameter, important for a calculation of the plane glide resistance, was the *dispersion* of the heights. Finally, for applications in thermal activation, one will have to know the *profile* of the typical barrier. In a mathematical model, one may say that linear barriers correspond to a one-dimensional Fourier analysis of the element resistance, of which the amplitude and wavelength of the first term are the two most essential parameters.

Similarly, *discrete obstacles* are a *two*-dimensional idealization of the general element glide resistance. They describe obstacles to slip whose dimensions are limited in both directions in the slip plane (although not necessarily perpendi-

cular to it). Particles and voids, precipitates and possibly individual (interstitial) solute atoms are discrete obstacles; so are dislocation loops that cut the slip plane and even those that do not, by virtue of their stress fields. The limits of the obstacle do not have to be sharp, they merely must be sharp enough for it to be treated as an individual: the element resistance profiles of neighboring obstacles should not overlap. In the present idealization, we will treat them as sharp, although generally of finite extent.

The two prime parameters of a discrete obstacle structure are the *height* and the *spacing* of the energy "hillocks" (or "wells") on the glide plane. A third parameter, important for a calculation of the plane glide resistance is their *dispersion*: in this case, a dispersion of the *spacings*, through an aperiodic arrangement of the obstacles in the slip plane, is as important as a dispersion in the height. Again, one may think of this idealization as a two-dimensional (though usually isotropic) Fourier analysis of the element glide resistance diagram, with the amplitude and wavelength of the first term being of prime interest.

Self stresses, in the case of linear barriers, were nonexistent along one path (the movement of straight dislocations), all-important along the other (nucleation of a double kink or a loop). In the case of discrete obstacles, self stresses are due to the bowing of dislocations between the obstacles and are always present. However, their effect averages out to zero for some of the macroscopic properties.

The Element Glide Resistance and the Resisting Force

Consider the simplest sort of discrete obstacle: one with a width w small compared to its spacing l_e (center-to-center distance) from the next obstacle, and independent of y (Fig. 25-1). Any element of dislocation between two obstacles experiences no resistance to its motion, since the obstacles are discrete and exert no influences outside their width w. But an element of width w at an obstacle experiences a *resisting force* to its motion in the y direction, due to a change in the (Helmholtz) free energy F of the crystal:

$$K \equiv \frac{\delta F}{\delta y} = \int_0^w \tau_{\text{ELEM}}\, b\, dx \equiv \bar{\tau}_{\text{ELEM}}\, bw. \qquad [25a]$$

This resisting force can have one of three general forms. First (Fig. 25-2a), free energy may be *stored* when the obstacle is cut, leading to an element resistance that is positive everywhere. Examples of such energy storing obstacles are the formation of a slip step at the surface of a precipitate; the creation of an anti-phase boundary in an ordered precipitate, or the creation of a jog in a forest dislocation. Second, the free energy may rise and fall again as the obstacle is cut (Fig. 25-2b). Examples of such *energy hills*, or *repulsive*

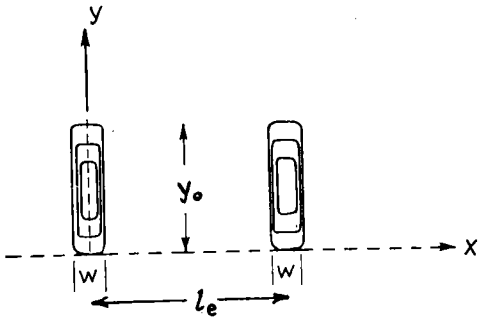

FIG. 25-1. Schematic element glide resistance contours of a pair of discrete obstacles.

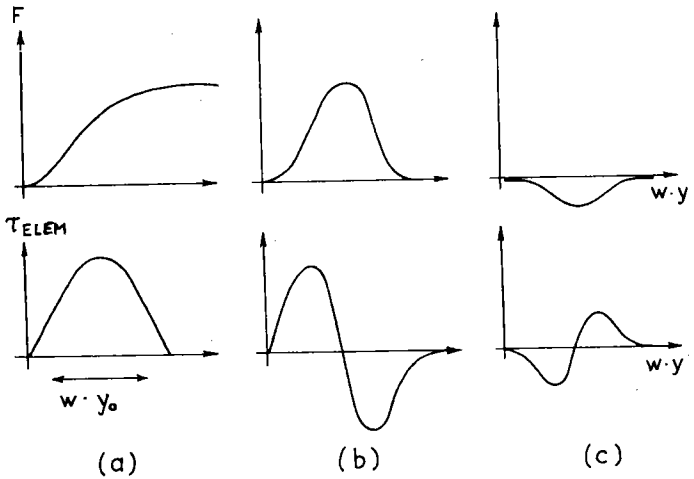

FIG. 25-2. Schematic free energy and glide resistance diagrams for (a) energy storing obstacle, (b) repulsive obstacle, (c) attractive obstacle.

obstacles, are coherent particles of larger shear modulus, or in which the stacking fault energy is larger than in the matrix; or any constrictions that may have to be temporarily formed in forest or mobile dislocations while they cross. Finally, the energy may first fall, then rise again (Fig. 25-2c). Examples of such *energy valleys*, or *attractive obstacles* are voids; coherent particles with lower shear modulus; or "attractive trees", i.e. forest dislocations that react with the mobile dislocation. Stress fields from misfitting particles, from dislocation loops, etc., act equally often as attractive and as repulsive obstacles.

To obtain some order-of-magnitude estimates, let us say the obstacle is of an average depth y_o and set

[25.1-]

For many obstacles—for instance, forest dislocations, loops, voids, internal stress peaks—τ_{ELEM} cannot exceed the theoretical shear strength of about $\mu/30$. Then an obstacle of atomic dimensions ($w \simeq y_o \simeq b$) cannot have an interaction energy F_o of more than $\mu b^3/30$, or a few tenths of an electron volt. If such obstacles exhibit interaction energies of order μb^3—a few eV—then they must be at least $5b$ wide and deep.

Certain solute atoms could behave differently. If the solute atom forms a strong, localized bond with its host (as carbon or nitrogen in iron may, for instance), then the bond must be broken and reformed as the dislocation moves. This energy of bond breaking could be as large as the activation energy for diffusion—about 1 eV for the atomic-sized obstacles (C and N) quoted above.

The Line Glide Resistance and the Force on the Obstacle

The line glide resistance was defined (eq. [23c]) to be the sum of the element resistance and the self stress; in equilibrium, it must equal the applied stress σ everywhere along the dislocation (eq. [23d]). To make this possible, the self stress must vary between two extreme limits in the presence of discrete obstacles: *near* the obstacles, it must counterbalance the high element resistance (minus the comparatively low applied stress), by developing a strong, concave-forward curvature; *between* the obstacles, the element resistance is zero and the self stress must balance the applied stress only, by developing a gradual, concave-backward curvature.

In one particularly simple case, we have seen (eq. [23q]) that a certain *average* of the self stresses must vanish despite these severe variations: namely, the forward component averaged over a quasi-straight piece of dislocation moving forward as a rigid body. Then, the average element resistance equals the average line resistance (eq. [23r]) which in turn, in equilibrium, equals the applied stress (eq. [23d]). Applying this to a piece of dislocation held up at two identical obstacles for motions perpendicular to their connecting line (Fig. 25-1) gives

$$\tau_{LINE}\, b l_e = K \qquad [25c]$$

since the element resistance is assumed zero outside the region w. Equation [25c] is a frequently used relation; it applies only under the rather severe conditions imposed above, and some other very special cases to be discussed below. In these cases, we find from eq. [25a]

$$\tau_{LINE} = \frac{w}{l_e}\,\bar{\tau}_{ELEM}. \qquad [25d]$$

In words, for discrete obstacles, *the line resistance is reduced from the element resistance by the ratio of width over spacing*.

Equation [25c] looks exactly the same as one that would have been derived for a rigid, *straight* dislocation: the ~~right~~-hand side is the total force exerted on it, the ~~left~~-hand side is the total resistance it experiences. Any effect of the bowing appears to have vanished. However, unless the obstacle has as ideal a shape as that illustrated

H left
H right

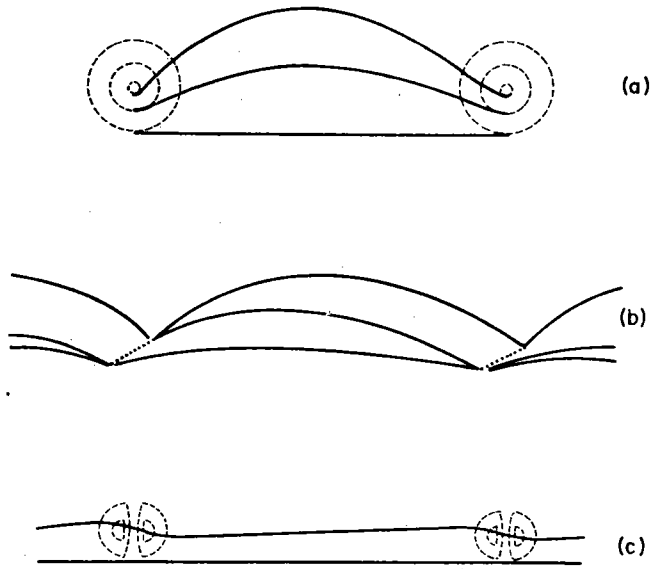

FIG. 25-3. The bowing of the dislocation determines the regions of the obstacle that are being sampled at any one stage.

in Fig. 25-1, the bowing does have an influence on the value of the resisting force K in different successive equilibrium positions: the shape of the dislocation determines the regions of the obstacle that are being sampled. Figure 25-3a shows this for circular obstacles, Fig. 25-3b for ribbon-like obstacles oriented skew to the x-direction. (Here, the force *in* the ribbon, which is physically prescribed, is *not* equal to K, KOCKS, 1968.) Finally, Fig. 25-3c shows the case of an element resistance that is due to a self-equilibrated stress field (such as that experienced by a screw dislocation near a misfitting particle, GLEITER, 1967). Here, the effect of the bowing is especially drastic, since the net force on a *straight* dislocation of the same average orientation would be always zero.

Another consequence of an arbitrary obstacle shape is that the distance δy of forward movement is then not as easily defined as for the idealized obstacle shown in Fig. 25-1. Yet it would be a useful quantity to complement the force K resisting forward motion. We choose a definition so that

$$\delta F = K\delta y = \tau_{\text{LINE}}\, b\delta a. \qquad [25e]$$

In most cases of practical interest, the dislocation will not overcome a series of obstacles simultaneously, as it would have to if the forward displacement were *constant* along the dislocation as we have assumed above. Instead, it will tend to overcome one obstacle at a time. This should be so for two reasons: first, thermal activation does not take place simultaneously at many obstacles even when they are stressed identically, as in Figs. 25-1 and 25-4a; second, in realistic cases, the obstacles are not in identical positions with respect to the dislocation: they are neither collinear nor equidistant (Fig. 25-4b). In this case, self stresses contribute in an important way to the force on the center

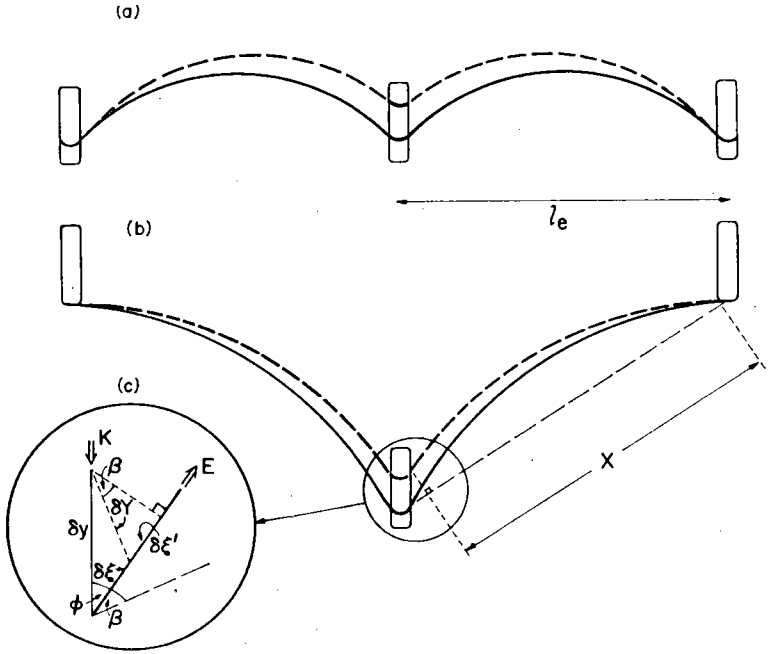

FIG. 25-4. When discrete obstacles are collinear and equidistant (a), the self stresses average out to zero; but in the more normal case (b), self stresses contribute significantly to the force on the obstacle. The insert (c) is used in the derivation of the line tension construction.

obstacle: the dislocation is getting shorter as it moves forward. Then, the simple relation [25c] is no longer true; putting it another way, the force σbX no longer points in the "forward" direction, to balance the "back" force K.

Figure 25-4a illustrates that, for the special case of a *periodic* distribution of discrete obstacles, which are small in extent compared to their spacing, eq. [25c] still holds. This is the geometry so frequently assumed.

For the more general geometry shown in Fig. 25-4b, a similarly simple relation can, however, be obtained, if one assumes the line tension approximation, and lumps together the effect of the self stress with that of the applied stress to make a *force on the obstacle* (KOCKS, 1968). For this purpose, we write the local free energy balance (including work terms) as follows:

$$(K - \sigma bw)\,\delta y = E \cdot 2\delta\xi + \sigma bX\,\delta Y. \qquad [25f]$$

With the symbols as they are defined in Fig. 25-4c, we see that the first term on the right is the change in line energy* of the free dislocation branches on either side of the obstacle, and the second term is the work done by the external forces as the free dislocation branches move. The branches are assumed pivoted at the two next obstacles on either side.

The simplification comes about when one replaces, in the same line tension approximation, the term σbX by $2E \sin\beta$, where β is the bow-out angle, and

*E is an effective line tension defined in eq. (25n).

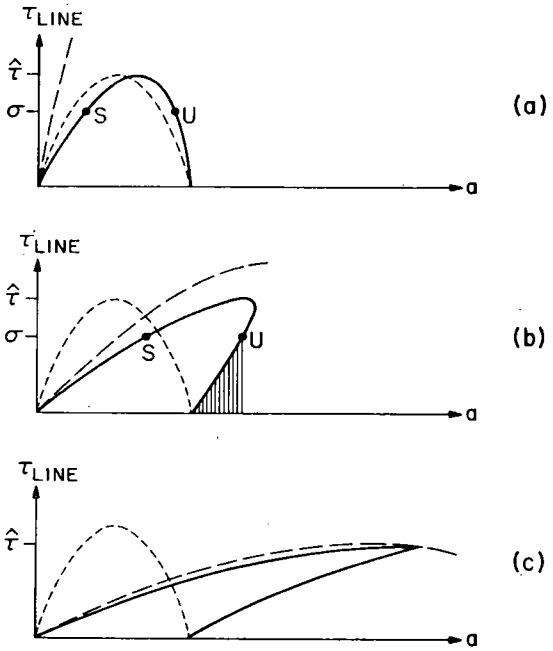

FIG. 25-5. Line glide resistance versus area swept: by forward translation through the obstacle (- - - -), by bowing between the obstacles (— —), and by both processes combined (——), for increasing obstacle spacing (a, b, c). In (c), the obstacle is bypassed rather than cut.

realizes that $\sin\beta\, \delta Y = \delta\xi'$. Then, the entire right-hand side becomes a single term equivalent to the "line tension construction":

$$(K - \sigma bw)\, \delta y = 2E \cos\phi \cdot \delta y \qquad (\textit{line tension approx.}) \qquad [25g]$$

or, when the width of the obstacles is negligible compared to their spacing:

$$\boxed{K \doteq 2\, E \cos\phi} \qquad (w \ll l_e). \qquad [25g']$$

This equation expresses *equilibrium* between the obstacle *resistance* K and the *force* on the obstacle $2E \cos\phi$.

Let us now plot the line resistance for one dislocation segment as a function of the area swept out between two obstacles. This area has two additive components: one due to the change in bow-out between obstacles, and one due to the proportional forward translation of the entire segment, l_e long, due to the compliance of the center obstacle, for example according to the element glide resistance diagrams shown in Fig. 25-2a. Figure 25-5 shows three cases: (a) when the contribution from bowing is smaller than the obstacle compliance; (b) when it is larger; and (c) when dislocation bowing dominates the compliance. The situation (c) must arise whenever the obstacle

spacing is large, since the bowing compliance is proportional to the third power of the obstacle spacing: geometric analysis of a circular arc for small bow-out angles shows, with eq. [23j], that initially

$$a_{\text{BOW}} \doteq \frac{1}{12} \cdot \frac{\sigma b}{\mathscr{E}} \cdot (l_e - w)^3. \qquad [25h]$$

As illustrated in these figures, the effect of the bowing is that the element glide resistance diagram (Fig. 25-2a) is sheared parallel to the area axis. Thus the *width* of the profile at any stress level is not affected; this is the most important parameter for thermal activation. However, the severe slant displayed in Fig. 25-5b is significant for two reasons. On the left side, where the dislocation comes from, it gives the actual spring constant felt by the dislocation in front of the obstacle, which controls its vibrational frequencies and influences whether these vibrations are overdamped or not. On the right side, it shows how the energy stored in the bowed-out dislocation gets dissipated immediately (shaded area), when the segment is released at the unstable point at the obstacle.

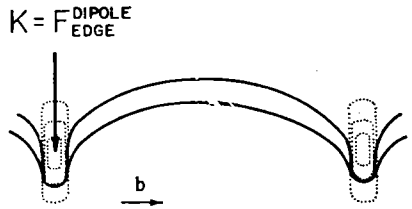

FIG. 25-6. The limiting effective strength of an obstacle is given by the free energy per unit length to draw out a dipole.

Finally, Fig. 25-5c shows a case where the bowing compliance is so large that the dislocation segment becomes unstable by "Orowan looping" (OROWAN, 1948) before the elements in front of the obstacle have moved to the point of maximum resisting force. Then the obstacle will never get *penetrated*, it will get *surrounded*. (In principle, a dislocation loop will then be left around the obstacle, which tends to shrink under the applied stress and its own high self stresses, and may thus eventually shear the obstacle.)

To derive this limiting effective strength of any obstacle, it is important to remember that the dislocation segment in front of the two obstacles considered cannot be isolated, but must be connected to other elements of dislocation line. They will tend to bow around the far sides of both obstacles (Fig. 25-6). An unstable dislocation shape is reached, when the two dislocation branches surrounding a single obstacle form a dipole, which may be extended by a rigid forward movement of the segments between the obstacles. The limiting effective resistance force of any obstacle is, therefore, the energy to draw out the respective dipole (ASHBY, 1966):

$$\left(1 - \frac{w}{l_e}\right) K_{\text{EDGE}} \leqslant \mathscr{F}_{\text{SCREW-DIPOLE}} = \frac{\mu b^2}{2\pi} \ln \frac{w}{r_o},$$
$$\left(1 - \frac{w}{l_e}\right) K_{\text{SCREW}} \leqslant \mathscr{F}_{\text{EDGE-DIPOLE}} = \frac{\mu b^2}{2\pi(1-\nu)} \ln \frac{w}{r_o}. \qquad [25i]$$

This limit is always lower than that to make an isolated half-loop, since the latter would involve the particle *spacing* as an outer cut-off radius in the logarithm, not the particle *diameter*.

The Effective Line Tension

We have seen that, during the virtual variation which corresponds to the overcoming of one discrete obstacle by a dislocation segment, the bowing of the free parts of the dislocation only played the role of the relaxation of another internal parameter to equilibrium; it had an influence only on such secondary problems as precisely which average of the element glide resistance is measured through the resisting force K.

There are other applications in which it is essential to have some knowledge of the shape of the dislocation between the obstacles. The most prominent one is the case where the crystal contains more than one pair of obstacles and more than one segment of dislocation line. One must then know, before one treats a particular obstacle pair, whether the dislocation segment between them encounters *another* obstacle while it bows out to equilibrate its self stresses, or whether it encounters (and possibly annihilates with) *another* segment of dislocation, such as the one on the far side of either obstacle along the same dislocation. The answer to the first question depends primarily on the *area* swept by the segment during bowing, that to the second question is determined by the *angle* the dislocation makes with its average direction, at the inflection point near the obstacle. Both of these parameters depend on the *effective line tension of the dislocation*

In the free regions between the obstacles, self stresses are the only contribution to the line glide resistance and, in equilibrium, this must be constant and equal to the applied stress:

$$\tau_{\text{SELF}}^{\text{free}} = \tau_{\text{LINE}} = \sigma \qquad (\textit{equilibrium}). \qquad [25j]$$

In the general case, in which the self stresses depend on the shape of the entire dislocation line, eq. [25j] determines this shape; more specific statements can only be made by detailed, usually numerical, calculations.

When the self stress depends only on the *local* shape (namely, the curvature κ), eq. [23j] provides a differential equation for the dislocation line (Fig. 25-7):

$$\mathscr{E}(\alpha) \frac{d\psi'}{d\xi} = b\tau_{\text{LINE}} \qquad (\textit{line tension approximation}) \qquad [25k]$$

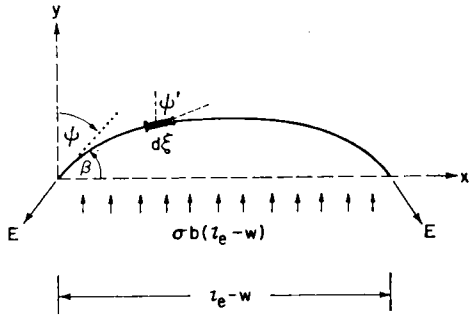

FIG. 25-7. Balance between the effective line tension E of a dislocation arc and the force exerted on it by an applied stress σ.

With

$$\kappa \equiv \frac{d\psi'}{d\xi} = \sin\psi' \frac{d\psi'}{dx} \qquad [25\ell]$$

and the equilibrium condition [25j], it can be integrated over the average direction x of the dislocation line (assuming that $\mathscr{E}$ is an even function of ψ'):

$$\int_{\psi}^{\pi-\psi} \mathscr{E}_{\bar{\alpha}}(\psi') \sin\psi' \, d\psi' = \sigma b(l_e - w) \qquad (\textit{equilibrium}). \qquad [25m]$$

Here, ψ' is the angle between the dislocation element and the y-axis (Fig. 25-7), and the dependence of the line tension $\mathscr{E}$ on the angle α between line element and Burgers vector has been replaced by a dependence on ψ' and on the character of the dislocation before it started bowing, which is defined by the average angle $\bar{\alpha}$ ($\bar{\alpha} = 0$: screw, $\bar{\alpha} = \pi/2$: edge).

The unknown in eq. [25m] is the integration limit, ψ, the complement of the bow-out angle. For convenience, let us define an *effective line tension*

$$\mathscr{E}_{\bar{\alpha}}(\psi) \equiv \frac{\int_{\psi}^{\pi-\psi} \mathscr{E}_{\bar{\alpha}}(\psi') \sin\psi' \, d\psi'}{\int_{\psi}^{\pi-\psi} \sin\psi' \, d\psi'} \qquad [25n]$$

which is defined such that eq. [25m] becomes

$$\boxed{2E\cos\psi = \sigma b(l_e - w)} \qquad (\textit{line tension approximation}). \qquad [25o]$$

Figure 25-7 illustrates this equation in terms of the "line tension construction".

For a collinear array of obstacles, or any quasi-straight dislocation piece, where the complement of the bow-out angle, ψ, equals the half cusp angle ϕ,

we regain (eqs. [25g], [25o])

$$K = 2E\cos\phi + \sigma bw = \sigma bl_e \qquad \textit{(line tension approximation, quasi-straight dislocation).} \qquad [25p]$$

It can now be seen that the same procedure (eq. [25m]) could have been used on the length of dislocation around the obstacle, which would have yielded the first equation [25p] with a similar definition [25n] of the (local) effective line tension.

The *effective* line tension E introduced in eq. [25n] is equal to the line tension and to the line energy, if these are orientation independent:

$$E = \mathscr{E} = \mathscr{F}_{\text{DIS}} \simeq \frac{\mu b^2}{2} \qquad \textit{(constant line energy approximation).} \qquad [25q]$$

In the more general case that the orientation dependence of the line energy is given by isotropic elasticity theory, the extreme values of the effective line tension, namely those applicable to a dislocation that starts out either as a pure screw or as a pure edge, can be derived from eqs. [23k], [23m], and [23n] to be (Fig. 25-8):

$$E_{\text{SCREW}} = \mathscr{F}_{\text{SCREW}}\left\{\frac{1+\nu}{1-\nu}\sin^2\phi + \frac{1}{1-\nu}\cos^2\phi\right\},$$

$$E_{\text{EDGE}} = \mathscr{F}_{\text{SCREW}}\left\{\frac{1-2\nu}{1-\nu}\sin^2\phi + \cos^2\phi\right\},$$

or, equivalently,

$$\boxed{\begin{aligned} E_{\text{SCREW}} &= \mathscr{E}_{\text{SCREW}}\sin^2\phi + \mathscr{F}_{\text{EDGE}}\cos^2\phi \\ E_{\text{EDGE}} &= \mathscr{E}_{\text{EDGE}}\sin^2\phi + \mathscr{F}_{\text{SCREW}}\cos^2\phi \end{aligned}} \qquad \textit{(isotropic elasticity).} \qquad [25r]$$

The latter form of these equations conveys directly that, for small bow-outs (large ϕ), the effective line tension is equal to the line *tension* of the *original* dislocation, for large bow-outs it is equal to the line *energy* of the *side* branches. For this reason, we prefer eqs. [25r] to the otherwise equivalent treatment employing both line *tensions* and line *torques* (see, for example, BROWN and HAM, 1971).

Equation [25o] was derived (using the definition [25n]) without any reference to a particular line shape such as a circle. In fact, it was specifically assumed that the curvature everywhere adjusts itself to the local value of the line tension, such that the product be constant. With the assumptions of isotropic elasticity theory, the shape of the dislocation segment will then approximately be an arc of an ellipse. Let us now, in an approximation that turns out to be very good, describe the shape by a *circular* arc, spanning the same obstacle distance and *starting with the same angle* ϕ as the true shape does. The radius R of that circle is then, by geometry and

$$R = \frac{l_e - w}{2\cos\phi} = \frac{E}{\sigma b} \qquad [25s]$$

with the same effective line tension E, defined in eq. [25n]. The area swept follows immediately as

$$a_{\text{BOW}}(\sigma,\phi) = \left(\frac{E}{\sigma b}\right)^2 \left\{\frac{\pi}{2} - \phi - \sin\phi\cos\phi\right\}. \qquad [25t]$$

Expansion of this formula for small bow-outs ($\phi \simeq \pi/2$) gives

$$a_{\text{BOW}}(R,\phi) \doteq \tfrac{2}{3} R^2 \left(\frac{\pi}{2} - \phi\right)^3 \qquad [25u]$$

which led to eq. [25h].

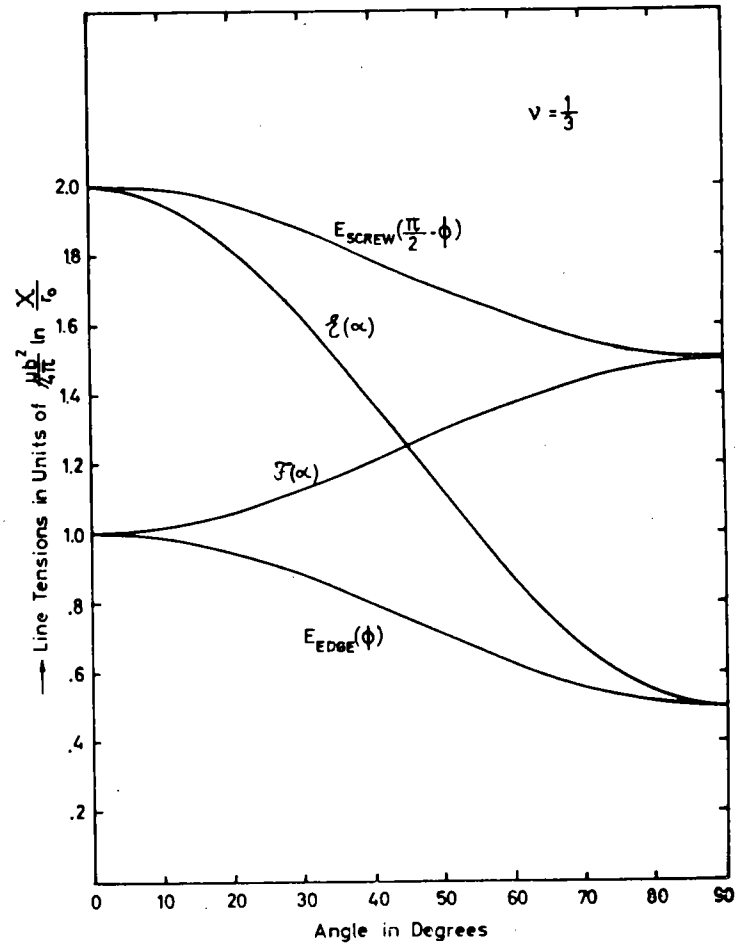

FIG. 25-8. The dependence of line energy $\mathscr{F}$ and line tension $\mathscr{E}$ on the angle α between line direction and Burgers vector and of the effective line tension E for an initial screw and an initial edge dislocation on the bow-out angle $(\pi/2-\phi)$. Isotropic elasticity theory.

The *orientation* dependence of the effective line tension having been fully discussed, the question remains, which *outer cut-off radius* X should be inserted into the logarithmic term in the line energy, eq. [23h], which enters E (eq. [25r]), to account for interactions of different parts of the same dislocation with each other.

In the case of Orowan by-passing, we have seen (eq. [25i]) that the interaction of the two branches of the dislocation on either side of each obstacle is all-important. On the other hand, the bowed-out dislocation between the obstacles may not be much affected by this dipole interaction. The computer calculation of equilibrium dislocation shapes by BACON *et al.* (1973), which is based on a self-stress model rather than on a line tension approximation, does in fact show that the major portion of the bowed-out dislocation between the obstacles is well described by a line tension with an outer cut-off radius $X = l$. (More exactly, $X = l_e - w$, which is here approximated by the average inter-obstacle spacing l to be introduced in eq. [25aa].)

Combining eqs. [23h], [23i], [23n], and [25p] and [25r], we obtain the final relation, in isotropic elasticity theory, between the strength K of an obstacle and the cosine of the breaking angle

$$f \equiv \cos \phi \qquad [25v]$$

as follows:

$$\boxed{\begin{aligned} K_{\text{SCREW}} &= f \cdot \frac{\mu b^2}{1-\nu} \cdot \frac{\ln l/r_o}{2\pi} \cdot (1 + \nu - \nu f^2) \cdot \frac{1}{1 - w/l_e}, \\ K_{\text{EDGE}} &= f \cdot \frac{\mu b^2}{1-\nu} \cdot \frac{\ln l/r_o}{2\pi} \cdot (1 - 2\nu + \nu f^2) \cdot \frac{1}{1 - w/l_e}. \end{aligned}} \qquad [25w]$$

We shall often use f as a measure of the obstacle strength. When orientation effects can be neglected, and when the width of the obstacles is small compared to their spacing, we have simply

$$f \simeq \frac{K}{2E}. \qquad [25w']$$

The quantity f is a geometric parameter that can be obtained from macroscopic measurements and an appropriate statistical theory. When l_e is known, we have from eqs. [25o] and [25q]:

$$\sigma \simeq f \cdot \frac{\mu b}{l_e - w} \qquad [25x]$$

The possibility of Orowan looping limits the possible values of f, by virtue of eqs. [25i], [25p], and [25v] to

$$f \leqslant \frac{\mathscr{F}_{\text{DIPOLE}}}{2E} \propto \frac{\ln (w/r_o)}{\ln (l/r_o)}. \qquad [25y]$$

The somewhat artificial representation of the equilibrium shape of the dislocation (Fig. 25-5) by two line tensions with different outer cut-off radii results in the idealized shape shown in Fig. 25-9: the dislocation is kinked near the obstacle by an angle given by eq. [25y] (BACON *et al.*, 1973). For reasonable values of w, l, and r_o, the angle ϕ at the kink is usually larger than 45°.

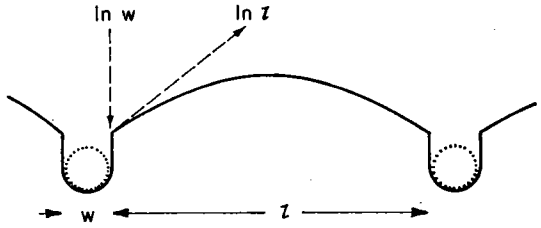

FIG. 25-9. Idealized shape of dislocation at the Orowan stress.

There is also a *lower* limit for reasonable values of the parameter f, the sine of the bow-out angle. This limit is given by the condition that the maximum excursion of the dislocation should be large compared to the lattice spacing for a continuum description of line tensions to be applicable. When the excursion is smaller, it would be more appropriate to treat the bow-out by the lateral travel of kinks; only when many kinks are necessary is this equivalent to a line tension description.

This condition reads, from geometry,

$$f \gg \frac{b}{\bar{l}_e}.$$

Since, for small relative obstacle strengths f, the obstacle spacing must also be small to give a non-negligible stress (eq. [25x]), the continuum model requires

$$f \gg \sqrt{\frac{\bar{\sigma}}{\mu}} \qquad [25z]$$

or $f \gg 1/100$ for $\sigma > 10^{-4}\mu$.

The Plane Glide Resistance (Friedel Statistics)

As in the case of linear barriers, the *plane* glide resistance may be significantly affected by any long-range heterogeneity in the *line* glide resistance; in particular, the maximum plane resistance may be smaller than the maximum line resistance. Heterogeneities in the line glide resistance of discrete obstacles may be due to a spectrum of obstacle *strengths*, as they were in the case of linear barriers; but they may here also be due to a spectrum in obstacle *spacings*: the line glide resistance of discrete obstacles depends both on the element resistance of a typical obstacle and on the obstacle spacing (eq. [25d]). Such heterogeneities in obstacle spacings are always present, unless the obstacles are arranged in a regular lattice.

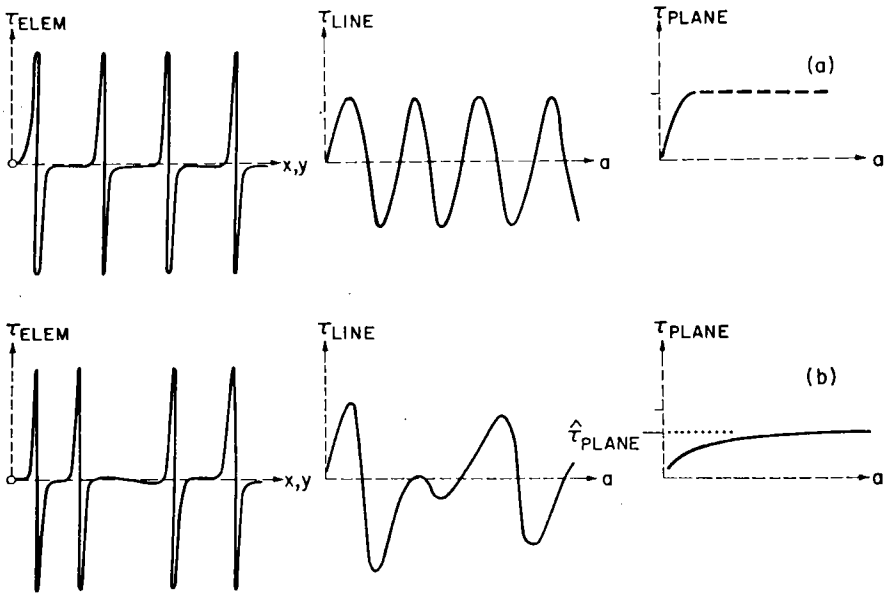

FIG. 25-10. An aperiodic line glide resistance diagram (b) gives rise to a lower plane glide resistance than a periodic one (a).

Figure 25-10 schematically shows the element, line, and plane glide resistance diagrams for (a) a periodic arrangement of obstacles, (b) an aperiodic distribution. The obstacle strengths were chosen the same in both cases: the variation in the "amplitude" of the line glide resistance in Fig. 25-10b is due only to the variation in obstacle spacing. While the plane glide resistance in the periodic case (a) reaches its maximum, beyond which no equilibrium is possible, after a small area has been swept, the plane glide resistance in the aperiodic case (b) approaches a much lower maximum in an asymptotic fashion: at $\hat{\tau}_{PLANE}$, an indefinite area may be swept out.

That such an asymptotic maximum in the plane glide resistance must exist has been shown by KOCKS (1966). The reason is the essentially two-dimensional nature of glide: dislocations are free to surround especially resistant areas of the slip plane. The level of the asymptote is not only lower than the maximum line glide resistance, it is also lower than the maximum in a *periodic* array of the same area density. If one imagines the aperiodic arrangement to be constructed from the periodic one by the removal of obstacles from some regions and their accumulation in some others, the regions of less-than-average density are bound to form a continuous area in the slip plane. A *clustered* arrangement of obstacles, rather than merely a *random* one enhances the effect: the asymptotic maximum is even lower (KOCKS, 1969).

Applied stresses $\sigma < \hat{\tau}_{PLANE}$ do not lead to long-range slip in this purely mechanical model; the term "plane glide resistance, τ_{PLANE}" gains significance at values

less than the maximum only when the possibility of thermal activation has been introduced (Chapter 4).

Derivations of the asymptotic maximum plane glide resistance fall into two classes, here called *Friedel statistics* and *Mott statistics*. In the remainder of this treatise, we will discuss discrete obstacles only when Friedel statistics are applicable; we shall outline the limits of their applicability in the next subsection under "Mott statistics".

FRIEDEL (1956, p. 205, or 1964, p. 224) provided a simple model for asymptotic maximum plane resistance based on the *steady-state* propagation of quasi-straight dislocation lines. In steady state, a dislocation released at one obstacle must, in the average, pick up exactly one more. This means that the area swept by the dislocation after overcoming one obstacle must, in the average, be equal to the average area per particle (assuming a random distribution). More exactly, for obstacles of finite width w, we may define

$$(l + w)^2 \equiv \frac{\text{slip plane area}}{\text{number of obstacles}}. \qquad [25aa]$$

Then, the square of the *average inter-obstacle spacing* l is a measure of the average area in which one new obstacle is encountered and must, according to FRIEDEL (1956), equal the area swept:

$$a_{\text{SWEPT}} = l^2 \qquad (\textit{steady state}). \qquad [25bb]$$

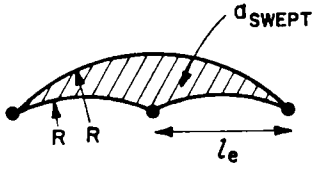

FIG. 25-11. Friedel's steady-state condition: the shaded area must in the average contain one obstacle point.

FRIEDEL (1956) calculated the area swept for small bow-outs of two dislocation segments of equal lengths between three collinear obstacles, assuming circular arcs of radius R (Fig. 25-11). This assumption amounts to neglecting any effects due to dislocation anisotropy or interaction, as well as any effects of viscous drag on the dislocation shape. The result is

$$a_{\text{SWEPT}} = \frac{1}{2}\frac{(l_e - w)^3}{R}$$

(6 times the bowing area given in eq. [25h]). Substituting for the numerator from eq. [25o], for the denominator from eq. [25s], and dividing by l^2, we have

$$\frac{a_{\text{SWEPT}}}{l^2} = \left(\frac{2E}{\sigma b l}\right)^2 \cos^3 \phi. \qquad [25cc]$$

If the left-hand side is 1, by virtue of eq. [25bb], for $\sigma = \tau_{\text{PLANE}}$, and if we replace $\cos\phi$ by the relative obstacle strength f (eq. [25v]), we have

$$\boxed{\tau_{\text{PLANE}} = f^{3/2}\frac{2E}{bl}.} \qquad [25dd]$$

The average center-to-center obstacle spacing $(l + w)$ is usually given geometrically in terms of the volume fraction and the dimension of the particles. For example, for uniform spheres of radius r, distributed at random in three dimensions and taking up a volume fraction c, one has

$$(l + w)^2 = r^2\frac{2\pi}{3c}. \qquad [25ee]$$

The average diameter of the circles formed by intersection of these spheres with the slip plane is

$$w = \frac{\pi}{2}r. \qquad [25ff]$$

The plane glide resistance (eq. [25dd]) then becomes

$$\tau_{\text{PLANE}} = (f(r)^{3/2}\cdot\frac{2E}{br}\cdot\sqrt{\frac{3c}{2\pi}}\cdot\frac{1}{1-\sqrt{3\pi c/8}} \qquad [25gg]$$

or approximately

$$\tau_{\text{PLANE}} \simeq f^{3/2}\frac{2E}{br}\frac{\sqrt{c/2}}{1-\sqrt{c}}. \qquad [25hh]$$

For a more refined measure of the plane glide resistance, one needs to know the distribution function of the obstacles and a criterion for large-scale slip. Figure 25-12 shows, in a qualitative way, the fraction P of peaks in the line resistance diagram at or below a level $\hat{\tau}_{\text{LINE}}$: it allows for a very few peaks at very low levels, but assumes that to get *all* of them ($P = 1$) one has to go to very high levels. The particular form shown is appropriate for a random distribution of obstacles of uniform strength (KOCKS, 1966). By contrast, a *periodic* arrangement of the same obstacles would make all of the peaks in the line resistance appear at the same level (dashed line in Fig. 25–12).

To derive the asymptotic maximum plane resistance, KOCKS (1966, 1967) has proposed a *percolation criterion*: the probability P must reach a critical value such that, whenever the dislocation has overcome one obstacle, it will in the average be able to overcome one more as a consequence. In the simplest case, this occurs at $P = 0.5$. Figure 25-13 shows a piece of quasi-straight dislocation which, at a stress at which it is released from one obstacle (B), must be able to move on to the left (A) or to the right (C).

This theory has the remarkable feature that the asymptotic maximum plane resistance, at which large-scale slip must occur, does not depend on the details of the distribution of line resistances, only on the value at a certain critical penetration probability. For example, this level does not depend on the maximum slope in Fig. 25-12, i.e. the half-width of the distribution. The value of $\hat{\tau}_{\text{PLANE}}$ thus makes for an excellent first-order description of the obstacle structure.

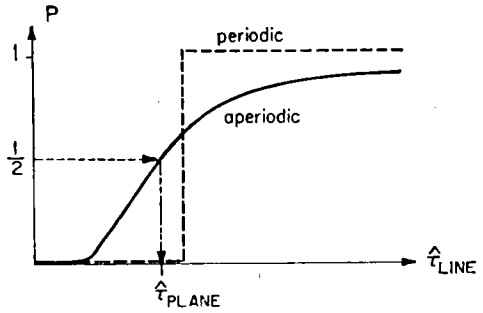

FIG. 25-12. Cumulative distribution of peaks in the line resistance diagram for periodic and aperiodic obstacle arrays (schematic). The maximum plane resistance corresponds to a critical probability, here for example chosen to be $P = \frac{1}{2}$.

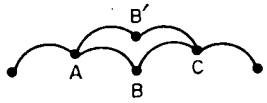

FIG. 25-13. The condition for continued glide is that either the dislocation segment AB' or $B'C$ is supercritical at the stress at which the dislocation gets released at B.

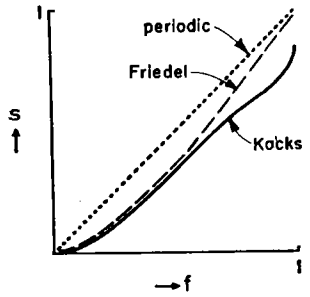

FIG. 25-14. General dependence of normalized plane glide resistance s on normalized obstacle strength f.

Unlike the simple development of FRIEDEL where the ratio of the area swept to the average area per obstacle was taken as 1, the more detailed statistical theories such as that of KOCKS (1966, 1967) and computer experiments such as those by FOREMAN and MAKIN (1966), involve this ratio as one important parameter, the breaking angle ϕ being the other one. At the critical limit, for example when a certain probability is reached, there exists a certain relation between these two parameters. Together with eq. [25cc], this relation determines the plane resistance as a function of f

$$\tau_{PLANE} = s(f)\frac{2E}{bl}. \qquad [25ii]$$

However, both of these statistical treatments have shown that FRIEDEL's simple development [25dd], which was an approximation for $f \ll 1$, actually holds very well up to at least $f \simeq 0.5$ (Fig. 25-14). This is in the neighborhood of the limiting (Orowan) strength (eq. [25y]).

Another way of looking at the results of a statistical treatment is that it gives a relation between the *average* inter-obstacle spacing l and the *effective* obstacle spacing l_e we used before to describe a local situation. Comparison of eqs. [25dd] with [25x] shows that

$$l_e - w = \frac{f}{s} l = \frac{l}{\sqrt{f}} = \frac{l}{(\sigma l/\mu b)^{1/3}}. \qquad [25jj]$$

Note that this "effective" spacing is the spacing between the *critical* obstacle pairs that make large-scale glide possible, not the (generally larger) *average* spacing of obstacles along a dislocation line in equilibrium with a certain applied stress. The latter is what has been calculated in the most complete form by LABUSCH (1962). Its relation to the stress is almost identical to that of FRIEDEL (1956).

Equation [25dd] is the basis for relating macroscopic measurements of the plane glide resistance to the microscopic properties of discrete obstacles: their average spacing l and their relative strength f. If $f = \hat{f}$ characterizes the *peaks* in the line resistance diagrams, τ_{PLANE} is at its asymptotic value $\hat{\tau}_{\text{PLANE}}$. If f characterizes a lower value, for example the effective obstacle strength under the influence of a certain level of thermal activation, τ_{PLANE} specifies the level of the applied stress that would lead to steady-state planar glide under those conditions.

The Plane Glide Resistance (Mott Statistics)

Above we have considered how the plane glide resistance can be obtained for a random distribution of point-like obstacles that interact with a dislocation only on contact. At zero stress, the dislocation was straight; at finite stresses, all obstacles with which the dislocation came in contact opposed its forward motion.

Real obstacles have a finite range of interaction w. If one introduced a straight dislocation into a crystal at zero applied stress, it would be attracted or repelled by all obstacles whose centers are inside a strip w wide around it. Their average spacing along the dislocation is

$$l_1 = l^2/w \qquad [25\ell\ell]$$

where l^2 is again the average slip plane area containing one obstacle. The dislocation would accommodate these interactions to some extent and would not remain straight.

Even if the obstacles were truly points, but were attractive, the dislocation could lower its energy by a certain amount of zig-zagging; this amount is determined by a balance between the binding energy F_{BIND} and the dislocation line energy. One can easily derive that, if an effective interaction range

$$w_{\text{eff}} = \sqrt{\frac{2F_{\text{BIND}}}{\mathscr{T}_{\text{DIS}}} \cdot l_1} \qquad [25mm]$$

is assigned to these point obstacles, their effects can be treated just like the finite-range obstacles to be considered in more detail below. This effect also increases the effective interaction range of finite-range attractive obstacles over that of repulsive ones.

The forces exerted on the dislocation by the "obstacles" are now in part forward and in part backward: the two signs must balance each other at zero stress. As a stress is applied, the distribution changes until, at the critical stress $\sigma = \hat{\tau}_{\text{LINE}}$, equilibrium is not longer possible. The rather difficult statistics of this process has been dealt with most extensively by LABUSCH (1970). The question that concerns us here is primarily, under what circumstances the initial zig-zagging of the dislocation becomes irrelevant at the flow stress, so that the Friedel statistics discussed above are in fact applicable.

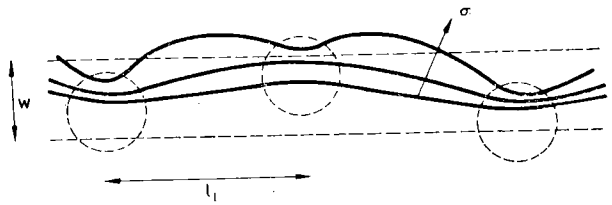

FIG. 25-15. Initially straight dislocation bent by interaction with three attractive "obstacles" of range w, at various stresses. The center obstacle exerts a "forward" force at zero stress, no force at the intermediate stress, and a resisting force at the highest stress shown.

Figure 25-15 shows that, for attractive obstacles, the "forward" forces on the dislocation turn into "backward" forces at a stress where a bow-out arc based on the length $2l_1$ has an excursion of about $w/2$. (For repulsive obstacles, the "forward" forces vanish at a critical excursion.) If at this stress the breaking strength of the "backward" obstacles has not yet been exceeded, the above treatment according to FRIEDEL (1956), FOREMAN and MAKIN (1966) and KOCKS (1967) is justified; i.e. when the cosine of half the minimum cusp angle fulfills the condition

$$\hat{f} \geqslant \frac{w}{l_1} = \frac{w^2}{l^2} \qquad (\textit{Friedel statistics}) \qquad [25nn]$$

with eq. [25ℓℓ]. Note that this condition is more restrictive than that which specifies that the obstacles may be treated as discrete:

$$\frac{w}{l} < 1 \qquad (\textit{discrete obstacles}). \qquad [25oo]$$

Obstacles whose range of interaction w is dictated by their spacing l, even if one treated them as quasi-discrete, would have to be quite strong before Friedel statistics can even approximately be applied; forest dislocations are probably a borderline case.

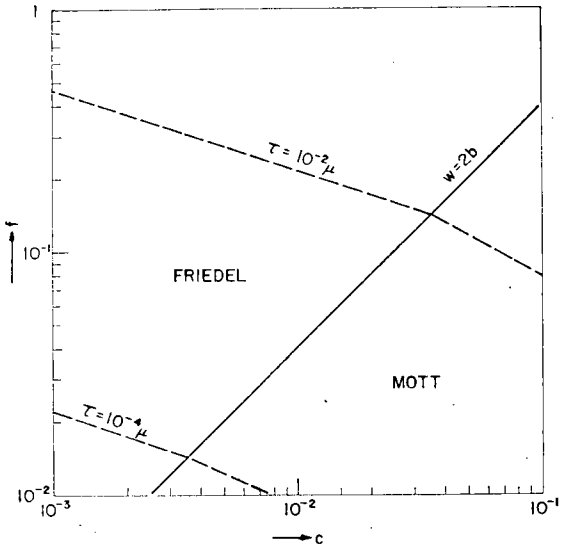

FIG. 25-16. A map showing the range of applicability of Friedel statistics (eq. [25dd]) and Mott statistics (eq. [25ww]), as a function of the normalized obstacle strength f and the solute concentration c, for an effective interaction range w twice the physical obstacle size b.

For solute atoms, $l^2 = b^2/c$, so that (NABARRO, 1972)

$$\boxed{\frac{c}{f}\left(\frac{w}{b}\right)^2 = 1} \qquad [25pp]$$

is the critical condition. It is plotted in Fig. 25-16, for the reasonable value $w = 2b$. In the interesting stress range between the broken lines, only very weak obstacles in fairly high concentrations, such as substitutional solute atoms, fall outside the range where Friedel statistics are justified. (LABUSCH, 1972, gives a critical value of 1/36 instead of 1 in eq. [25pp] and thus finds Friedel statistics rarely justified.)

We shall now give a brief outline of the basic features underlying various theories of the yield strength when condition [25nn] is *not* fulfilled. They are primarily due to MOTT and NABARRO (1948), RIDDHAGNI and ASIMOW (1968), and LABUSCH (1970); with apologies to the other authors, we adopt the characterization given by NABARRO (1972) to this type of statistical treatment by calling it "Mott statistics". All approaches of the above authors give the same result to within a numerical constant, if the various detailed assumptions are made comparable (LABUSCH, 1972; NABARRO, 1972).

We start with a description of the shape of a quasi-straight dislocation in a field of many weak discrete obstacles. As we have seen, an initially straight dislocation would acquire small bends due to the various interactions, sometimes in one direction, sometimes in the other. Due to statistical fluctuations, a given length l_n may have an excess of one sign of bend or the other. If one assumes for simplicity that the *amount* of each bend is always the same, i.e. that the interaction *always* has

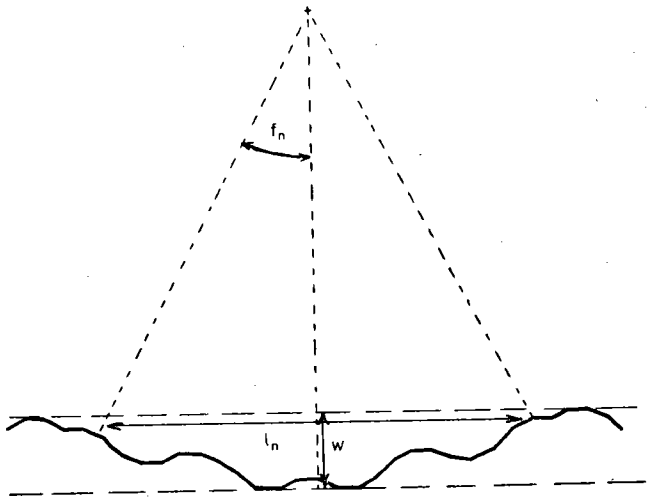

FIG. 25-17. Schematic of fluctuation in dislocation line shape at zero stress, when it is bent by many weak obstacles of range w through identical angles f of randomly distributed signs.

the *average* strength $\bar{f}$ and that the *signs* of the bends are randomly distributed, the angle f_n accumulated over n bends is, in the average,

$$f_n = \bar{f} \cdot \sqrt{n}. \qquad [25qq]$$

Over the length l_n of this fluctuation, the dislocation will have an average curvature (Fig. 25-17). If it is to stay within the strip of width w, as originally implied, the height of the arc must be about w; this gives the condition

$$w = \tfrac{1}{4} l_n f_n. \qquad [25rr]$$

(Summation over repeated subscripts is here *not* implied.) Finally, the average number of obstacles n in a strip of length l_n and width w is

$$n = \frac{l_n w}{l^2} = \frac{l_n}{l_1}. \qquad [25ss]$$

The unknown l_n can be eliminated from eqs. [25qq], [25rr], [25ss], and a condition for the equally unknown number n in an average fluctuation established:

$$n^{3/2} = \frac{w^2}{l^2} \frac{1}{\bar{f}} \qquad (n \gg 1). \qquad [25tt]$$

Note that we have made the assumption of a *large* number n throughout; nevertheless, for $n = 1$, eq. [25tt] is precisely the condition [25nn] for Friedel statistics to apply. The number n may be read off Fig. 25-16 for the case of solute atoms with $w = 2b$: the largest it becomes is 12, in the bottom right corner of this figure. Thus, it is probably necessary to take better account of the discrete bends than we have done above using circle geometry.

Over the length l_n, there is a net backwards force $K_n = 2Ef_n$, even at zero stress. If one applied a stress to balance this force, namely

$$\tau_{\text{PLANE}} = \frac{K_n}{b l_n} \qquad [25uu]$$

the configuration should be unstable—presuming that the configuration does not *change* much during the application of the stress. Another way of arriving at eq. [25uu] is to say that the angle

$$\Sigma f_i = \frac{1}{2R(\tau)} \cdot \Sigma l_i$$

accumulated in all the little arcs between two individual obstacles must just equal f_n—so that, under the stress τ_{PLANE}, the dislocation would just be straight. It is evident that the changed cusp angles at all obstacles must in fact lead to earlier yielding.

Taking eq. [25uu] for the plane glide resistance and inserting from the previous equations for n and l_n, we find

$$\tau_{PLANE} = \frac{2E}{bl} \cdot f^{3/2} \cdot n^{1/4}. \qquad [25vv]$$

This is written as the Friedel formula [25dd] with a correction term $n^{1/4}$. It thus appears that Mott statistics must always give a higher flow stress than Friedel statistics. On the other hand, eq. [25vv] contains a somewhat vaguely defined *average* obstacle strength f whereas the Friedel equation [25dd], written also for zero temperature, contains the *maximum* strength $\hat{f}$. A proper calculation would give a smooth transition from eq. [25dd] to eq. [25vv], which was here derived for $n \gg 1$ only.

The important difference between Mott and Friedel statistics is not so much the absolute magnitude of the flow stress as its dependence on f and c. Inserting for n from eq. [25tt], using $l^2 = b^2/c$ for solute atoms, and $2E = \mu b^2$, we get

$$\boxed{\tau_{PLANE} = \mu f^{4/3} c^{2/3} \cdot \left(\frac{w}{b}\right)^{1/3} \quad (\textit{Mott statistics}).} \qquad [25ww]$$

The functional form of this result is the same for all theories based on *fluctuations* in the sign of the obstacle interaction (LABUSCH, 1972; NABARRO, 1972). Proportionality constants of order 1 were here neglected.

Screws versus Edges

The propagation of slip over an entire slip plane requires that *both* screw and edge dislocations move. The plane glide resistance is thus determined by the ones that are harder to move (not the ones that are easier to move, SEEGER, 1955b, and not some combination, GILMAN, 1969).

Equations [25dd] and [25ee] suggest, at first glance, that these are always the screws, since their effective line tension is always larger (eqs. [25r]). This is in fact true when f is independent of the character of the dislocation. As one can see from the simplified form [25w'] of f, this is only true when the obstacle strength K is itself proportional to the line tension. Discounting the small differences in the exact, orientation dependent, line tension, the Orowan stress (eq. [25i]) is a case in point, and so are all other dislocation (self) interactions, such as forest hardening.

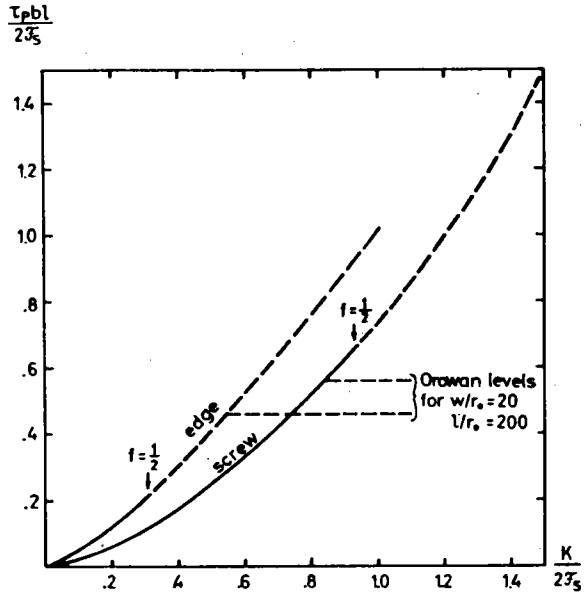

FIG. 25-18. Normalized plane glide resistance τ_P versus normalized obstacle strength K for screw and edge dislocations, using orientation dependent effective line tension and isotropic elasticity theory ($\nu = 1/3$). $\mathscr{F}_S$ is the free energy per unit length of screw dislocations, l^2 the slip plane area per obstacle point, and f the sine of the bow-out angle.

On the other hand, when the element glide resistance is only due to the shear produced by the passing dislocation, which is the same for screws and edges, the appearance of $E^{-3/2}$ in the term $f^{3/2}$ of eq. [25dd] dominates the explicit E, and the dislocations with the *lower line tension* determine the plane resistance: the edges. An example of this is the cutting of coherent precipitates. Figure 25-18, which was derived from the exact relation [25w], illustrates the change from edge control to screw control as the Orowan strength limits the precipitate strength.

The relative values of the glide resistance to screw and to edge dislocations may, under some circumstances, have a far-reaching influence on the slip habit. This occurs when the applied stress necessary to drive the *edge* components through their obstacles at a prescribed rate and temperature exceeds the *maximum* glide resistance of the screws: then, the screws must be in continuous motion and have no opportunity and no driving force for cross slipping. As a consequence, slip remains planar and this fact may lead to more severe stress concentrations and to difficulties in propagating slip throughout the volume of a specimen. On the other hand, when the maximum glide resistance to screws is *not* exceeded, slip may be wavy or planar depending on other factors affecting the ease of cross slip (temperature, stacking fault energy, etc.). If wavy slip should be observed in a particular case, this establishes that the propagation of screws is not easy (KOCKS, 1969).

Same as presumably applies to b.c.c. metals when edges are easier than screws at high values of τ/μ

26. Dragging Obstacles

In secs. 24 and 25, we discussed some examples of glide resistance diagrams due to structural features of the crystal that vary with position in some way. But there are some effects that are not fixed in the crystal, which produce a resistance to dislocation motion. One example is a dragging Cottrell cloud of solute atoms, from which the dislocation may nevertheless tear loose under a high enough stress or a high enough imposed strain rate. We have excluded effects requiring diffusion in this article and will, therefore, not treat this case further. (See, for example, Schoeck, 1974.)

Another example of a glide resistance that moves along with the dislocation, as it were, is the necessity of extending a dipole trailing behind the dislocation, which may once have been formed at a jog in a screw dislocation. This case has been of some interest in the literature and we will discuss it briefly.

Jogs

A *jog* on a screw dislocation can act as an obstacle to its motion. We are concerned here with temperatures below that at which diffusion becomes important.

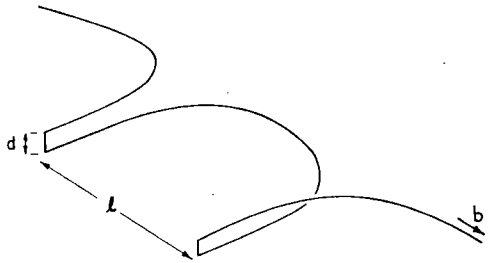

Fig. 26-1. Screw dislocation drawing out edges dipole at jogs.

Then, if the dislocation advances, it pulls out a dipole behind it, as shown in Fig. 26-1. If the height d of the jog is large—much larger than the size of the atom—the energy associated with the dipole is mainly elastic. By advancing unit distance, it creates unit length of dipole, of energy

$$F_{\text{DIPOLE}} \simeq \frac{1}{1-\nu}\cdot\frac{\mu b^2}{2\pi}\ln\frac{d}{r_o} \qquad [26a]$$

where r_o is an inner cut-off radius. This energy per unit length is the resisting force K exerted locally on the dislocation. It is here not the strength of a fixed obstacle, but is dragged along with the dislocation as it advances. For a constant jog spacing l, the line glide resistance is then constant and of a value

$$\tau_{\text{LINE}} = \frac{K}{bl} = \frac{\mu}{1-\nu}\cdot\frac{b}{l}\cdot\frac{\ln\,(d/r_o)}{2\pi}. \qquad [26b]$$

The resulting line resistance diagram is shown in Fig. 26-2. The free energy of the body increases (initially as a^2) as the dislocation bows out between jogs, driven forward by an applied stress. At a sufficiently large bow-out, a dipole is pulled out at the place where the dislocation was jogged. The free energy then increases

linearly with area, so the line resistance is constant. As we have seen (sec. 22), such motion cannot be thermally activated.

The energy of a dipole of *atomic* height is mainly core energy. It may be regarded as a row of associated point defects. On forming such a jog, the free energy probably undulates with a wavelength of atomic dimensions, as shown in the figure. The amplitude of the oscillations is difficult to estimate (it depends on the details, at an atomic level, of the formation of the dipole) but it is likely to be small compared with the bow-out energy. The oscillation permits a small degree of thermal activation of dislocation motion.

The (plane) glide resistance for continued flow must here follow from a statistical treatment of the jog spacing as it develops with glide.

Energy is stored, as the self energy of the dipoles, during jog dragging. At temperatures above 0 K, this energy is slowly released by the annealing-out of the dipoles. But at the temperatures that concern us in this review, this process is very slow. (The first detailed discussion of jog dragging was given by SEEGER, 1955b.)

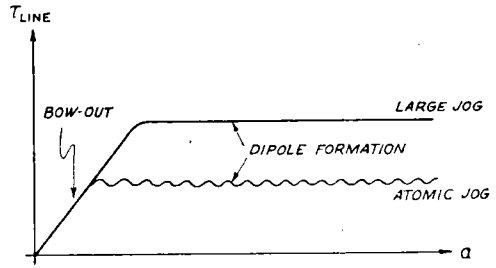

FIG. 26-2. Schematic line resistance diagram for dipole formation at jogs.

27. EXTENDED DISLOCATIONS

Dissociation in the Slip Plane

Up to now we have characterized a crystal by its glide resistance: a quantity with the dimension of a stress which describes its resistance to the motion of a single dislocation of strength $\vec{b}$ (a lattice translation vector). The magnitude of the glide resistance depends on the magnitude of b, and thus on the ability of the dislocation to dissociate.

In fcc crystals, the unit perfect dislocation may dissociate into two partials separated by a stacking fault. In ordered fcc alloys it may dissociate into four partials, separated by antiphase boundary, stacking fault, or both. In more complicated structures (MoS_2 is an example), the dissociation may involve the splitting of the dislocation into six or more partials, each separated by a fault from the next. In all cases the faults tend to bind the partials together (opposing their elastic interaction which tends to separate them) so that they move as a *glissile group*.

If the fault energy is sufficiently high, the partials move as a tightly-bound group of width η. For many practical purposes the dissociation can be ignored, and the behavior of the group is well approximated by that of a single dislocation of strength:

$$\vec{b} = \Sigma \vec{b}_p \qquad [27a]$$

where the $\vec{b}_p$ are the partial Burgers vectors. But when the glide resistance varies rapidly with distance, the total force on the leading partial may be sufficiently

different from that on the trailing partial to dissociate the two or at least change their spacing.

Complete separation cannot occur when the glide resistance is controlled by *discrete obstacles* the spacing of which is large compared to the equilibrium separation of the partials, under the given stress. The local glide resistance gradients can then only have the effect of causing local constrictions or bulges in the extended dislocation. The associated element free energy changes must be incorporated in the element glide resistance of the "obstacle". In fact, these changes alone form the basis of some proposed mechanisms of precipitation hardening (GLEITER and HORNBOGEN, 1965; HIRSCH and KELLY, 1965).

More extensive changes in the treatment are necessary for dislocations held up at isolated (or dragging) *linear barriers*. Dissociation along the entire length of the dislocation is here conceivable, and it is easy to derive under which circumstances it will occur when the barrier half-width δ (Fig. 24-3) is smaller than the equilibrium separation of the partials η. For then the difference in force on the two partials is exactly equal to the maximum glide resistance $\hat{\tau}_{\text{ELEM}}$ times b, and dissociation must occur when this force exceeds the fault free energy per unit area χ_{FAULT}. In normalized variables, using the shear stiffness in the glide plane, μ':

$$\frac{\tau_{\text{ELEM}}}{\mu'} > \frac{\chi_{\text{FAULT}}}{\mu' b}, \qquad \delta < \eta \qquad \text{(dissociation)}. \qquad [27b]$$

For a quantitative estimate, we have listed in Table 2-III some typical values for the stacking fault energy parameter $\chi_{\text{SF}}/\mu' b$ and the equilibrium partial separation η. As noted by SEEGER (1955a), most materials fall into two extreme classes. Most pure elements and compounds have stacking fault energies so high that their equilibrium partial separation is of the order of the lattice spacing and that it would require stresses in excess of $\mu/100$ to dissociate them. Since for linear barriers we always have $\hat{\tau}_{\text{LINE}} = \hat{\tau}_{\text{ELEM}}$, such stresses are of no practical interest, unless $\hat{\tau}_{\text{PLANE}} \ll \hat{\tau}_{\text{LINE}}$ through the action of dynamic pile-ups (sec. 24).

Table 2-III.

Stacking fault energies χ_{SF} (compromise from *a*, *b*, *c*), normalized by the shear modulus* μ' (Table 3-I) and the Burgers vector (Table 2-I); and equilibrium separation η of partials in screw and edge dislocation (*c*, *d*)

	$\frac{\chi_{\text{SF}}}{\mu' b}$	η_{SCREW}/b	η_{EDGE}/b
Some elements with allotropic transformations, many solid solutions	$< 10^{-3}$	> 10	> 50
Ag	0.2×10^{-2}	7	30
Cu	0.4×10^{-2}	5	15
Au	0.6×10^{-2}	3	10
Most other elements and compounds	$> 10^{-2}$	~ 1	~ 1

Notes:

(*a*) CLAREBROUGH *et al.* (1967).
(*b*) LÜCKE and MECKING (1973).
(*c*) COCKAYNE, *et al.* (1971).
(*d*) From values in first column, values for ν_{eff} from Table 2-I and fig. 122 in SEEGER (1955a)

* SEEGER uses the inverse compliance rather than the stiffness μ'.

On the other hand, most solution hardened alloys and some elements that exhibit allotropic transformations (such as cobalt) have rather extended dislocations, and their partial separation may be changed significantly, up to the point of dissociation, by differences in the glide resistance experienced of $10^{-3}\mu$ or less. In such materials, the element glide resistance of an isolated linear barrier must be taken to be that applying to a single partial. Moreover, the *line* glide resistance for bulge formation (sec. 24) must be severely affected by the stacking fault extending throughout the area of the bulge for the leading partial, and by the necessity to also form a bulge in the trailing partial.

In cases more complicated than the narrow linear barrier discussed above (eq. [27b]), the equilibrium partial separation can be derived, provided the functional relationship $\eta(\chi)$ is known (SEEGER, 1955a, fig. 122), by subtracting from the stacking fault energy χ_{SF} the difference in total force on the two partials:

$$\chi_{eff} = \chi_{SF} - [b(\sigma - \tau_{LINE})]_2 + [b(\sigma - \tau_{LINE})]_1. \qquad [27c]$$

The line glide resistance incorporates the element resistance as above and any "curvature stresses" exerted on each partial by itself (but not their interaction stress); and the term $b\sigma$ in each bracket signifies the Peach-Koehler force exerted on the respective partial by the applied stress.

Periodic linear barriers are the hardest to treat when the finite extension of the dislocation is taken into account. Only some extreme cases can be judged with some confidence. Firstly, long-wavelength ($\lambda \gg \eta$) variations in the element resistance, such as by internal stresses, are not expected to have an appreciable influence on the partial separation in any material, since here the difference in force felt by the leading and the trailing partial becomes insignificant. Secondly, when the period λ of the element glide resistance and the equilibrium spacing η of the partials are the same (such as they may be for the lattice resistance in all high-stacking-fault-energy materials) the variation of the partial separation and the concomitant variation of the element free energy become part and parcel of the element glide resistance diagram. But when one stacking fault spreads over many wavelengths of the glide resistance, it should be important how close the spacing is to an integer multiple of the wavelength (since then the difference in force is zero). This problem would become very sensitive to the details of the model; one may, however, expect some degree of smoothing of the element glide resistance. This could be one of the reasons for the low Peierls stress in fcc metals.

Dissociation out of the Slip Plane

In some materials, crystallographic symmetry demands that any dissociation of stationary dislocations be nonplanar. For example, in bcc metals, the slip vector is the $\langle 111 \rangle$ direction, and the core of the screw dislocation must, therefore, have three-fold symmetry. Even if part of the dissociation may be in a slip plane, some other part must be out of the slip plane.

For such a dislocation to glide without atomic shuffling in the core, it must recombine into a full dislocation or at least into one with a planar core. Depending on whether this recombination occurs only for forward travels of atomic distances or is retained for longer times, this process may be described as a periodic lattice resistance ("pseudo-Peierls stress") or as a linear barrier that is not localized at a fixed position but is re-established wherever the dislocation comes to rest.

In either case, the line resistance to glide may be lower than the element resistance through the activation of an alternative path: in the case of a lattice resistance, the nucleation and lateral propagation of kink pairs or bulges; in the case of a dragged linear barrier, the nucleation of a loop in the manner discussed for isolated attractive linear barriers.

3. KINETICS

Summary

In the last Chapter, we have derived the *driving force* for dislocation motion. For an element of a continuous dislocation line, it is the difference between the applied stress σ and the line glide resistance τ_{LINE}. We have considered equilibrium situations by letting the dislocation adjust its shape and thus its self stresses such as to make τ_{LINE} constant along its length—and then adjusting the applied stress to the same value. For different positions of the dislocation in the glide plane, a different applied stress σ would, in general, be required to maintain equilibrium.

For a *constant* applied stress σ, a dislocation element experiences, in general, a varying driving force. It responds to a finite value of $(\sigma - \tau_{\text{LINE}})$ by accelerating until its velocity is limited by energy dissipating drag mechanisms—or, eventually, by relativistic effects near the speed of sound. *Dislocation dynamics* is concerned with the relations between forces, energies, velocities, and accelerations. We discuss it in sec. 31, and introduce the relevant material properties: the *mass* $\mathscr{M}$ per unit length of a dislocation, and the *drag coefficient* B.

If the driving force varies *rapidly*, two special dynamic effects may come into play: the oscillatory motion superposed on the forward velocity of the dislocation may lead to radiation losses; and the *inertia* of the dislocation may help it overcome obstacles even when the stress is less than the maximum glide resistance. We find that inertial effects have been unduly neglected in the past. At low temperatures, and for short-range obstacles, they may well be important.

For the more usual slow variations in driving force, in which the velocity is drag controlled everywhere, we find it convenient to distinguish between two regimes of stress: one in which the stress is *below* the mechanical threshold and the other in which it is *above*. When $\sigma > \hat{\tau}$, the driving force is positive everywhere and dislocations must keep moving. We call this *continuous glide* and discuss it in sec. 32. Calculation of the average velocity leads one to define an *effective stress* which, in contradistinction to the (local) driving force, is *not* equal to the difference between applied stress and glide resistance, but is a more complicated function of them; for a sinusoidal variation in glide resistance, for example, it is the geometric mean of the minimum and maximum driving force.

When the applied stress σ is *smaller* than the mechanical threshold $\hat{\tau}$, dislocations must stop at various obstacles. They may be released by thermal fluctuations and then travel at a drag controlled velocity to the next obstacle.

We call this *jerky glide* and treat it in sec. 33. The most important problem here is the derivation of the conditions for continued plastic flow or *steady state*, and the associated possibility of transient behavior at short times.

The mechanical threshold $\hat{\tau}$, which separates jerky from continuous glide, may be the maximum value of τ_{LINE} or of τ_{PLANE} depending on whether the behavior of individual dislocations is studied or continued slip over an entire plane.

The *kinematic relations* linking the velocities of individual dislocations (or dislocation segments) to the macroscopic strain rate demand a knowledge of the density of mobile dislocations (or mobile dislocation segments). The *kinetics of slip* is thus controlled not only by the kinetics of dislocation glide, but also by the kinetics of the number of participating elements. Again, this will usually involve time dependent behavior leading to a steady state.

The relation between strain rate and stress, and its dependence on other variables such as temperature (i.e. the *deformation kinetics*) may be described in empirical or phenomenological form (sec. 34). If one wishes to avoid the strain-time history as an explicit set of variables, it is imperative that one introduce *structure* variables; it will be discussed how many are necessary under various conditions for a meaningful "constitutive relation".

There have been many excellent discussions of the kinetics of motion of individual dislocations in continuous glide and jerky glide, and of the kinetics establishing the mobile dislocation density, as well as how these kinetic relations can furnish a basis for phenomenological constitutive equations. Of these references we find the following limited selection most useful:

ALEXANDER and HAASEN (1968), *Dislocation Dynamics and Plastic Flow in the Diamond Structure;*
GILMAN and JOHNSTON (1962), *Dislocations in Lithium Fluoride Crystals;*
KLAHN, MUKHERJEE, and DORN (1970), *Strain Rate Effects;*
LEIBFRIED (1955), *Gittertheorie der Mechanischen und Thermischen Eigenschaften der Kristalle;*
NABARRO (1967), *Theory of Crystal Dislocations;*
OROWAN (1940), *Problems of Plastic Gliding;*
RICE (1970), *On the Structure of Stress Strain Relations for Time-dependent Plastic Deformation in Metals;*
ROSENFIELD, HAHN, BEMENT, and JAFFEE (Editors) (1968), *Dislocation Dynamics.*

31. Dislocation Dynamics

The Equation of Motion

Like the classical body of Newtonian mechanics, a dislocation or a kink that is not in (static) equilibrium is governed by a (dynamic) *equation of motion*. The force that an applied shear stress exerts on it tends to cause it to accelerate, at a rate which is determined by its inertial *mass*, which we define below. This tendency is opposed by mechanisms which dissipate energy (*drag*, or *damping* mechanisms) and by any other internal forces opposing the motion (the glide resistance treated in sec. 23).

The dislocation element or kink moves when the force σb applied externally

first exceeds the glide resistance $b\tau_{\text{LINE}}$ due to both element resistance and self-stress (eq. [23c]). The equation of motion of a unit length is

$$\boxed{\mathscr{M}\ddot{y} + B\dot{y} = b(\sigma - \tau_{\text{LINE}}).} \qquad [31a]$$

The "inertial force" $\mathscr{M}\ddot{y}$ and the "drag force" $B\dot{y}$ balance the "driving force" $b(\sigma - \tau)$. The integral over y gives the energy balance:

$$\tfrac{1}{2}\mathscr{M}v^2 + \int B\dot{y}\,dy = \sigma by - \tau_{\text{STOR}}\,by \qquad [31b]$$

The kinetic energy $\frac{1}{2}\mathscr{M}v^2$, the dissipated energy $\int B\dot{y}\,dy$, and the stored energy $\tau_{\text{STOR}}\,by$ (where τ_{STOR} is the average glide resistance felt by the element, eq. [22g]) are all supplied by the external work σby.

Experiments frequently show that the velocity of a dislocation is a *nonlinear* function of stress, suggesting that B in the equations above itself depends on velocity. All the evidence for close-packed crystals, however, indicates that a dislocation moving through an *obstacle free* crystal experiences a *linear-viscous drag*, and that a nonlinear relation reflects the thermally activated motion of a dislocation through obstacles (to be discussed in Chapter 4).

In some applications, the dislocation motion of interest is the vibration of a "string" constrained by "pinning points" at both ends but under no glide resistance in between. Along the free length, the line glide resistance is then equal to the self stress. In the line tension approximation (eq. [23j]), this is proportional to the curvature or, for small excursions, to the second derivative y'' of y with respect to the average line direction x. The equation of motion [31a] reads then

$$\mathscr{M}\ddot{y} + B\dot{y} + \mathscr{E}y'' = \sigma b. \qquad [31c]$$

For larger excursions of dislocations in a field of discrete obstacles, one may still wish to treat dislocation *segments* as a whole, rather than individual elements. Integration of eq. [31a] over a segment between two points l apart gives then, with eqs. [25c], [25d],

$$\mathscr{M}\ddot{a} + B\dot{a} = \sigma bl - K(a). \qquad [31d]$$

Before discussing the two coefficients $\mathscr{M}$ and B in the equation of motion in some detail, let us introduce two quantities that appear in all time dependent dislocation phenomena: the speed of sound and the atomic frequency.

Speed of Sound and Atomic Frequency

The "speed of sound" in a solid may depend on many variables: the longitudinal or transverse character of the waves being considered, the direction of propagation and (in the case of shear waves) of polarization, and the frequency. In dislocation problems, the "speed of sound" is often meant to refer to the "terminal velocity" of the dislocations, in which case it depends on whether it is a screw or an edge dislocation (the definition is, in fact, more

complicated for an edge dislocation)—or the "speed of sound" may refer to the rate at which information travels along a dislocation line (to be derived, for instance, from the wave equation [31c]).

We are here not concerned with dynamic problems except as limiting cases, and will thus ignore these subtle differences. For the purposes of normalization of various quantities, and of order-of-magnitude estimates, however, we wish to use the "speed of sound", and for these purposes, we shall use the value obtained from

$$\boxed{v_S \equiv v_{SOUND} \equiv \sqrt{\frac{\mu'}{\rho}}} \qquad [31e]$$

where μ' is the shear constant in the slip plane and slip direction (stiffness, not inverse compliance) and ρ is the mass density of the material.

In many problems, the ratio of the speed of sound to the Burgers vector appears: an "atomic frequency". We define

$$\boxed{\omega_A \equiv \omega_{ATOM} \equiv \frac{v_S}{b}} \qquad [31f]$$

and we shall use for all order-of-magnitude estimates

$$\omega_A \simeq 10^{13}\ \text{sec}^{-1}. \qquad [31g]$$

Values of v_S and ω_A for some materials will be listed, along with damping data, in Table 3-I.

The atomic frequency ω_A introduced in eq. [31f] is 2π times the frequency of vibration of one atom in a crystal otherwise at rest; also, it characterizes a phonon with wave number $1/b$. Sometimes the Einstein frequency

$$\nu_E = \frac{\omega_A}{2} \qquad [31h]$$

is used as a typical atomic frequency, and sometimes the Debye frequency (LEIBFRIED, 1955, p. 251):

$$\nu_D = v_S \left(\frac{3}{4\pi\Omega}\right)^{1/3}, \qquad [31i]$$

which is approximately $0.7\omega_A$ for both close-packed and bcc lattice structures (Ω = atomic volume). We chose ω_A as a parameter, because v_S and b are in fact the quantities that primarily enter the equations and there is no reason for introducing any proportionality constants.

The Mass of Dislocations and Kinks

We may formally identify $\mathcal{M}$ as the (inertial) *mass* per unit length of the dislocation. It could, in principle, be calculated by deriving the stress necessary to provide *uniform acceleration* of a straight dislocation in the absence of any damping and of any element glide resistance, in a given lattice at a given

temperature. This has not been done, partly because of the difficulty of describing the force on a moving dislocation (see NABARRO, 1967, p. 496). Instead one may calculate the kinetic energy of a straight dislocation moving at *uniform velocity*. For a *screw* dislocation, geometric requirements lead to the well-known (FRANK, 1949, see also WEERTMAN, 1961) relation for the total elastic-plus-kinetic energy, $\mathscr{U}_v$, of a unit length of dislocation moving at a constant velocity v

$$\mathscr{U}_v = \frac{\mathscr{U}}{\sqrt{1 - v^2/v_S^2}} \simeq \mathscr{U}\left(1 + \tfrac{1}{2}\frac{v^2}{v_S^2} + \ldots\right), \qquad [31j]$$

which, when expanded as shown above for $v/v_S \ll 1$, allows us to formally identify the first term $\mathscr{U}$ with the energy of unit length of a screw dislocation at rest (approximately equal to its free energy $\mathscr{F}_{DIS}$), and the second term with its *kinetic energy*. If the latter is set equal to $\frac{1}{2}\mathscr{M}v^2$, this leads to an expression for the mass $\mathscr{M}$ in terms of $\mathscr{U}$ and the speed of sound v_S:

$$\mathscr{M}_{SCREW} = \frac{\mathscr{U}}{v_S^2}. \qquad [31k]$$

The relativistic energy of a moving *edge* dislocation cannot be described by eq. [31j] (ESHELBY, 1949). However, a relation has been derived (WEERTMAN, 1961) between the effective mass of an edge dislocation and that of a screw:

$$\mathscr{M}_{EDGE} = \left[1 + \left(\frac{v_t}{v_l}\right)^4\right]\mathscr{M}_{SCREW}. \qquad [31\ell]$$

These masses are very similar, since the transverse speed of sound v_t is usually about half the longitudinal speed of sound v_l. We can thus use eq. [31k] for the mass of both kinds of dislocations, using the *line energy of a screw dislocation for* $\mathscr{U}$.

Kinks in dislocations can be treated more easily, inasmuch as they are point-like defects traveling in one dimension only. Their self-energy per unit length is roughly an order of magnitude lower than that of an element of a long straight dislocation, due to the absence of a far-reaching strain field of a kink. Thus we may set (ESHELBY, 1962):

$$\mathscr{M}_{KINK} = \frac{\mathscr{U}_{KINK}}{v_S^2} \simeq \frac{1}{10}\frac{\mathscr{U}}{v_S^2}\ (v \ll v_S). \qquad [31m]$$

The line energy of a screw dislocation is approximately $\mu b^2/2$. With the atomic frequency introduced in eq. [31f], we thus have for both screw and edge dislocations

$$\boxed{\mathscr{M} \simeq \tfrac{1}{2}\frac{\mu}{\omega_A^2}} \qquad [31n]$$

and for kinks:

$$\mathscr{M}_{\text{KINK}} \simeq \frac{1}{20}\frac{\mu}{{\omega_A}^2}. \qquad [31o]$$

The order of magnitude of $\mathscr{M}$ can be obtained by substituting

$$\mathscr{U} \simeq \tfrac{1}{2}\mu b^2$$

and [31e]

$${v_S}^2 = \frac{\mu'}{\rho}$$

into eq. [31k]. The result is

$$\mathscr{M} \simeq \tfrac{1}{2}\rho b^2 \qquad \textit{per unit length.}$$

The mass of a length b of dislocation is $\frac{1}{2}\rho b^3$, or roughly half the mass of one atom.

The Drag Coefficient

At steady state under a constant driving force $b(\sigma - \tau_{\text{LINE}})$, a dislocation moves with a constant velocity. Then, assuming its velocity is sufficiently smaller than that of sound,

$$Bv = b(\sigma - \tau_{\text{LINE}}). \qquad [31p']$$

In crystals with a Peierls potential, the drag force Bv may be due to the lattice friction, and be nonlinear (that is, B may depend on v). But in close-packed crystals without an appreciable lattice friction, B is determined by the interaction of the moving dislocation with phonons, and, at very low temperatures, with electrons; both impose a linear-viscous drag on the moving dislocation.

More than one type of interaction is possible (see LOTHE, 1962; NABARRO, 1967; KLAHN *et al.*, 1970; BRAILSFORD, 1972; GRANATO, 1973). First, thermal shear-stress fluctuations can set the dislocation into fluttering vibration, radiating elastic energy into the crystal (the "flutter mechanism"). Second, the nonlinear elastic strains around a dislocation scatter phonons because of the locally changed lattice compliance, and the changed density near the core of the dislocation scatters both phonons and electrons ("phonon and electron scattering"). Both the flutter mechanism and the scattering mechanisms exert a retarding force because a moving dislocation encounters more phonons from the forward direction than from behind. Third, a moving dislocation builds up and relaxes elastic strains at any point in the lattice. This process is opposed by the same phonon viscosity that damps out elastic waves ("phonon viscosity"). This process, again, applies to electrons also, and may appear as a low-temperature electron drag.

All the phonon mechanisms lead to a drag coefficient of the same general form,

$$\boxed{B \simeq \frac{kT}{\Omega \omega_A}} \qquad [31q]$$

so that the drag controlled steady-state velocity becomes

$$v \simeq \frac{\Omega(\sigma - \tau)}{kT} v_S. \qquad [31r]$$

The interactions become stronger as the temperature rises—although not necessarily according to the simple linear law [31q]. This means that, at constant stress, *the velocity decreases as the temperature rises*, so that a formally defined "activation energy" would be negative:

$$\left.\frac{\partial \ln v}{\partial(-1/kT)}\right|_{\sigma} = -kT. \qquad [31s]$$

Experimental measurement of the drag coefficient is possible in principle though difficult in practice. Three techniques have been used: direct measurement, internal friction studies, and high-strain-rate tensile or compression testing. The "direct" measurement involves measuring the distance moved by a dislocation during a given stress pulse; it gives a lower limit to the instantaneous velocity, thus an upper limit to B. Etch pit (GILMAN and JOHNSTON, 1962) or x-ray imaging techniques (TURNER *et al.*, 1968) have been used to locate the dislocation before and after the stress pulse. Here it is imperative that the applied stress exceed the mechanical threshold considerably, if a linear velocity-stress relation is to be observed (see sec. 32). On the other hand, $v \ll v_S$ must also hold so that

$$\hat{\tau}_{\text{LINE}} \ll \sigma \ll \frac{kT}{\Omega}.$$

These conditions are fulfilled in the experiments of POPE and VREELAND (1969) on zinc, of GORMAN *et al.* (1969) on aluminum, and of JASSBY and VREELAND (1970) on copper; but not in those of TURNER and VREELAND (1970) on iron and in the LiF experiments by JOHNSTON and GILMAN (1959) and by NAGATA and VREELAND (1970).

An indirect measurement of the damping constant can be obtained by studying the macroscopic strain-rate effects, using a tensile machine (FERGUSON *et al.*, 1967). This indirect method is subject to uncertainty since the mobile dislocation density must be known in order to derive B, and can only be determined by a separate experiment.

Internal friction measurements give information from which the mobile dislocation density and the drag coefficient can be derived. Studies must be made at such low strain amplitudes that the dislocations do not have to overcome discrete obstacles, but simply vibrate, like damped elastic strings, between points where they are pinned (ALERS and THOMPSON, 1961; MASON and ROSENBERG, 1967; FANTI *et al.*, 1969). FANTI *et al.* (1969) measured the

dislocation density and (assuming that all dislocations are mobile) combined this information with the frequency of the internal friction peak to give a reliable value for the damping constant.

The three techniques, when they have been properly applied, show broad agreement. The data have been reviewed recently by KLAHN *et al.* (1970). Their compilation shows that, over the temperature range from 4.2 K to 300 K, B lies between 10^{-4} and 10^{-3} dyn sec/cm^2 [that is, between 10^{-5} and 10^{-4} N s/m^2] for most metals and ionic crystals. In general, B increases with temperature, though certain experiments suggest that it becomes independent of temperature close to 0 K.

In Table 3-I, we have listed some room temperature data we consider reliable. (For more data see KLAHN *et al.*, 1970.) It may be seen that eq. [31q] represents these data to within a factor of 2. We will see below (Fig. 31-1) that this is true even for some other temperatures.

Due to many uncertainties, the detailed theories of the phonon and electron drags are themselves no more than order-of-magnitude estimates. Although all of them give a linear temperature dependence in the high temperature approximation, different treatments differ in their predictions for low temperatures. It has sometimes been suggested (GRANATO, 1968) that some of these theories should be related by being different ways of looking at the same physical mechanism. This is important, because additivity of drag requires independence of the different mechanisms of energy dissipation. Below we summarize what we believe to be the physical bases for the most important treatments, both with reference to dislocations and to kinks, and then proceed to compare these with the scant experimental evidence available.

Thermal waves produce local fluctuations in shear stress (LEIBFRIED, 1950). This stress, producing a force on the dislocation element like any other stress, has an amplitude for which an estimate can be obtained from the energy balance in an atomic volume:

$$\frac{1}{2\mu}\,\tau_{\text{THERM}}^2 = \frac{1}{10}\,E_{\text{THERM}} \qquad [31t]$$

where E_{THERM} is the thermal energy density and the factor 1/10 is a close approximation to an exact orientation factor derived by Leibfried, and to which longitudinal waves contribute only negligibly (τ_{THERM} is large: typically $\mu/30$ at 100 K). A free dislocation element oscillates in response to these stresses and to the self stress arising from its connection to other parts of the dislocation. A kink in a dislocation responds directly to the stress given by eq. [31t] (ESHELBY, 1962; LOTHE, 1962).

This *flutter* of the dislocation leads to a *reradiation* of energy proportional to the incident energy [31t], which may be formally described by a scattering radius R_{FLUT} (scattering cross section per unit length of the dislocation). The dislocation element moving with a drift velocity v feels a net force proportional to (v/v_S), in the manner of a radiation pressure, giving rise to a drag coefficient

$$B_{\text{FLUT}} \simeq \frac{1}{10}\,\frac{E_{\text{THERM}}}{\omega_{\text{ATOM}}}\,\frac{R_{\text{FLUT}}}{b}. \qquad [31u]$$

Clearly, the entire physical mechanism is hidden in the scattering radius R_{FLUT}, which was set equal to b by LEIBFRIED (1950) as a "first estimate", while ESHELBY (1962) derived a complicated formula for kinks with widths of a few b, again giving $R_{\text{FLUT}} \simeq b$. In most references to Leibfried, the factor R_{FLUT}/b is simply omitted. We prefer to treat it as an adjustable parameter with the proviso that nothing in

Table 3-I. Some Dynamic Properties at Room Temperature

Shear modulus μ', speed of sound v_S, atomic frequency ω_A, Debye temperature T_D, atomic volume Ω, and the lowest[(a)] observed drag coefficient B for edge dislocations

Property Defin. eq. Reference Units	μ' * (*b*) 10^{10} N m^{-2}	v_{SOUND} [31e] (*c*) km s^{-1}	ω_{ATOM} [31f] 10^{13} s^{-1}	T_{DEBYE} (*c*) K	B [31a] → *Ref.* 10^{-5}N s m^{-2}†	Ω (*c*) Å^3	$\frac{B}{kT/\Omega\omega_A}$ [31q]	$\frac{\mu' b}{B v_S} \simeq \frac{\mu'\Omega}{kT}$ [31z, bb, hh]
Al	2.51	3.06	1.07	428	1.8 (*d*)	16.50	0.8	130
Cu	4.08	2.14	0.84	343	1.7 (*e*)	11.81	0.4	300
Zn	3.83	2.33	0.88	310	5.0 (*f*) 3.7 (*screw*)	13.29	1.4 1.0	110 150
LiF	4.40	4.11	1.44	732	2.4 (*g*)	8.17	0.7	130
NaCl	1.63	2.73	0.69	321	1.6 (*g*)	22.41	0.6	140

* $\mu' = (c_{11}-c_{12}+c_{44})/3$ for fcc, $\mu' = c_{44}$ for cph basal glide. † 10^{-4} dyn s cm^{-2}.

References:

(*a*) T. VREELAND, JR. and K. M. JASSBY (1971) *Mater. Sci. Eng.* **7**, 95.
(*b*) H. B. HUNTINGTON (1958) *Solid State Physics* (SEITZ and TURNBULL, eds.) **7**, 213.
(*c*) *American Institute of Physics Handbook*, 2nd ed. 1963: McGraw-Hill.
(*d*) J. A. GORMAN, D. S. WOOD, and T. VREELAND, JR. (1969) *J. Appl. Phys.* **40**, 833.
(*e*) K. M. JASSBY and T. VREELAND, JR. (1970) *Phil. Mag.* **21**, 1147.
(*f*) D. P. POPE and T. VREELAND, JR. (1969) *Phil. Mag.* **20**, 1163.
(*g*) F. FANTI, J. HOLDER, and A. V. GRANATO (1969) *J. Acoust. Soc. Am.* **45**, 1356.

the mechanism should let R_{FLUT} depend on temperature or velocity in any sensitive way, for $v/v_s \ll 1$.

While the flutter mechanism discussed above relies on the force exerted by any stress field on an elastic incompatibility, there is also an interaction between two elastic fields that is due to *nonlinear elasticity*: when two stress fields superpose nonlinearly, there is an interaction energy that is temporarily stored during the time of the superposition and is then released again to the thermal reservoir. This mechanism is therefore intimately linked to some transport property. For this reason, and for the reason that nonlinear dislocation effects are hard to treat, no detailed theory seems to be available.

Formally, one may again describe it by a scattering radius, R_{NONL}. Since *all* components of the "thermal stresses" are subject to this scattering mechanism, the orientation factor 1/10 in eq. [31u] would be missing:

$$B_{NONL} \simeq \frac{E_{THERM}}{\omega_{ATOM}} \frac{R_{NONL}}{b}. \qquad [31v]$$

NABARRO (1951) provided an estimate that shows the effect to be negligible. SEEGER and ENGELKE (1968, p. 623) claim that it is important for wide kinks, and obtain an expression of the same order as [31u]. (They show it to be large compared to the flutter contribution from *longitudinal* waves, which, however, is itself negligible.)

Finally, phonons can interact with the strain field of a dislocation in the same way they interact with each other, whether the strain field is linear-elastic or not. The effect is due to the dependence of the phonon spectrum on volume and other strains (MASON, 1960) and involves transfer of energy between different volume elements ("thermo-elastic effect") or between different modes of the phonon spectrum ("phonon viscosity", MASON, 1960, 1968) as the strain in each volume changes when a dislocation moves. This effect too depends on a transport property: in the case of the thermo-elastic effect on the total thermal resistance (appreciable only in insulators); in the case of the phonon viscosity effect on the mean free path Λ_{pp} for phonon–phonon interactions. For the latter effect, MASON (1968) derives a formula (his eqs. 4 and 12) which reads, in slightly rephrased terminology,

$$B_{MASON} \simeq \frac{1}{15} \frac{E_{THERM}}{\omega_{ATOM}} \frac{b\Lambda_{pp}}{r_p^2}, \qquad [31w]$$

where the proportionality factor depends on the relative magnitude of the nonlinear elastic constants and r_p is an inner cut-off radius appropriate to this macroscopic theory, which turns out to be its most important parameter. While MASON sets it to be slightly less than b, other authors (e.g. LOTHE, 1962) have argued that it should be equal to the phonon mean free path so that (his eqs. 10–15)

$$B_{LOTHE} \lesssim \frac{1}{2} \frac{E_{THERM}}{\omega_{ATOM}} \frac{b}{\Lambda_{pp}} + B_{CORE}. \qquad [31x]$$

Since Λ_{pp} is generally larger than about $10b$, the selection of the cut-off parameter can change the predicted value of the drag coefficient by a large amount—even though we have inserted, in eq. [31x], an upper estimate of the proportionality constant derived by LOTHE in a different way and have added a core relaxation contribution given by LOTHE (his eqs. 36, 37). Since Λ_{pp} rises substantially as the temperature is lowered, the predicted temperature dependence would also be noticeably different. At the present time, we regard the question as unsettled. For kinks there should be little phonon viscosity drag on account of the absence of a far-reaching strain field.

In all these theories the drag coefficient is proportional to the thermal energy density E_{THERM}, the temperature dependence of which is given by the Debye theory.

(BRAILSFORD, 1972, derived a somewhat less sensitive function of temperature.) The only disagreement in the literature is about the zero-point energy $\frac{9}{8}kT_{\text{DEBYE}}$ (T_{DEBYE} = Debye temperature), whether it should be included (LEIBFRIED, 1950) or not (LOTHE, 1960; ESHELBY, 1962). If it is not, we have, with the atomic specific heat c_v,

$$E_{\text{THERM}} = \frac{1}{\Omega}\int c_v \, dT \qquad [31y]$$

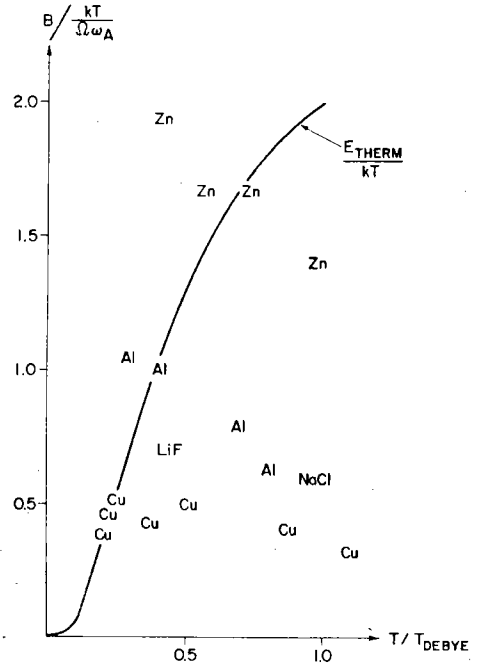

FIG. 31-1. Observed drag coefficient B, divided by the order-of-magnitude estimate (eq. [31q]), as a function of temperature. The points should follow the solid line if B were proportional to the thermal energy density E_{THERM} (eqs. [31t] through [31y]). References as in Table 3-I.

which tends to $k(3T - T_{\text{DEBYE}})/\Omega$ for high temperatures; a good approximation for all temperatures above half the Debye temperature is $2kT/\Omega$, instead of $3kT/\Omega$ as is often used. At lower temperatures, the value of E_{THERM}/kT decreases in the manner shown in Fig. 31-1. It is seen that the experimental temperature dependence agrees at least as well with the order-of-magnitude formula (31q) than with one in which the kT-term is replaced by E_{THERM}. A similar conclusion was reached by ALERS and THOMPSON, 1961. (See, however, recent experiments by HIKATA *et al.*, 1970, on Al, and 1972 on NaCl.)

We now turn to the motion of a dislocation through a crystal with an appreciable Peierls potential. If the driving force is less than the Peierls stress ($b\tau_p$ per unit length), then the dislocation can only move by the thermally activated penetration of the Peierls hills. We discuss this in Chapter 5: the dislocation moves as if acted on by a drag which is (usually) strongly nonlinear. Here we are concerned with driv-

ing forces which *exceed* $b\hat{\tau}_P$, when the dislocation velocity is limited by some other energy-dissipating process.

One such mechanism was proposed by OROWAN (1940) and has been re-examined by HART (1955a). Suppose the dislocation energy fluctuates through an amplitude $a\mathscr{U}$, with a wavelength b, as it moves through the lattice. Then an oscillatory motion is superimposed on the steady motion of the dislocation resulting in the radiation of elastic energy into the crystal which must be supplied by the external stress (NABARRO, 1967, p. 510). The resulting drag, B_{OSC}, at first increases with v, then reaches a maximum resembling a damped resonance peak at which a maximum occurs in the radiated energy, and finally, at high velocities, decreases again towards zero.

If the Peierls barrier has any significant height, the velocity of a dislocation under a driving force which exceeds $\hat{\tau}_P\, b$ is large; so large, in fact, that B_{OSC} is rarely, if ever, important. The steady part of the dislocation motion is then limited either by the linear drags discussed earlier, or by relativistic effects as the dislocation approaches the speed of sound.

As the dislocation approaches the velocity of sound, larger drags operate on it. This is in part because the mechanisms described above are linear at low velocity only ($v \ll 0.5v_S$); as the speed of sound is approached the mechanisms become nonlinear, exerting an increasingly large drag on the moving dislocation. It is in part because the relativistic contraction of the dislocation causes its elastic energy to increase rapidly when $v > 0.5v_S$; and most drag mechanisms are linked to the dislocation energy. Finally, new mechanisms for radiating energy not significant at low velocities come into play. The net result is that, above $\frac{1}{2}v_S$, the dislocation dissipates energy at a steeply increasing rate.

In a linear-elastic continuum, the velocity of a dislocation would be limited to a maximum value of v_S since its energy would then become infinite. The discrete atoms of a crystal actually set a limit to the relativistic contraction of the stress field, and allow, at least in principle, dislocations to achieve supersonic velocities. Such high speeds are rare. In subsequent sections, we shall assume that an upper limiting velocity, equal to v_S is imposed on the dislocation motion. The stress is then limited to values

$$\frac{\sigma}{\mu} < \frac{\sigma_{LIM}}{\mu} \equiv \frac{Bv_S}{\mu b} \simeq \frac{kT}{\mu\Omega}. \qquad [31z]$$

Table 3-I includes this limit for some materials. For others, it may be estimated by the last expression in [31z], given by [31q].

Inertial Effects

We have now considered the *mass* $\mathscr{M}$ of a dislocation in connection with the kinetic energy it carries while moving at constant velocity; and we have considered the *drag coefficient* B in connection with the dissipation of energy while a dislocation moves at its steady-state velocity under an essentially constant driving force. Nonuniform motion has entered only through the rapid oscillations that may be superposed on the "essentially constant"

velocity due to thermal fluctuations or periodic variations in glide resistance.

A dynamic interaction between mass forces and drag forces comes into play when the driving force varies abruptly: for example, when the applied stress is suddenly dropped, or when the dislocation suddenly experiences an increased glide resistance by, say, running into an isolated barrier. In principle, the kinetic energy must then be dissipated before the dislocation comes to rest. Under certain circumstances, a dislocation may be able to overcome an obstacle by *inertia*: when the mass is large, the drag coefficient small, and the change in net driving force abrupt.

Such inertial effects have, in the past, been largely neglected: dislocations have been considered to be *overdamped*, i.e. moving at their drag-limited velocity, at all times. There are two reasons for this. First, the time constant of the equation of motion [31a],

$$t_{\mathrm{ACC}} \equiv \frac{\mathcal{M}}{B} \qquad [31aa]$$

is very short. Inserting the value [31n] for the mass, we find that, in units of lattice vibrations, it is just half the value given in Table 3-I for $\mu/\sigma_{\mathrm{LIM}}$:

$$t_{\mathrm{ACC}}\,\omega_{\mathrm{A}} = \frac{1}{2}\frac{\mu b}{B v_{\mathrm{S}}} \simeq \frac{1}{2}\frac{\mu\Omega}{kT} \qquad [31bb]$$

or of the order of 100 at room temperature. This means that any oscillatory motion of the dislocation with a frequency of less than about 10^{11} Hz is overdamped at room temperature. Reliable measurements at frequencies as high as this have not yet been achieved. Thus, internal friction studies always show dislocations to be overdamped. The time t_{ACC} also measures the time the dislocation takes to accelerate to a new steady velocity when the force acting on it is suddenly changed—and for most practical purposes t_{ACC} is so short that the new steady velocity can be considered to be reached instantaneously.

A second reason for ignoring inertial effects in the past has been the practice of considering long dislocations impeded only by an average plane glide resistance. Yet the glide resistance, even when it is averaged along the dislocation line, varies substantially with distance traveled: from positive to negative when little energy is stored. Moreover, the glide resistance sampled by individual elements of the dislocation varies much more widely (Fig. 25-10) if the dislocation has not reached equilibrium shape. Thus, dislocation elements in real materials experience rapidly changing driving forces, and the possibility of inertial effects must be considered.

When one deals with the small dimensions and short times for which inertial effects may be important, the macroscopic concept of a drag coefficient may no longer be valid. For a rough estimation,* we shall neverthe-

* GRANATO (1971) independently developed a treatment of inertial effects similar to the one developed here but based on the string model. He emphasizes the fact that B becomes small at temperatures near absolute zero, and that it is here that inertial effects will be most important. He has applied his model to the observed increased plasticity in the superconducting state, with considerable success.

less use the equation of motion [31a] with the values for material properties $\mathscr{M}$ and B as given above. For this purpose, we rewrite eq. [31a] in the following dimensionless form:

$$\frac{B}{b\hat{\tau}}\,dv = \frac{\sigma - \tau}{\hat{\tau}}\,\frac{B}{\mathscr{M}}\,dt - \frac{B^2}{\mathscr{M}\hat{\tau}}\,\frac{dy}{b} \qquad [31cc]$$

with

$$v = \frac{dy}{dt}.$$

(All τ's are line glide resistances in this section, and we have referred all stresses to their maximum, $\hat{\tau}$. For some general applications, one may instead wish to normalize with the shear modulus μ.)

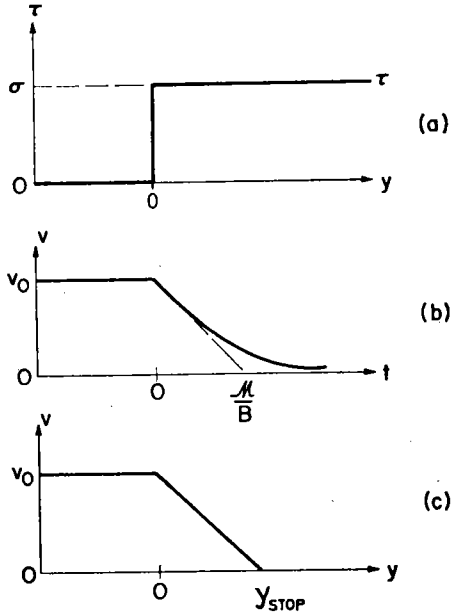

FIG. 31-2. Velocity v of a dislocation for which the line glide resistance τ abruptly rises from zero to the level of the applied stress σ.

An important characteristic of the behavior expressed by eq. [31cc] is the "stopping distance". It can be easily derived by considering the case where a kink or other dislocation element, which has an initial velocity v_o, suddenly finds itself under zero driving force (Fig. 31-2); then the term with the time differential vanishes. By setting $dy = v\,dt$, one can immediately see the exponential decay (Fig. 31-2b) of the velocity with *time*; the relation between the *distance* y and the velocity is seen to be linear. The velocity becomes zero when the distance traveled is

$$y_{STOP} = v_o \frac{\mathscr{M}}{B}. \qquad [31dd]$$

(This also holds as a first approximation when the driving force is negative, where the distance y_{STOP} in eq. [31dd] now defines the point at which the dislocation reverses direction.) Since we have seen that $\mathscr{M}/B$ is generally less than $100b/v_S$ at room temperature (eq. [31aa], Table 3-I), the dislocation comes to rest in a distance smaller than b if its initial velocity $v_o < v_S/100$.

If v_o was the steady-state velocity under an applied stress σ in an obstacle-free region, eq. [31dd] becomes, with eqs. [31n] and [31q],

$$\frac{y_{STOP}}{b} = \frac{\sigma}{\mu}\frac{\mu\mathscr{M}}{B^2} = \frac{\sigma}{\mu}\frac{1}{2}\left(\frac{\mu b}{Bv_s}\right)^2 \simeq \frac{\sigma}{\mu}\frac{1}{2}\left(\frac{\mu\Omega}{kT}\right)^2. \qquad [31ee]$$

To provide an order-of-magnitude estimate, we list below the stopping distances and velocities of dislocations that moved under $\sigma \simeq 10^{-4}\mu$ (both quantities are linear in stress), for $\mu b/Bv_S \simeq 140$ as an average at room temperature from Table 3-I.

Table 3-II

T [K]	30	100	300
v/v_S	1/7	1/20	1/70
y_{STOP}/b	100	10	1

The kinetic energy of the dislocation helps to overcome an obstacle when a characteristic width, y_o, of the obstacle becomes smaller than this stopping distance, i.e. when

$$\boxed{\frac{y_o}{b} < \frac{\mathscr{M}\hat{\tau}}{B^2} \simeq \frac{1}{2}\left(\frac{\hat{\tau}\Omega}{kT}\right)^2.} \qquad [31ff]$$

This is reminiscent of the condition for subcritical damping of a harmonic oscillator, i.e. a linearized obstacle:

$$\frac{dy}{a\hat{\tau}b} < 4\frac{\mathscr{M}}{B^2}. \qquad [31gg]$$

To determine the effects to be expected for some idealized obstacles, numerical solutions for eq. [31cc] have been obtained (KOCKS, unpublished work). Figure 31-3 shows the results for sinusoidal isolated linear barriers, 10 wavelengths λ apart. When the parameter (eq. [31ff]), $y_o/y_{STOP} = B\lambda/(4\mathscr{M}b\hat{\tau})$, with $y_o = \lambda/4$, assumes values of the order 1 or below, the obstacles are in fact overcome dynamically at stresses substantially below $\hat{\tau}$. It is also seen that, once they are so overcome, the average velocity of the dislocations is essentially the drag-controlled one. One can thus speak of a *dynamic theshold.*

A number of other glide resistance diagrams have also been investigated, among them an isolated inverse square, and a continuous sinusoidal variation. For the

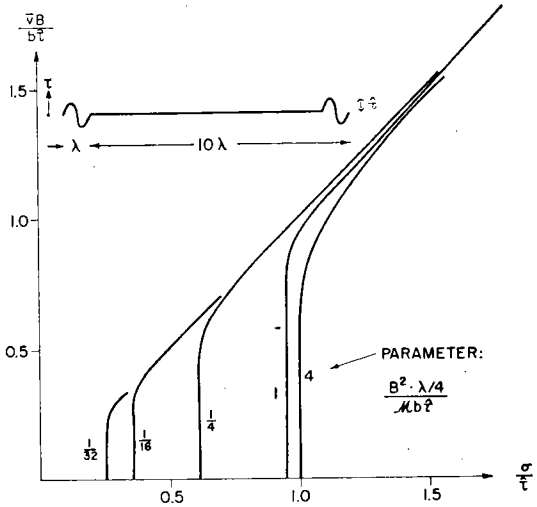

FIG. 31-3. Computer results for the dynamic behavior of a dislocation (or kink) under the influence of a constant applied stress σ and a variable line glide resistance τ as shown.

latter, it was assumed that the average velocity over each period was constant; the dislocation would have had to be brought to this velocity by a higher initial stress or by a preceding obstacle-free area. In both of these cases, the dynamic threshold varied with the parameter in the same manner as in Fig. 31-3.

A slightly different behavior is shown by attractive obstacles, where the driving force first increases, then decreases. Here, the dislocation element can first accumulate additional kinetic energy, which then helps it overcome the repulsive part at even lower stresses.

The results are combined in Fig. 31-4 which shows the dynamic threshold τ_{DYN} as a fraction of the static threshold, $\hat{\tau}_{LINE}$, plotted against the normalized range of the obstacle. At stresses just below this line, a dislocation would have some kinetic energy left when it first arrives at a position of zero driving force; subsequent thermal activation may therefore be somewhat affected though we expect the effect to be small.

These relations were derived under the assumption that the dislocation will follow the same path under dynamic and static conditions. We do not expect this to be true for bowing dislocations, but consider it to be probably correct for kinks.

It remains for us to assess some practical conditions under which these dynamic effects could occur—again providing the macroscopic parameters remain appropriate. The structure independent material property that determines the critical dimensions may be expressed as

$$\frac{B}{\sqrt{\mu\mathcal{M}}} \simeq \frac{Bv_s}{\mu b} \simeq \frac{kT}{\mu\Omega}. \qquad [31hh]$$

These quantities can be calculated for the cases where B is known experimentally, and may be estimated by the above relation for others. Table 3-I

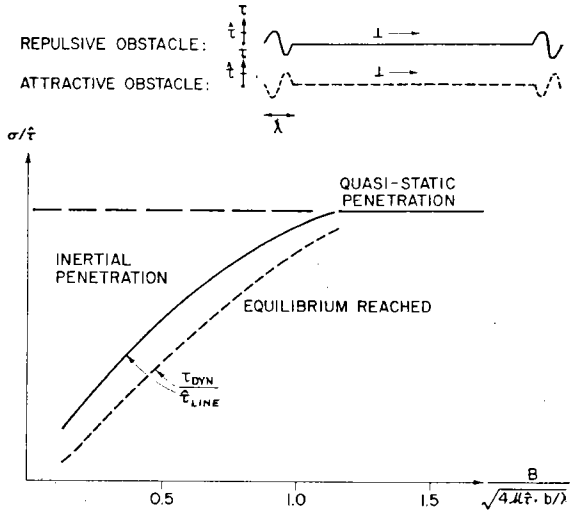

FIG. 31-4. Dynamic threshold τ_{DYN}, over static threshold $\hat{\tau}_{LINE}$, as a function of the drag coefficient B and the mass $\mathcal{M}$ of the dislocation per unit length, and of the stiffness $\hat{\tau}/\lambda$ of the obstacle.

listed the inverse of this parameter for some materials at room temperature; it is the same as $2t_{ACC}\omega_A$ (eq. [31bb]) or as μ/σ_{LIM} (eq. [31z]).

The values in the table refer to dislocations. For sharp kinks, we expect the mass to be substantially smaller (eq. [31o]) and the damping to be somewhat smaller (since the phonon viscosity mechanism does not contribute). The ratio [31hh] may thus be unaffected in first order.

For obstacles of a width of no more than a few b, we should thus expect inertia effects when (eq. [31ee])

$$\frac{\hat{\tau}_{LINE}}{\mu} > 5\left(\frac{kT}{\mu\Omega}\right)^2. \qquad [31ii]$$

Even at room temperature, such a maximum ~~element~~ line glide resistance may be achieved with a number of atomic-size obstacles. At low temperatures, it is hard to see how dynamic effects can be avoided.

Some ways in which inertial effects might be observed are: a lowering of the observed flow stress with decreasing temperature according to Fig. 31-4; a dependence of the flow stress on the superconducting or normal state through the corresponding change in the drag coefficient (see also GRANATO, 1971); the possibility of a very mild solution softening for solutes that attract kinks; and the absence of normal annihilation between kinks of opposite sign under a certain applied stress.

All these effects rely on the *short range* of the barrier. For example, two *dislocations* of opposite sign, which have a much longer range of interaction than two kinks, annihilate each other even at very high stresses.

The most important case of any effectively long-range interaction is that of strong discrete obstacles; namely those whose cutting is accompanied by significant dislocation bow-outs. Although the work of FROST and ASHBY (1971) suggests that the bowing may in fact not proceed to its equilibrium extent, the considerable compliance associated with any bowing (eqs. [31d] and [25t]) makes the effective y_o in eq. [31ff] always larger than the stopping distance.

When the discrete obstacles are weak and closely spaced, the degree of bow-out is small; so small in fact that we doubt the applicability of the bowing concept to this situation. Whether the bowing mechanism is used or the motion of kinks, weak obstacles may well be overcome inertially at high stresses or low temperatures.

32. KINETICS OF CONTINUOUS GLIDE

Long-range dislocation motion can be classified in one of two categories: continuous glide or jerky glide. In the former, the applied stress is above the (static or dynamic) mechanical threshold everywhere and, while dislocations may move with varying speed, they must always move. In jerky glide, which will be considered in sec. 33, the applied stress is below the mechanical threshold in at least some places, so that dislocations are occasionally stopped; they may be released by thermal fluctuations (Chapter 4). In the following, we treat continuous glide of a single dislocation at a varying, drag-controlled velocity, and then proceed to consider the superposition of the movement of *many* dislocations in continuous glide.

Drag over a Varying Glide Resistance

In the preceding section we have, in the main, discussed dislocations and kinks under constant driving force. Only *rapid or short-range* variations in glide resistance were considered, with respect to their influence on acceleration losses and on inertial penetration. We now turn to the very common case of *slow or long-range variations in glide resistance*, such as it would occur in the presence of internal stresses.

The velocity may then be assumed to attain its drag controlled limit [31p] everywhere—provided it does not get too close to the velocity of sound. This condition imposes an *upper* limit to the stresses to be admitted (eq. [31z]); a *lower* limit is the maximum line glide resistance. Thus, for continuous glide:

$$\hat{\tau}_{\text{LINE}} < \sigma < \frac{kT}{\Omega}. \qquad [32a]$$

For simplicity, we will first consider a one-dimensional variation in glide resistance: either due to *linear* barriers to the motion of *dislocations*, or due to *any* kind of obstacle to the motion of *kinks*. The glide resistance may then be described by $\tau \equiv \tau_{\text{LINE}} = \tau_{\text{ELEM}}$. The average velocity is obtained by

dividing the periodicity distance λ by the integrated time spent at all positions:

$$\bar{v} = \frac{\lambda}{\int_0^\lambda \frac{dy}{v}} \qquad [32b]$$

or

$$\frac{1}{\bar{v}} = \frac{1}{\lambda}\int_0^\lambda \frac{B\,dy}{b[\sigma - \tau(y)]}. \qquad [32c]$$

For a sample calculation with some generality, we take a sinusoidal variation of the line glide resistance (ARSENAULT and LI, 1967; ARGON, 1968; KLAHN *et al.*, 1970), but with a non-zero mean value:

$$\tau = \tau_{\text{STOR}} + \tilde{\tau}\sin\frac{2\pi y}{\lambda}. \qquad [32d]$$

The source of this glide resistance is usually assumed to be an internal stress. As an example, a square array of dislocations of strength b leads to a fluctuating internal stress which can be approximated by eq. [32d] with

$$\tau_{\text{STOR}} = 0; \quad \tilde{\tau} = \hat{\tau}_{\text{INT}} \simeq \frac{\mu b}{\lambda} \qquad [32e]$$

and eq. [32d] can be thought of as the principal Fourier component of the real internal stress. (If, instead, groups of n dislocations of the same Burgers vector are arrayed on a square lattice, $\tilde{\tau}$ is greater by the factor n, but the dislocations can move in cooperative groups and the effective amplitude is the same as eq. [32e], see eq. [24r].)

Insertion of [32d] into [32c] then gives an elementary integral with the solution

$$\bar{v} = \frac{b}{B}\sqrt{(\sigma - \tau_{\text{STOR}})^2 - \tilde{\tau}^2}. \qquad [32f]$$

This relation is plotted in Fig. 32-1. It gives zero velocity for

$$\sigma \leq \hat{\tau} = \tau_{\text{STOR}} + \tilde{\tau} \quad \text{and approaches} \quad \bar{v} = \frac{b(\sigma - \tau_{\text{STOR}})}{B}$$

for high stresses. Note, however, that the deviation from a straight line through the origin is still substantial at $\sigma = 2\hat{\tau}$.

One may now wish to define an "effective stress" σ_{eff}, or an "average driving force" $b\sigma_{\text{eff}}$, by

$$b\sigma_{\text{eff}} \equiv B\bar{v} \qquad [32g]$$

which (from [32f]) is the *geometric mean* of the local driving forces:

$$\sigma_{\text{eff}} = \sqrt{(\sigma - \tau_{\text{MAX}})(\sigma - \tau_{\text{MIN}})}. \qquad [32h]$$

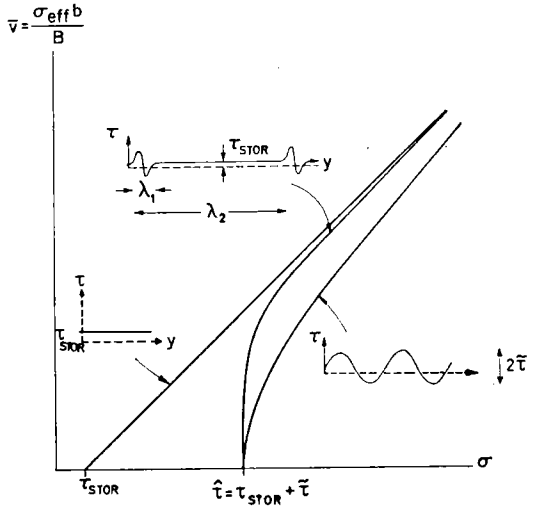

FIG. 32-1. Average velocity $\bar{v}$ or equivalently effective stress σ_{eff}, as a function of an applied stress σ larger than the maximum $\hat{\tau}$ of the variable line glide resistance. Only a *constant* $\tau = \tau_{STOR}$ gives a linear relation.

Finally, one may write for the case of internal stresses (which must average to zero, as in equation [32e])

$$\sigma^2 = \hat{\tau}_{INT}^2 + \sigma_{eff}^2. \qquad [32i]$$

In other words, the *square* of the internal stress and the *square* of the effective drag resistance add to give the *square* of the applied stress.

While the term "effective stress" is often used in a context that implies the same definition we have used here (eq. [32g]), it is nevertheless usually assumed to be linearly additive to the internal stress. This does hold trivially on a local basis, but not on an average. The "local effective stress" (times b) is what we have here called "driving force". Note again that, in this context, "internal stresses" are in no way different from any other glide resistances we have considered (e.g. incoherent inclusions). We shall encounter one more definition of an "effective stress": this is merely the component of the flow stress provided by one of two threshold mechanisms (usually when the other is athermal). We shall use the term *only* in the sense of eq. [32g].

Figure 32-1 also shows the results for a glide resistance profile consisting of a series of single periods of a sine curve of wavelength λ_1, spaced λ_2 apart, with only the uniform energy-storing τ_{STOR} in between. Again, one merely has to add the times spent over the distance λ_2, with the result

$$\bar{v} = \frac{b\bar{\sigma}_{eff}/B}{\frac{\lambda_1}{\lambda_2} + \frac{\bar{\sigma}_{eff}}{\sigma - \tau_{STOR}}\frac{\lambda_2 - \lambda_1}{\lambda_2}} \qquad [32j]$$

where $\bar{\sigma}_{eff}$ refers only to the sine part (eq. [32h]). This kind of behavior may be relevant, for example, to the motion of kinks along a dislocation with solute atoms on it. The velocity closely approaches the drag limited value immediately above $\hat{\tau}$.

Discrete obstacles present a more complicated problem. At the lowest level of approximation, the obstacles introduce a mechanical threshold $\hat{\tau}_{\text{LINE}}$. One could regard this as the peak value of an oscillating internal stress, when (according to the reasoning above) the dislocation velocity would be given by

$$\bar{v} = \frac{\sigma_{\text{eff}}\, b}{B} \qquad [32k]$$

with

$$\sigma_{\text{eff}} = \sqrt{\sigma^2 - \hat{\tau}^2} \qquad [32\ell]$$

leading to a velocity-stress diagram of the same form as that of Fig. 32-1. More detailed treatments of the way in which a dislocation bows between and by-passes, or cuts, the discrete obstacles shows that this is a reasonable qualitative description (FROST and ASHBY, 1971; KLAHN *et al.*, 1970). A diagram, calculated by considering the rate of bowing of the dislocation between the obstacles, will be shown later (Fig. 34-3).

Kinematic Equations

A *kinematic equation* relates the microscopic motion of dislocations to the macroscopic strain. In what follows, we limit ourselves to motion on one slip system only; slip on several systems presents no new problems and can be handled along the lines described in sec. 22 (cf. KOCKS, 1970a).

In the simplest case the element glide resistance is zero everywhere (no obstacles are present). All dislocations remain straight and move at a velocity determined only by a drag coefficient and the applied stress; and every part of every dislocation moves with the same velocity. If the total length of dislocation per unit volume is ρ_m, the area da swept out during an increment of strain dγ is $V\rho_m \mathrm{d}y$ so that (eq. [22c]):

$$\mathrm{d}\gamma = b\rho_m\, \mathrm{d}y \qquad [32m]$$

or

$$\dot{\gamma} = b\rho_m\, v. \qquad [32n]$$

In the case of *linear barriers* to kink or dislocation motion, the velocity of each element varies with time; eq. [32b] gave a prescription for obtaining the average velocity $\bar{v}$ over a period of the glide resistance diagram. With it, we may write

$$\dot{\gamma} = b\rho_m \bar{v}. \qquad [32o]$$

When many dislocations are moving in the crystal, they sample different regions of the glide resistance diagram in the same way an individual dislocation does in the course of time. The *instantaneous strain rate*, which follows directly from the basic kinematic relation [22c],

$$\dot{\gamma} = \frac{b}{V}\int_0^{\rho_m V} v\, \mathrm{d}\xi \qquad [32p]$$

is thus, in this case, the same as the long-term average. We may use eq. [32o] for continuous glide in general, with the *spatial average velocity* defined by

$$\bar{v} \equiv \frac{1}{\rho_m V} \int_0^{\rho_m V} v \, d\xi. \qquad [32q]$$

Equations [32p] and [32q] are usable even when the glide resistance diagram varies in both dimensions in the slip plane. The velocity will then not be the same for different elements of the same dislocation, just as before it was not the same for different dislocations. The integral over $d\xi$ runs over *all* elements of all dislocations. The time average is here not easily obtained in detail, primarily because the dislocations do change length on a local basis. The integrals in eqs. [32p] and [32q] assume that the total dislocation length is very large: there will then always be regions in which the dislocation length decreases and others in which it increases, so as to keep $\rho_m V$ constant. For the *instantaneous* strain rate, to reiterate, eq. [32p] is completely general and, for example, not restricted to large dislocation lengths.

When dislocation motion must be considered as motion of kinks along the dislocation line, the velocity of the dislocation is given by

$$v = v_{KINK} \, \lambda / x_{KINK} \qquad [32r]$$

where v_{KINK} is the kink velocity along the dislocation, λ the height of the kink, and x_{KINK} the instantaneous average spacing of running kinks along the dislocation. The strain rate becomes

$$\dot{\gamma} = b \cdot \rho_m \frac{\lambda}{x_{KINK}} \cdot \bar{v}_{KINK}. \qquad [32s]$$

The center term may be regarded as the total length of *kinks* per unit volume.

The Mobile Dislocation Density

The macroscopic strain rate is, according to eq. [32o], proportional to the mobile dislocation density ρ_m. This quantity has been the subject of much discussion. The main questions are: what relation does ρ_m bear to the *total* dislocation density such as might be measured in electron micrographs or etch ~~discussion. The main questions are: what relation bears ρ_m to the *total* dislocation density such as it might be measured in electron micrographs or etch~~ pit studies; can ρ_m change *instantaneously* with a change in external variables such as the stress; and, can either this instantaneous or a steady-state value of ρ_m depend *sensitively* on the stress?

In a material with *zero* glide resistance, in which flow is controlled only by drag, *all* dislocations should be mobile. For the present treatment of continuous glide, we have not demanded that the glide resistance be zero, only that it be smaller than the applied stress everywhere (eq. [32a]). One may, however, be willing to admit the presence of *some* dislocations for which the glide resistance exceeds the applied stress; for example, dislocations in dipoles

by some impurity; or Lomer–Cottrell locks. Such dislocations would be seen in electron micrographs and might contribute to the glide resistance, but they would not contribute to strain.

When such immobile dislocations are present, it is conceivable that some of them might become mobile by the sole action of an increase in stress; then, the mobile dislocation density could increase instantaneously. We consider such mechanical release a part of jerky, rather than continuous, glide and shall treat it in the next section.

Even at constant stress, however, there must be some generation of mobile dislocations. This is because mobile dislocations tend to disappear as a consequence of their very mobility: they may exit through the surface or annihilate each other on the way, or be trapped to form dipoles. It can easily be estimated that the strain achieved before a reasonable initial mobile density has been decimated is very small. Continued flow thus depends on a mechanism to generate new mobile dislocations at sources or to multiply dislocations as they move.

The kinetics of the development of a mobile dislocation density ρ_m are then described by a differential equation stating that the net increase in ρ_m per unit time equals the rate of generation minus the rate of trapping. Let the rate of trapping be described by a mean free path y_m, and the rate of generation, for a simple example, by the sufficient decrease of the back stress on (linear) sources of density ρ_{SOURCE} after previously emitted dislocations have traveled a distance y_{BACK}; then the kinetic balance reads

$$\frac{d\rho_m}{dt} = \rho_{SOURCE} \frac{\bar{v}}{y_{BACK}} - \rho_m \frac{\bar{v}}{y_m}. \qquad [32t]$$

This equation may have a steady-state solution, i.e. such that the left-hand side vanishes; when any initial mobile dislocation density does not happen to have the appropriate steady-state value, eq. [32t] describes the development of ρ_m with time.

The physical content of eq. [32t] depends on the mechanisms that prescribe ρ_{SOURCE}, y_{BACK}, and y_m; they may depend on the applied stress σ, on ρ_m, and, of course, on various structure constants. For example,

$$\rho_{SOURCE} = \text{const} \qquad [32u]$$

would be true for fixed sources, but

$$\rho_{SOURCE} \propto \rho_m \qquad [32u']$$

would describe a multiplication mechanism of the mobile dislocations;

$$\frac{1}{y_{BACK}} \simeq 2\pi \frac{\sigma - \hat{\tau}_{PLANE}}{\mu b} \qquad [32v]$$

would mean that the source feels the back stress from the last dislocation which it previously emitted; whereas

$$\frac{1}{y_{\text{BACK}}} \simeq \sqrt{\rho_m} \qquad [32v']$$

would only demand that the back stress must decrease below the level of the random stresses at the source due to other mobile dislocations.

The mean free path y_m may be given by a structure constant, such as the distance to the free surface, as suggested above. However, one must consider the interaction between mobile dislocations on different slip planes. The average spacing d to the next slip plane on which another mobile dislocation moves in the opposite direction, while one mobile dislocation traverses its free path y_m is given by

$$\rho_m = \frac{1}{2y_m d}. \qquad [32w]$$

But the stress necessary for these dislocations to pass each other (OROWAN, 1941) is of order

$$\hat{\tau}_{\text{INT}} \simeq \frac{\mu b}{4\pi} \frac{1}{d} \qquad [32x]$$

and must be added to the glide resistance (i.e. to its maximum value $\hat{\tau}_{\text{PLANE}}$, if the wavelength with which τ varies is small compared to d, see sec. 53), and the sum must, by the premise of continuous glide, be smaller than the applied stress:

$$\sigma - \hat{\tau}_{\text{PLANE}} - \hat{\tau}_{\text{INT}} \geqslant 0. \qquad [32y]$$

This puts an upper limit on the mean free path y_m, which corresponds to dipole trapping (eqs. [32w], [32x], and [32y]):

$$y_m = \frac{1}{2\rho_m d} \leqslant 2\pi \frac{1}{\rho_m b} \frac{\sigma - \hat{\tau}_{\text{PLANE}}}{\mu}. \qquad [32z]$$

Inserting this upper limit into the kinetic equation [32t], along with the assumptions [32u] and [32v] for ρ_{SOURCE} and y_{BACK}, respectively, gives a steady-state mobile dislocation density

$$\rho_m \simeq 2\pi \sqrt{\rho_{\text{SOURCE}}} \cdot \frac{\sigma - \hat{\tau}_{\text{PLANE}}}{\mu b} \qquad [32aa]$$

or, with the alternative assumptions [32u'] and [32v'],

$$\rho_m \propto \left(\frac{\sigma - \hat{\tau}_{\text{PLANE}}}{\mu b} \right)^2. \qquad [32aa']$$

The foregoing examples illustrate that the mobile dislocation density can have a steady-state value that depends on a small power of the excess stress (over the maximum glide resistance). Such a relation is very similar to that between *velocity* and stress in the continuous-glide regime (Fig. 32-1). The *product* of mobile density and velocity, i.e. the strain rate, can thus not even give any approximate information on either one of the factors. However, we have seen that a decrease in stress in a time interval short compared to y_m/v cannot change ρ_m, while it can certainly change v. We shall return to questions relating to measurable parameters in Chapter 6.

Certain combinations of mechanisms cannot lead to a steady state of the mobile dislocation density for finite ρ_m (e.g. eqs. [32u'], [32v] and constant y_m), but it is

unlikely that they play any role. Finally, the steady state may not be reached in practical cases; an example is treated in the following.

The mobile dislocations may directly contribute to a glide resistance through their mutual interaction: even when they do not trap each other, the mobile dislocations of opposite sign, which move in opposite directions, exert varying internal stresses on each other. HAASEN (1962) assumed that, in a first approximation, the internal stress experienced by one dislocation varies sinusoidally with distance traveled, with an amplitude equal to the mean passing stress:

$$\tau_{INT} \simeq \frac{\mu b}{2\pi} \rho_m^{1/2} \sin 2\pi y \rho_m^{1/2}. \qquad [32bb]$$

If the dislocation maintains the drag controlled velocity appropriate to the driving force $\sigma - \tau_{INT}$ at all points, and there is no other glide resistance, the average velocity is (eq. [32f]):

$$\bar{v} = \frac{b}{B} \sqrt{\sigma^2 - \left(\frac{\mu b}{2\pi}\right)^2 \rho_m} \qquad [32cc]$$

and thus the strain rate

$$\dot{\gamma} = \frac{b^2 \rho_m}{B} \cdot \sigma \cdot \sqrt{1 - \left(\frac{\mu}{2\pi\sigma}\right)^2 b^2 \rho_m}. \qquad [32dd]$$

In steady state, where ρ_m is determined by the kinetic balance (e.g. eqs. [32aa] or [32aa']), the strain rate comes out proportional to the second or third power of the stress. However, the elastic interaction between the mobile dislocations described by eqs. [32bb] to [32dd] holds for any mobile dislocation density, whether it is in steady state or not. ALEXANDER and HAASEN (1968) treated, in some detail and in remarkable agreement with experiments on germanium and silicon, the behavior of a material in which the mobile density rises from very low values. For example, the

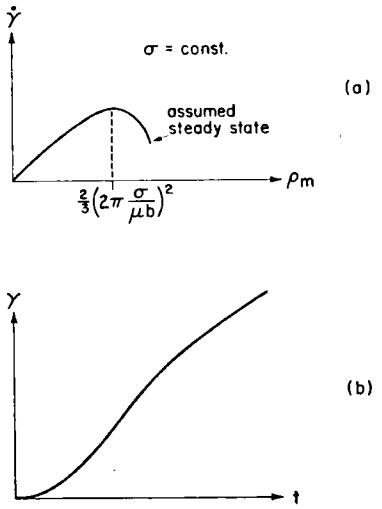

FIG. 32-2. (a) Dependence of strain rate $\dot{\gamma}$ on mobile dislocation density ρ_m at constant stress σ, as influenced by mutual interaction; (b) resulting sigmoidal creep curve.

development of the strain rate as a function of this rising density in a creep test would be described by eq. [32dd] at σ = constant, which is shown in Fig. 32-2. The strain rate first rises with ρ_m in the expected manner, but then drops again when the glide resistance due to the mobile dislocation interaction comes close to the fixed applied stress. If the steady-state density is larger than the value at the maximum, or irrelevant because of a lack of sinks (as assumed by ALEXANDER and HAASEN), one obtains a *sigmoidal creep curve*. The mobile density at the maximum creep rate is easily calculated from eq. [32dd] and is proportional to the square of the stress:

$$\rho_m = \frac{2}{3}\left(\frac{2\pi\sigma}{\mu b}\right)^2. \qquad [32ee]$$

In a complete theory of the dependence of strain rate on stress, through both the velocity and the mobile dislocation density, the effects of an elastic interaction between the moving dislocations and those of their mutual trapping would be parts of the same mechanism. The proposal by ARGON (1970) is a step in this direction.

33. JERKY GLIDE

"Jerky glide" refers to dislocation motion at stresses *below* the mechanical threshold. Between obstacles, the dislocations are assumed, at the lowest level of approximation, to move in zero elapsed time—at the next higher level, with a drag-controlled velocity. At obstacles, they may be released either by thermal fluctuations or by a change in the applied stress or in the obstacle structure. The "mobile" dislocations then fall into two classes: those actually "running", and those "waiting" to be released at obstacles. Three levels of *steady state* are established: that between the waiting and the running dislocations; that in the slip plane, assuring continued plastic flow (introduced with the definition of the plane glide resistance); and, in the case of thermally instable structures, that between work hardening and recovery. Below, we shall give a general rate equation, which describes the kinetics of jerky glide when the first two levels of steady state have been achieved.

Thermal and Mechanical Release

The basis for distinguishing "jerky" from "continuous" glide is that, on a local basis, there may be long periods of zero glide rate, interspersed with short periods of a finite glide rate (Fig. 33-1). On a time scale long compared

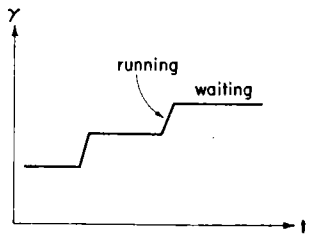

FIG. 33-1. Strain due to one dislocation in jerky glide.

with these "short periods", glide occurs in finite increments $\delta\gamma$, at intervals determined by the rate of release at the obstacles. If P describes the fraction of obstacles that would, under given conditions, *not* hold a dislocation back, δP is the fraction released under a given change of these conditions. Then, from the kinematic relation [22c],

$$\delta\gamma = b\, N_{\text{WAIT}}\, a_{\text{RUN}}\, \delta P \qquad [33a]$$

where N_{WAIT} is the number of waiting segments per unit volume, and a_{RUN} is the area swept out by a segment after its release. In the special case of one-dimensional dislocation motion, which one might expect when the barriers are linear, one may instead use the total dislocation *length* per unit volume that is waiting, ρ_{WAIT}, and the *distance* traveled after release, y_{RUN}:

$$\delta\gamma = b\, \rho_{\text{WAIT}}\, y_{\text{RUN}}\, \delta P. \qquad [33b]$$

We shall often use the more common relation [33b] with the understanding that, in the case of two-dimensional glide, it is merely meant to represent eq. [33a]; for example, by introducing an average segment length l and setting

$$\rho_{\text{WAIT}} = N_{\text{WAIT}}\, l \quad y_{\text{RUN}} = a_{\text{RUN}}/l. \qquad [33c]$$

For general usage, we also define γ_o so that

$$\delta\gamma = \gamma_o\, \delta P. \qquad [33d]$$

The reason for the release of a dislocation (segment) from an obstacle, i.e. for a finite δP, may be thermal fluctuations occurring at a rate P_t per unit time:

$$\delta P_{\text{THERM}} = P_t\, \delta t. \qquad [33e]$$

Here, P_t may be a simple Arrhenius term

$$P_t = \nu_G \exp\left(-\frac{\Delta G}{kT}\right) \qquad [33f]$$

or other appropriate forms to be discussed in Chapter 4.

On the other hand, the reason for the release may be mechanical: if the applied stress is increased, an additional fraction of obstacles can be overcome by the dislocation:

$$\delta P_{\text{MECH}} = P_\sigma\, \delta\sigma \qquad (\delta\sigma \geqslant 0). \qquad [33g]$$

This is precisely the same effect as was described in connection with the influence of any aperiodicity of the obstacle arrangement on the plane glide resistance (sec. 25). From Fig. 25-12 we see that P_σ should be of order $1/\hat{\tau}_{\text{PLANE}}$. A *decrease* in stress does not change the number of obstacles that hold back a waiting dislocation.

Finally, a dislocation may be released at an obstacle point, if this point disappears through recovery. This effect may be described as a change in the plane glide resistance, which is proportional to the density of obstacles along

the dislocation and furnishes the *scale* of Fig. 25-12. Taking $\hat{\tau} = \hat{\tau}_{\text{PLANE}}$ as a representative value, we set

$$\delta P_{\text{STRUCT}} = P_\tau \, \delta\hat{\tau}. \qquad [33h]$$

If obstacle points *disappear*, $\delta\hat{\tau}$ is negative; for a *release* of dislocations ($\delta P_{\text{STRUCT}} > 0$), P_τ must then be negative also. In fact, if the situation is described by a one-parameter diagram such as Fig. 25-12, the penetration probability is a function of the ratio $\sigma/\hat{\tau}$ only, and we have

$$P_\tau = -\frac{\sigma}{\hat{\tau}} \cdot P_\sigma \qquad (P = P(t,\sigma/\hat{\tau})). \qquad [33i]$$

When there is more than one set of obstacles, the relation is more complex. For example, when there is a linear superposition with a flow stress $\hat{\tau}_1$ due to an obstacle set whose density does not change, such as inclusions, eq. [33i] must be replaced by

$$P_\tau = -\frac{\sigma - \hat{\tau}_1}{\hat{\tau} - \hat{\tau}_1} P_\sigma. \qquad [33i']$$

Additional obstacles may *appear*, under some circumstances, through work hardening; however, it is extremely unlikely that they would appear exactly at a waiting dislocation. Thus, a positive $\delta\hat{\tau}$ would not affect δP_{STRUCT}, and we have for the total release probability

$$\delta P = \delta P_{\text{THERM}} + \delta P_{\text{MECH}} + \delta P_{\text{STRUCT}}$$

with each term positive. The strain increment becomes

$$\delta\gamma = \gamma_o (P_t \, \delta t + P_\sigma \, \delta\sigma + P_\tau \, \delta\hat{\tau}). \qquad [33j]$$

This is a general, statistical-kinematic relation for jerky glide. It was introduced by KOCKS (1970b). We will discuss it again in the form of time *rates*, under certain restrictions concerning the times over which the rates are smoothed out, after dealing with the mobile dislocation density contained in the term γ_o.

Waiting, Running, and Mobile Dislocations

Until now, we have only discussed virtual variations, in which dislocations were transferred from one "waiting" position to another without consideration of the time involved in this transfer. In reality, a finite time is required. Then, the (potentially) *mobile* dislocations fall, at any one time, into two classes: those that are actually *running*, and those that are *waiting*.

At any *instant*, the macroscopic strain rate is provided only by those dislocations that are running (eq. [32o]):

$$\dot{\gamma} = b \, \rho_{\text{RUN}} \, \bar{v}_{\text{RUN}}. \qquad [33k]$$

These are "generated", or rather transferred into the running from the waiting

state, by release at the occupied obstacles, at a rate $\rho_{WAIT}\dot{P}$; and they are transferred back into the waiting state after they have traveled a distance y_{RUN} (eq. [33b]). One may look at this as a generation-and-trapping problem much as was discussed, for continuous glide, in eq. [32t], only for the *running* dislocations:

$$\dot{\rho}_{RUN} = \rho_{WAIT}\dot{P} - \frac{\rho_{RUN}\bar{v}_{RUN}}{y_{RUN}}. \qquad [33\ell]$$

The solution to this differential equation, for zero initial running density is

$$\rho_{RUN} = \rho^{SS}_{RUN}[1 - \exp(-t/t_{RUN})] \qquad [33m]$$

where $\rho^{SS}_{RUN} = \rho_{WAIT}\dot{P}t_{RUN}$ is the steady-state density, and the running time is

$$t_{RUN} = y_{RUN}/\bar{v}_{RUN}. \qquad [33n]$$

At times long compared to t_{RUN}, when a steady state has been achieved between the running and the waiting densities, the left-hand side of eq. [33ℓ] must vanish. The strain rate (eq. [33k]) then becomes equal to

$$\boxed{\dot{\gamma} = by_{RUN}\rho_{WAIT}\dot{P}} \qquad (\textit{steady state mobile density}). \qquad [33o]$$

This relation is similar to eq. [33b], with the virtual variation replaced by a rate of change with time. *When two states are allowed for the mobile dislocations, they must be in kinetic balance with each other for the simple rate equation to hold.* We can then replace eq. [33d] by

$$\dot{\gamma} = \gamma_o\dot{P} \qquad [33p]$$

where $\dot{P}$ is the *total* derivative of P with respect to time and may involve terms proportional to $\dot{\sigma}$ and $\dot{\tau}$ (eq. [33j]).

Equations [33k] and [33o] are not in a truly useful form, since one of them relates only to the *running* dislocations, the other only to the *waiting* ones. During all transfers between these two states, the *total* length of dislocations in both states is constant. This is the mob*ile* dislocation density

$$\rho_m \equiv \rho_{WAIT} + \rho_{RUN}. \qquad [33q]$$

With this definition, one can combine eqs. [33k] and [33o] to give the most commonly used relation for the strain rate:

$$\boxed{\dot{\gamma} = \frac{b\rho_m y_{RUN}}{t_{WAIT} + t_{RUN}}} \qquad (\textit{steady state mobile density}) \qquad [33r]$$

where, for esthetic reasons, we have set $\dot{P} \equiv 1/t_{WAIT}$. (Note that this refers to the *total* differential $\dot{P}$, not to the partial P_t.)

All these relations have been written for one-dimensional glide; but they may, by virtue of the definitions [33c], be used for two-dimensional jerky glide

as well. Explicitly, one may write eqs. [33o] and [33r] as

$$\dot{\gamma} = b\, a_{\mathrm{RUN}}\, N_{\mathrm{WAIT}}\, \dot{P} = \frac{b a_{\mathrm{RUN}}\, N_{\mathrm{m}}}{t_{\mathrm{WAIT}} + t_{\mathrm{RUN}}}. \qquad [33s]$$

Using the general term γ_o introduced in eq. [33d], one must identify

$$\gamma_o \equiv b y_{\mathrm{RUN}}\, \rho_{\mathrm{m}} \cdot \frac{1}{1 + \dot{P}\, t_{\mathrm{RUN}}} \equiv b a_{\mathrm{RUN}}\, N_{\mathrm{m}} \cdot \frac{1}{1 + \dot{P}\, t_{\mathrm{RUN}}}. \qquad [33t]$$

The fractional correction factor is usually quite close to 1: the running time is small compared to the waiting time, and almost all mobile dislocations are waiting rather than running.

It is a characteristic of jerky glide that eq. [33r] does not involve a *velocity*, but *times*. In an entirely arbitrary fashion, one may *define* an average velocity of all mobile dislocations (i.e. both the waiting and the running ones) in steady state as

$$\bar{v}_{\mathrm{m}} \equiv \frac{y_{\mathrm{RUN}}}{t_{\mathrm{WAIT}} + t_{\mathrm{RUN}}} \qquad [33u]$$

so that

$$\dot{\gamma} = b \rho_{\mathrm{m}} \bar{v}_{\mathrm{m}}. \qquad [33v]$$

Conversely, with at least as much justification, one may define

$$\dot{\rho}^{+} \equiv \rho_{\mathrm{WAIT}}\, \dot{P} \qquad [33w]$$

so that in steady state (OROWAN, 1940)

$$\dot{\gamma} = b y_{\mathrm{RUN}} \dot{\rho}^{+}. \qquad [33x]$$

Here, $\dot{\rho}^{+}$, by the definition [33w], is the rate of generation of running dislocations; it is not a *total* differential as all other dotted quantities are in this article. Nothing is gained by either the formulation [33v] or [33x], and we shall remain with eqs. [33p] with [33t], or [33r], or [33s].

Other recent discussions of the dichotomy between "velocity" and "generation" treatments, and of steady-state problems with mobile dislocations in general, were given by MECKING and LÜCKE (1970) and by DEROSSET and GRANATO (1970).

Mobile Dislocation Density and Active Slip Plane Spacing

We have now answered the question, how the density of dislocations actually *running* is related to those potentially *mobile*. But what determines the *mobile* density? In a sense, one might say that the introduction of a "mobile" density, which comprises both the running and the waiting dislocations (eq. [33q]), and of an average velocity of these mobile dislocations (eq. [33u]), is tantamount to describing jerky glide in terms of continuous glide. The same arguments as were used in sec. 32 must then apply here: maintenance of a sufficient density of mobile dislocations requires the existence of sources, to balance the unquestioned existence of sinks, at least at the surface. Equation [32t] then describes the kinetic balance. The source density ρ_{SOURCE}, and the distance y_{BACK} that controls its frequency of operation, may have one of the

forms outlined in the case of continuous glide, or they may be different, as discussed in an example below. The distance y_m traveled by the mobile dislocations may, however, be different in principle, since it could be determined by the peaks in the glide resistance allowed in jerky glide.

If the glide resistance may be considered to consist of two components, such as in Fig. 24-6, one may elect to treat the small-amplitude variations as smoothed out and overcome in quasi-continuous glide and the large peaks as the sinks and sources of the "mobile" dislocations in the quasi-continuous-glide region (MECKING and LÜCKE, 1970; DEROSSET and GRANATO, 1970). If the distance between the peaks is L and the slip plane spacing is d, this model would correspond to setting

$$\rho_{\text{SOURCE}} = \frac{1}{Ld}; \qquad y_m = L. \tag{33y}$$

Depending on whether y_{BACK} is also set equal to L, signifying a direct correlation between neighboring sources, or whether it is related to the internal stress variations associated with the other mobile dislocations in the manner of eq. [32v'], the steady-state results are, from eq. [32t],

$$y_{\text{BACK}} = L \quad \rightarrow \quad \rho_m = \frac{1}{Ld}; \qquad \gamma_o = \frac{b}{d}, \tag{33z}$$

$$y_{\text{BACK}} = \frac{1}{\sqrt{\rho_m}} \quad \rightarrow \quad \rho_m = \frac{1}{d^2}; \qquad \gamma_o = \frac{bL}{d^2}. \tag{33aa}$$

In the first case, there is always exactly one dislocation mobile between each pair of peaks; in the second, there are L/d. The case in which the average number of mobile dislocations between peaks is much *less* than one, as it was apparently envisaged by MECKING and LÜCKE and by DEROSSET and GRANATO, does not lead to a determination of γ_o—it is rather a higher-order treatment of jerky glide between the peaks.

The slip plane spacing d appears again in both of the above equations. In the case of continuous glide (sec. 32), we had estimated a value for d from the requirement that dislocations moving in opposite directions on parallel slip planes must bypass each other. In jerky glide, one may allow these dislocations to trap each other in dipoles: if these dipoles are not completely free to move in the slip plane, they may provide an added glide resistance. The statistics of such a process are very complicated and have been worked out under various assumptions by ARGON (1969) and by NEUMANN (1971).

In one simple case, the slip plane spacing can be given explicitly; namely, when the glide resistance consists of well-separated discrete obstacles or, more generally as above, of well-separated large peaks with a small-scale variation in between, which is approximated as a "friction" stress τ_1. In that case, even those dislocations that are waiting at the high peaks may translate under the action of parallel mobile dislocations until they are both in the quasi-continuous regime. The passing stress (eq. [32x]) must then be provided by the difference between the applied stress σ and the "friction" stress τ_1; no added contribution to the glide resistance is necessary if

$$\sigma = \tau_{\text{PLANE}}. \tag{33bb}$$

The smallest spacing d, providing the highest strain rate without affecting the flow stress is thus given by

$$\frac{b}{d} = 4\pi \frac{\sigma - \tau_1}{\mu}. \qquad [33cc]$$

Equations [33cc] and either [33z] or [33aa] combine to give a result (OROWAN, 1941) that the steady-state mobile dislocation density depends linearly on the applied stress (minus any friction stress). Other evaluations of [33aa] may give a quadratic law. In the case of jerky glide treated here, *this is a very insensitive dependence* compared to that of the "velocity" or $\dot{P}$ (provided the stress is large compared to τ_1). Under those conditions, one may then well consider the pre-exponential factor in the Arrhenius relation to be constant.

Work Hardening and Recovery

In the expression for mechanical release from obstacles (eq. [33g]), we allowed for a variation in structure described by a change in $\hat{\tau}$. This was, in part, in anticipation of including recovery in the rate equation. It is apparent that the disappearance of some obstacles through recovery releases dislocations in the same manner as thermal fluctuations do. The only difference is that, in recovery, the change of the obstacle is permanent.

On the other hand, some additional obstacles may *appear* through work hardening. They cannot release dislocations; but their number must be subtracted from the number of those disappearing through recovery to obtain the net change in obstacle density.

The density of discrete obstacles is one parameter that enters, through their average spacing l, into the relation for the line or plane glide resistance and, in particular, into its maximum value $\hat{\tau}$. When the nature of the obstacles, and thus their strength, remains constant, we may use $\hat{\tau}$ as a measure of the obstacle density as it changes through work hardening or recovery:

$$\delta\hat{\tau} = h\delta\gamma - r\delta t. \qquad [33dd]$$

The meaning of this equation is that the flow stress (the asymptotic plane glide resistance) is measured at zero temperature, once as a function of prestrain in the absence of thermal fluctuations, and once as a function of recovery time (at some temperature and possibly some stress in the elastic range) in the absence of (net) glide. Formally, one may then define the coefficients h and r as partial derivatives at constant time and strain, respectively:

$$h \equiv \left.\frac{\partial\hat{\tau}}{\partial\gamma}\right|_t, \qquad [33ee]$$

$$r \equiv -\left.\frac{\partial\hat{\tau}}{\partial t}\right|_\gamma. \qquad [33ff]$$

We are here primarily interested in the *total* time derivative of $\hat{\tau}$:

$$\dot{\hat{\tau}} \equiv \frac{\mathrm{d}\hat{\tau}}{\mathrm{d}t} = h\dot{\gamma} - r. \qquad [33gg]$$

The rate equation [33p] for a steady-state running dislocation density then reads, with eqs. [33i] and [33j], for a one-parameter obstacle structure

$$\boxed{\dot{\gamma} = \gamma_0 P_t + \gamma_0 P_\sigma \left\{\dot{\sigma} - \frac{\sigma}{\hat{\tau}} \cdot (h\dot{\gamma} - r)\right\}.} \qquad [33hh]$$

If the structure is in steady state (or if it is constant for other reasons), the left-hand side of eq. [33gg] vanishes, and so does the last term in eq. [33hh]. In a creep test ($\dot{\sigma} = 0$), we are then left with the conventional Arrhenius relation

$$\dot{\gamma} = \gamma_0 P_t. \qquad [33ii]$$

Equations [33gg] and [33ii] are two simultaneous equations for steady state at all levels, from which the structure parameter $\hat{\tau}$ can be eliminated to obtain a constitutive relation (KOCKS, 1974a).

In addition to changes in obstacle *density*, there may be changes in obstacle *arrangement* with time (ALDEN, 1972, 1973). If they lead to more extensive clustering, they, too, should lead to a partial lowering of the flow stress. In contrast to recovery, this "metarecovery" may be reversible.

34. PHENOMENOLOGICAL KINETICS

We have discussed two sets of physical kinetic laws: one for continuous glide above the mechanical threshold $\hat{\tau}$, one for jerky glide below. They are

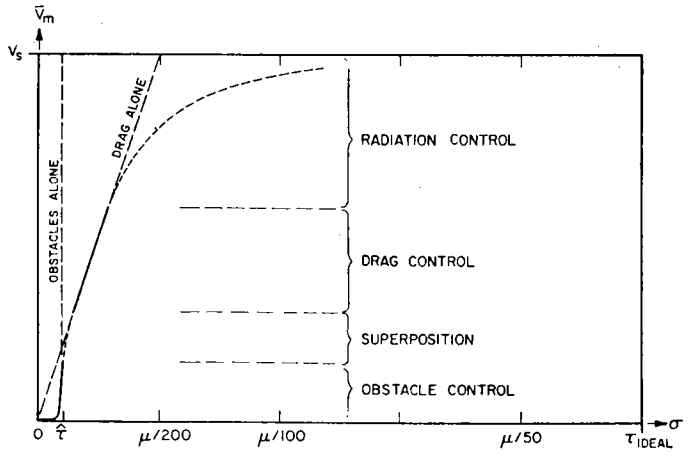

FIG. 34-1. Schematic velocity-stress diagram up to the respective natural limits.

displayed together in Fig. 34-1, a linear diagram of (average) dislocation velocity versus stress up to their respective natural limits, the speed of sound $\overline{v}_S$ and the theoretical shear strength τ_{IDEAL}. The strain rate $\dot{\gamma}$ observed macroscopically contains, in addition, the kinetics of the mobile dislocation density, which was also discussed in physical terms in secs. 32 and 33.

The general diagram of dislocation velocity (or of strain rate) versus stress has been described, in whole or in part, by various empirical laws. It is of the essence of plasticity that such laws contain structure parameters. Before discussing empirical descriptions, we shall therefore consider the problem of "structure" in its relevance to constitutive relations.

Constitutive Relations

An "equation of state" for plasticity, when it is assumed, has frequently been written in the form

$$f(\gamma, t, \sigma, T, \ldots) = 0. \qquad [34a]$$

The dots stand for additional variables such as pressure or other components of stress, magnetic fields, etc. In addition, the equation contains material constants. If one is interested in rates, one may differentiate this equation with respect to time and write

$$f(\dot{\gamma}, \dot{\sigma}, \dot{T}, \gamma, t, \sigma, T, \ldots) = 0 \qquad [34b]$$

The chief problem with such equations is that two of the variables, namely γ and t, do not describe any "state", but a *history*: they specify differences against some assumed initial state. (See also HART, 1970; KOCKS, 1974b.) Moreover, they are only *two* parameters of the thermo-mechanical history, and many more may be relevant:

$$\{\gamma, t\} \subset \{\text{History}\}.$$

If one inserted the entire set of history variables into eq. [34b] instead of γ and t, the equation would have to be correct, but it would then, by definition, not be an equation of *state*.

The premise made to deal with such problems in Physical Metallurgy is that history has an effect on properties only through the *structure* developed while it passed; the present properties are uniquely determined by the current structure (in other words, the current *state*):

$$\{\text{History}\} \rightarrow \{\text{Structure}\}.$$

In fact, different histories may lead to the same structure, and then the properties must be the same. The "Structure" is a set of *parameters of state*, and one might thus call the resulting general relation

$$f(\dot{\gamma}, \dot{\sigma}, \dot{T}, \sigma, T, \{\text{Structure}\}, \{\text{Structure Changes}\}) = 0 \qquad [34c]$$

an "equation of state". HART (1970) has recently re-introduced this term in a more restricted sense, namely for the case that there is but one "Structure"

variable (the "hartness"), which can then be uniquely expressed by the values of all external variables. We shall simply refer to equations of the form [34c] as *constitutive laws.*

For plastic deformation by dislocation glide, we have found how the structure influences the properties: through the glide resistance τ at all positions in the crystal. For macroscopic slip, we further need the mobile dislocation density ρ_m or an equivalent parameter, which may be included in the general set of structure variables. If we characterize the glide resistance by a finite number of parameters such as its overall average τ_{STOR} and its effective maximum values under various conditions, we may write

$$\{\tau_{STOR}, \hat{\tau}_{PLANE}, \hat{\tau}_{LINE}, \ldots, \rho_m\} \subset \{\text{Structure}\}. \qquad [34d]$$

The dots may stand, for example, for a particular contribution to the glide resistance such as from lattice friction.

Under various conditions, some of these parameters become irrelevant, and then the problem may become tractable. We have encountered three of these conditions, all *steady states* in their respective variables.

First, the mobile dislocation density may attain its steady-state value under constant stress, structure, and temperature. It is then uniquely given by these variables and is no longer an independent variable:

$$\rho_m \subset \{\text{Structure}\}.$$

Equation [34c] becomes

$$\boxed{f(\dot{\gamma},\sigma,T,\tau) = 0} \qquad (\textit{steady-state mobile dislocation density}) \qquad [34e]$$

where τ stands, in principle, for the entire glide resistance profile throughout the crystal, i.e. all parameters of structure except the mobile dislocations.

Second, dynamic arrangements of mobile dislocations may form in the slip plane such as to smooth out variations in the line glide resistance. Then, $\hat{\tau}_{LINE}$ becomes irrelevant:

$$\hat{\tau}_{LINE} \notin \{\text{Structure}\}$$

and we may write

$$f(\dot{\gamma}, \sigma, T, \hat{\tau}_{PLANE}) = 0 \qquad (\textit{steady-state dynamic dislocation structure}) \qquad [34f]$$

if we neglect τ_{STOR} and any possibility to differentiate between various contributions to $\hat{\tau}_{PLANE}$. Choosing $\hat{\tau}_{PLANE}$ as the first or most important structure parameter is suggested by Fig. 34-1, and we shall use constitutive relations of the form [34f] unless macroscopic observations warrant the introduction of additional parameters. For generality (or as an abbreviation for the first approximation [34f]), we shall write it in the form [34e].

Finally, at temperatures where the structure is not thermally stable, $\hat{\tau}_{PLANE}$ may attain a steady-state value that is uniquely determined by a balance between work hardening and recovery at a given strain rate, temperature, and

stress (sec. 33). Then,

$$\hat{\tau}_{\text{PLANE}} \notin \{\text{Structure}\}$$

and the constitutive relation becomes

$$f(\dot{\gamma}, \sigma, T, \tau_{\text{STOR}}) = 0 \qquad (\textit{steady-state structure}). \qquad [34g]$$

Note that the average glide resistance τ_{STOR}, which describes the rate of energy *storage* associated with flow, can never disappear from the equation for thermodynamic reasons (eq. [22h]). It may vanish for certain mechanisms, but it could be nonzero even when the "Structure" that enters the rate equation is constant as in eq. [34g]; for example, internal surfaces may yet be generated by glide (or climb) and not be capable of recovery at the same temperature in a time comparable with the experiment.

These examples illustrate the general phenomenon that each level of steady state reduces the number of independent variables by one. Conversely, successive approximations to an adequate description of "Structure" in the constitutive relation can be obtained when the time resolution of the experiments is increased and the various transients are analyzed.

Empirical Laws

An empirical law is meant to be a simple relation that describes experimental observations tolerably well over a limited range of the variables. Good empirical laws can be used to extrapolate slightly beyond the range of observations, although extrapolation far beyond the intended range may often violate some known physical limitation. For example, the most frequently used law to describe the relation between strain rate and stress,

$$\dot{\gamma} = A\sigma^{m} \qquad [34h]$$

implies no upper limit for the strain rate or for the stress. For physical reasons, however, the strain rate can at most correspond to the case where all dislocations (of length ρ per unit volume) are running at the speed of sound v_S:

$$\dot{\gamma} < b\rho v_S \qquad [34i]$$

and the stress cannot be larger than the ideal or "theoretical" shear strength:

$$\sigma < \tau_{\text{IDEAL}}. \qquad [34j]$$

Within this range, eq. [34h] may nevertheless describe the behavior tolerably well. For example, we have seen that, in continuous glide well above the mechanical threshold $\hat{\tau}$, a power law with a small exponent should obtain:

$$\dot{\gamma} = \dot{\gamma}_o \left(\frac{\sigma}{\sigma_o}\right)^{m}; \quad \sigma \gg \hat{\tau}; \quad 1 \leqslant m \lesssim 4. \qquad [34k]$$

Here, we have split up the single empirical parameter A in eq. [34h] into

two, $\dot{\gamma}_o$ and σ_o, which have the dimensions of the variables under discussion. Their relation to known material properties may, under some circumstances, be guessed rather easily. For example, in the absence of any glide resistance of influence, the shear modulus μ would be a logical material constant to be substituted for σ_o. Some further insight into the physical process that limits deformation rates in continuous glide would, on the other hand, lead one to expect the combination $\sigma\Omega/kT$ (Ω = atomic volume), which is proportional to the drag limited dislocation velocity (eq. [31r]). If the excess of the exponent m over 1 is due to mobile dislocation interactions (sec. 32), we could rewrite eq. [34k] as follows:

$$\dot{\gamma} = \dot{\gamma}_o \frac{\mu\Omega}{kT}\left(\frac{\sigma}{\mu}\right)^m \qquad \sigma \gg \hat{\tau};\ 1 \leqslant m \lesssim 4. \qquad [34\ell]$$

This equation contains an additional variable, the temperature T, but still only two unknown parameters—only one of which, $\dot{\gamma}_o$, is likely to depend on material and dislocation structure. It could thus be a very useful empirical law.

With additional sophistication, one would want to take account of the mechanical threshold $\hat{\tau}$. However, we know from physical cases treated in sec. 32, that it cannot simply be subtracted from the applied stress σ to obtain an "effective stress". More likely to succeed would be an empirical equation of the form

$$\dot{\gamma} = \frac{A}{T}(\sigma^p - \hat{\tau}^p)^{m/p} \qquad \sigma > \hat{\tau};\ p \geqslant 1. \qquad [34m]$$

But this equation contains four unknown parameters and still only three variables. It thus has little predictive value. Furthermore, the applicability of the physical picture near the limit $\sigma \simeq \hat{\tau}$ is restricted to obstacles that cannot be overcome thermally.

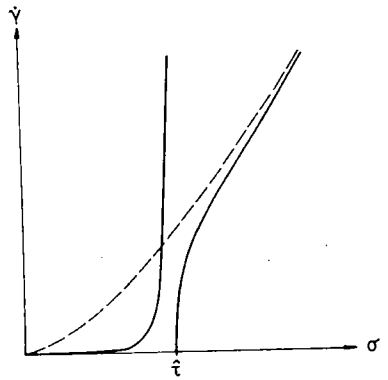

FIG. 34-2. Schematic strain-rate versus stress diagrams suggested by physical mechanisms below and above the mechanical threshold $\hat{\tau}$ separately. Dashed: continuous glide in the absence of a threshold.

Figure 34-2 shows the qualitative predictions for the physical mechanisms of continuous glide and jerky glide separately, and also (dashed) a schematic representation of eqs. [34k] or [34ℓ]. It is clear that for $\sigma \simeq \hat{\tau}$, neither picture can be adequate, and eq. [34m] provides little if any improvement over eq. [34ℓ].

FROST and ASHBY (1971) have treated the threshold region exactly for a particular physical model. As a guideline for possible empirical equations, their results are shown in Figs. 34-3 and 34-4. (The mobile dislocation density is here assumed constant, and thus m = 1.)

The double-logarithmic diagram suggests that, even for $\sigma < \hat{\tau}$, a power law (eq. [34h]) may be a reasonable empirical description, except that the exponent m would now have to be rather large. Any number that is very large or very small compared to 1 is unlikely to be a merely geometric parameter, but more likely to be the ratio of some physical quantities. Indeed, the large value of m necessary if a power law description is formally applied below the mechanical threshold $\hat{\tau}$, follows from a description of jerky glide in terms of an Arrhenius law:

$$\dot{\gamma} = \dot{\gamma}_0 \exp - \frac{\Delta G(\sigma)}{kT}; \qquad \tau_{\text{STOR}} < \sigma \leqslant \hat{\tau} \tag{34n}$$

where, for a simple demonstration, we may assume

$$\Delta G = F_0 \left(1 - \frac{\sigma}{\hat{\tau}}\right). \tag{34o}$$

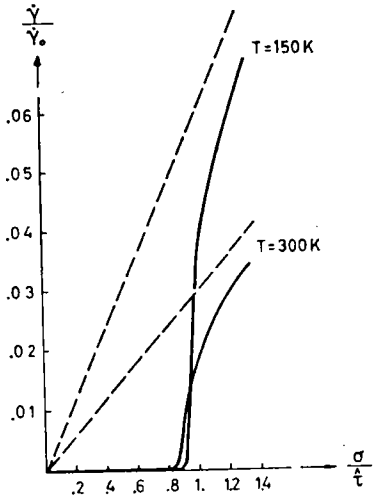

FIG. 34-3. Results of FROST and ASHBY (1971) for jerky glide with drag, adapted to show transition near mechanical threshold.

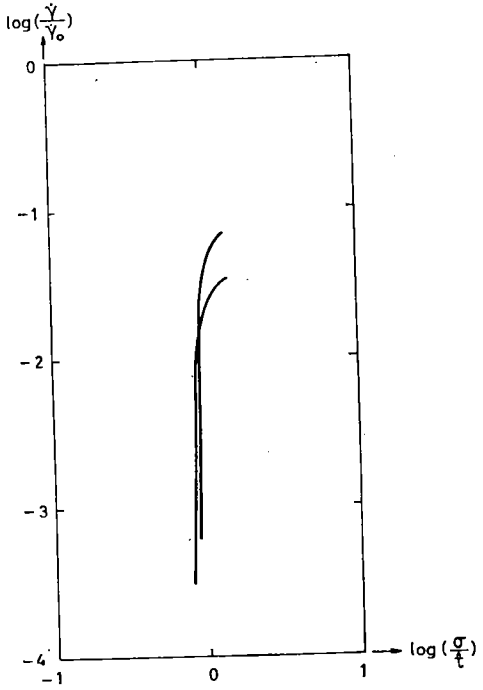

FIG. 34-4. Same as Fig. 34-3, but on double-logarithmic scale.

The terms F_o and $\hat{\tau}$ may here be regarded as empirical parameters. Equation [34n] then becomes

$$\dot{\gamma} = \dot{\gamma}_o \left[\exp\left(\frac{\sigma}{\hat{\tau}} - 1\right)\right]^{F_o/kT} \qquad [34p]$$

which, for values of σ not too far below $\hat{\tau}$, may be approximated by

$$\dot{\gamma} = \dot{\gamma}_o \left(\frac{\sigma}{\hat{\tau}}\right)^{F_o/kT} \quad | \quad \tau_{STOR} \ll \sigma < \hat{\tau}. \qquad [34q]$$

In other words, eq. [34k] holds with

$$\sigma_o = \hat{\tau}; \qquad m = \frac{F_o}{kT} \qquad (\textit{jerky glide}). \qquad [34q']$$

The large number m thus corresponds to the ratio of an "activation energy" to kT—and a new physical variable has again been introduced into eq. [34k].

Of course, m may not be strictly independent of σ, if the more exact eq. [34p] holds, or if ΔG is a different function of σ than that shown in eq. [34o]. For these cases, when m depends on σ, it is more appropriately defined as the

slope in the diagram of Fig. 34-4:

$$m \equiv \left.\frac{\partial \ln \dot{\gamma}}{\partial \ln \sigma}\right|_T . \qquad [34r]$$

Any dependence $m(\sigma)$ could only be seen in Fig. 34-4, if the scales were changed such as to make the lines less steep.

As in the continuous glide case discussed above, basic physical arguments actually provide a better proposal for an empirical relation between the activation energy and the stress than the linear one given in eq. [34o] (see sec. 44). With it, eq. [34p] could be replaced by

$$\dot{\gamma} = \dot{\gamma}_o \exp\left\{-\frac{F_o}{kT}\left[1 - \left(\frac{\sigma}{\hat{\tau}}\right)^p\right]^{3/2}\right\}; \qquad 0 < p \leqslant 1. \qquad [34s]$$

Again, the number of parameters has now risen to four, for three variables. Nevertheless, this may be an acceptable empirical relation, since it is rather insensitive to one of the parameters, namely $\dot{\gamma}_o$. If p should be observed to have a value small compared to 1, this may be an indication for an additional physical mechanism, say with maximum glide resistance τ_1; then, σ has to be replaced by $(\sigma - \tau_1)$ or a similar "effective stress".

Regardless of the particular form of the empirical law, the combination of variables to be used to describe flow below the mechanical threshold is suggested by general physical arguments for jerky glide to be

$$\frac{kT}{F_o} \ln \frac{\dot{\gamma}_o}{\dot{\gamma}} \quad \text{versus} \quad \frac{\sigma}{\hat{\tau}}.$$

Structure parameters in addition to $\hat{\tau}$ should be used only when warranted by the observations. Some authors have used the value of the stress, "where the strain rate goes to zero", as it appears, for example, in Fig. 34-3 at about $0.8\hat{\tau}$, as a parameter associated with some additional mechanism ("internal stress"). It is clear from the same figure, however, that the exponential dependence alone, with the high exponent F_o/kT, implies such a severe decrease of the strain rate with mildly decreasing stress. The "internal stress level" could, therefore, serve merely as a measure of the *maximum* glide resistance $\hat{\tau}$, provided it is agreed what "vanishingly small" strain rates are, but it need not be an *additional* parameter.

The exponential laws, like the power laws, do not account for the natural upper limits to strain rate and stress; in addition, the exponential laws imply a finite strain rate at zero stress. Again, a different mechanism must prevail here. In fact, we have seen from thermodynamic arguments, that long-range slip is impossible below $\sigma = \tau_{STOR}$. Near this value, the response should be linear; we shall discuss the reasons in more detail in sec. 45. A sensible empirical law for the low-stress range should then be

$$\dot{\gamma} = A \frac{\sigma - \tau_{STOR}}{kT} \exp -\frac{F_o}{kT} \qquad \tau_{STOR} \leqslant \sigma \ll \hat{\tau}. \qquad [34t]$$

This is another power law, with m = 1 and with a corrected stress. In addition, it describes the temperature dependence, using a total of three parameters.

Summarizing, we have found three acceptable empirical relations, all power laws, for three different ranges of the strain rate versus stress relationship: eqs. [34ℓ], [34q], and [34t]; only the regime of very high $\dot{\gamma}$ (where the dislocation velocity gets close to the speed of sound) shall remain undescribed.

Some general rules about empirical laws, which we have more or less explicitly used in this survey are:

(1) The minimum number of parameters in an empirical law is one less than the number of variables with different dimensions.
(2) The number of additional parameters, which are now dimensionless, should be no larger than is warranted by the experimental observations over the range of interest.
(3) A dimensionless parameter whose value is large or small compared to 1 is likely to hide additional physical variables that should be considered.
(4) Physical mechanisms can often suggest dimensionless combinations of variables; when these have been found, the predictive value of the empirical law beyond the range of observations is enhanced. On the other hand, physical mechanisms will also usually suggest natural limits for the applicability of an empirical law.
(5) When different physical mechanisms are expected in different ranges of the variables, it is of little value to attempt description by a minimum number of parameters, or even by a single empirical law.

Such overall descriptions of many ranges of the strain rate versus stress diagram have been attempted. For one, the overlap between the very-low-stress and the "jerky glide" regimes has been given by

$$\dot{\gamma} = \dot{\gamma}_0 \sinh \frac{2V_0(\sigma - \tau_{\text{STOR}})}{kT} \exp -\frac{F_0}{kT}. \qquad [34u]$$

We shall show in detail later (sec. 45) that this law provides no improvement over the linear equation [34t], except when the glide resistance diagram has the rather pathological shape of a square wave.

An empirical law that could qualitatively describe the *entire* strain rate versus stress diagram as shown in Fig. 34-1, without the very-low-stress range, but including the very-high strain rate range, is

$$\dot{\gamma} = \dot{\gamma}_0 \exp\left[-\frac{\sigma_0}{\sigma}\right] \qquad [34v]$$

with

$$\dot{\gamma}_0 = b\rho v_S; \quad \sigma_0 \propto \hat{\tau}. \qquad [34v']$$

But obviously this law has *too few* parameters for the large range. The parameter choices [34v'] were made with the high-speed and the jerky-glide regimes in mind; it is very unlikely that they describe the drag-controlled region for all but a single temperature (namely, the one deliberately chosen in Fig. 34-1). Note that, for other

temperatures, the direction in which the curve changes is different in the different regimes (cf. Fig. 34-4).

We also know that the dependence on stress given in [34v] is wrong in each range. If the parameters were chosen such as to represent the correct dependence in any one range (say, the jerky-glide region) as well as possible, there is no reason why they should even approximately describe another region (say, why $\dot{\gamma}_0$ should then have anything to do with the speed of sound). For these reasons, we find eq. [34v] of little use.

Multi-axial Stress States

From sec. 22 on, and for the remainder of this article, we have assumed all stresses and strains to be resolved in the slip plane and slip direction, and have discussed the kinetic laws governing their relation to each other. Constitutive relations comprise, in addition, statements concerning the *yield condition* when many components of stress are present, and concerning the *plastic potential* that describe the relation between the "direction" of strain increments and the "direction" of stress.

In their classic form, the yield condition and plastic potential are only defined in the absence of rate effects. Their superposition with kinetic laws is, however, possible. Without discussing this problem in detail, we merely wish to point out here how the concept of a yield surface fits into the framework we have presented.

The definition of the mechanical threshold $\hat{\tau}_{\text{PLANE}}$ as the highest stress at which static equilibrium can be attained in a slip plane may easily be extended to all slip systems in the crystal. In this way, one would obtain the "yield surface" of the crystal at zero temperature. If any combination of applied stresses *exceeds* this yield surface, dislocations are under positive driving force everywhere and must accelerate or do work against strictly dissipative mechanisms. On the other hand, if a combination of stresses lies *inside* this "zero temperature yield surface", or *mechanical threshold surface*, finite rates of deformation are also possible: namely, with the aid of thermal fluctuations. Thus, for most normal situations, the yield surface for a particular finite strain rate lies *inside* the "static" yield surface, defined as the limit of static equilibrium states (KOCKS, 1970a, 1974b).

Instead of using the mechanical threshold $\hat{\tau}$, one may wish to consider τ_{STOR} and extend its definition (sec. 22) to all slip systems. In this way, one would obtain a "yield surface" below which macroscopic plastic deformation is thermodynamically impossible. Such a definition may have been implied in conventional treatments of mathematical plasticity; however, it defines a critical stress that is, in most practical circumstances, very much smaller than a "yield" or "flow" stress in any macroscopic sense: most of the work done in plastic deformation is dissipated, not stored.

4. THERMAL ACTIVATION

Summary

While Chapter 3 dealt with the motion of dislocations at stresses *above* the peaks of the glide resistance, we shall here be concerned with the thermal release of dislocations from regions in which the stress is *below* some of the peaks of the glide resistance. Each dislocation is supposed to start at rest in a position of static equilibrium (the problem of superposition of the dynamic motion *between* the obstacles and the thermal release *at* the obstacles having been treated on a formal basis in Chapter 3).

Thermal activation is a statistical process. It is never possible to say at which time a particular dislocation segment may be released. In this sense, we will always be dealing with *averages*. The *fraction* of a large number of identically situated dislocation segments that is released per unit time has been introduced in eq. [33e] as P_t. The ensuing macroscopic strain rate

$$\dot{\gamma} = \gamma_o P_t$$

contains, in addition, the total number of dislocation segments taking part in the process and the average strain achieved with each activation event; these have been lumped together (eqs. [33d] and [33ii]) into a term γ_o that, in this Chapter, is treated as a phenomenological parameter that may depend weakly on stress (and possibly on temperature through the shear modulus).

In principle, thermal activation events may occur in the "reverse" ($\leftarrow$) as well as in the "forward" ($\rightarrow$) direction. The net rate of strain is then given by the difference

$$\dot{\gamma} = \overrightarrow{\gamma_o P_t} - \overleftarrow{\gamma_o P_t}$$

In most dislocation problems, the rate of thermal release in the reverse direction, $\overleftarrow{P_t}$, can be neglected because, under the applied driving force, dislocations move large distances after each forward activation event. Cases in which reverse jumps must be considered are therefore postponed to the end of this Chapter (sec. 45).

The activation rate $\overrightarrow{P_t}$ depends, in a simple picture, on the *frequency of attempts* at overcoming a particular obstacle, and on the *chance of success*. In a more macroscopic picture, it depends on the frequency with which the total energy of the crystal is redistributed between its various parts, and on the probability that one of the fluctuations in energy exceeds a certain magnitude. Very precise statements can be made about the *probability* of a fluctuation between specified equilibrium states (sec. 41). The *frequency* with which

fluctuations occur is much harder to calculate (sec. 42). Fortunately, for many problems, it is sufficient to know this frequency factor to within about one order of magnitude accuracy, since it occurs in a pre-exponential term.

The probability of an energy fluctuation of sufficient magnitude to cause activation is, in all cases of interest here, given by a Boltzmann distribution. The activation energy depends sensitively on stress; for example, it must go to zero when σ reaches the maximum glide resistance $\hat{\tau}$. This stress dependence is at the heart of all thermal activation problems in plasticity. It will be discussed on a formal basis in sec. 43; some examples based on physical models will be given in Chapter 5.

The "activation energy" will also, in general, depend on temperature. If it does, there is a difference between the activation enthalpy ΔH and the *free* enthalpy (or Gibbs free energy) of activation ΔG. In principle, ΔH is not only more easily obtained from experiments, but also with more certainty from theory. In practice, however, any difference between ΔH and ΔG can only be dealt with when the reason for the temperature dependence is known; for example, when it is due to the temperature dependence of the shear modulus. We come to the conclusion (sec. 43) that, because there is usually more than one mechanistic contribution to the glide resistance, it is preferable to deal with ΔG only, in the form

$$\Delta G = \mu b^3 \cdot \mathrm{g}\left(\frac{\sigma}{\mu}\right)$$

or simply

$$\Delta G = \Delta G(\sigma)$$

when there are no temperature effects.

The calculation of ΔG, which is an equilibrium property, is based on the equilibrium properties of the dislocation segment involved: they are described by the *line* glide resistance diagram $\tau_{\mathrm{LINE}}(a)$. The length of dislocation that is in direct contact with the obstacle is much shorter: it feels the *element* glide resistance τ_{ELEM} of the obstacle and is influenced by it in its vibration frequencies. Macroscopically, however, neither the detailed behavior of the short length of dislocation in contact with the obstacle, nor that of the segment undergoing a local thermal activation process can be observed: only the average behavior of certain critical, or "rate controlling", obstacles can. This is described by the *plane* glide resistance τ_{PLANE}. In this Chapter, all of these different glide resistances, which were discussed in detail in sec. 23, become important at various places; it is thus necessary to keep them well identified.

We will eventually introduce (sec. 44) one further material property designated by the symbol τ: the *flow stress* $\tau_{\mathrm{FLOW}} \equiv \tau$. It is a macroscopic measure of the structure through the (plane) glide resistance at a standard temperature and strain rate and will be extensively used in data analysis (Chapter 6).

There have been many excellent discussions on the details of thermally activated processes in solid state diffusion and dislocation motion. Of these

we find the following especially useful for further reading:

BASINSKI (1959), *Thermally Activated Glide in Face-Centered Cubic Metals and its Application to the Theory of Strain Hardening;*
BURKE (1965), *The Kinetics of Phase Transformations in Metals;*
CHRISTIAN and MASTERS (1964), *Low-temperature Deformation of Body-Centered Cubic Metals: II. Mechanism of Thermally Activated Flow;*
deMEESTER, YIN, DONER, and CONRAD (1973), *Thermally Activated Deformation of Crystalline Solids;*
DORN (1968), *Low Temperature Dislocation Mechanisms;*
FRANK (1968), *Thermally Activated Dislocation Motion in a Solid Containing a Multiple Spectrum of Dislocation Obstacles;*
GIBBS (1965), *The Thermodynamics of Thermally Activated Dislocation Glide;*
GIBBS (1969), *Thermodynamic Analysis of Dislocation Glide Controlled by Dispersed Local Obstacles;*
GLASSTONE, LAIDLER, and EYRING (1941), *Theory of Rate Processes;*
GRANATO, LÜCKE, SCHLIPF, and TEUTONICO (1964), *Entropy Factors for Thermally Activated Unpinning of Dislocations;*
HIRTH and NIX (1969), *An Analysis of the Thermodynamics of Dislocation Glide;*
LI (1965), *Thermodynamics of Dislocation Mobility and the Third-law Analysis of the Activation Process;*
SCHOECK (1965), *The Activation Energy of Dislocation Movement;*
SCHOECK (1974), *Thermodynamics and Thermal Activation of Dislocations;*
SEEGER (1958), *Kristallplastizität;*
VINEYARD (1957), *Frequency Factors and Isotope Effects in Solid State Rate Processes.*

41. FLUCTUATIONS IN THERMAL EQUILIBRIUM

Almost always, the glide resistance is not uniform, but has peaks and valleys associated with the cutting or bypassing of linear barriers or localized obstacles. At absolute zero (and ignoring the zero-point energy of the atoms) these barriers cannot be overcome unless σ exceeds the local peak glide resistance, $\hat{\tau}_{\text{LINE}}$. But at any temperature above absolute zero, thermal fluctuations redistribute energy; this means that a finite probability exists that the dislocation can penetrate the peaks in the τ–a curve, provided only that, macroscopically, the Second Law is obeyed ($\sigma \geqslant \tau_{\text{STOR}}$).

These fluctuations constitute a part of the *equilibrium* properties of a body kept at constant temperature. In this sense, it was inconsistent to treat, in Chapter 2, the equilibrium of dislocations with obstacles without regard to thermal fluctuations: we dealt only with *static* equilibrium. This static state will now serve as a reference state; for example, the energy necessary to overcome an obstacle quasi-statically is precisely the energy that must be supplied by thermal fluctuations, if the obstacle is to be overcome by thermal activation (see, for example, HART, 1958).

Activation Free Energies, Activation Work and Activation Area

Figure 41-1 shows a glide resistance diagram and an applied stress σ that is lower than the maximum value $\hat{\tau}_{\text{LINE}}$. A dislocation traveling from left to right is under a positive driving force $b(\sigma - \tau)$ in some regions, but would be in (static) equilibrium at position S. A finite increment of area further on

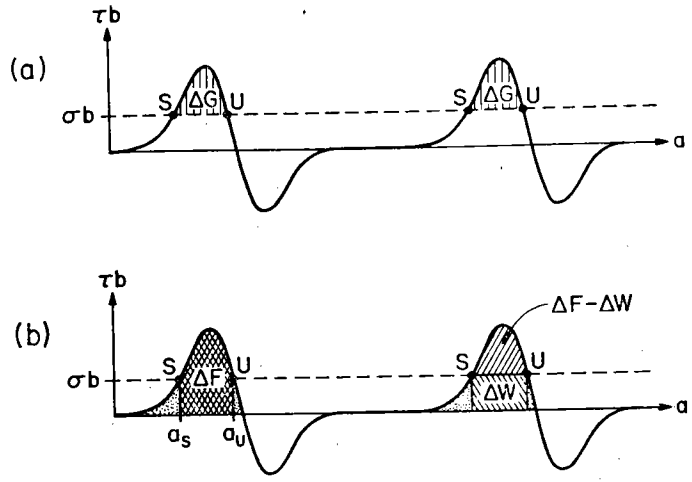

FIG. 41-1. (a, b) A glide resistance diagram illustrating the quantities ΔG, ΔF, ΔW and Δa.

would be a second equilibrium position, U. The first one is stable, the second unstable. If thermal fluctuations transferred the dislocation from the stable to the unstable equilibrium position, it would then again be under positive driving force.

The difference in energy between the stable and the unstable equilibrium states, at the given stress and temperature, is the shaded area in Fig. 41-1a:

$$\Delta G = \int_{a_S}^{a_U} (\tau_{\text{LINE}} - \sigma) b \, \mathrm{d}a. \qquad [41a]$$

We have identified it with a difference in free enthalpy, ΔG, and shall discuss this nomenclature below.

The probability, p_B, of an equilibrium fluctuation in energy greater than a given value ΔG, at a given temperature T, is equal to a Boltzmann term involving this energy, that is,

$$p_B = \exp - \frac{\Delta G}{kT} \qquad [41b]$$

where k is Boltzmann's constant. (See, for example, SLATER, 1939; TURNBULL and FISHER, 1949; but also ESCAIG, 1970.)

Figure 41-1b shows a different illustration of the same process. Consider a dislocation that is reversibly, with stress rising from zero, brought to the stable equilibrium position S: a certain amount of work (given by the stippled area) is done during this process. If the dislocation were removed from the unstable position U in a reversible manner also, an additional amount of work (given by the second stippled area) would have to be done. The remaining area under the glide resistance diagram (cross-hatched area) is the (Helm-

holtz) free energy necessary for activation:

$$\Delta F(\sigma) = \int_{a_S(\sigma)}^{a_U(\sigma)} \tau_{\text{LINE}}\, b\, \mathrm{d}a \qquad [41c]$$

Not all of this free energy must be applied by thermal fluctuations, since at constant applied stress, some work ΔW would be done *during* activation (in addition to the work done as the dislocation was brought up to S and was removed from U):

$$\boxed{\Delta W(\sigma) = b\sigma\Delta a(\sigma)} \qquad [41d]$$

where

$$\boxed{\Delta a(\sigma) \equiv a_U - a_S} \qquad [41e]$$

is the difference in area swept between the unstable and stable *equilibrium* states, or the *activation area*. We call ΔW the *activation work*; its geometric representation in a glide resistance diagram is shown in Fig. 41-1b.

Subtracting the work done by the applied stress during activation from the (Helmholtz) free energy necessary for such an activation to take place, we obtain the *energy that must be supplied by thermal fluctuations at constant temperature and stress*:

$$\boxed{\Delta G \equiv \Delta F - \Delta W.} \qquad [41f]$$

Insertion of the expressions [41c] and [41d] shows that this is, of course, the same ΔG as was introduced in eq. [41a]; Figs. 41-1a and b illustrate the relation as well. A third, equivalent, expression for ΔG, which will be used most extensively, is self-evident from Fig. 41-1:

$$\boxed{\Delta G = \int_{\sigma}^{\tau_{\text{LINE}}} b\Delta a\, \mathrm{d}\tau_{\text{LINE}}.} \qquad [41g]$$

The energy ΔG to be supplied by thermal fluctuations at constant temperature and stress is commonly called the *activation free enthalpy*, or the *Gibbs free energy of activation*. This nomenclature, and the use of the symbol G, is not identical with that common in thermodynamics, where the conventional definition is $G = U - TS + pV$, and the difference expression at constant temperature and *pressure* reads $\Delta G = \Delta F + p\Delta V$. It would indeed be the correct activation energy *in the absence of any other work terms*. The usage according to eq. [41f] (e.g. SCHOECK, 1965; GIBBS, 1965) comes from an analogy with this conventional definition for the case that a different work term (eq. [41d]), *but again only one*, is present, and the respective stress component is prescribed. One can then set

$$G = U - TS - \sigma ba$$

and eq. [41f] follows as the difference between two states at the same T and σ.

This nomenclature is unfortunate in the sense that, *when other work terms are present, they must all be included in* ΔW to give the activation energy $\Delta F - \Delta W$. The activation energy [41f] is thus exactly analogous to the quantity $-\Delta\Psi$ defined (as a virtual variation and with the opposite sign) in eq. [21r]. The analogy is also obvious in Fig. 41-1a: where the driving force $\sigma - \tau$ is *positive*, the area between the glide resistance diagram and the horizontal line corresponding to the applied stress is the energy *dissipated* when the dislocation moves at constant stress; where the driving force is *negative*, the area between these two lines is the energy to be supplied from thermal fluctuations if the dislocation is to move at constant stress. The restriction proscribed by the Second Law takes on a direct physical meaning: the energy taken out of the heat reservoir during activation cannot exceed that put into the heat reservoir through dissipation, in the average. Exactly this inequality is expressed in eq. [22h]: $\sigma > \tau_{\text{STOR}}$.

We will retain the convention [41f], with the work term [41d], and call the activation energy at prescribed T and σ the "activation free enthalpy" or "Gibbs free energy of activation", ΔG, for two reasons. First, the subtleties as to which work terms should be included are immaterial when, as is usual, all work terms except one are negligible. Second, the use of the name "free enthalpy" emphasizes the fact that the quantity G, with or without other work terms, is a state function.

In Fig. 41-2, we have plotted all three representations of the "obstacle" properties, in correlated fashion, versus the glide area: (a) the line glide resistance τ_{LINE}, exactly as in Figs. 41-1a and b; (b) its integral, the (Helm-

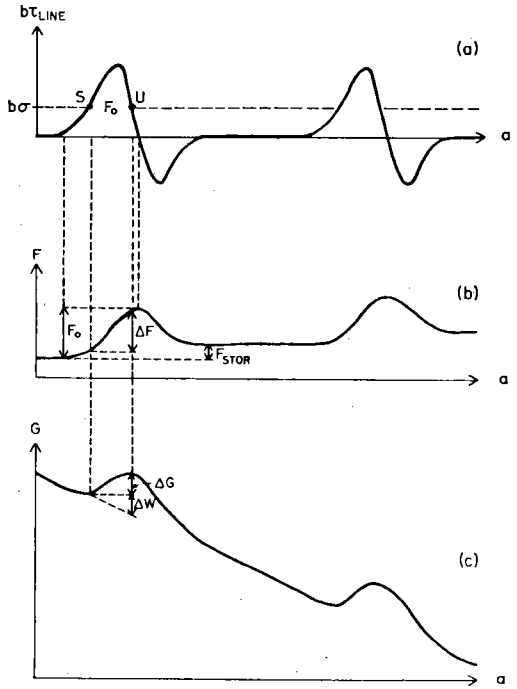

FIG. 41-2. The glide resistance diagram and its relation to the *F–a* and the *G–a* diagrams.

holtz) free energy F; and (c) the free enthalpy (or Gibbs free energy) G, obtained from F by subtracting a term proportional to a. This last diagram may be viewed as an inclined plane, with obstructions, down which a ball is made to roll in quasi-static fashion (i.e. without inertia effects). Thermal activation must help it get from the bottom of a "valley" to the top of the "hill". Apart from this obvious analogy, the diagram is not very useful, since it would have to be redrawn with a different "slant" for every new value of the stress. In the free energy diagram, Fig. 41-2b, the stable and unstable equilibrium positions have the same *slope*, though a different one for each stress; this is again less convenient than the glide resistance diagram, Fig. 41-2a, where different stresses merely correspond to different horizontal *levels*, σb. It is for this reason that we prefer to use the glide resistance diagram for most applications. Sometimes, it is also the one most directly derived although, in other cases, it is itself obtained by differentiation of a free energy diagram.

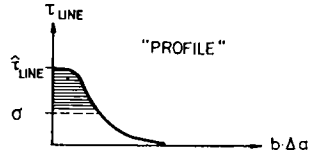

FIG. 41-3. The sheared glide-resistance diagram, now a diagram of the glide resistance against activation area Δa (not total area a) times b.

The appearance of Δa, rather than of a_S and a_U separately, in the expressions for activation work [41d] and activation energy [41g] suggests that the glide resistance diagram, Fig. 41-2a, might be simplified even further by a shear parallel to the a-axis so that the abscissa becomes Δa. This is done in Fig. 41-3 for one "obstacle" or other glide resistance unit. The resulting diagram may be called the *glide resistance profile*; it is the basic material property on which thermal activation theory rests. In principle, this sheared profile can be derived from experimental measurements; the unsheared obstacle shape cannot.

Only the resistive part of the glide resistance diagram, Fig. 41-2a, has been used for the profile of Fig. 41-3; negative glide resistances do not enter activation problems (except in reverse glide, sec. 45). The profile would, in fact, be exactly the same, if the dislocation encountered the region of negative glide resistance first, and the region of positive resistance second; that is if the obstacle were attractive rather than repulsive (Fig. 25-2).

One quantity often used to characterize an obstacle or other glide resistance unit, namely the total free energy necessary to overcome the resistive part, without the aid of external work, is

$$F_o \equiv \Delta G(0) \equiv b \int_0^{\hat{\tau}} \Delta a \, d\tau_{LINE}. \qquad [41h]$$

It is the total area under the positive part of a "unit" in the glide resistance diagram, or the total height of a "hill" (from the approaching side) in a free energy diagram (Fig. 41-2).

The *net* free energy associated with one "obstacle" in both its regions of positive and (if any) of negative glide resistance is in the free energy stored, F_{STOR}, introduced in eq. [22g]; for generality, it was left finite in Fig. 41-2.

Activation Enthalpy and Activation Entropy

In general, the total activation free energy F_o, and the glide resistance, will depend on temperature in some unknown way schematically shown in Fig. 41-4a. The negative slope in this diagram may be called the *total activation entropy*

$$S_o \equiv -\frac{dF_o}{dT} \qquad [41i]$$

and the intercept of the tangent on the ordinate is the total activation *energy* proper:

$$U_o \equiv F_o + TS_o. \qquad [41j]$$

For thermal activation at constant stress, we may similarly define the *activation entropy* (Fig. 41-4b)

$$\Delta S \equiv -\left.\frac{\partial \Delta G}{\partial T}\right|_\sigma \qquad [41k]$$

and

$$\Delta H \equiv \Delta U - \Delta W = \Delta G + T\Delta S. \qquad [41\ell]$$

This is the *activation enthalpy*, the quantity usually meant when one simply refers to an "activation energy". As ΔG, it should, in principle, contain *all* work terms, not just the one deemed most important in eq. [41d].

The usefulness of ΔH in rate theory stems from the fact that it exactly equals the derivative

$$\Delta H = \left.\frac{\partial(\ \Delta G/kT)}{\partial(1/kT)}\right|_\sigma \qquad [41m]$$

even when ΔG depends on temperature, as can be easily verified by use of eqs. [41k] and [41ℓ].

The *curvature* in a plot of $\Delta G/kT$ versus $1/kT$ at constant stress then is

$$\left.\frac{\partial \Delta H}{\partial T}\right|_\sigma = T\left.\frac{\partial \Delta S}{\partial T}\right|_\sigma. \qquad [41n]$$

In principle, this provides a means of determining the activation entropy by integration (Li, 1965; Arsenault, 1971):

$$\Delta S(\sigma,T) = \Delta S(\sigma,0) + \int_0^T \left.\frac{\partial \Delta H}{\partial T'}\right|_\sigma \frac{dT'}{T'}. \qquad [41o]$$

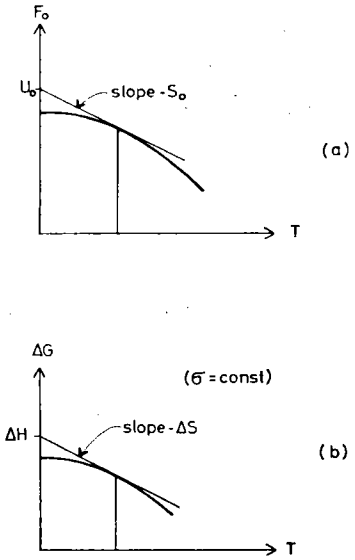

FIG. 41-4. The dependence of the total free energy of activation (a) and of the activation free enthalpy at a given stress (b) on temperature. The slope of the diagram is the (total) activation entropy.

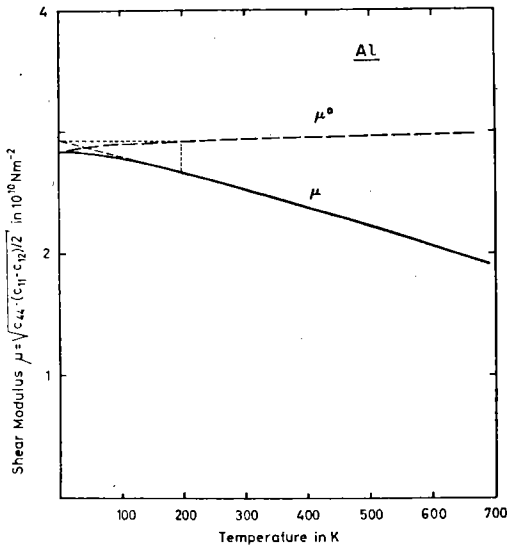

FIG. 41-5. The dependence of the shear modulus on temperature for aluminum (after SUTTON, 1953). If μ° is obtained by extrapolating from a finite temperature T to absolute zero, the result depends mildly on the choice of T as shown.

The integral is hard to evaluate in practice when all the curvature in Fig. 41-4 or in the Arrhenius plot is concentrated at low temperatures, as Fig. 41-5 would suggest when the temperature dependence of the elastic constants is responsible for the entropy (JONAS and LUTON, 1971a,b; JONAS *et al.*, 1972).

The first term in eq. [41o], the entropy at zero temperature, is not necessarily zero (LI, 1965). It may then depend on stress, and the complete formula would be

$$\Delta S(\sigma, T) = \Delta S(0,0) + \int_0^{\sigma} \left.\frac{\partial \Delta S}{\partial \sigma'}\right|_{T=0} d\sigma' + \int_0^{T} \left.\frac{\partial \Delta H}{\partial T'}\right|_{\sigma} \frac{dT'}{T'} \qquad [41o']$$

or

$$\Delta S(\sigma, T) = \Delta S(0, 0) + \int_0^{\sigma} \left.\frac{\partial \Delta S}{\partial \sigma'}\right|_{T} d\sigma' + \int_0^{T} \left.\frac{\partial \Delta H}{\partial T'}\right|_{\sigma=0} \frac{dT'}{T'} \qquad [41o'']$$

depending on whether it is easier to extrapolate to zero temperature or to zero stress. Note that the stress dependence of the entropy is identical to the temperature dependence of the apparent activation area (eqs. [41k], [43g]).

Any calculation of an element glide resistance is usually based on a continuum approximation; that is, on an assumption that a change in some microscopic parameters (such as in the number of atomic bonds between different atoms) may be represented by a macroscopic material property (such as the interface free energy, or "surface tension"). In many cases, specifically those involving internal stresses or self stresses, the material property of importance is the shear modulus; in others, such as the example given above, it is some surface tension; in others it may be the stacking fault energy.

All these material properties depend, albeit weakly, on temperature. The assumption, also usually made, that the temperature dependence of the microscopic property "glide resistance" is the same as that of the macroscopic property "shear modulus" is a more stringent one. For example, it implicitly asserts that only the long-wavelength limit of the phonon spectrum enters; local changes of vibrational frequency at dislocation cores, jogs, or kinks, or at surface steps left by cutting, are ignored. Once this assumption is made, the integral of this glide resistance over some glide area, evaluated using the shear modulus for a given temperature, is precisely the free energy for this temperature. For one entire obstacle, for example, we would have

$$F_o(T) \propto \mu(T)\, b^3(T). \qquad [41p]$$

(The temperature dependence of b is often negligible, but, in principle, it must be included as was pointed out by GIBBS, 1965.)

A more realistic impression of these temperature effects may be gleaned from Fig. 41-5, in which we have reproduced the actual temperature dependence of the shear modulus μ (the precise combination of elastic constants defined in Table 2-I) for aluminum; it is weak and, to a good approximation, linear over a wide temperature range (JONAS *et al.*, 1972). If the free energy were really proportional to μ (eq. [41p]), the *internal* energy of activation U_o would be essentially temperature independent and proportional to μ^o, the value of the shear modulus obtained by *extrapolation* to zero temperature (Fig. 41-5). Clearly the value of this extrapolated modulus depends on the point on the curve from which the extrapolation is made; this extrapolated value is plotted as μ^o on Fig. 41-5. It does not vary much at higher temperatures.

From this point of view, a calculation of U_0 rather than F_0, or equivalently of the glide resistance at *zero temperature* (but without zero-point effects), would be based on fewer assumptions; it would leave room for activation entropies other than that due to the temperature dependence of the macroscopic shear modulus, surface free energy, etc. In practice, however, the material properties at room temperature are usually inserted, and so room temperature is used as a reference state. We continue the practice of defining the glide resistance as derivatives of the *free* energy (eq. [22e]), in part because of difficulties encountered with glide resistance diagrams that stem from two distinct mechanisms (sec. 43).

42. Activation Rates

In the last section, we have discussed the probability p_B of *fluctuations*. The quantity of interest for the kinetics of dislocation glide is, however, the *rate* P_t at which such fluctuations occur. It is given by the product of p_B with a *frequency factor*; its magnitude will be discussed in this section.

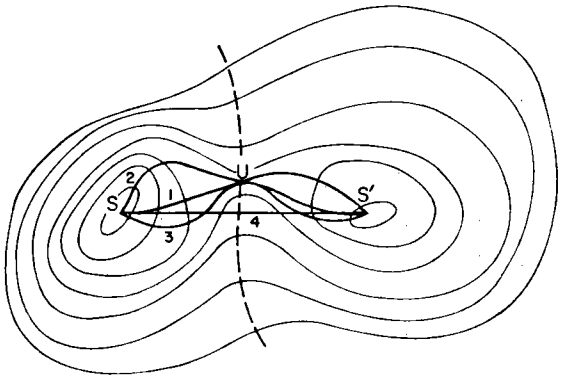

FIG. 42-1.i A schematic representation of contours of constant free enthalpy, G for a two-dimensional configuration space. S represents the ground state, U the activated state. Four hypothetical reaction paths are illustrated.

The problem is complicated by the fact that a large number of different paths may be available for the fluctuation to occur. The sequence of states is then not described by a single coordinate like a in Fig. 41-2. Figure 42-1 illustrates the case in which there are two degrees of freedom. The free enthalpy G, described by a single curve as a function of a in Fig. 41-2c, is now described by contour lines, and the maximum in G at the unstable equilibrium point U has turned into a saddle point. This point U and the two stable equilibrium points S and S′ are the only points at which the whole body is in equilibrium at the given stress. The free enthalpy G at all other points in Fig. 42-1 is calculated on the assumption that the body is in equilibrium with respect to all degrees of freedom except the two that are especially plotted in the figure, and with applied stresses and a temperature bath. (In this sense, G is not quite a complete free enthalpy of the body.)

The one-dimensional diagram in Fig. 41-2c may now be looked upon as a *section* of the two-dimensional diagram in Fig. 42-1 along the (generally

curved) *reaction coordinate*; for example, one of the lines drawn in Fig. 42-1. The difference ΔG in the free enthalpy of the ground state S and the activated state U is independent of the reaction path, it is a "static" equilibrium property; but the *rates* of transfer across the saddle point may be different for the different paths.

Two approaches are commonly used to calculate, or rather estimate, activation *rates*. In *kinetic models*, the reaction coordinate is assumed to be known. The activation rate then follows from the *attempt frequency*, i.e. the frequency of vibration in the ground state *in the direction of the reaction coordinate*, multiplied by the *chance of success* given by the Boltzmann term p_B. The difficulty lies in the determination of the reaction coordinate. It is illustrated in Fig. 42-1 by plotting four different paths, each one of which has some phenomenological plausibility, and which generally do not coincide. They leave the ground state: (1) in the direction parallel to the reaction coordinate in the saddle point (where it is well defined); (2) in the direction of the "lowest mode"; (3) in the direction of "steepest ascent"; and finally (4) in the direction heading straight for the new stable equilibrium point S′.

An alternative approach is provided by the *statistical* theory of fluctuations (also called *transition state theory* or "*absolute rate theory*"). It avoids the difficulty of identifying the actual reaction path by considering *all* paths. In a diagram like Fig. 42-1, all states on the line (dashed in the figure) that separates the initial and final states are compared with all states in the half-space to the left of this line. The fact that these two regions have different dimensions, and thus a different number of degrees of freedom for vibrations, leads to a transition rate. In general, the theory means to consider *all* degrees of freedom of the system; Fig. 42-1 would then have to be replaced by a multidimensional configuration space, in which the *potential* energy is defined at every point, but the free enthalpy only follows from the proper averaging procedure. For practical applications, the hyperspace is narrowed down again to only as many dimensions as are considered relevant and noninteracting with the rest. In this matter of judgment lies one of the difficulties of the theory, the other one being that a harmonic approximation must be made to obtain any usable results.

We shall summarize some results of both the statistical and the kinetic approaches in this section, but will first outline various definitions and order-of-magnitude estimates. For background reading, we recommend the treatment of the kinetic and statistical approaches to chemical reactions by HINSHELWOOD (1940, chap. 9) and to solid state diffusion by SEEGER (1955a, sec. 12), as well as the far-reaching first paper on absolute reaction rates by POLANYI and WIGNER (1928).

Frequency Factors and Activation Entropies

The net rate P_t of thermal release from a region of negative driving force (see sec. 33) is, in principle, the result of two competing processes: the rate

of activation from the stable to the unstable state (e.g. "S" and "U" in Fig. 41-1), and the rate of activation in the reverse direction, from a newly reached stable state back to the unstable state. In sec. 45, we will discuss cases where both rates are important and shall call them $\vec{P}_t$ and $\overleftarrow{P}_t$. Here, we concentrate on the rate of thermal activation in the *forward* direction and call it P_t.

This rate of activation is the product of a *frequency factor* and a *Boltzmann factor*, together called an *Arrhenius term*. Depending on whether a description in terms of the *free* enthalpy or of the enthalpy is desired, it may be written as:

$$P_t = \nu_G \exp\left\{-\frac{\Delta G}{kT}\right\} \qquad [42a]$$

or as

$$P_t = \nu_H \exp\left(-\frac{\Delta H}{kT}\right). \qquad [42b]$$

Here we have introduced effective frequency factors with subscripts that indicate the equation in which they are used. The two frequency factors may be formally related to each other by using eq. [41ℓ]:

$$\nu_H = \nu_G \exp\frac{\Delta S}{k}. \qquad [42c]$$

From a mechanistic point of view, ν_G or ν_H might, for a first estimate, be related to one of two extreme frequencies: either the "atomic" frequency ω_A (eq. [31f]) or (for discrete obstacles) the dislocation ground frequency (Fig. 42-2a),

$$\nu_o \equiv \omega_A \frac{b}{4l_e}. \qquad [42d]$$

In most practical cases, these two frequencies are orders of magnitude apart. Better estimates are therefore needed; they will be sketched below and

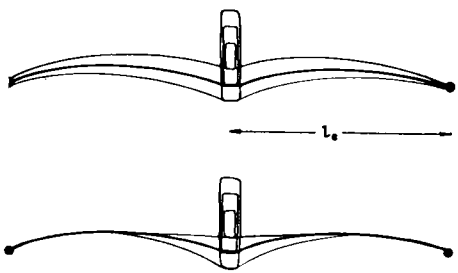

FIG. 42-2. (a) A fluctuation with wavelength $4l_e$. (b) A fluctuation of shorter wavelength.

generally give values for ν_G or ν_H that are between these two limits; that is:

$$\nu_o \leqslant \nu_G \leqslant \omega_A. \qquad [42e]$$

The meaning of the limits may be seen as follows. The value ω_A corresponds to the frequency of uncorrelated atomic motions. The dislocation, however, through its line tension, provides some correlation between the atomic motions of interest: their wavelength should thus be longer. On the other hand, a wavelength longer than $4l_e$ would correspond to a correlated overcoming of many obstacles at the same time, which is not necessary. Thus, eq. [42d] should give a lower limit for discrete obstacles.

A mechanistic estimate of a form similar to eq. [42d] is due to FRIEDEL (1956, p. 47, or 1964, p. 66) who derived it via a classical treatment of the lowest natural frequency of a taut string (the dislocation) of length l_e, mass ρb^2 per unit length, and line tension μb^2. His result:

$$\nu_{\text{FRIEDEL}} \simeq \frac{v_S}{l_e} \qquad [42f]$$

was rationalized as follows. Suppose (Fig. 42-2b) a short length of dislocation around the obstacle vibrated away from the equilibrium position (solid line). The rest of the dislocation segment would then immediately tend to reverse the non-equilibrium curvatures at the point of juncture—unless the whole dislocation segment "knew" about the activation event. The frequency in eq. [42f] is just the inverse of the time necessary to propagate a sound wave along this dislocation segment.

Further consideration of the problem (GRANATO *et al.*, 1964) shows that FRIEDEL's argument is not dynamic enough. One may say that not only one pulse travels along the dislocation segment during an activation event; many do, and they interfere with each other. Treatments in terms of standing waves, which we shall summarize below, then show that the "effective" wavelength is indeed much shorter than l_e, and is a property of the obstacle and the dislocation line tension, but *not* of the obstacle *spacing* (unless it is especially small).

The result obtained by GRANATO *et al.* (1964), and discussed further below is:

$$\boxed{\nu_G \simeq \tfrac{1}{10}\,\omega_A C} \qquad (\textit{discrete obstacles}) \qquad [42g]$$

where C is the normalized *obstacle stiffness*

$$C \equiv \frac{\mathrm{d}(K/\mu' b^2)}{\mathrm{d}(y/b)} = \frac{1}{\mu' b}\frac{\mathrm{d}K}{\mathrm{d}y}. \qquad [42h]$$

The stiffness of the obstacles (that is, the slope $\mathrm{d}K/\mathrm{d}y$ of its force-distance curve) enters because this determines the local vibration frequencies of a dislocation segment at and near the obstacle. Unless the force-distance curve

is linear, the stiffness depends on the applied force, i.e. on the applied stress times the effective obstacle spacing. The frequency ν_G may, therefore, be a weak function of stress and structure.

The order of magnitude of ν_G may be estimated by noting that

$$0.01 < K/\mu' b^2 < 0.5$$

for discrete obstacles sufficiently strong to be interesting, yet not so strong that Orowan looping occurs (eq. [25i]); and that y/b varies between about 1 for the weak obstacles (substitutional solute atoms, for example) and about 10 for obstacles that are stronger (e.g. Guinier–Preston zones) yet which are still sufficiently small that thermal activation can help in overcoming them. It follows that

$$\frac{1}{100} \lesssim C \lesssim \frac{1}{10} \qquad [42i]$$

and therefore that

$$\left.\begin{aligned} &\frac{\omega_A}{1000} \lesssim \nu_G \lesssim \frac{\omega_A}{100} \\ &\text{or typically} \quad \boxed{\nu_G \lesssim 10^{11}\ \mathrm{s}^{-1}.} \end{aligned}\right\} \qquad [42j]$$

We shall use this value for estimates in subsequent sections.

At low temperatures some frequencies cease to be available in the lattice spectrum. As a rough estimate, one may say that the "effective Debye temperature" T_ν, below which such effects must be considered, is given by

$$kT < kT_\nu \equiv h\nu_G \quad (\textit{quantum effects}). \qquad [42k]$$

By virtue of the estimate [42j], this temperature is less than one hundredth of the Debye temperature and thus, in most cases, too low to be of interest for plastic flow problems. The various considerations necessary at those low temperatures have been reviewed by ALEFELD (1964) and SCHOECK (1974).

It is appropriate at this point to introduce a word of caution. The Boltzmann probability expression, and the Arrhenius rate equations that are based on it (e.g. eq. [42a]) are valid only if certain conditions are met. First, the probability of a fluctuation exceeding ΔG in magnitude is only described by a Boltzmann distribution provided $\Delta G \gg kT$. When $\Delta G \approx kT$, the velocity of a dislocation is determined by dynamic effects (Chapter 3), not by rates of thermal release from obstacles. At the other extreme, when $\Delta G/kT$ is very large, backward jumps (to be discussed in sec. 45) may be important, and the release rate is no longer given by a single Arrhenius term. Finally, there are statistical restrictions. The total number of dislocation segments in a position to be activated, or the total number of activated events that a single segment undergoes, must be sufficiently large that the statistical averaging implicit in the Arrhenius equations has proper significance.

The difference between the frequency factors ν_G and ν_H was meant, in the above discussion (eqs. [42c], [41k]), to stem from the temperature dependence of ΔG, which is a property of the individual obstacles; one may call ΔS in eq. [42c] the "obstacle entropy". Some authors, following GRANATO *et al.* (1964), consider the vibrations of the free dislocation segment to lead to another entropy term, so that one could write

$$\nu_G = \nu_o \exp \frac{\Delta S_{DIS}}{k} \qquad [42\ell]$$

or

$$\nu_H = \nu_o \exp \frac{\Delta S + \Delta S_{DIS}}{k} \qquad [42m]$$

where

$$\boxed{\Delta S \equiv \Delta S_{OBSTACLE}} \qquad [42n]$$

as before. However, the value of ΔS_{DIS} depends, according to eq. [42ℓ], on the choice of ν_o. The value [42d] might be logical, since ΔS_{DIS} would then always be positive, but others have been proposed (VINEYARD, 1957). Furthermore, ΔS_{DIS} would have to depend on l_c, if indeed ν_G does not; the introduction of a structure parameter into an equation such as [42i] at two places in a manner that it exactly cancels out again, is clearly confusing. For these reasons, we continue to regard the activation entropy to be a property of the obstacle only (eq. [42j]) and will not use ν_o as a frequency factor.

It is true that ΔS_{DIS} should, in principle, be measurable through its temperature derivative (eq. [41o]). As the above discussion shows, this would require going to temperatures below $h\nu_G/k$: at all useful temperatures, ΔS_{DIS} is thus constant with temperature.

Transition State Theory

The transition state theory was developed for crystalline solids—although without explicit consideration of applied stresses—by VINEYARD (1957). It considers configuration space divided into two halves and derives the partition function of all states in the half that contains the initial stable state by assuming them to be reached by vibrations around this stable state in a harmonic potential. Similarly, it derives the partition function of all unstable states by assuming them to be harmonic vibrations around the state "U" (Fig. 42-1) in unstable static equilibrium; this is of course, not possible in any direction in which the curvature of the potential is negative—and there must be (at least) one of these to make the state unstable.

As discussed in the introduction to this section, the transition state theory considers, in principle, all degrees of freedom of the system, but, in practice, only those assumed relevant according to a particular model. GRANATO *et al.* (1964) assumed that the relevant degrees of freedom were those associated with the vibrations of the two dislocation segments on either side of a (discrete) "pinning point". If these vibrations have N + 1 independent modes in the "stable" position of the dislocation, they have N in the "unstable" position. Figure 42-1 may be looked upon as a two-dimensional representation of the N + 1 degrees of freedom. The free enthalpy G plotted in it is then associated with all other degrees of freedom of the system (which are still many more than N), but does not contain any "entropy" terms associated with the vibration of the dislocation "string", in accordance with the

terminology we have previously adopted. In this terminology, the result of GRANATO *et al.* (1964) is that the (forward) activation rate is

$$P_t = \frac{\prod_{1}^{N} \nu_i^S}{\prod_{1}^{N} \nu_i^U} \exp\left[-\frac{\Delta G}{kT}\right] \qquad [42o]$$

where the ν's are the frequencies of the harmonic oscillators around the stable (ν^S) and unstable (ν^U) states, respectively; the index 0 has been chosen for the mode in the stable state that has no equivalent in the unstable state.

Dividing eq. [42o] through by P_t, one sees that the transmission rate P_t plays the role of a "frequency" in the direction of the reaction coordinate in the point U. The right-hand side of the equation is then the ratio of two complete partition functions, which must be 1, since both states are supposed to be in equilibrium.

The ratio of products of frequencies in eq. [42o] would be easy to evaluate if the terms in the numerator and denominator canceled in a pairwise manner, at least approximately. For example, if all frequencies with the same mode number i were the same in the S and the U state, one would be left with

$$\nu_G = \nu_o \qquad (\textit{false assumption}) \qquad [42p]$$

which is about twice the lowest possible frequency ν_o (eq. [42d]).

The evaluation by GRANATO *et al.* (1964) showed, however, that this is not even approximately true for discrete obstacles. While the terms with equal mode number are similar at the high-frequency end of the spectrum, the frequency of a *low-lying* mode in the stable state is approximately equal to that in the *next higher* mode in the unstable state. By an elegant graphical evaluation, GRANATO *et al.* estimated which of the intermediate frequencies in the stable state is essentially uncanceled by one in the unstable state. Their result, quoted earlier (eq. [42g]), is

$$\nu_G \simeq \tfrac{1}{10}\,\omega_A C \qquad [42q]$$

where C is a normalized stiffness, defined by eq. [42h].

The most noteworthy feature of this result is that the effective frequency factor does not depend on the length l_e of the free dislocation segments. One can only conclude that the number N of degrees of freedom that were considered relevant to the problem was already too large. The fact that ν_o of eq. [42d] depends on l_e is a property of the Friedel model, which considers dislocation segments stretched between rigid pinning points. The statistical-mechanical treatment emphasizes that the compliance of the obstacle itself is of vital importance. We shall come back to this point in our discussion of kinetic fluctuation models.

Some treatments of the transition state theory, we must note for completeness, retain a factor kT/h in the frequency factor, following GLASSTONE *et al.* (1941). Both the appearance of an explicit temperature dependence and of Planck's constant are fortuitous since they fall out in more complete treatments for solid state applications (see, for example, SEEGER, 1955a, p. 412; VINEYARD, 1957; and even POLANYI and WIGNER, 1928).

Kinetic Fluctuation Models

Instead of looking at the stable and unstable states as being in equilibrium with respect to *all* their coordinates, as in the transition state theory, one may look at the

fluctuation by the amount ΔG defined in eq. [42a] as the result of a kinetic process, in which the Boltzmann term gives the probability of success and the frequency factor gives the "attempt frequency".

For a very simple model which, unrealistic though it is, may be used for order-of-magnitude estimates, consider a piece of straight dislocation of length $\mathscr{L}$ in front of a linear barrier, with an equilibrium position y_σ at the applied stress σ. Linearize the force–distance diagram of the barrier in the neighborhood of this position so that

$$(\tau - \sigma)b\mathscr{L} = \mu' bC(y - y_\sigma) \qquad [42r]$$

where C is the normalized stiffness defined in eq. [42h]. Set the drag coefficient B to zero for the small excursions considered (this will be discussed further below), and set the mass per unit length of the dislocation to the value [31n]. Then the equation of motion for this piece of dislocation becomes

$$\tfrac{1}{2}\mathscr{L}\frac{\mu'}{\omega_A{}^2}\ddot{y} + \mu' bC(y - y_\sigma) = 0. \qquad [42s]$$

An appropriate solution is

$$y = \sin 2\pi\nu t$$

with the frequency

$$\nu = \frac{\omega_A}{2\pi}\sqrt{2Cb/\mathscr{L}}. \qquad [42t]$$

Since, for a linear barrier, the resisting force and thus the stiffness C is itself proportional to $\mathscr{L}$ (eq. [25d]), one may write eq. [42t] more appropriately

$$\nu = \frac{\omega_A}{2\pi}\cdot\sqrt{2\frac{\mathrm{d}(\tau_{ELEM}/\mu')}{\mathrm{d}(y/b)}}. \qquad [42t']$$

A real piece of dislocation would not remain straight but vibrate in various modes, depending in some measure on the boundary conditions to be discussed below. However, these vibrations do not tend to carry the piece as a whole forward, and for this reason the frequency [42t] may be taken to be a mode "in the direction of the reaction coordinate".

To obtain an estimate for the attempt frequency ν_G to be inserted into eq. [42a], let us consider two extreme examples. The first concerns a *long* piece of dislocation attempting the nucleation of a pair of kinks of atomic height (Fig. 42-3). If the interaction between these kinks is neglected for the *long* piece of dislocation, eq. [42t'] already gives the attempt frequency, except for one complication, which was pointed out by CELLI *et al.* (1963) and, more generally, already by POLANYI and WIGNER (1928): the nucleated kink pair has *two* degrees of freedom that do not qualify as vibration states. One of these consists of their spreading as envisaged in the nucleation process; the other of their lateral translation as a rigid body.

Using the transition state theory for this aspect (LOTHE and HIRTH, 1959), we

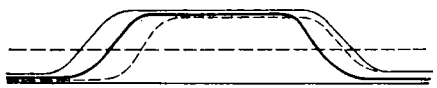

FIG. 42-3. Expansion (——) versus translation (- - -) of a critical double kink (——).

would have to replace one of the frequencies in the denominator of eq. [42o] by a translational term such as the thermal velocity

$$v_{\text{TRANS}} = \sqrt{\frac{kT}{4\pi M_{\text{KINK}}}} \qquad [42u]$$

divided by the length of the dislocation, where M_{KINK} is the mass of one kink, which is U_{KINK}/v^2_s (eq. [31m]). Furthermore, the assumption is made that the additional uncanceled frequency in the numerator of eq. [42o] is approximately equal to [42t']. This gives, *per length b*,

$$\boxed{\nu_G = \frac{\omega_A}{\pi\sqrt{2\pi}} \cdot \sqrt{\frac{2U_{\text{KINK}}}{kT}} \cdot \frac{d(\tau_{\text{ELEM}}/\mu)}{d(y/b)}} \qquad \textit{(linear barriers)}. \qquad [42v]$$

In this case, the effective frequency depends mildly on temperature, in addition to depending possibly on stress through the stiffness term. An order-of-magnitude estimate may be obtained by setting $F_o \simeq 0.4$ eV, $\hat{\tau}_{\text{ELEM}} \simeq \mu'/100$, and $\hat{y}/b \simeq \frac{1}{2}$; this gives, for room temperature, again the value $\omega_A/100$ (eq. [42g]).

FIG. 42-4. A *local* forward fluctuation of a dislocation segment at an obstacle is opposed by the line tension of the dislocation itself.

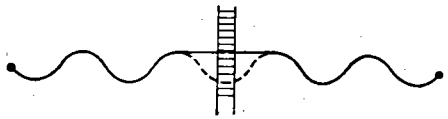

FIG. 42-5. The activated segment has a length equal to the wavelength of a natural frequency of the dislocation line.

The other application is to a shorter piece of dislocation in front of a discrete obstacle. Here it becomes of paramount importance that the piece of dislocation is in fact connected to other parts of the dislocation. If they vibrated only to the extent enforced by the piece we are considering, the situation illustrated in Fig. 42-4 would develop; the substantial line tension forces from the rest of the dislocation would have to be incorporated into the equation of motion [42r] and would effectively prevent all independent vibrations of the element. One must instead consider the element vibrations to be part of a standing-wave spectrum of the whole dislocation segment. The interaction would vanish, if the length $\mathscr{L}$ of the piece were just equal to one wavelength of the standing wave (Fig. 42-5)—and *its* vibration frequency equalled that of the piece:

$$\mathscr{L} \simeq \lambda \frac{v_s}{\nu}. \qquad [42w]$$

Inserting this value into eq. [42t] and solving for ν, we find (KOCKS and LÜCKE, unpublished)

$$\nu_G \simeq \frac{1}{2\pi^2}\,\omega_A C. \qquad [42x]$$

This is within a factor 2 of the calculation by GRANATO *et al.* (1964), eq. [42q].

Finally, we need to justify the neglect of a damping term $B\mathcal{L}\dot{y}$ in the equation of motion [42r]. This is justified so long as the dislocation is not overdamped for the vibrations under consideration. This is so when the square of the coefficient of $\dot{y}$ is smaller than 4 times the coefficient of $\ddot{y}$, times the coefficient of y. With the value [31q] for B and eq. [42t], this means

$$\frac{kT}{\mu b^3} < \frac{2\pi\nu}{\omega_A} \qquad [42y]$$

which is easily fulfilled with the estimate [42g].

43. The Stress Dependence of Thermal Activation

When the strain rate at a given stress and temperature is governed by thermal release (eq. [33ii]), and the net rate of release may be approximated by the rate of *forward* activation $\vec{P}_t$ (eq. [42a]), the rate equation reads

$$\boxed{\dot{\gamma} = \gamma_o \nu_G \exp -\frac{\Delta G}{kT}.} \qquad [43a]$$

The dependence of strain rate on stress at a given temperature may be expressed as

$$\left.\frac{\partial \ln \dot{\gamma}}{\partial \sigma}\right|_{T,\tau} = \left.\frac{\partial \ln \gamma_o}{\partial \sigma}\right|_{T,\tau} + \left.\frac{\partial \ln \nu_G}{\partial \sigma}\right|_{T,\tau} - \frac{1}{kT}\left.\frac{\partial \Delta G}{\partial \sigma}\right|_{T,\tau} \qquad [43b]$$

or, with the definition [34r],

$$m \equiv \left.\frac{\partial \ln \dot{\gamma}}{\partial \ln \sigma}\right|_{T,\tau} = \left.\frac{\partial \ln \gamma_o}{\partial \ln \sigma}\right|_{T,\tau} + \left.\frac{\partial \ln \nu_G}{\partial \ln \sigma}\right|_{T,\tau} - \frac{1}{kT}\left.\frac{\partial \Delta G}{\partial \ln \sigma}\right|_{T,\tau}. \qquad [43c]$$

The index τ at the partial differentials indicates that the entire obstacle structure is assumed constant in the variation.

We have seen in secs. 32 and 33 that the contribution to m from the stress dependence of γ_o, through the mobile dislocation density, is usually between 1 and 3; and in sec. 42 that the contribution to m from the stress dependence of ν_G, through the obstacle stiffness, may be positive or negative, but also usually of order 1. The stress dependence of the activation energy ΔG may, however, be considerably larger, to the point that the first two terms in eqs. [43b] and [43c] can rightly be neglected. In that case, experimentally measured relations between strain rate and stress can give important information about ΔG, and thus about the nature of the rate-controlling obstacle. This case will be analyzed here.

When, instead, the term involving ΔG in eq. [43c] is small compared to the others, the value of m reflects mainly the way in which the mobile dislocation density and frequency factor vary with stress. The appropriate way of handling experimental data for these two situations is discussed in Chapter 6.

Activation Volume and Apparent Activation Area

In applications of thermal activation analysis outside plasticity, a dependence of the activation energy on a particular component of applied stress—the hydrostatic pressure, p—is frequently encountered. One commonly describes this behavior by the derivative

$$\Delta V \equiv \left.\frac{\partial \Delta G}{\partial p}\right|_T \qquad [43d]$$

called the *activation volume*. The effect on the activation energy of pressures comparable with that of the atmosphere is usually very small.

Similarly, the activation energy for plastic flow may depend on hydrostatic pressure, although again the effect is usually small. For example, the number of point defects with which the dislocation might interact, or their stress field, might depend on pressure, as might the width of the dislocation core. Such an effect would be properly described by the activation volume [43d].

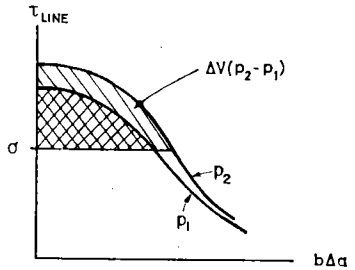

FIG. 43-1. A change of pressure from p_1 to p_2 will, in general, change the obstacle profile. When p_1 and p_2 are comparable with atmospheric pressure, the effect is negligible.

One may think of the influence of hydrostatic pressure as one on the glide resistance diagram. Figure 43-1 shows two profiles for different pressures and the two activation energies as differently shaded areas. Note that, since the glide resistance was defined as a derivative of the free energy F (eq. [22e]), the present interpretation amounts to including a "work term" in ΔF, not in ΔW.

The width of the dislocation core may well depend on *other components of stress*, too. As an example, the conversion of a screw dislocation core in bcc crystals from the rest configuration of three-fold symmetry into the ribbon-like configuration necessary for glide must depend on the entire stress tensor. The activation energy for glide may, thus, in general depend on all components of stress. The derivatives

$$\left.\frac{\partial \Delta G}{\partial \sigma_{ij}}\right|_{T,\ \text{other}\ \sigma}$$

could all be different from zero.

The shear stress in glide plane and glide direction here simply called σ (eq. [22d]) is of special importance. In addition to its possible influence on core structures and other atomic configurations, it provides the very driving force for the glide process

under consideration. Its effect on the activation energy is not small and is our prime concern. In particular, the activation energy will vanish as σ approaches $\hat{\tau}_{\text{LINE}}$.

It would obviously be convenient to have a general name and symbol for stress derivatives of the activation energy. In analogy to eq. [43d], and because they have the dimensions of volume, it was common for some time to call them all "activation volume", in particular also $-\partial\Delta G/\partial\sigma$. This terminology has been felt to be confusing (if not "wrong") by many recent authors. The now more common term "activation area (times b)" is, however, at least as confusing: it has a very specific geometric meaning (eq. [41e]), which sometimes equals $-\partial\Delta G/\partial\sigma$ and sometimes not (eq. [43h]). The term is also applied to $-\partial\Delta H/\partial\sigma$ which is, in general, different again (eqs. [43p], [43r]). The worst feature of these geometrically inspired names is that their correspondence to $-\partial\Delta G/\partial\sigma$ relies on a *model*; but $-\partial\Delta G/\partial\sigma$ is *measurable*, at least in principle.

One way out of this problem is to define a set of "activation strains" (or "activation strain volumes" $V\Delta\epsilon_{ij}$, as Li *et al.*, 1973)

$$\Delta\epsilon_{ij} \equiv \frac{1}{2V}\left\{\left.\frac{\partial\Delta G}{\partial\sigma_{ij}}\right|_T + \left.\frac{\partial\Delta G}{\partial\sigma_{ji}}\right|_T\right\}. \qquad [43e]$$

The activation volume of eq. [43d] is then simply

$$\Delta V = V\Delta\epsilon_{ii}/3 \qquad [43e']$$

and the derivative of the activation energy with respect to the shear stress σ could be described by

$$V\Delta\gamma \equiv 2V\Delta\epsilon_{12} = -\left.\frac{\partial\Delta G}{\partial\sigma}\right|_T. \qquad [43e'']$$

Note, however, that $V\Delta\gamma$ is the quantity of interest, not $\Delta\gamma$, where V is the volume of the entire body.

Although this terminology has certain attractions, we will not use it because of its unfamiliarity (and because we could not find an acceptable name for $V\Delta\gamma$). We shall use an "apparent activation area" $\Delta a'$ to describe the dependence of ΔG on the shear stress σ, as outlined below, and will not consider dependences on other stress components.

The (*true*) *activation area* was defined in eq. [41e] as

$$\Delta a = a_U - a_S. \qquad [43f]$$

It has a straightforward geometric interpretation: it is the area swept out by a dislocation segment between the equilibrium configurations belonging to the stable and unstable positions, as shown in Fig. 41-1.

We now define the *apparent activation area* as

$$\boxed{\Delta a' \equiv -\frac{1}{b}\left.\frac{\partial\Delta G}{\partial\sigma}\right|_{T,r}.} \qquad [43g]$$

It is the stress dependence of the activation energy, and is equal to Δa only under special circumstances. The two can be related by noting (eq. [41g]) that

$$\Delta G = \int_{\sigma}^{\hat{\tau}_{\text{LINE}}} b\Delta a \, \mathrm{d}\tau_{\text{LINE}}$$

and thus that

$$\Delta a' = \Delta a - \int_{\sigma}^{\tau_{\text{LINE}}} \left.\frac{\partial \Delta a}{\partial \sigma}\right|_{\tau} \mathrm{d}\tau_{\text{LINE}}. \qquad [43h]$$

The second term in this equation may be viewed as the dependence of the glide resistance profile itself on σ, such as, in Fig. 43-1, it depends on pressure. But here only the combined effect can be measured. As shown later, this term amounts to $\frac{1}{3}\Delta a$ for the case of discrete obstacles, and thus is far from negligible.

Finally, we note that the experimentally measurable quantity, which might be termed the *operational activation area*, is

$$\frac{kT}{b}\left.\frac{\partial \ln \dot{\gamma}}{\partial \sigma}\right|_{T} = \frac{\mathrm{m}kT}{b\sigma}. \qquad [43i]$$

Similarly the *true activation work*

$$\Delta W \equiv \sigma b \Delta a \qquad [43j]$$

is the actual work done by the applied stress during a thermally activated event. The *apparent activation work*

$$\Delta W' \equiv \sigma b \Delta a' \equiv -\left.\frac{\partial \Delta G}{\partial \ln \sigma}\right|_{T} \qquad [43k]$$

is not necessarily equal to ΔW (for randomly distributed discrete obstacles, for instance, $\Delta W' = \frac{2}{3}\Delta W$).

The best that can be achieved from experiment, without invoking a model, is a measurement of $\Delta W'$ as a function of σ (or ΔG as a function of σ). Figure 43-2(a) schematically shows such a curve. With suitable model assumptions it can be translated into a τ_{LINE}–Δa diagram (Fig. 43-2(b)).

Profile Dependent on Temperature

There are two difficulties with an experimental determination of $\Delta a'(\sigma)$ or $\Delta G(\sigma)$ diagrams. The first has already been mentioned and concerns the possible stress dependence of the pre-exponential factors. It occurs again, if one attempts to determine $\Delta G(\sigma)$ as (eq. [43a])

$$\Delta G = kT \ln (\gamma_o \nu_G / \dot{\gamma}), \qquad [43a']$$

e.g. by measurement of the stress necessary to achieve different strain rates at the same temperature: the stress dependence of $\gamma_o \nu_G$ would have to be known to obtain any information about $\Delta G(\sigma)$.

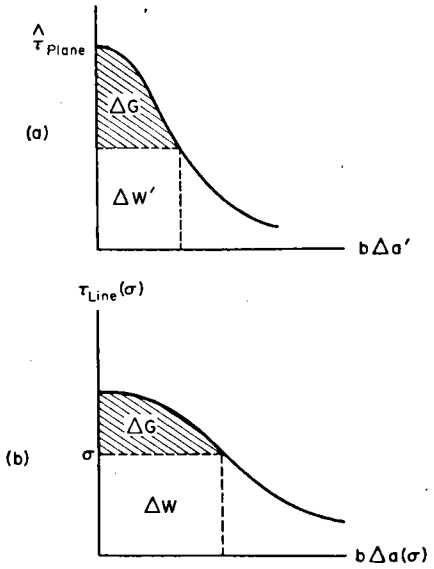

FIG. 43-2. Experiments allow the "apparent profile" shown at (a) to be determined. A model is needed to translate this into the obstacle profile shown at (b). Note that the area ΔG is the same in both diagrams.

The second difficulty lies in the fact that the strain rate cannot in practice be varied sufficiently to cover the entire range from $\sigma \simeq 0$ to $\sigma \simeq \hat{\tau}$ at any one temperature. Equation [43a'] suggests that then a determination of the stress to achieve the *same* strain rate at *different temperatures* would give $\Delta G(\sigma)$ over the entire range (again assuming any stress dependence of the pre-exponentials to have been taken care of). However, this is not necessarily true, since the functional relation $\tau(\Delta a)$ and thus $\Delta G(\sigma)$ may itself depend on temperature as was discussed in sec. 41.

This (very likely) possibility is sketched in Fig. 43-3a: the thin lines show theoretical $\tau(\Delta a)$ curves for four different temperatures; the heavy lines illustrate the range over which each curve might be measured by varying the strain rate (assuming the connection between $\Delta a'$ and Δa is known); using a single strain rate over a range of temperatures thus gives a distorted curve. In the same way, Fig. 43-3b illustrates the situation in a $\Delta G(\sigma)$ diagram, and Fig. 43-3d in a $\Delta H(\sigma)$ diagram. The latter may be thought of as the integral of a modified line resistance diagram, Fig. 43-3c, in which the derivative of the *free* energy (eq. [22e]) has been replaced by a derivative of the *internal* energy. Here, the effects of temperature on the resistance and on the Burgers vector go in the same direction.

The explicit temperature dependence of τ and ΔG may, in principle, be determined by a more extensive thermal activation analysis, to be outlined below. But it is usually more fruitful to assume, on theoretical grounds, some temperature dependence, for example via the shear modulus. We shall treat

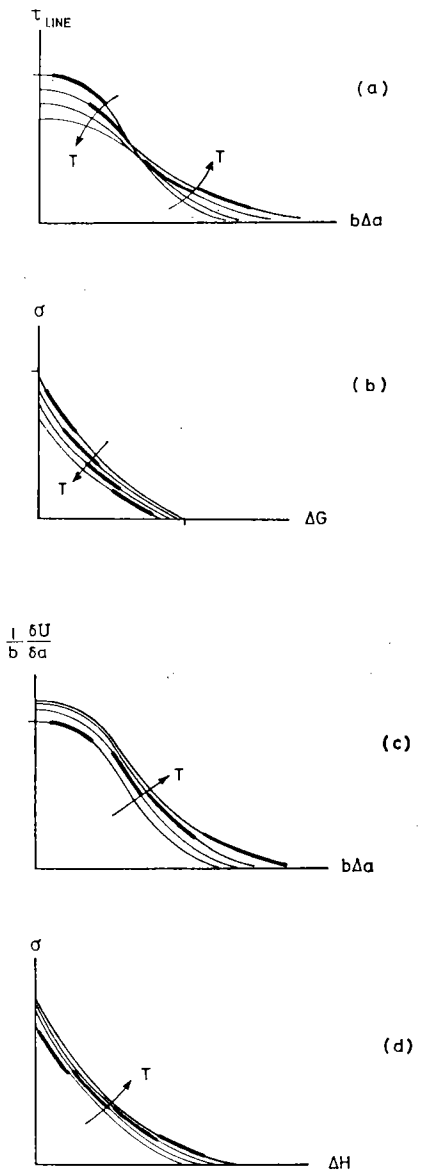

FIG. 43-3. (a–d) If the obstacle profile depends on temperature, and the experiments at different temperatures (four, in these figures) are used to determine it, then four segments of four different obstacle profiles are obtained. If an explicit temperature dependence for the profile is known, or assumed, a single *normalized profile* can be derived.

this case first. It permits an analysis even when the pre-exponential terms are, in a certain manner, stress dependent and even when, as will be shown later on, the flow stress is in part determined by an internal stress contribution.

Profile Scaled by Shear Modulus and Burgers Vector

The glide resistance may be assumed to be proportional to the shear modulus, and the activation area proportional to the square of the Burgers vector:

$$\tau_{\text{LINE}} \propto \mu(T); \qquad \Delta a \propto b^2(T). \qquad [43\ell]$$

The proportionality to the modulus is obviously true when the glide resistance is due to some kind of internal stress or a longer-range dislocation property. When it is due to the generation of some internal surface or of some length of dislocation core or some area of stacking fault, the glide resistance is instead proportional to the respective surface, core, or fault energy. It is often assumed that the temperature dependence of these macroscopic properties is similar to that of the shear modulus. In some cases, this may be reasonable, in others it is certainly not; for example, when the glide resistance depends on the *difference* in stacking fault energy in matrix and second phase in an alloy hardened by coherent precipitates.

The assumption [43ℓ] allows one to rewrite eq. [41g] to read (with $\tau = \tau_{\text{LINE}}$)

$$\frac{\Delta G}{\mu b^3} = \int_{\sigma/\mu}^{\hat{\tau}/\mu} \frac{\Delta a}{b^2} \, \mathrm{d}\frac{\tau}{\mu}$$

where, as before $\hat{\tau}$ is the maximum value of τ_{LINE}. If $\Delta a/b^2$ is assumed to be a function τ/μ and σ/μ at most, this implies

$$\boxed{\Delta G = \mu b^3 \cdot \mathrm{g}\left(\frac{\sigma}{\mu}\right)} \qquad [43\ell']$$

where g is any function of σ/μ. It immediately follows that

$$\Delta a' = -b^2 \frac{\mathrm{dg}}{\mathrm{d}(\sigma/\mu)}. \qquad [43\ell'']$$

Equation [43ℓ'], together with [43a], would suggest plotting a modified Arrhenius diagram of $\ln \dot{\gamma}$ vs. $\mu b^3/kT$ at constant σ/μ (Fig. 43-4). For the slopes in this diagram, we have

$$\left.\frac{\partial \ln \dot{\gamma}}{\partial(-\mu b^3/kT)}\right|_{\sigma/\mu} = \left.\frac{\partial \ln (\gamma_o \nu_G)}{\partial(-\mu b^3/kT)}\right|_{\sigma/\mu} + \mathrm{g}\left(\frac{\sigma}{\mu}\right). \qquad [43\mathrm{m}]$$

Thus even when the pre-exponential factors depend on stress and temperature,

so long as they do so only through the reduced variable σ/μ, the slope in Fig. 43-4 is the function g. If indeed σ/μ is the only variable, the lines in this diagram must be straight.

The dependence of the slope on σ/μ gives, by eq. [43ℓ''], the apparent activation area as a function of σ/μ. One can compare this to values derived directly from eq. [43b] in the reduced form

$$\left.\frac{\partial \ln \dot{\gamma}}{\partial(\sigma/\mu)}\right|_T = \left.\frac{\partial \ln (\gamma_o \nu_G)}{\partial(\sigma/\mu)}\right|_T + \frac{\mu b \Delta a'}{kT}. \qquad [43n]$$

When the first differential does not vanish, it can be determined by inserting $-\,\mathrm{dg/d}(\sigma/\mu)$ for $\Delta a'/b^2$.

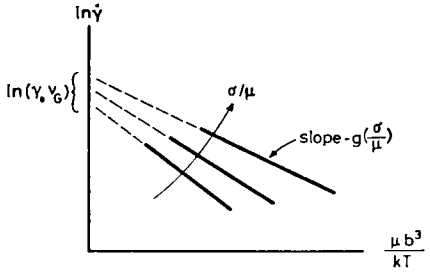

FIG. 43-4. The modified Arrhenius diagram, corrected for the temperature dependence of μ and b. Its slope gives the function $g(\sigma/\mu)$.

Fortunately, the analysis of experimental data is usually simplified by the fact that *either* the stress dependence of the pre-exponentials *or* the explicit temperature dependence of ΔG can be neglected. These cases will be discussed in some detail in Chapter 6. In the following, we treat the case in which not even the present assumptions [43ℓ] are believed justified.

Stress Dependence of Activation Enthalpy and Entropy

We have seen that the stress dependence of the activation *free* enthalpy ΔG, which is related to the activation area and is thus of physical interest, may sometimes be hard to determine because of a stress dependence of the pre-exponential factors in the rate equation. In such cases, one may want to resort to a determination of the stress dependence of the activation enthalpy ΔH, which is free of these difficulties—though it introduces others.

The activation enthalpy is, according to eq. [41m], given by the temperature derivative of the Boltzmann term. It thus can be obtained from the slope of an Arrhenius plot (eq. [43a]), that is, from the equation

$$\left.\frac{\partial \ln \gamma}{\partial(-1/kT)}\right|_{\sigma,\tau} = \left.\frac{\partial \ln (\gamma_o \nu_G)}{\partial(-1/kT)}\right|_{\sigma,\tau} + \Delta H, \qquad [43o]$$

provided that the *temperature* dependence of the pre-exponential factors is known or negligible. This is usually true to a much better approximation than that their *stress* dependence (eq. [43b]) is negligible; for example, ν_G may be proportional to

$1/\sqrt{T}$ (eq. [42v]), in which case the first term on the right in eq. [43o] is $-kT/2$ and always negligible compared to ΔH.

The stress dependence of ΔH then follows from the stress dependence of the Arrhenius slopes, and is related to the apparent activation area by (KOPPENAAL and ARSENAULT, 1966)

$$-\left.\frac{\partial \Delta H}{\partial \sigma}\right|_{T,\tau} = b\Delta a' - T\left.\frac{\partial \Delta S}{\partial \sigma}\right|_{T,\tau} \qquad [43p]$$

from eq. [41ℓ].

The stress dependence of the activation entropy ΔS thus becomes of interest. We have seen in sec. 41 that, while the activation entropy itself may have non-negligible values of a few k, its *temperature dependence* is usually negligible over the range of temperatures investigated. As we shall show below, the *stress dependence* may, under different circumstances, be very small or very large.

First, let us use one of the "Maxwell relations" for plastic flow, which were listed *in extenso* by LI (1965):

$$\left.\frac{\partial \Delta S}{\partial \sigma}\right|_T \equiv \frac{\partial}{\partial \sigma}\left(-\left.\frac{\partial \Delta G}{\partial T}\right|_\sigma\right)_T = \frac{\partial}{\partial T}\left(-\left.\frac{\partial \Delta G}{\partial \sigma}\right|_T\right)_\sigma \equiv \left.\frac{\partial (b\Delta a')}{\partial T}\right|_\sigma . \qquad [43q]$$

The stress dependence of the activation entropy equals the temperature dependence of the "activation volume". Now, we express this in dimensionless form by separating the temperature dependence of b^3 from that of $\Delta a'/b^2$, and by expanding the latter to show the functional relations:

$$\boxed{\left.\frac{\partial(\Delta S/k)}{\partial \ln \sigma}\right|_T = \frac{\sigma b \Delta a'}{kT}\left\{\frac{\mathrm{d} \ln b^3}{\mathrm{d} \ln T} - \left.\frac{\partial \ln (\Delta a'/b^2)}{\partial \ln \sigma}\right|_T \left.\frac{\partial \ln \sigma}{\partial \ln T}\right|_{\frac{\Delta a'}{b^2}}\right\}.} \qquad [43q']$$

The left-hand side is now the contribution to m from the activation entropy, the factor on the right is the main component of m—that from ΔG.

The expression in braces contains two opposite contributions: the stress dependence of the activation entropy may thus be positive or negative. The negative contribution has as one factor any temperature dependence of the stress that does *not* come from thermal activation ("at constant $\Delta a'/b^2$"). For example, this term could be $\mathrm{d} \ln \mu/\mathrm{d} \ln T$, which is typically about 0.1 and usually larger than $\mathrm{d} \ln b^3/\mathrm{d} \ln T$, typically about 0.02. But it is multiplied by a factor, which determines the entire behavior of $\partial \Delta S/\partial \sigma$, namely the *slope of the (apparent) profile*.

Figure 43-5 illustrates the meaning of the stress dependence of the activation entropy. It shows two profiles for two different temperatures; the stresses are chosen *smaller* for the higher temperature, but the apparent activation areas $\Delta a'$ are chosen

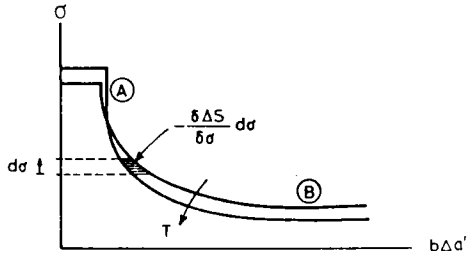

FIG. 43-5. Diagram illustrating the stress dependence of the activation entropy.

larger. The shape of the profile was chosen to illustrate the two extreme possibilities: (A) when the profile has a vertical drop, the negative contribution to $\partial\Delta S/\partial\sigma$ is zero (eq. [43q']) and only the small positive one from the temperature dependence of the Burgers vector remains; but (B) when the profile has a plateau, $\partial\Delta S/\partial\sigma$ can have very large negative values.

For any short-range obstacle, the glide resistance decreases with distance by an inverse second or third power, for example; $(\partial \ln (\Delta a'/b^2)/\partial \ln \sigma)_T$ is then approximately $-\frac{1}{2}$ or $-\frac{1}{3}$, and the two terms in braces in eq. [43q'] compensate each other quite well.

In conclusion, *the stress dependence of the activation entropy should be negligible for all short-range obstacles*, and then $-(\partial\Delta H/\partial\sigma)_{T,\tau}$ and $b\Delta a'$ are approximately equal (eq. [43p]). But for obstacles with "shoulders" or "plateaus", one must use (eqs. [43p] and [43q'])

$$\boxed{-\left.\frac{\partial\Delta H}{\partial\sigma}\right|_{T,\tau} = b\Delta a'\left\{1-\frac{\mathrm{d}\ln b^3}{\mathrm{d}\ln T}+\left.\frac{\partial\ln(\Delta a'/b^2)}{\partial\ln\sigma}\right|_T\left[\frac{\partial\ln\sigma}{\partial\ln T}\right]_{\frac{\Delta a'}{b^2}}\right\}.} \qquad [43r]$$

This is especially important for two-stage profiles.

Two-stage Profiles

A particular obstacle profile may look like the curve shown in Fig. 43-6a. It appears to consist of two stages: a long-range and a short-range one. Similarly, its integral may have the two-stage appearance of Fig. 43-6b.

The profile, Fig. 43-6a, may have been derived theoretically as a superposition of an "internal stress" field and a localized resistance—be they due to the *same* physical obstacle such as a coherent precipitate, or to two different obstacles such as parallel dislocations and solute atoms. The glide resistance due to internal stress would have its own maximum value $\hat{\tau}_\mu$, so called because it would be proportional to some shear modulus. In fact, *any* contribution to the glide resistance that is proportional to μ, such as Orowan looping around incoherent inclusions, would qualify for τ_μ in this sense, even if it could not be measured as an "internal stress".

The Figs. 43-6 may, on the other hand, have been obtained experimentally. It would then be logical to hypothesize that two distinct mechanisms contribute to this profile—and that the longer-range one would be proportional to the shear modulus. If one suspected that the two mechanisms might be due to different physical obstacles (such as forest dislocations and solute atoms), one could try to vary their respective concentrations independently, in order to decompose the observed "profile" into parts attributable to each sort of obstacle. (We shall discuss a particular prescription for such a procedure in sec. 44.) But when a single obstacle is responsible for the observations, the diagrams of Figs. 43-6a and b are all that can be learned from experiment. One may draw a τ_μ-level and a total free energy $F_0^{(1)}$ for the short-range

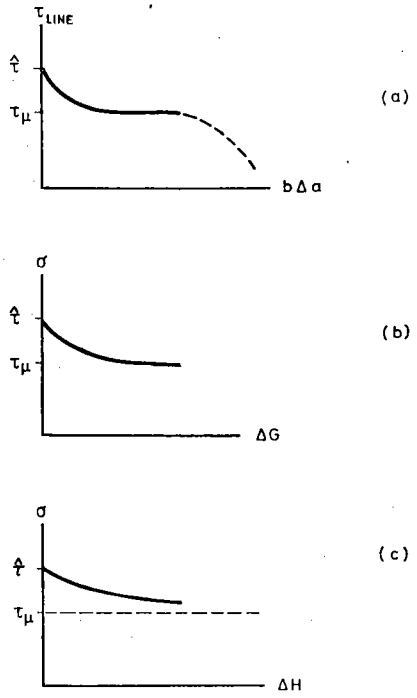

FIG. 43-6. (a–c) In (a) and (b) a two-stage obstacle, having a short-range "peak" and a long-range "tail". A plot of σ against ΔG has a well-defined asymptotic value. A plot of σ against ΔH does not (c).

mechanism into the plots to whatever accuracy may be warranted by the observations.

Many authors (for example, SEEGER, 1957, 1958) introduce the notion of an "internal stress" contribution τ_μ and of an "effective stress" $\sigma - \tau_\mu$ (meaning "effective" on the short-range mechanism) at an earlier stage, before the evaluations that led to Fig. 43-6a or b. They may be misleading if τ_μ is not accurately known—and is not necessary when the free enthalpy of the short-range mechanism depends on temperature through the shear modulus. This is because eq. [43ℓ']

$$\Delta G = \mu b^3 \cdot \mathrm{g}\left(\frac{\sigma}{\mu}\right)$$

is not altered by the replacement of σ by $\sigma - \tau_\mu$, except in the form of the function g. The entire analysis presented in formulas [43ℓ] through [43n] is thus applicable, whether there is a distinct internal stress contribution or not. It is this analysis that is here meant to have led to Figs. 43-6a and b in the first place.

The situation is, however, different when an analysis in terms of ΔH is attempted, which is necessary when the short-range mechanism has an explicit temperature dependence that *cannot* be described by that of the shear modulus. The difficulty may be appreciated by writing the expression for ΔH for the case in which the temperature dependence is in fact that of the shear modulus (i.e. when the exercise would not be necessary).

For this case, the free enthalpy is (eq. [43ℓ'])

$$\Delta G = \mu b^3 \cdot \mathrm{g}\left(\frac{\sigma}{\mu}\right)$$

and the enthalpy (eq. [41ℓ])

$$\Delta H \equiv \Delta G + T\Delta S$$

follows from this with the activation entropy (eq. [41k])

$$\Delta S \equiv -\left.\frac{\partial \Delta G}{\partial T}\right|_{\sigma} = -\frac{\mathrm{d}(\mu b^3)}{\mathrm{d}T}\cdot \mathrm{g} - \mu b^3 \cdot \frac{\mathrm{dg}(\sigma/\mu)}{\mathrm{d}(\sigma/\mu)} \cdot \left(-\frac{\sigma}{\mu^2}\right)\frac{\mathrm{d}\mu}{\mathrm{d}T}$$

or, with eq. [43ℓ'],

$$\boxed{T\Delta S = -\frac{\mathrm{d}\ln(\mu b^3)}{\mathrm{d}\ln T}\Delta G - \frac{\mathrm{d}\ln\mu}{\mathrm{d}\ln T}\Delta W'.} \qquad [43s]$$

Parenthetically, this expression simplifies considerably when the temperature dependence of b is neglected and $(\partial \Delta a/\partial\sigma)_\tau = 0$ so that $\Delta W' = \Delta W$ (eq. [43h]); then (SUREK, *et al.*, 1973a),

$$T\Delta S = -\frac{\mathrm{d}\ln\mu}{\mathrm{d}\ln T}\cdot\Delta F \simeq \frac{\Delta F}{10} \quad (\textit{special case}) \qquad [43s']$$

where the order-of-magnitude estimate is based on eq. [43r].

The activation enthalpy becomes, returning to the general case,

$$\boxed{\Delta H = \left(1 - \frac{\mathrm{d}\ln(\mu b^3)}{\mathrm{d}\ln T}\right)\cdot\Delta G - \frac{\mathrm{d}\ln\mu}{\mathrm{d}\ln T}\cdot\Delta W'.} \qquad [43t]$$

While ΔG refers to the "top" of the glide resistance profile only, and may thus be regarded as a property of the short-range obstacle so long as $\sigma > \tau_\mu$, ΔH depends on σ, the entire applied stress, through $\Delta W'$. Thus, ΔH increases indefinitely as σ decreases towards the τ_μ-level (Fig. 43-6c). On the other hand, ΔG (Fig. 43-6b) reaches a finite value at this level and *then* becomes indefinite. This explains the wide range of values quoted for ΔH in the case of work-hardened fcc crystals (MECKING, 1973).

If one wished to ascribe an "effective" activation enthalpy ΔH_1 to the short-range mechanism only, one would have to define it as

$$\Delta H_1 = \left(1 - \frac{\mathrm{d}\ln(\mu b^3)}{\mathrm{d}\ln T}\right)\cdot\Delta G - \frac{\mathrm{d}\ln\mu}{\mathrm{d}\ln T}\cdot\Delta W_1'. \qquad [43t']$$

In other words, one must know τ_μ.

As a corollary to eq. [43t'], one may then also define an "effective" activation

entropy (CONRAD and WIEDERSICH, 1960):

$$\Delta S_1 = -\left.\frac{\partial \Delta G}{\partial T}\right|_{(\sigma-\tau_\mu)}. \qquad [43t'']$$

Since this procedure would eliminate the plateau from the glide resistance profile, it also eliminates the large negative stress dependence of the activation entropy (eq. [43q'], Fig. 43-5): ΔS_1 would be approximately constant.

Note that this procedure depends on an accurate knowledge of τ_μ. It is of value only when the temperature dependence of ΔG is severely different from that of the shear modulus (i.e. the lines in Fig. 43-3 are curved). (See also GIBBS, 1964.)

Phenomenological Description of Glide Resistance Profiles

For rough estimates, obstacles have often been assumed to be box-shaped. For such obstacles, Δa is obviously constant for $0 < \sigma < \hat{\tau}$, or, in terms of the stress dependence of the free enthalpy of activation:

$$\Delta G = F_0 \cdot \left(1 - \frac{\sigma}{\hat{\tau}}\right). \qquad [43u]$$

Although the flat top of this obstacle profile may be a realistic expression of some core cut-off, real obstacles would usually have a tail in which τ decreases as some negative power of Δa:

$$\left.\begin{aligned} &\tau \propto \frac{1}{(\Delta a)^n} \qquad (\tau \ll \hat{\tau}) \\ &\text{with} \\ &n > 1 \qquad \text{for } \textit{short-range obstacles} \\ &\text{and} \\ &n \leqslant 1 \qquad \text{for } \textit{long-range obstacles}. \end{aligned}\right\} \qquad [43v]$$

The distinction between long and short range has here been made according to whether the activation energy diverges at large Δa or not.

For short-range obstacles, which are especially sensitive to thermal activation, a useful phenomenological generalization of eq. [43u] is

$$\boxed{\Delta G = F_0 \cdot \left\{1 - \left(\frac{\sigma}{\hat{\tau}}\right)^p\right\}^q}. \qquad [43w]$$

This equation still contains the physical parameters of prime interest, viz. the maximum (plane) glide resistance $\hat{\tau}$ and the total free energy F_0 necessary to overcome the obstacle without the aid of external work. The activation energy ΔG decreases from F_0 to 0 as σ is raised from 0 to $\hat{\tau}$, provided p and q are both positive.

The appearance of *two* adjustable parameters, p and q, in a phenomenological relation may seem at first sight disturbing. However, it is quickly realized that p

essentially describes the shape of the "tail" ($\sigma \simeq 0$), with (eqs. [43g], [43v])

$$p = 1 - \frac{1}{n}$$

whereas q describes the shape of the "top" ($\sigma \simeq \hat{\tau}$). For example, it would be

$$q = 1 + \frac{1}{k}$$

in a phenomenological glide resistance profile of the form

$$\tau = \hat{\tau} \cdot (1 - [\Delta a]^k). \qquad [43v']$$

Furthermore, the possible range of values for p and q is limited by the requirement that the activation area increase continuously as σ decreases. Double differentiation of eq. [43v'] with respect to σ shows that this means

$$0 < p \leqslant 1; \qquad 1 \leqslant q \leqslant 2 \qquad [43w']$$

or, in terms of the exponents in eqs. [43v] and [43v']: $n > 0$, $k \geqslant 1$. (The upper limit for q comes from the supposition that obstacles cannot have a sharp point.)

Figure 43-7 shows the profiles for some representative values of p and q. The case $p = \frac{1}{2}$ may stand for any value $0 < p < 1$, the case $q = 3/2$ for any value $1 < q < 2$. In fact, one may consider these values of the exponents to be a sufficiently accurate description for all cases and write (ONO, 1968)

$$\Delta G = F_o \cdot \left\{1 - \left(\frac{\sigma}{\hat{\tau}}\right)^{\frac{1}{p}}\right\}^{3/2}. \qquad [43w'']$$

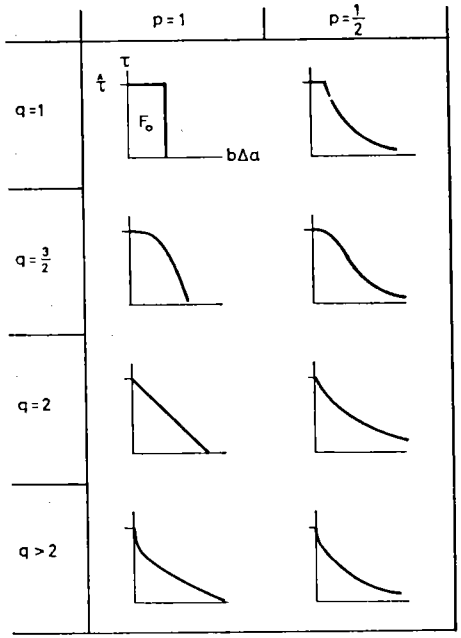

FIG. 43-7. "Short-range" profiles ($F_o < \infty$) described by $\Delta G = F_o \cdot \{1 - \sigma/\hat{\tau}^p\}^q$.

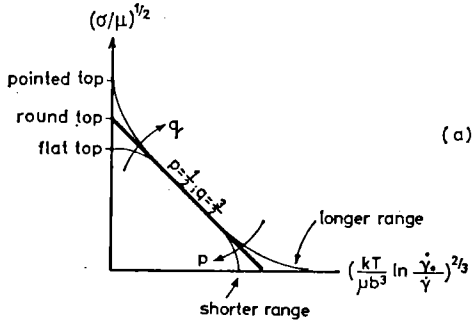

FIG. 43-8. (a) A plot based on eq. [43w″], showing deviations from linearity caused by deviations in the obstacle shape from a norm of $q = \frac{3}{2}$, $p = \frac{1}{2}$.

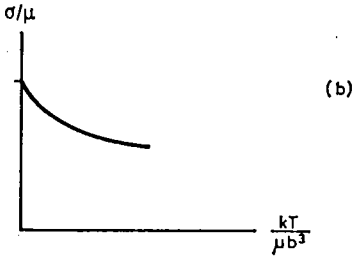

FIG. 43-8. (b) Hypothetical experimental results showing the effect of an "internal stress".

If this equation were exactly correct, one would obtain, with eq. [43a′], a straight line in a plot of $\sigma^{1/2}$ vs. $T^{2/3}$. This is shown in Fig. 43-8a in corrected variables assuming again (eq. [43ℓ′]) that $F_0 \propto \mu b^3$ and $\hat{\tau} \propto \mu$. When real observations show curvatures on such a plot, and especially when they approach the coordinate axes with vanishing or infinite slopes, immediate conclusions can be drawn as indicated in the figure, concerning the real values of p and q for this case, i.e. the real shape of the obstacle in the tail and near the top.

A real curve in a normalized stress vs. temperature diagram may appear to level out at a finite stress, such as that shown on Fig. 43-8b. This may indicate the existence of a separate flow stress contribution τ_2 (for example, an "internal stress" τ_μ). In that case, decreasing the value of p (the exponent of σ/μ) should sharpen up the kink. If so, one may wish to introduce τ_2 as an extra parameter into eq. [43w] and write

$$\Delta G = \mathrm{F}_1 \cdot \left\{ 1 - \left(\frac{\sigma - \tau_2}{\hat{\tau} - \tau_2} \right)^{\mathrm{p}_1} \right\}^{\mathrm{q}} \qquad [43\mathrm{w}'''']$$

with new values F_1 and p_1 that relate to the short-range portion only. Note that in this case it is especially important to have *both* axes in Fig. 43-8b normalized by the shear modulus: while the τ_μ-level would appear even if only σ had been corrected, the shape of the curve would be distorted if T had not.

On the other hand, a curve such as that in Fig. 43-8b could be indicative merely of a single long-range obstacle; it would then theoretically approach the abscissa asymptotically, only at extremely high temperatures. A plot according to Fig. 43-8a would then remain concave upward at the right end even when very small values of

p are chosen. It is then appropriate to assume that $n \leqslant 1$ in eq. [43v] and, consequently (eq. [41g]), that

$$\Delta G \propto \ln\left(\frac{\hat{\tau}}{\sigma}\right) \qquad (n = 1) \qquad [43x]$$

or

$$\Delta G \propto \left(\frac{\hat{\tau}}{\sigma}\right)^{r} \qquad \left(r = \frac{1}{n} - 1 > 0\right). \qquad [43x']$$

The first of these relations is phenomenologically important, since it is equivalent to a *power* dependence of the strain rate on stress, rather than an exponential function: the exponent m (eq. [43c]) is then independent of stress (although still inversely proportional to temperature). Two physical mechanisms have been proposed to be approximately described by such a logarithmic stress dependence of the activation energy: cross slip away from a linear barrier (SCHOECK and SEEGER, 1955); and double kink nucleation over Peierls hills in a particular (and peculiar, see sec. 51) model by SEEGER (1956).

The second type of long-range $\Delta G(\sigma)$ relation (eq. [43x']) has also been used on occasion, especially with $r = 1$. Such a proportionality between ΔG and $1/\sigma$ is typical of dislocation unlocking from a linear barrier (FISHER, 1955). It follows directly by integration [41g] from eq. [24d], a dependence of τ_{LINE} on $1/\sqrt{\Delta a}$, and is shown as ~~a dashed~~ line in Fig. 43-9a. It has the obviously unrealistic feature of an infinite mechanical threshold, which is a direct consequence of assuming a "square well" energy profile for the locking mechanism (Fig. 24-2). If one allows for a finite unlocking force, for example by assuming a triangular energy profile (Fig. 24-3), one obtains (eqs. [24g'], [41g])

$$\Delta G \propto \frac{\sqrt{1 - \sigma/\hat{\tau}}}{\sigma} \qquad [43x'']$$

or, in general, some combination of a typical "short-range" function $\Delta G(\sigma)$ in the numerator and a σ in the denominator (SUZUKI, 1957; TEUTONICO *et al.*, 1964; FELTHAM, 1968). In order to extract the short-range law characteristic of the linear barrier, it would then be opportune to plot $\sigma\Delta G$ as a function of σ, as is done in Fig. 43-9b.

In all these phenomenological relations, we have used $\hat{\tau}$ as a structure parameter without specifying whether the maximum value of τ_{LINE} or of τ_{PLANE} was meant. We have, until now, dealt with the overcoming of a particular "obstacle" (or other line glide resistance unit); for that case, of course, $\hat{\tau}_{LINE}$ limits the possible values of the stress.

When there are many obstacles, they may have different values of $\hat{\tau}_{LINE}$ (Figs. 24-8 and 25-10). In that case, macroscopic measurements cannot relate to the individual profiles, nor do they relate to the absolute maximum value of τ_{LINE} in the entire slip plane; instead, as was discussed in detail in Chapter 2, they relate to the plane glide resistance and its maximum value $\hat{\tau}_{PLANE}$. It may

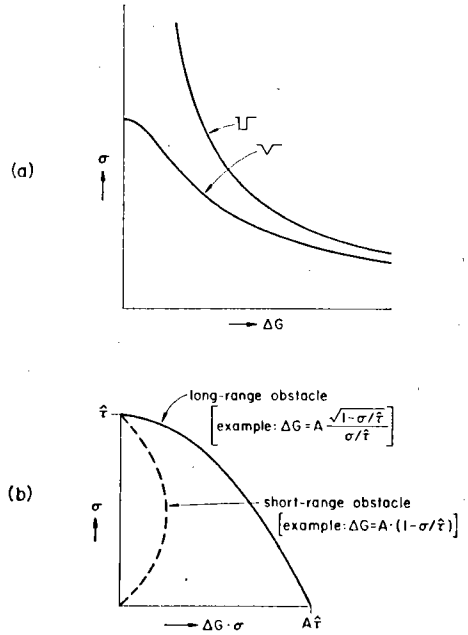

FIG. 43-9. Dislocation unlocking from attractive linear barrier: (a) conventional $\Delta G(\sigma)$ plot; (b) suggested a plot to establish $1/\sigma$-dependence and isolate numerator. In plot (b), a typical short-range obstacle (here: $p = q = 1$) would give the dashed curve.

be thought of as the average value of $\hat{\tau}_{\text{LINE}}$ over particularly critical obstacles (the "gates" in a random array of discrete obstacles, for example), or the value of $\hat{\tau}_{\text{LINE}}$ felt by the leading dislocation in a dynamic pile-up (eq. [24n]). The case of randomly dispersed discrete obstacles will be dealt with in detail in sec. 44.

Linearized Stress Dependence

We have seen that the activation energy ΔG generally depends on stress in a nonlinear manner. For a long time, the dependence was assumed to be linear, following SEEGER (1954). Strictly speaking, this would be correct only for a *box*-shaped obstacle (and in addition only for a *periodic* arrangement of these obstacles, if they are discrete, as we shall see in the next section). However, as had been realized earlier (COTTRELL and AYTEKIN, 1950), a linear dependence can always be assumed for small changes in stress, no matter what the shape of the profile; the constant "activation energy" from which the stress term is subtracted then generally depends on the mean stress level.

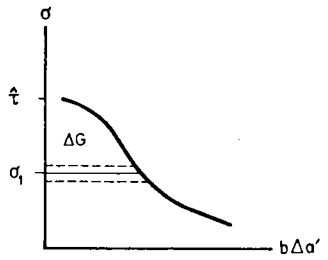

FIG. 43-10. A general apparent obstacle profile. For small changes of stress around $\sigma = \sigma_1$, the activation free enthalpy ΔG appears to be a linear function of σ.

Figure 43-10 shows a general apparent profile, i.e. a plot of stress σ vs. apparent activation area $\Delta a'$ (times b). Let us assume that a standard strain rate $\dot{\gamma}_1$ and a standard temperature T_1 were chosen, from which small variations in either variable were then made. The Arrhenius equation for the standard conditions then defines a stress σ_1 necessary to maintain the rate $\dot{\gamma}_1$ at the temperature T_1:

$$\dot{\gamma}_1 = \dot{\gamma}_o \exp - \frac{\Delta G(\sigma_1)}{kT_1}. \qquad [43y]$$

(We assume constant structure, and thus constant stress, for the moment and will discuss the general case in the next section.)

The activation energy for conditions slightly different from the standard one may then be written as an expansion:

$$\Delta G(\sigma) = \Delta G(\sigma_1) - (\sigma - \sigma_1) b \Delta a' - \frac{(\sigma - \sigma_1)^2}{2} b \frac{\partial \Delta a'}{\partial \sigma} + \ldots \qquad [43z]$$

Provided the fractional variation in apparent activation area is small compared to 1, as it would be in the illustration, Fig. 43-10, for all stresses not too close to $\hat{\tau}$, this series may be broken off after the first two terms:

$$\Delta G(\sigma) \doteq \Delta G(\sigma_1) + \sigma_1 b \Delta a'(\sigma_1) - \sigma b \Delta a'(\sigma_1). \qquad [43z']$$

The first two terms on the right-hand side are constants, and so is the coefficient of σ; we thus have a linearized dependence of the activation free enthalpy on stress.

The expression may again be considerably simplified when $\Delta a' = \Delta a$ (i.e. when the second term in eq. [43h] can be neglected) for then the second term in [43z'] is the activation work and

$$\Delta G(\sigma) \doteq \Delta F(\sigma_1) - \sigma b \Delta a(\sigma_1) \qquad (\textit{special case}). \qquad [43z'']$$

Thus the constant "activation energy" from which the stress term must be subtracted is the *free energy of activation under the standard stress* and, not, for example, the total free energy F_o. But even this simple interpretation is not applicable to discrete obstacles where $\Delta a' \neq \Delta a$.

44. Application to Discrete Obstacles

We have described discrete obstacles in sec. 25 as obstructions for which the element glide resistance is strictly limited in both directions in the slip plane (such as precipitates or voids), or at least for which the element glide resistance diagram can be idealized to consist of isolated peaks with little overlap (such as forest dislocations and possibly solute atoms). We shall here employ the idealization of an obstacle of strictly limited width w, small compared to the spacing l_e (Fig. 25-1). The element glide resistance may then be integrated over the width to give the obstacle strength (eq. [25d])

$$K \equiv \tau_{\text{ELEM}}\, bw$$

which, however, may be a function of the penetration y into the depth of the obstacle—a function concisely described in the obstacle *profile* $K(\Delta y)$.

The plane glide resistance encountered by individual dislocations that move long distances through a random dispersion of such obstacles is connected to the strength of the individual obstacles and their spacing l by the Friedel relation (eqs. [25w'], [25dd]):

$$\left.\begin{aligned} \tau_{\text{PLANE}} &= s\cdot\frac{2E}{bl}, \\ s &\simeq \left(\frac{K}{2E}\right)^{3/2}. \end{aligned}\right\} \qquad [44a]$$

To describe the influence of thermal activation at constant structure (l), we assume the effective obstacle strength to depend on temperature and strain rate, and thus

$$s = s(T,\dot{\gamma}). \qquad [44b]$$

This assumption implies that the dislocations follow the same path through the obstacle structure at all temperatures and strain rates, namely the path that led to the purely geometrical derivation of eq. [44a].

Such a hypothesis may not be justified under all circumstances (Diehl *et al.*, 1965). In fact, computer experiments of Klahn *et al.* (1972) leave the possibility that it may be violated, although they found the Friedel relation [44a] well satisfied. This strengthens our belief that eqs. [44a] and [44b] form an adequate basis for a description of thermal activation of dislocations through discrete obstacles. The general averaging procedure that must, in principle, be followed when this approximation is inappropriate, has been written down by Frank (1968). A very useful generalization of the Friedel model has been given by Labusch (1962).

In this section, we shall first describe the properties of *individual* obstacles, then the influence of a random dispersion of obstacles on the macroscopically measured quantities, and finally the possibilities offered by a variation in the number or concentration of the obstacles.

Obstacle Strength and Activation Distance

Figure 44-1a shows four successive equilibrium positions of two neighboring dislocation segments in front of three obstacles. In all cases, the dislocation is in *stable* equilibrium with respect to the two outside obstacles and with respect to its own shape in the obstacle-free region; but with respect to the center obstacle, the first two positions are in stable equilibrium at two different stresses, the last two in *unstable* equilibrium at the *same* two stresses. Figure 44-1b shows all four points on a line glide resistance diagram similar to Fig. 25-4b, and Fig. 44-1c shows the same in profile form.

All effects of bowing have vanished from Fig. 44-1c. The distance l_e between obstacles, however, is still implicitly contained in this profile; for the areas Δa would clearly grow if l_e were increased, but the properties of the obstacle should not be affected. (Here enters the essential condition of negligible overlap between "discrete obstacles".)

The parameter l_e, which was arbitrarily prescribed in Fig. 44-1a, can be eliminated again from the results by defining the activation distance

$$\Delta y = \Delta a / l_e \qquad [44c]$$

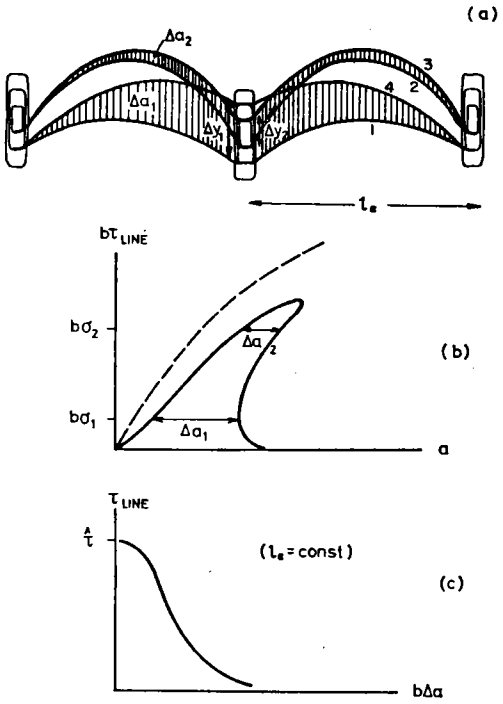

FIG. 44-1. (a) Successive equilibrium positions (1, 2, 3, 4) of two neighboring segments of dislocation at an obstacle. (b) The glide resistance diagram. (c) The sheared diagram or obstacle profile.

and remembering the equilibrium equation [25e]

$$K = \tau_{\text{LINE}}\, bl_e. \qquad [44d]$$

In this way, one can obtain a diagram of obstacle strength versus activation distance, or *force-distance diagram*, or *obstacle profile*, as shown in Fig. 44-2.

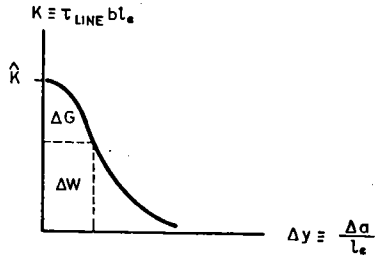

FIG. 44-2. The force-distance diagram for a discrete obstacle.

It is identical to Fig. 44-1c except for scale factors. These scale factors do not, however, influence the areas corresponding to ΔW and ΔG. Equations [44c] and [44d] give for the activation work (remembering $\tau_{\text{LINE}} = \sigma$ in equilibrium)

$$\Delta W = \tau_{\text{LINE}}\, b\Delta a = K\Delta y \qquad [44e]$$

and (eq. [41g])

$$\Delta G = \int_{\sigma}^{\hat{\tau}} b\Delta a \, \mathrm{d}\tau = \int_{K(\sigma)}^{\hat{K}} \Delta y \, \mathrm{d}K \qquad [44f]$$

where

$$K(\sigma) = \sigma b l_e. \qquad [44d']$$

Finally, one may turn eq. [44f] around and write

$$-\frac{\mathrm{d}\Delta G}{\mathrm{d}K} = \Delta y(K). \qquad [44f']$$

The activation parameters have thus been expressed in obstacle properties only.

An essential condition for writing eq. [44f] as we did was that l_e was assumed constant; otherwise, the derivative $\mathrm{d}\tau/\mathrm{d}K$ might have brought in terms from l_e. In real materials, l_e is not known, only the average spacing l is (at best). In the model we use for randomly dispersed obstacles, the ratio l_e/l depends on the applied stress (eq. [25jj]). This leads to a substantial complication to be dealt with presently.

Effective Obstacle Spacing and Apparent Activation Area

We have seen that in a material with a random dispersion of obstacles of average planar spacing l, the relation between obstacle strength and plane

glide resistance is given by eq. [44a]. Conversely, at an applied stress $\sigma = \tau_{PLANE}$, the force exerted by the dislocation on the critical obstacle that makes long-range slip possible (now, the "rate-controlling" obstacle), is

$$K(\sigma) = 2E \cdot \left(\frac{\sigma b l}{2E}\right)^{2/3}. \qquad [44g]$$

This relation must replace eq. [44d'] in the lower limit for the integral [44f], if the activation energy ΔG described by it is to refer to the rate-controlling obstacle in the random dispersion. The stress derivative of this activation energy, i.e. the apparent activation area times b is then given by

$$b\Delta a' \equiv -\left.\frac{\partial \Delta G}{\partial \sigma}\right|_l = \Delta y(K) \cdot \left.\frac{\partial K}{\partial \sigma}\right|_l = \tfrac{2}{3}\frac{K}{\sigma}\Delta y = \tfrac{2}{3} b\Delta a \qquad [44h]$$

where it is explicitly stated that the average obstacle spacing l (along with the nature of the dispersion and of the individual obstacles, in other words, the entire glide resistance diagram) is held constant. The model treated above of a single obstacle triplet for which the (local) spacing l_e was known and held constant would instead give (eqs. [44f] and [44d'])

$$-\left.\frac{\partial \Delta G}{\partial \sigma}\right|_{l_e} = \Delta y(K) \cdot \left.\frac{\partial K}{\partial \sigma}\right|_{l_e} = b l_e \, \Delta y = b\Delta a. \qquad [44h']$$

While in this latter case, which refers to a *local model*, the apparent activation area is equal to the true activation area, in the former case it is not. It is for this reason that we have introduced the symbol $\Delta a'$ and the name apparent activation area. The case described by eq. [44h] is, if anything, the more important one, since it describes *macroscopic behavior* which can be controlled or measured. This fact was recognized first by LABUSCH (1962); a recent different treatment (MACEWEN, 1973) is in error (SUREK *et al.*, 1973b).

An elaboration of the role of the effective obstacle spacing may here be helpful. In Fig. 44-3, it is treated as a free parameter and different $\tau - \Delta a$ diagrams are calculated for the same $K - \Delta y$ diagram. But in a real material, l_e cannot be chosen

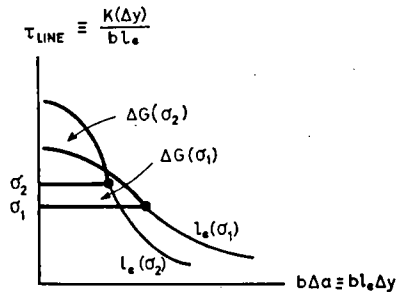

FIG. 44-3. The influence of the effective obstacle spacing on the glide resistance diagram.

arbitrarily. Comparison of eqs. [44d'] and [44g] shows that

$$\frac{l_e}{l} = \left(\frac{2E}{\sigma b l}\right)^{1/3}. \qquad [44i]$$

At constant structure (l), l_e is thus a function of the applied stress. For the two stresses corresponding to the two values of l_e in Fig. 44-3, the relevant parts of the glide resistance profiles are outlined. Only the two heavy points correspond to measurable pairs of σ and Δa. Evidently, the stress derivative of ΔG is here not $-b\Delta a$.

On a formal basis, we may calculate $\Delta G(\sigma)$ by inserting the proper value for the activation area:

$$\Delta a(\sigma,\tau) = l_e(\sigma)\Delta y(K) \qquad [44c']$$

where K depends on σ and τ through eq. [44d']. Inserting this dependence explicitly into the expression [41f], we get for the activation energy

$$\Delta G(\sigma) = \int_{\sigma}^{\tau_{\text{LINE}}} b \cdot l_e(\sigma) \cdot \Delta y(\tau_{\text{LINE}} b l_e(\sigma)) \cdot d\tau_{\text{LINE}}. \qquad [44j]$$

The integration is, as specified, only over $\tau = \tau_{\text{LINE}}$, with the applied stress σ held constant during the process. In terms of Fig. 44-1a, this means that, while the *activation energy* is calculated through a series of equilibrium processes, during which the dislocation sweeps out substantial areas by bowing out, *the effective length l_e is held constant* and not decreased by any encounter of new obstacles. This is realistic, since the *path* of the dislocation during the activation process will obviously not follow the tremendous bow-outs required in equilibrium.

The above argument also shows that it would be incorrect to execute the integral [44f] for ΔG over τ_{PLANE} instead of τ_{LINE}: this would correspond to adjusting the effective length continuously during the integration.

Strictly speaking, one must assume that even in whatever area the dislocation does sweep out, it encounters no new obstacles. This area should be of the order of the activation area, so this assumption means

$$\Delta a \ll l^2. \qquad [44k]$$

Drawing a general conclusion from this discussion of randomly dispersed discrete obstacles, we see that the only "profile" we can measure even in principle is an apparent one: a diagram of applied stress σ against apparent activation area $\Delta a'$ (Fig. 44-4a). This quantity $\Delta a'$ is derived from the slope in a $\sigma - \Delta G$-diagram (Fig. 44-4b); if this is not available,

$$-\frac{1}{b}\left.\frac{\partial \Delta H}{\partial \sigma}\right|_{\tau}$$

could instead be used, as taken from the slope in a $\sigma - \Delta H$-diagram (Fig. 44-4c); or, finally, simply the operational activation area (eq. [43i]) from a $\sigma - \ln \dot{\gamma}$-diagram.

Even the apparent activation area $\Delta a'$ is generally not equal to the true activation area Δa; in the above case, it is two-thirds of it. Similarly, the apparent activation work $\Delta W'$ is not generally equal to the true activation work ΔW; in the above case, it is again two-thirds of it. Only the activation

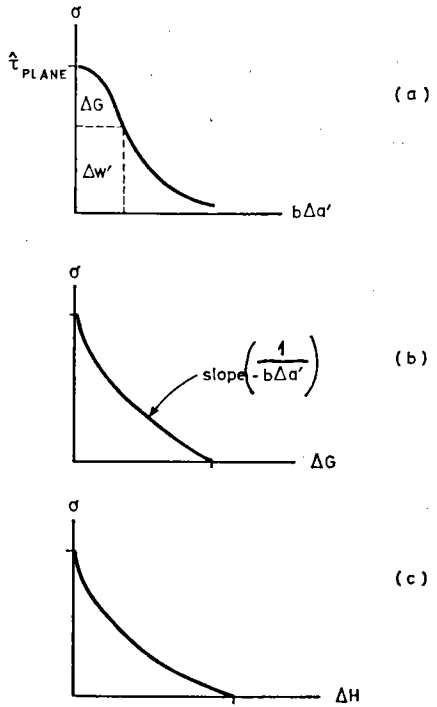

FIG. 44-4. (a) The apparent obstacle profile. (b) The plot of stress vs. activation free energy, used to derive the apparent profile. (c) An alternative plot that may be used to obtain a profile.

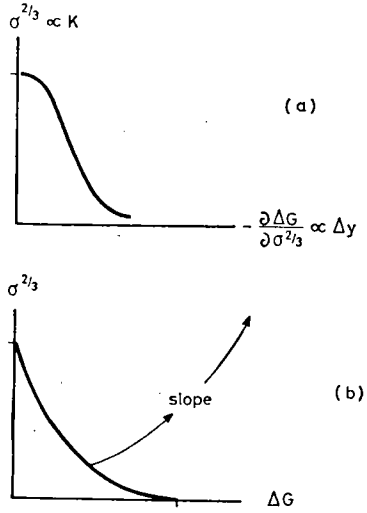

FIG. 44-5. (a, b) An alternative to the method of Fig. 44-4 when the obstacle distribution is known to be random.

energy is, by definition, always the area above any particular σ-level (Fig. 44-4a).

When it is known that one deals with randomly dispersed discrete obstacles, it would make sense to plot $\sigma^{2/3}$ against ΔG, and then the slope in this diagram again against $\sigma^{2/3}$ (Fig. 44-5). In the latter diagram, Fig. 44-5a, the ordinate is then proportional to K, the abscissa to Δy. One thus obtains a correct impression of the shape of the obstacle profile—although one would have to know the obstacle spacing and the dislocation line energy to get numerical values for either K or Δy. Note, however, that both ΔG and ΔW are directly obtained from such a diagram, without a knowledge of the scale factors.

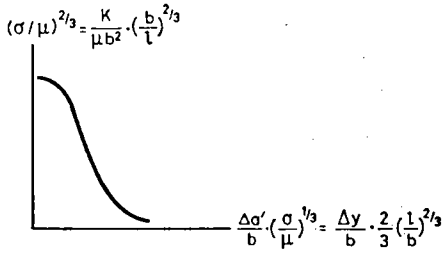

FIG. 44-6. A plot of force K vs. activation distance Δy derivable from experiments in which the flow stress is controlled by one set of randomly dispersed discrete obstacles. The scale factors depend on the obstacle spacing, which would have to be measured metallographically.

Finally, one may wish to again incorporate the temperature dependence of the shear modulus into this apparent profile. For discrete obstacles, one then obtains the plot shown in Fig. 44-6. Only for the interpretation of the two coordinates, we have used $2E = \mu b^2$.

When the obstacle profile can be described by a phenomenological relation equivalent to eq. [43w], so that

$$\Delta G = F_o \cdot \left\{ 1 - \left(\frac{K}{\hat{K}} \right)^{p'} \right\}^q \qquad [44\ell]$$

this can be translated into the respective relation for the macroscopically observed stress by means of eq. [44g]:

$$\Delta G = F_o \cdot \left\{ 1 - \left(\frac{\sigma}{\hat{\tau}} \right)^{2p'/3} \right\}^q \qquad [44\ell']$$

where $\hat{\tau}$ is now meant to be $\hat{\tau}_{\text{PLANE}}$. The $\frac{2}{3}$ power is a direct consequence of the randomness of the obstacle distribution. Since the arguments that limited the exponent p in the general relation [43w] to $\leqslant 1$ now hold for p′ the net stress exponent p is now even more limited:

$$0 < \tfrac{2}{3}p' = p \leqslant \tfrac{2}{3}. \qquad [44\ell'']$$

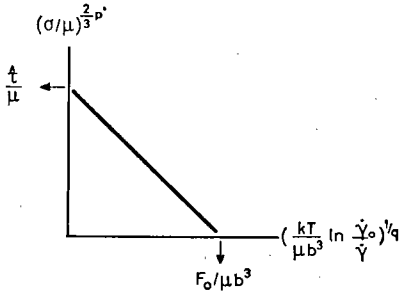

FIG. 44-7. Test for the exponents in the phenomenological relation [44*l'*] if it is obeyed over the entire temperature range.

By the trial-and-error method, one may find the correct exponents that give straight lines, at least at either end, in Fig. 44-7 (cf. Fig. 43-8a).

The Interpretation of Activation Entropies and Enthalpies

The activation entropy defined in eq. [41k] as

$$\Delta S \equiv -\left.\frac{\partial \Delta G}{\partial T}\right|_{\sigma}$$

and the activation enthalpy defined in eq. [41ℓ] as

$$\Delta H \equiv \Delta G + T\Delta S$$

are not as closely related to obstacle properties as the activation free enthalpy

$$\Delta G = \int_{\sigma}^{t} b\Delta a \, d\tau_{\text{LINE}} = \int_{K(\sigma)}^{\hat{K}} \Delta y \, dK.$$

We have discussed one instance of this general fact in the case of two-stage profiles (sec. 43). The case of randomly dispersed discrete obstacles provides another example, which was first described by GIBBS (1967).

Here, the effective obstacle spacing l_e is, for a given average obstacle spacing l, a function of σ/μ according to eq. [44i]. If the shear modulus μ depends on temperature, then l_e/l depends on temperature at constant stress and this dependence enters into the thermodynamically defined activation entropy, above, and consequently into ΔH. The local activation process, however, which is not accessible to direct macroscopic measurement, occurs at *fixed* l_e. The problem is most easily avoided by using reduced variables σ/μ, $\Delta G/\mu b^3$, and $kT/\mu b^3$, as we have done before—although, in principle, such a normalization procedure assumes some minimal knowledge of the physical nature of the local process, namely that μ and b are the proper material properties to be used.

The problem is a general one, as we mention in passing. An example relating to *linear barriers* would be the nucleation of a pair of kinks with a finite constriction energy. This constriction energy would depend on the width η of the stacking fault in the neighboring unactivated region which, in general, depends on the applied stress and on some temperature-dependent material property such as the stacking fault energy. However, during activation, η in the *unactivated* region is to be held

constant. Thus the macroscopic derivatives with respect to stress at constant temperature, and with respect to temperature at constant stress, do not directly relate to the local process.

In this sense, ΔS and ΔH are "apparent" activation parameters just as the apparent activation area (eq. [43g])

$$\Delta a' \equiv -\left.\frac{\partial \Delta G}{\partial \sigma}\right|_T.$$

GIBBS (1967) called them "experimental" (index e), which is unfortunate because truly experimental parameters (here called operational) involve the pre-exponential factors also. In the case of ΔS and ΔH, we have decided to use a single definition only, the thermodynamic one, and no further adjectives. In the case of $\Delta a'$, this seemed unadvisable because of the obvious geometric interpretation of the name activation area, which is $\Delta a \neq \Delta a'$.

The Flow Stress as a Structure Parameter

Until now, we have always assumed the structure to be constant. Often this is not so. For example, in an experiment at constant stress (i.e. a "creep" experiment), the strain rate often decreases as the straining progresses. While one interpretation of this phenomenon is based on an exhaustion of the number of *mobile* dislocations, the currently preferred one is that this is due to work hardening, i.e. an increase in the number of *obstacles*, and thus a decrease in the obstacle spacing. For another example, precipitation from solid solution could be going on during straining; this increases the number of precipitates but decreases the number of atoms in solution—the two hardening mechanisms would thus be affected in opposite directions.

The maximum plane glide resistance is a direct measure of the average obstacle spacing l, so long as the nature of the individual obstacles does not change (eq. [44a]):

$$\hat{\tau}_{\text{PLANE}} = s(\hat{K})\frac{2E}{bl} = \tau(l). \qquad [44m]$$

Its magnitude can change, for example, with strain according to a work hardening coefficient Θ:

$$\mathrm{d}\hat{\tau} = \hat{\theta}\,\mathrm{d}\gamma. \qquad [44n]$$

Unfortunately, both $\hat{\tau}_{\text{PLANE}}$ and $\hat{\theta}$ would have to be measured by extrapolation to absolute zero temperature.

To make a measure of "structure" more accessible, one can make use of the fact that, so long as the nature of the individual obstacles does not change, the same temperature and strain rate will lower the obstacle strength by the same amount. The stress necessary to achieve a standard strain rate at a standard temperature could thus serve as a measure of the structure. We call it the *flow stress*:

$$\tau_{\text{FLOW}} \equiv s(T_{\text{STD}}, \dot{\gamma}_{\text{STD}})\cdot\frac{2E}{bl} \equiv \tau(l) \qquad [44o]$$

or, expressing the same thing in another description:

$$\dot{\gamma}_{\text{STD}} = \dot{\gamma}_o \exp - \frac{\Delta G(\tau_{\text{FLOW}})}{kT_{\text{STD}}} \qquad [44o']$$

(provided, of course that $\dot{\gamma}_{\text{STD}}$ is not so small that the structure changes with time, nor so large that dislocation motion is drag-controlled).

This flow stress is (like all quantities we have called τ) a material property: *it is a first-order description of structure.* In this same first order, we may now reinterpret the nomenclature "at constant τ" we have already used with many partial derivatives to mean "at constant flow stress". (In reality, it implies "at constant structure" in *all* possible parameters.) We shall often just use the symbol τ for τ_{FLOW}.

The case of work hardening discussed above may now be described by

$$d\tau = \theta \, d\gamma \qquad [44n']$$

θ being the work hardening coefficient at the standard temperature and strain rate.

The effects of a change of structure on the strain rate at constant stress is now described by (CHENG and KOCKS, 1970):

$$\boxed{\left.\frac{\partial \Delta G}{\partial \tau}\right|_T = b\Delta a'.} \qquad [44p]$$

It is exactly equal to the apparent activation area (times b). This may be seen easily in two ways. First, the identity

$$\left.\frac{\partial \Delta G}{\partial \tau}\right|_\sigma = - \left.\frac{\partial \Delta G}{\partial \sigma}\right|_\tau \cdot \left.\frac{\partial \sigma}{\partial \tau}\right|_{\Delta G} \qquad [44p']$$

degenerates into [44p] at the standard temperature and strain rate specified by ΔG, where $\sigma = \tau$. Second, one may take the derivative [44p] explicitly from the integral [44f] with the lower limit [44g]; in expanded form:

$$\left.\frac{\partial \Delta G}{\partial \tau}\right|_\sigma = \frac{d\Delta G}{dK} \cdot K \left.\frac{\partial \ln K}{\partial \ln l}\right|_\sigma \cdot -\frac{1}{\tau} \frac{d \ln l}{d \ln \tau}.$$

The three terms separated by dots on the right-hand side are, respectively, $-\Delta y$, $\frac{2}{3} K$, and $-1/\tau$, by eqs. [44f'], [44g], and [44m], respectively. Since $K/\tau = bl_e$, the right-hand side is $\frac{2}{3} b\Delta a$.

We make use of eq. [44p] in the interpretation of creep and stress relaxation experiments.

Discrete Obstacles Plus Internal or Friction Stress

Not only the flow stress, but also the activation area depends on the obstacle density. With eqs. [44c], [44i], and [44a], it is

$$\Delta a = l_e \cdot \Delta y = l \cdot \Delta y \cdot s^{-1/3} \qquad [44q]$$

where Δy and s are properties of the individual obstacle only, but l is a function only of their area density (eq. [25aa]; the obstacle width is again neglected with respect to the obstacle spacing).

This density dependence may be expressed through the flow stress; for example, by

$$\frac{1}{b\Delta a(l)} = \frac{\tau(l)}{\Delta W(T_{STD}, \dot{\gamma}_{STD})} \qquad [44r]$$

as may be verified by explicit insertion of eq. [44o] into [44q], with (eq. [44a])

$$\Delta W(T_{STD}, \dot{\gamma}_{STD}) = \Delta y \cdot 2Es_{STD}^{2/3} = K\Delta y \qquad [44r']$$

which is again a property of the individual obstacle.

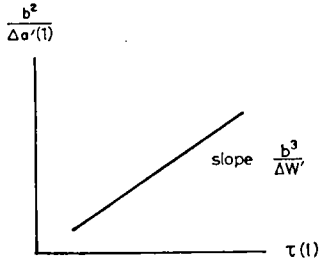

FIG. 44-8. Test for flow stress control by a single set of discrete obstacles: the inverse activation area must be proportional to the flow stress as the obstacle spacing is varied (Cottrell–Stokes law).

Equation [44r] may be experimentally tested (with eq. [44h]) by varying the obstacle concentration and plotting $b^2/\Delta a'$ versus τ: it should give a straight line through the origin (Fig. 44-8). Note that l, or even the concentration, does not have to be known for each obstacle, only the macroscopic mechanical properties are needed.

Figure 44-8 can be used to test an implicit assumption we have made above: namely, that the obstacles under discussion provide the *only* contribution to the flow stress. The plot becomes really useful, when there is a possibility of other contributions. We will illustrate this on two simple examples; in one there is an additional "constant" glide resistance, in the other there is a second set of discrete obstacles.

First, let us postulate that the element glide resistance diagram (such as in Fig. 23-2) contains, in addition to a contribution from the discrete obstacles, one that may be described by a significantly different "wavelength"; for example, a lattice resistance that may, on the scale of the obstacle spacing, be smoothed out to a "friction stress"; or an internal stress that varies slowly compared to the obstacle spacing. In both cases, not only the element resistances, but also the line glide resistances are additive. The plane glide resis-

tance would also consist of two additive contributions:

$$\tau_{\text{PLANE}} = s_1 \frac{2E}{bl_1} + \tau_2 \qquad [44s]$$

although τ_2 is then not necessarily the amplitude of the nondiscrete component: in the case of the long-range internal stress, it may be smoothed out by a dynamic pile-up as in eq. [24n]. For our purposes here, τ_2 is a constant.

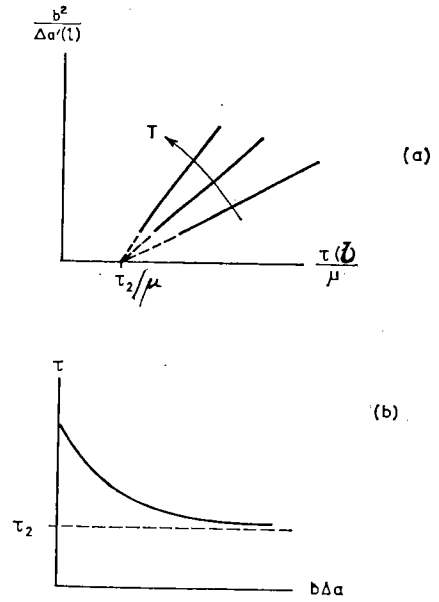

FIG. 44-9. The case of linear superposition of an "athermal" flow stress contribution $\tau_2 \propto \mu$ and a contribution from an independent set of activatable discrete obstacles: (a) plot (eq. [44t]) of inverse apparent activation area vs. total flow stress, as the density of discrete obstacles is varied; (b) apparent glide resistance profile.

If the discrete obstacles, marked here by the index 1, are the only flow stress contribution that may be lowered by thermal activation, nothing has evidently changed in the above description of a single set of obstacles, except that all symbols in eq. [44q] should obtain an index 1, and τ in eq. [44r] should be replaced by $\tau - \tau_2$:

$$-\frac{1}{b\Delta a(l_1)} = \frac{\tau(l_1) - \tau_2}{\Delta W_1(T_{\text{STD}}, \dot{\gamma}_{\text{STD}})}. \qquad [44t]$$

Figure 44-9a illustrates this equation, again making use of the proportionality between true and apparent activation area (eq. [44h]), and furthermore allowing a number of different "standard" temperatures to enter ΔW. For this purpose, τ_2 is assumed to be proportional to the shear modulus; its slight

temperature dependence is then taken account of by plotting τ/μ in the abscissa. In this case, the lines for different temperatures must all extrapolate to the same point τ_2/μ on the abscissa.

Figure 44-9b shows the glide resistance profile as it would be macroscopically measured: a combination of the two distinct obstructions. Only the part above τ_2 is supposed to be changed by changing l_1, and only to this part does the quantity $\Delta W_1'$ refer, which determines the slopes in Fig. 44-9a. Obviously, if the profile in Fig. 44-9b were due to a single kind of discrete obstacles (although possibly different resistance mechanisms as in a forest dislocation), both parts would change with the spacing l, and a behavior as in Fig. 44-8 should be observed. This is what actually happens in strain-hardened pure fcc materials; this proportionality between the two contributions to the plane glide resistance is an example of the Cottrell-Stokes Law (COTTRELL and STOKES, 1955; HAASEN, 1958).

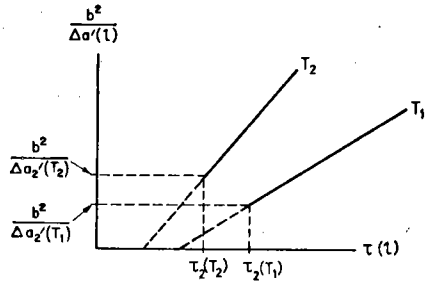

FIG. 44-10. As Fig. 44-9a, but with a temperature dependent τ_2 (eq. [44t']).

The interpretation of τ_2 as an internal stress, independent of temperature except through the shear modulus μ, was not necessary for the separability of the two contributions. In the other example given in the introduction, that of a lattice friction stress, τ_2 could also be lowered by thermal activation. In that case, we obtain (eq. [44h])

$$\frac{b^2}{\Delta a'(l_1)} = \frac{b^2}{\Delta a'_2} + \frac{3}{2}\frac{b^3}{\Delta W'_1}\{\tau(l_1) - \tau_2\} \qquad [44t']$$

which is plotted in Fig. 44-10.

Finally, there may be cases when an internal or a friction stress superpose with a flow stress contribution due to discrete obstacles in a *nonlinear* fashion (although we cannot think of an example). If the discrete obstacles are the only ones thermally activated, the activation area must again be proportional to their spacing, and their flow stress contribution τ_1 must be inversely proportional to this spacing. In this sense, a diagram of $1/\Delta a'$ vs. τ, as that in Fig. 44-9a, amounts to a diagram of τ_1 vs. τ: of the relation between "effective stress" and "flow stress". Figure 44-11 demonstrates this in the case where the superposition law is

$$\tau^2 = \tau_1^2 + \tau_2^2 \qquad [44u]$$

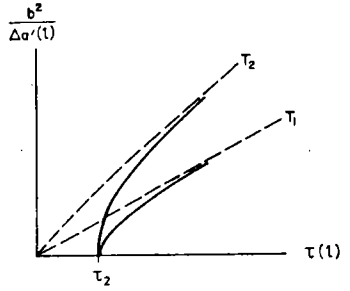

FIG. 44-11. As Fig. 44-9a, but with superposition of the *squares* of the flow stress contributions (eq. [44u']).

in which

$$\frac{1}{\Delta a'(l_1)} \propto \frac{1}{l_1} \propto \sqrt{\tau^2(l_1) - \tau_2^2}. \qquad [44u']$$

Note that in all cases where the exponent in eq. [44u] is larger than 1, the asymptotic relation for large flow stresses is a straight line through the origin. This could sometimes be mistaken for the case of a single obstacle (Fig. 44-9a).

Two Sets of Discrete Obstacles

When there are two sets of discrete obstacles, the statistics can obviously get very complicated. One extreme case is, however, relatively simple and should be of particular interest: namely, when there are many weak obstacles and few strong ones, so that the contributions to the flow stress may be comparable. It is then, in principle, possible to vary the concentration of either set and obtain rather complete information. Typical cases could be small precipitates or solute atoms as the weak obstacles, and large inclusions or forest dislocations as the strong ones.

For this case, imagine three successive positions of a dislocation segment under the same applied stress (Fig. 44-12a). In position (1), it is a quasi-straight piece of dislocation between two of the strong obstacles. Let us assume that the force it exerts on each weak obstacle is almost enough to break through it. In that case, thermal activation near the weak obstacles could help the dislocation overcome this particular row of weak obstacles in a reasonable time.

The force exerted on the strong obstacle would be very small compared to its breaking strength. Thus, in the next position (2), we consider the segment still held up at the strong obstacles, but at a new set of weak ones. Since the dislocation must now have an average curvature between the two strong obstacles, the angle included at each weak one is smaller. Thus, the force exerted by the dislocation on these obstacles is now a smaller fraction of the

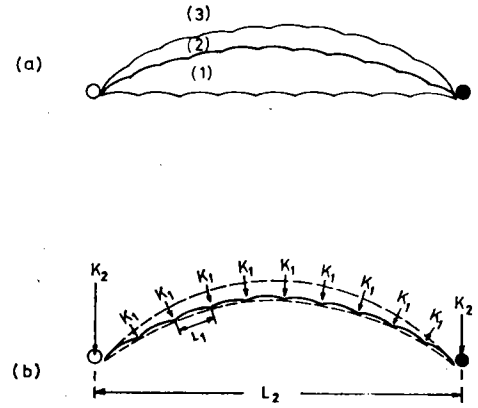

FIG. 44-12. A dislocation segment acted on by many weak discrete obstacles between two strong ones: (a) three successive positions under the same applied stress; (b) the critical configuration.

breaking strength and thermal activation will take longer. On the other hand, the force exerted on the strong obstacles has now risen and thus thermal activation near the strong obstacles may come into the realm of possibilities.

Let us assume that the dislocation can still break through the weak obstacles earlier, so that it arrives at position (3). Let this position be characterized by the condition that the waiting time for thermal activation has become equal at the strong obstacles and at the weak ones. There is then no further time scale during which the segment may be considered to be in equilibrium in front of these two strong obstacles. This condition was postulated by KOCKS (1968) to be a critical one.

Figure 44-12b illustrates the geometry at the critical condition. The dislocation segment has an *average* curvature that is less than that prescribed by the applied stress σ: the individual forces K_1 exerted by the weak obstacles on the dislocation may be smoothed out into a kind of "back stress" given by K_1/bL_1—provided there are *many* weak obstacles between two strong ones. The angle ϕ near each strong obstacle (Fig. 44-12b), which corresponds to this curvature is then given by

$$\sigma - \frac{K_1}{bL_1} \doteq \frac{2E\cos\phi}{bL_2} \qquad (L_1 \ll L_2). \qquad [44v]$$

The numerator on the right-hand side equals the force K_2 only when $\phi_2 \simeq \phi$, i.e. when the bow-out between two obstacles on the set ❷ is small compared to that between set ❶; in other words, when set ❷ is weak compared to set ❶:

$$K_2 \doteq 2E\cos\phi \qquad (K_1 \ll K_2). \qquad [44v']$$

Under this same condition, the area swept out by the whole segment is

almost the same as that swept out by the arc (dashed) that would give rise to same force K_2 on the strong obstacles in the absence of the weak ones; thus the L_2 is approximately equal to the effective spacing l_{e2} of the strong obstacles. Since $L_1 \simeq l_{e1}$ when $L_1 \ll L_2$, we have at the end

$$\sigma = \frac{K_1}{bl_{e1}} + \frac{K_2}{bl_{e2}} \qquad [44w]$$

or

$$\sigma = s_1(T, \dot{\gamma}) \frac{2E}{bl_1} + s_2(T, \dot{\gamma}) \frac{2E}{bl_2}. \qquad [44w']$$

This equation may be used in two ways: for the flow stress as a function of the average obstacle spacings l_1 and l_2:

$$\tau = \tau_1(l_1) + \tau_2(l_2) \qquad [44w'']$$

and for the reciprocals of the apparent activation areas

$$\boxed{\frac{1}{\Delta a'} \equiv -b \frac{\partial \sigma}{\partial \Delta G} = \frac{1}{\Delta a'_1} + \frac{1}{\Delta a'_2}.} \qquad [44x]$$

Together, these two equations give the equations of two straight lines in a diagram of $1/\Delta a'$ vs. τ, one for the case that l_1 is varied, the other for the case that l_2 is varied:

$$\begin{aligned} \frac{b^2}{\Delta a'(l_1)} &= b^3 \cdot \left\{ \frac{\tau(l_1) - \tau_2}{\Delta W'_1} + \frac{\tau_2}{\Delta W'_2} \right\}, \\ \frac{b^2}{\Delta a'(l_2)} &= b^3 \cdot \left\{ \frac{\tau_1}{\Delta W'_1} + \frac{\tau(l_2) - \tau_1}{\Delta W'_2} \right\}. \end{aligned} \qquad [44y]$$

These two straight lines are shown in Fig. 44-13. The slope of each line is given by a property of the individual obstacles whose number is being varied. It is steeper for the more rate-sensitive material.

Furthermore, one can determine the contributions from each set to both the flow stress and the apparent activation area of the "alloy" corresponding to the intersection of the two lines (i.e. with the obstacle spacing l_2 that was held constant when set 1 was varied, and the obstacle spacing l_1 that was held constant when set 2 was varied). The ratios of these contributions follow directly from the intercepts (KOCKS, 1968), as may be seen directly from eqs. [44y]:

$$\frac{\tau_1}{\tau_2} = \frac{Y_2}{|Y_1|}; \quad \frac{\Delta a'_1}{\Delta a'_2} = \frac{X_1}{|X_2|}. \qquad [44y']$$

A particularly useful application of this technique is to work-hardening materials: when a variation of strain (and thereby presumably of the forest

a truly long-range internal stress (or image stress) that has a nonzero mean value over the area actually swept out in the slip plane.

Low-stress Limit for the Boltzmann Term

For the classical box-shaped obstacle, where the activation energy depends linearly on stress, the "probability of success" given by the Boltzmann term does not go to zero for zero stress. Apart from any correction due to reverse jumps, which will be considered later, the mild stress dependence of the *preexponential factors* in the rate expression will then become important. Even the frequency factor, which must enter all measurements, depends on stress through the obstacle stiffness (sec. 42).

The first question to be answered here is: when does the stress dependence of the activation energy become negligible with respect to that of the pre-exponential factors? We shall discuss it in terms of the phenomenological exponent m (eq. [34r]) and assume that in order of magnitude

$$m_o = \left.\frac{\partial \ln \dot{\gamma}_o}{\partial \ln \sigma}\right|_T \approx 1. \qquad [45a]$$

The contribution to m from the Boltzmann term is, with eq. [43g],

$$\boxed{m_G \equiv -\frac{1}{kT}\left.\frac{\partial \Delta G}{\partial \ln \sigma}\right|_T = \frac{\Delta a'}{b^2}\frac{\sigma}{\mu}\frac{\mu b^3}{kT}} \qquad [45b]$$

where $\mu b^3/kT \simeq 100$ (Table 3-I). Thus, when $\Delta a'$ is very small (say $10b^2$) m_G is dominant (exceeding m_o) only for stresses above $10^{-3}\mu$. But for discrete obstacles where typically $\Delta a' \simeq 1000b^2$, the contribution from m_G is dominant at all stresses above $\sigma \simeq 10^{-5}\mu$.

For long-range obstacles, in which $\Delta a'$ depends inversely on stress (or a higher power of it), m_G retains, of course, its constant value over all stresses (or even increases to lower stresses). But even for short-range obstacles where, in principle, the contribution m_G goes to zero for zero stress, our conclusion is that it may well have values comparable to m_o at all stresses of practical interest. It would only be negligible if

$$\sigma \ll \frac{kT}{b\Delta a} \quad \rightarrow \quad m_G \ll 1. \qquad [45b']$$

Reverse Jumps

Figure 45-1 is a copy of Fig. 41-1, showing *two* successive stable positions, 1 and 2, under the same applied stress. A "reverse jump" is a process that would bring a dislocation back from the stable position 2 to the unstable position U, from where it would, under positive driving force, go back to the

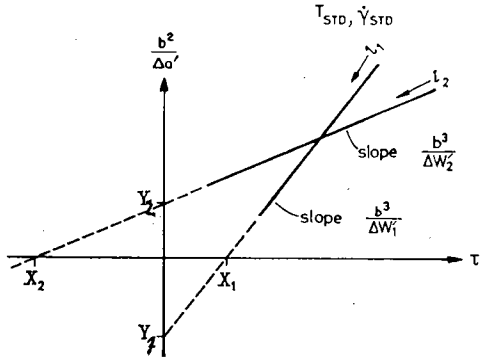

FIG. 44-13. A method of separating two contributions to the flow stress from two sets of obstacles the densities of which can be independently varied.

dislocation spacing) gives a straight line that does not go through the origin, there must be other obstacles; when the τ-intercept is negative, these are *more* subject to thermal activation than the forest dislocations, when it is positive they are *less* rate sensitive.

45. Low Stresses and High Temperatures

Until now, we have explicitly neglected reverse jumps of dislocations over activation barriers. These may become important at low stresses, where an Arrhenius-type rate equation can no longer apply. The analysis below, which differs from conventional ones in a number of important points, shows that the stresses at which reverse jumps must be taken account of are much too low to be of any practical interest, except when the obstacle *spacing* is no more than a few atomic dimensions. The propagation of kinks over second-order Peierls hills (sec. 24) or the generation of vacancies at jogs in screw dislocations (sec. 26) may be examples.

The condition for "low" stresses, in the above problems, turns out to be one in which the stress must be small compared to some term linear in the temperature. In that sense, one may also call this a "high-temperature" case. The condition for phonon drag to become important during thermal activation involves a similar comparison. On the other hand, an approximation may sometimes be of interest, in which the stress is merely small compared to the maximum glide resistance, irrespective of the temperature; or in which kT is high compared to the total activation energy, irrespective of the stress. These cases will also be discussed in the following.

The stresses to be used below are again total applied stresses, not any kind of "effective" stress. However, any long-range *average* glide resistance, which leads to energy *storage*, must always be subtracted from the applied stress. This is again a consequence of the Second Law, but will be explicitly derived. As was pointed out in the introduction of τ_{STOR} (sec. 22), this term may include

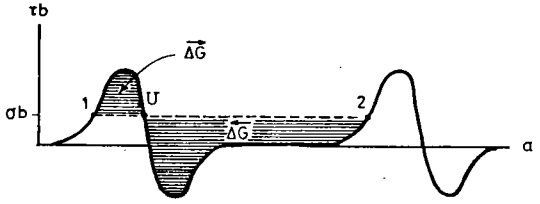

FIG. 45-1. A glide resistance profile showing the activation energies for forward jumps ($\vec{\Delta G}$) and for reverse jumps ($\overleftarrow{\Delta G}$).

stable position 1. This can happen under the action of thermal fluctuations, despite the adverse influence of the applied stress.

Just as the activation free enthalpy for the forward process (which we now mark by an arrow pointing to the right) could be described by (eq. [41a], $\tau = \tau_{\text{LINE}}$).

$$\vec{\Delta G} = \int_{a_1}^{a_U} (\tau - \sigma) b \, da$$

so the activation free enthalpy for reverse jumps is

$$\overleftarrow{\Delta G} = \int_{a_2}^{a_U} (\tau - \sigma) b \, da = \int_{a_1}^{a_U} (\tau - \sigma) b \, da - \int_{a_1}^{a_2} (\tau - \sigma) b \, da$$

$$= \vec{\Delta G} - (\sigma - \tau_{\text{STOR}}) ba \quad [45c]$$

where

$$\int_{a_2}^{a_1} \tau b \, da \equiv \tau_{\text{STOR}} ba = F_{\text{STOR}} \quad [45d]$$

is the free energy stored during the unit process, and

$$a \equiv a_2 - a_1 \quad [45e]$$

is the same as the area swept out after a successful jump, roughly l^2 in the case of discrete obstacles.

The net rate of thermal release is now

$$P_t = \vec{P}_t - \overleftarrow{P}_t = \vec{\nu} \exp - \frac{\vec{\Delta G}}{kT} - \overleftarrow{\nu} \exp - \frac{\overleftarrow{\Delta G}}{kT}. \quad [45f]$$

The frequency factors $\vec{\nu}$ and $\overleftarrow{\nu}$ must be assumed equal in order to proceed:

$$\overleftarrow{\nu} = \vec{\nu} \equiv \nu_G. \quad [45g]$$

This is a reasonable assumption when the two obstacles are identical.

With the expression [45c] for $\Delta\overleftarrow{G}$, we obtain the result

$$\boxed{P_t = \nu_G \exp - \frac{\Delta G(\sigma)}{kT}\left\{1 - \exp - \frac{(\sigma - \tau_{STOR})ba}{kT}\right\}} \qquad [45h]$$

which is *the most general rate equation for thermal activation* at constant stress and structure. (The right arrow above ΔG has been dropped again: ΔG refers to forward jumps.) The correction factor becomes equal to 1 and thus *reverse jumps can be neglected for*

$$\frac{\sigma - \tau_{STOR}}{\mu} \gg \frac{kT}{\mu b^3}\left(\frac{b}{l}\right)^2. \qquad [45i]$$

For stronger discrete obstacles, the average obstacle spacing l is generally in excess of 100 Burgers vectors; then, reverse jumps can be neglected above $\sigma \simeq 10^{-6}\mu$. But weaker obstacles or other glide resistance profiles that repeat after distances of the order of $10b$ or less may show effects of reverse jumps at stresses around $\sigma \simeq 10^{-4}\mu$ or somewhat higher.

When the inequality [45i] is reversed, the correction factor in eq. [45h] may be expanded, with the result

$$\boxed{P_t \doteq \nu_G \cdot \frac{(\sigma - \tau_{STOR})ba}{kT} \cdot \exp - \frac{\Delta G(\sigma)}{kT} \quad \Big| \quad \sigma - \tau_{STOR} < \frac{kT}{ba}.} \qquad [45j]$$

This equation differs from conventional ones in three significant respects:

(1) The net rate vanishes, in general, at a finite applied stress, equal to the *average* glide resistance. Only when no energy at all is stored during plastic deformation does the strain rate become proportional to the applied stress in the limit of vanishing stress.

(2) The proportionality factor of the stress is not the activation area Δa, but the area per "obstacle" a: it is often significantly larger, and it is *independent of stress* (LI, 1970; NICHOLS, 1971). Thus, the linearity of the pre-exponential factor in $(\sigma - \tau_{STOR})$ occurs for *all* forms of the stress dependence of ΔG, not only for a linear one.

(3) The stress-dependent Boltzmann term has *not* disappeared from the equation through the linearization. While, in theory, this provides a correction of "second order", the discussion under the last subtitle showed that this can be numerically significant (eq. [45b]).

An approximately linear stress dependence of the activation rate thus occurs only under very restrictive conditions (eqs. [45j], [45b]):

$$m = m_o + 1 \quad \text{for} \quad \tau_{STOR} \ll \sigma < \frac{kT}{ba} \ll \frac{kT}{b\Delta a'}. \qquad [45k]$$

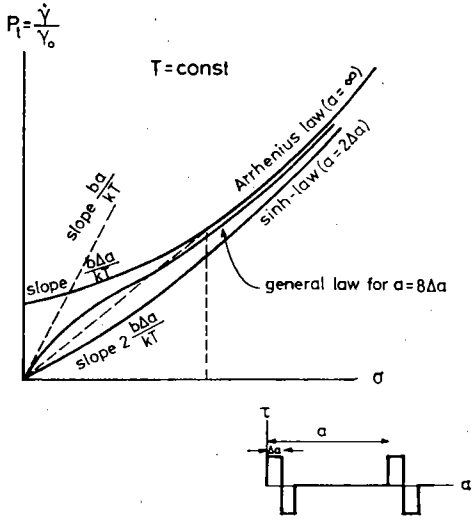

FIG. 45-2. The activation rate P_t, plotted against stress, for the exponential Arrhenius equation, the general law (eq. [45h]) and the sinh-law (eq. [45n]). All slopes in units of $\nu_G \exp(-F_o/kT)$.

An example would be $F_{STOR} \simeq 10^{-3}$ eV, $\sigma \simeq 10^{-4}\mu$, $a \simeq 100\ b^2$, $\Delta a' \simeq \Delta a \simeq 10\ b^2$, $T = 300$ K.

Figure 45-2 shows an actual plot of the activation rate versus stress according to the general equation [45f], for $\tau_{STOR} = 0$, $\Delta a = \text{const}$, and $a = 8\,\Delta a$. An inflection like the one shown must occur, when the initial slope ba/kT is larger than that of the tangent to the Arrhenius curve from the origin, which is $2.7\ b\Delta a/kT$, as is the case for most realistic obstacles.

A special case that has attracted much attention occurs when $a = 2\Delta a$. If this is to be true over a range of stresses, Δa must be constant; the glide resistance diagram is then a "square wave" (Fig. 45-3). For generality, we allow a finite level of τ_{STOR}. This case could then be an idealization of jog dragging (Fig. 26-2). With $\tau_{STOR} = 0$, it could describe the motion of a kink over a second-order Peierls potential.

For this case, we can write the general equation [45f] in the form

$$P_t = \nu_G \exp -\frac{F_t}{kT}\left\{\exp \frac{\Delta\overrightarrow{W}_t}{kT} - \exp \frac{\overleftarrow{\Delta W}_t}{kT}\right\}. \qquad [45\ell]$$

But since here

$$\Delta\overrightarrow{W}_t = -\overleftarrow{\Delta W}_t = (\sigma - \tau_{STOR})b\Delta a \qquad [45m]$$

eq. [45ℓ] is exactly equal to

$$P_t = \nu_G \exp -\frac{F_t}{kT}\sinh\left\{\frac{2b\Delta a}{kT}(\sigma - \tau_{STOR})\right\}. \qquad [45n]$$

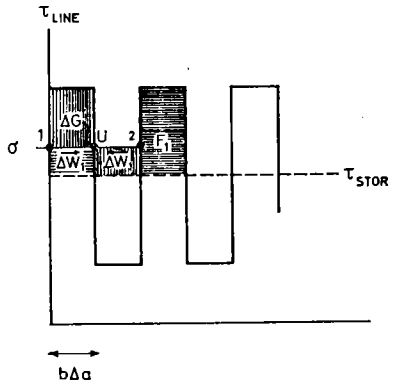

FIG. 45-3. The special obstacle profile that leads to a "sinh-law" (eq. [45n]).

The low-stress limit is again as in eq. [45j], for the special case $a = 2\Delta a$, since $\Delta G = F_1$ to first order.

Note that a sinh-law, eq. [45n], would not have been possible, had the forward and reverse work terms not been equal and opposite (eq. [45m]). This is clearly a very special condition (KAUZMANN, 1941); the complicated law [45n] has thus rarely any advantage over the linear law [45j]: the latter covers *any* obstacle profile, although it is limited to lower stresses.

The sinh-law can be useful in one respect: as Fig. 45-2 shows, it describes the limiting behavior for the maximum reasonable influence of reverse jumps.

High Temperatures

Without reverse jumps, the temperature dependence of the stress to achieve a certain strain rate came only from the stress dependence of the activation energy. A simple linear dependence $\Delta G(\sigma)$, for example, gave a linear law for $\sigma(T,\dot{\gamma}_{STD})$; it is shown again in Fig. 45-4, labeled "Arrhenius Law". When the stress goes to zero, the activation energy becomes F_o, and the temperature is

$$kT_o \equiv F_o/\ln(\dot{\gamma}_o/\dot{\gamma}). \qquad [45o]$$

But, at this limiting temperature, the Arrhenius Law cannot describe thermal activation over short-range obstacles; clearly, the influence of a strain rate on the temperature at *zero* stress (eq. [45o]) cannot be real. Once again the general eq. [45h] for the *net* rate of thermal release in the presence of reverse jumps remedies the situation: the net rate goes to zero as the stress approaches zero (or, more exactly, τ_{STOR}). The approximation [45j] shows that then, for $\Delta G = F_o$, the stress decreases exponentially with temperature, rather than having a sharp kink at T_o:

$$\sigma = \frac{\dot{\gamma}}{\dot{\gamma}_o} \cdot \frac{kT}{ba} \exp \frac{F_o}{kT}. \qquad [45p]$$

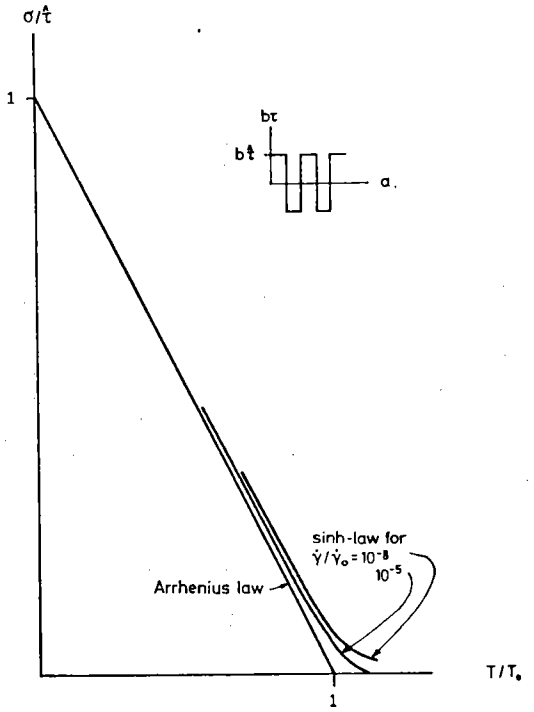

FIG. 45-4. The decrease of stress with temperature for the Arrhenius law and the "sinh-law".

Figure 45-4 illustrates this behavior, using instead the sinh-law over the entire range to obtain the limiting case. It is seen that, at the temperature T_0 belonging to a particular strain rate, a finite stress is still necessary to achieve net flow. For experimental determinations of T_0 as a measure of F_0, it is important that the extrapolation be made from higher stresses. When the obstacle is not box-shaped, and thus the $\sigma - T$ relation due to the Arrhenius Law not linear, this may be difficult. The procedure suggested in Fig. 43-8a may then be useful.

The stress-temperature relation [45p] for a certain strain rate contains not only an exponential, but also a linear temperature term. It should lead to an eventual *rise* of the stress with temperature at high temperatures. Straightforward analysis of eq. [45p] shows that, for this reason, a minimum would occur in the σ–T diagram at

$$kT = F_0. \qquad [45q]$$

But at this temperature, the application of a Boltzmann term becomes questionable. Actually, such a temperature is not accessible unless the total activation energy of the "obstacle" is less than 0.1 eV (900°C), and then T_0 would typically be 20 times smaller or 60 K.

Another effect can become important at lower temperatures than that given by

[45q], which also leads to an eventual linear rise in stress with temperature, and that is phonon drag. At zero glide resistance (between obstacles), it can be approximately described by eq. [31r]:

$$\sigma = \frac{kT}{\Omega}\cdot\frac{v}{v_s}. \qquad [45r]$$

Although the superposition between thermal activation and viscous drag is more complicated (e.g. eq. [33r]), the location of the minimum in the σ–T diagram can be estimated by setting the positive slope due just to the drag mechanism (eq. [45r]) equal to the negative slope due just to thermal release (eq. [45p]). This gives approximately

$$\frac{F_o}{kT}\exp\frac{F_o}{kT} = \frac{a}{b^2}\frac{v}{v_s}\frac{\dot\gamma_o}{\dot\gamma}.$$

To estimate the last ratio on the right, we must compare velocities with release rates and use

$$v = yP_t \doteq y\nu_G\frac{\dot\gamma}{\dot\gamma_o}$$

where y is the forward distance moved by a dislocation segment after thermal release. Equations [42j] and [31f] give $\nu_G \simeq v_s/100b$. Thus we obtain

$$\frac{F_o}{kT}\exp\frac{F_o}{kT} \simeq \frac{1}{100}\frac{ay}{b^3} \qquad [45s]$$

as the condition for the minimum.

Inserting the temperature [45q] into [45s], we see that phonon drag effects become important at lower temperatures so long as $ay > 270b^3$, i.e. for most realistic obstacles.

On the other hand, to see whether such effects could ever be of practical interest, let us insert the temperature T_o from eq. [45o], and take a typical value of $\dot\gamma/\dot\gamma_o$ to be 10^{-10}. Then eq. [45s] would require

$$ay > 10^{13}b^3.$$

Such a value is very unrealistic.

In conclusion, we find that an exponential decay of the stress with temperature near T_o, due to reverse jumps, describes high temperature processes sufficiently well. For all obstacles that are spaced more than a few atomic dimensions, this decay is so rapid as to be virtually equal to a kink.

5. MODELS FOR MACROSCOPIC SLIP

Summary

In this Chapter we show, with two examples, how the methods developed in Chapters 2, 3, and 4 may be applied to derive the dependence of the macroscopic strain rate on stress, temperature, and structure parameters from specific microscopic models. We are not especially concerned with whether the particular model is a completely adequate description of the deformation process; rather, we wish to point out the macroscopically observable consequences that must ensue if it were. In this way, one may eventually be able to distinguish between different mechanisms on the basis of macroscopic observations; conversely, one sometimes finds that different models lead to essentially indistinguishable macroscopic behavior.

As an example of a *linear barrier*, we treat the lattice resistance to full dislocations ("Peierls stress") in sec. 51. There exist two common models: one is based on the nucleation of a continuous bulge under a macroscopic line tension; the other on the nucleation of an atomic-sized double kink. We give new derivations and simple end formulae for both and find the results to be similar, thus softening physical objections against either. Variational energy principles are illustrated in the nucleation part of the problem; the kink propagation part demonstrates the use of steady-state kinetics.

Isolated linear barriers of the repulsive kind were shown (sec. 24) to be identical in their nucleation aspects to periodic ones; the results of sec. 51 should, therefore, be directly applicable. Attractive or energy-storing linear barriers can also be treated by the bulge method; the results, however, are significantly different (see secs. 24 and 43).

The mobilization of screw dislocations in bcc metals—an important thermally-activated process in these materials—is not treated explicitly. Screw motion must be preceded by a change in core structure: a constriction normal to the slip plane (sec. 27). If this activated configuration is retained for forward movements of a few atomic distances at least, the process is formally identical to the unlocking from an attractive linear barrier; if, on the other hand, the dislocation merely progresses to the next possible low-energy configuration, it is better described as a lattice resistance (*pseudo-Peierls stress*). An important complication is the asymmetry between forward and backward movement. We feel that, at present, no self-consistent and realistic model has been established sufficiently well to warrant presentation in this article. The current status was reviewed by HIRSCH (1968) and by CHRISTIAN (1970b); a more recent development is due to BASINSKI *et al.* (1971).

A *precipitation hardened* crystal is the prototype of a material with discrete

obstacles. The element glide resistance, or local force-distance, diagrams for various mechanisms are outlined in sec. 52, the method for their superposition is derived, and the characteristics of the line and plane glide resistance are given as a function of temperature. While the temperature dependence is generally slight, it may be sufficiently strong at very low temperatures to allow a macroscopic discrimination between various mechanisms. It is also strong enough to significantly influence expected age-hardening observations.

The mechanism of *solution hardening* presents some problems. An extension of the precipitation hardening model to individual solute atoms may, at best, apply to very dilute solutions when only interstitial solutes cause any appreciable strengthening. Randomly dispersed substitutional solute atoms do not act as discrete obstacles when they are in concentrated solution, but interact with a dislocation cooperatively. A model due to LABUSCH (1972) for cooperative interactions of solutes with a dislocation, and applicable at absolute zero temperature was discussed in sec. 25. The high-temperature behavior is, in our opinion, not well enough understood to be discussed here.

The mechanism of *forest dislocation cutting* exhibits unusual complexities. Forest dislocations can interact with glide dislocations to form attractive junctions where small nodal segments of a dislocation can form to significantly lower the local energy of the two intersecting dislocations, making a thermally assisted intersection nearly impossible. Alternatively the interaction between a forest dislocation and a glide dislocation can be a repulsive one for which a thermally assisted intersection is possible. In work-hardened crystals not only are the points of intersection of forest dislocations with the slip plane nearly always clustered into cell walls giving a distinctly nonrandom distribution, but they can also be displaced significantly under the forces exerted by an impinging glide dislocation. All such complex effects prevent us from presenting a detailed model for forest dislocation intersections. In spite of this, a satisfactory first-order approximation can often be had by considering forest dislocations as a collection of fixed and randomly distributed point obstacles.

The macroscopic behavior of almost all real materials reflects the superposition of effects due to many types of obstacles and mechanisms, and occasionally also of effects due to drag and inertia. The superposition problem is thus of major importance for any comparison of theory and experiments. We summarize some examples of binary superposition in sec. 53. In general, they involve many subtleties and lead to a large variety of results. However, many practical cases are reasonably well described by one of the well-known limits: additivity of the flow stress contributions; significant contribution only from the mechanism that requires the higher flow stress (or furnishes the lower rate); and additivity of the strain rates.

The procedure of the Chapter, namely to hypothesize a microscopic mechanism and derive macroscopic consequences from it, is reversed in Chapter 6, where macroscopic data are presumed given and the necessary or likely properties of the underlying mechanisms are derived.

There have been many detailed discussions of specific mechanistic models

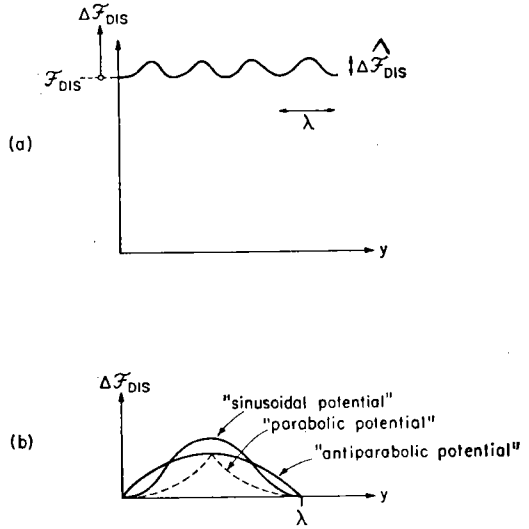

FIG. 51-1. (a) The total free energy per unit length of a dislocation as a function of the position y in a lattice of spacing λ. (b) Limiting shapes of the Peierls potential $\Delta\mathcal{F}_{DIS}$. (The parabolic potential is not used in the following evaluations.)

governing the glide resistance for dislocation motion. Of these we find the following limited selection most directly related to the mechanisms which we have discussed:

ALEXANDER and HAASEN (1968), *Dislocations and Plastic Flow in the Diamond Structure;*
ASHBY (1970), *The Mechanical Effects of Dispersion of a Second Phase;*
BROWN and HAM (1971), *Dislocation-Particle Interactions;*
CHRISTIAN (1970a), *Plastic Deformation of BCC Metals;*
FRIEDEL (1964), *Dislocations;*
GUYOT and DORN (1967), *A Critical Review of the Peierls Mechanism;*
HIRTH and LOTHE (1968), *Dislocation Theory;*
KELLY and NICHOLSON (1963), *Precipitation Hardening;*
OROWAN (1954), *Dislocations and Mechanical Properties.*

51. LATTICE RESISTANCE

The Mechanism

In most crystalline solids the core energy of a dislocation undulates as it moves (PEIERLS, 1940; NABARRO, 1947): the slip plane appears to be energetically rough (Fig. 51-1a). This periodic roughness has a wavelength equal to the appropriate lattice spacing λ and an amplitude, $\Delta\hat{\mathcal{F}}_{DIS}$ (the *Peierls energy*) small compared to the total free energy, $\mathcal{F}_{DIS}$, of unit length of the dislocation. Figure 51-1b shows two simple but useful approximations for the shape of the Peierls energy: the "*sinusoidal*" *potential*:

$$\Delta\mathcal{F}_{DIS} = \frac{\hat{\tau}_P b\lambda}{2\pi}\left(1 - \cos 2\pi\frac{y}{\lambda}\right) \qquad [51a]$$

and the *anti-parabolic potential* introduced by GUYOT and DORN (1967) (and called "quasi-parabolic" by them):

$$\Delta\mathscr{F}_{\text{DIS}} = \hat{\tau}_{\text{P}} b\lambda \cdot \frac{y}{\lambda}\left(1 - \frac{y}{\lambda}\right); \quad (0 \leqslant y \leqslant \lambda). \qquad [51b]$$

They are normalized to give the same maximum slope, $\hat{\tau}_{\text{P}} b$, where

$$\hat{\tau}_{\text{P}} = \left(\frac{\text{d}\Delta\mathscr{F}_{\text{DIS}}}{b\ \text{d}y}\right)_{\text{MAX}}$$

is called the *Peierls stress*: in our terminology it is the maximum element glide resistance. (The results of models for lattice-resistance controlled flow are less sensitive to the choice of a potential thus normalized than to potentials normalized to the same Peierls *energy*—an observation first made by GUYOT and DORN). For the two potentials listed above, the Peierls energy is, respectively,

$$\Delta\hat{\mathscr{F}}_{\text{DIS}} = \frac{\hat{\tau}_{\text{P}} b\lambda}{\pi} \qquad (\textit{sinusoidal potential}) \qquad [51a']$$

and

$$\Delta\hat{\mathscr{F}}_{\text{DIS}} = \hat{\tau}_{\text{P}} b\lambda/4 \qquad (\textit{anti-parabolic potential}). \qquad [51b']$$

The undulating free energy of Fig. 51-1 reflects two physical quantities: the interaction potentials of the atoms that make up the crystal, and the structure—principally, the width—of the dislocation core. If the ideal shear strength, τ_{IDEAL}, is high (say $\mu'/10$, see KELLY, 1966) so that the dislocation core is narrow and of order b, the motion of the dislocation can be thought of as distorting, breaking, and remaking atomic bonds. The stress required to do this is the ideal strength τ_{IDEAL}. But if the ideal strength is low so that the core is wide, serious distortion of bonds occurs some distance ahead of, and behind, the dislocation. Regions exist which contain bonds in all stages of being stretched, broken, and remade; and since these regions are elastically coupled, the free energy increase of some is compensated for by the decrease in others. Then, the maximum lattice resistance $\hat{\tau}_{\text{P}}$ may be considerably less than the ideal strength. If the core is sufficiently wide, this coupling smooths out the periodic lattice potential completely: apparently this occurs in fcc metals. But in a much larger class of materials that includes the covalently bonded elements and practically all inorganic compounds, the smoothing is incomplete.

In general, the maximum lattice resistance to the motion of a dislocation (the Peierls stress) is thus limited to

$$\hat{\tau}_{\text{P}} \leq \tau_{\text{IDEAL}} \lesssim \frac{\mu'}{10} \qquad [51c]$$

where μ' is the shear modulus in the glide plane and glide direction (see KELLY, 1966). This limits the Peierls energy—the amplitude of the energy undulations—to a maximum value given by eqs. [51a'] or [51b']:

$$\Delta\hat{\mathscr{F}}_{\text{DIS}} \lesssim \frac{\mu' b\lambda}{10\pi}. \qquad [51c']$$

Even for a high lattice resistance, then, the *fractional* change in energy as the dislocation moves is still relatively small. We shall take, as typical orders of magnitude

$$\frac{\Delta \hat{\mathscr{F}}_{\text{DIS}}}{\mathscr{F}_{\text{DIS}}} \simeq 10^{-2}$$

and [51c″]

$$\frac{\hat{\tau}_{\text{P}}}{\mu} \simeq 10^{-2}.$$

A sinusoidal shape is a logical choice for a first guess at the Peierls potential. But more detailed thinking suggests that the maximum should be flatter than this: the ability of the dislocation to dissociate, for example, flattens the peak while leaving the maximum slope (and thus $\hat{\tau}_{\text{P}}$) unchanged. So deviations from the sinusoidal potential will tend towards the anti-parabolic, rather than the parabolic potential (shown as a dashed line in Fig. 51-1b). Thus, in spite of its unrealistic, sharp cusp the anti-parabolic potential is a useful limiting case, and is mathematically convenient.

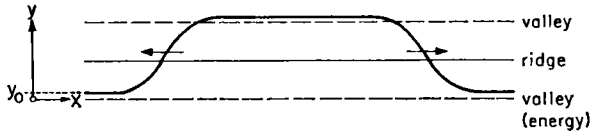

FIG. 51-2. Final configuration after double kink nucleation. This is never the critical configuration.

How does a dislocation move through this energetically undulating terrain? The end result of thermal activation is that a sufficiently long segment of a dislocation—initially straight and lying in an energy valley—now lies in an identical position in the next valley; two full kinks (i.e. kinks of height λ) connect it to the rest of itself, and, if the crystal is stressed, they move apart (Fig. 51-2). But this is not the *critical* configuration: the configuration corresponding to the energetic saddle point over which the system must pass to reach the next valley. The main task of the following pages is to derive *critical configurations for all stresses*, and hence the energy of nucleation of a bulge or kink pair.

As a simple example, consider the limiting case of kink nucleation at very low stresses. (See, for example, ALEXANDER and HAASEN, 1968; HIRTH, 1970). (Although the forward dislocation does not lie *past* the next valley, as will be shown below). Here, the critical configuration must tend to that depicted in Fig. 51-2: a pair of full kinks of a critical spacing. Two kinks interact such that the glide resistance each exerts on the other is (sec. 24, eq. [24h'], Fig. 51-3):

$$\tau_{\substack{\text{INT} \\ \text{KINKS}}} = \frac{\mu b \lambda^3}{4\pi(\Delta a)^2} \qquad [51d]$$

Using eq. [41g], the low-stress limit for the activation free enthalpy is

$$\Delta G_{\text{NUCL}} = b \int_{\sigma}^{\hat{\tau}} \Delta a \, d\tau = F_{\text{NUCL}} \cdot \left\{ 1 - \sqrt{\frac{\sigma}{\hat{\tau}}} \right\}; \text{ for } \sigma \simeq 0 \qquad [51d']$$

where F_{NUCL} is the free energy of the two isolated kinks; $\hat{\tau}$ is an upper cut-off stress

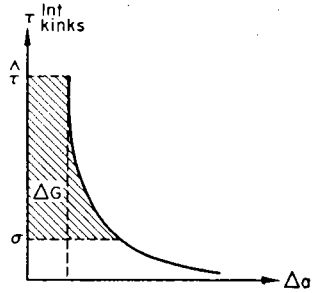

FIG. 51-3. Glide resistance diagram for kink interaction. The total area under the curve up to the upper cut-off stress $\hat{\tau} \simeq \tau_{\text{IDEAL}}$ is the free energy $2F_{\text{KINK}}$ of two isolated kinks in this elastic model.

where the ideal shear strength is approached. With this (somewhat arbitrary) cut-off procedure, the total self energy of two kinks becomes

$$F_{\text{NUCL}} = \mu b^3 \sqrt{\frac{\hat{\tau}}{\pi\mu}} \left(\frac{\lambda}{b} \right)^{3/2}. \qquad [51e]$$

It is the area under the curve of Fig. 51-3. Note, however, that the "core energy" in this model, namely the part of the area (dashed box) affected by the cut-off, is fully one-half the total area F_{NUCL}.

It is useful to have an estimate for the quantity F_{NUCL}. In typical cases, the forward lattice spacing λ is about equal to b (or a little smaller), the upper cut-off stress $\hat{\tau}$ is about equal to the ideal shear strength $\mu'/20$ (or a little smaller for kinks). Inserting these values into eq. [51e] gives an upper limit

$$F_{\text{NUCL}} \lesssim \frac{\mu b^3}{8}. \qquad [51e']$$

In other words, the free energy of one kink ($F_{\text{NUCL}}/2$) is about one-tenth of that of a dislocation of the same length—a common order-of-magnitude estimate also arrived at by methods that focus more on core energy than on elastic energy.

Kinks such as these exist in thermal equilibrium at reasonable temperatures. Their average spacing along dislocation lines is of order

$$b \cdot \exp\left\{ \frac{F_{\text{KINK}}}{kT} \right\}$$

where F_{KINK} is the free enthalpy of formation of a kink: $F_{\text{NUCL}}/2$ in this model. This spacing (for typical values of μ and b) is larger than 1 μm at room temperature and larger than 1 cm at 150 K. Since this is more than the typical length of free dislocation segments, *nucleation* of kink pairs under stress must be of prime importance in real materials. We will treat it by two different models, in the next two subsections. Subsequently, we consider the motion of the kinks thus generated.

For a review of various models of the lattice resistance and of experimental results, we recommend that by GUYOT and DORN (1967). For background material, we have made extensive use of the book by HIRTH and LOTHE (1968).

The Energy to Nucleate a Continuous Bulge

An alternative to the discrete-kink model—which neglects line tension, replacing it by the kink–kink interaction—is the *continuous bulge* model. It treats the nucleation step involved in the microscopic forward displacement of a dislocation in the same way that a macroscopic displacement would be treated—by the self-stress approach. The problem is further simplified if long-range interactions between segments of dislocation are neglected: then the self-stress becomes a local property of the dislocation, and expressible as a line tension. Let us in addition assume for simplicity that the line tension is orientation independent and equal to $\mathscr{F}_{\mathrm{DIS}}$; the small contributions from $\Delta\mathscr{F}_{\mathrm{DIS}}$ can be neglected.

Under such circumstances, as we have seen in sec. 24, the dislocation will take up varying local curvatures in response to the stress. Starting from a straight dislocation at the position y_0 where it is in stable equilibrium under the applied stress σ, given by:

$$\frac{\partial \Delta\mathscr{F}_{\mathrm{DIS}}}{b\,\partial y} = \tau_{\mathrm{ELEM}}(y_0) = \sigma \qquad [51f]$$

it will accumulate an angle β to the x-axis, which is given as a function of y by

$$\frac{\beta^2}{2} \doteq \int_{y_0}^{y} \frac{\tau_{\mathrm{ELEM}}(y') - \sigma}{\mathscr{F}_{\mathrm{DIS}}} \cdot b\,\mathrm{d}y'; \qquad \beta(y_0) = 0. \qquad [51g]$$

This is an adaptation of eq. [24e'] for $y_0 \neq 0$, for a constant line tension $\mathscr{F}_{\mathrm{DIS}}$, and for $\beta \ll 1$. Integration of the right-hand side, as in eq. [24f'], leads directly to

$$\beta(y,\sigma) \doteq \sqrt{2\,\frac{\Delta\mathscr{G}_{\mathrm{DIS}}(y,\sigma)}{\mathscr{F}_{\mathrm{DIS}}}} \qquad [51g']$$

where the lattice free enthalpy per unit length of dislocation is

$$\Delta\mathscr{G}_{\mathrm{DIS}} \equiv \Delta\mathscr{F}_{\mathrm{DIS}}(y) - \Delta\mathscr{F}_{\mathrm{DIS}}(y_0) - \sigma b(y - y_0). \qquad [51g'']$$

Equation [51g'] describes the equilibrium shape of a bulge on the dislocation line.

The activation free enthalpy for the nucleation of such a bulge is

$$\Delta G_{\mathrm{NUCL}} = \mathscr{F}_{\mathrm{DIS}} \int (d\xi - \mathrm{d}x) + \int \{\Delta\mathscr{F}_{\mathrm{DIS}}(y) - \Delta\mathscr{F}_{\mathrm{DIS}}(y_0)\}\,\mathrm{d}\xi - \sigma b \int (y - y_0)\,\mathrm{d}x \qquad [51h]$$

where $\mathrm{d}\xi$ is an element along the dislocation line, and the integration extends

over the entire length of the dislocation. The first term in eq. [51h] describes the rise in energy due to the increase in length of the dislocation line; the second that due to the increased line energy of the dislocation elements in the bulge; and the third term is the work done by the applied forces in forming the bulge.

Since all integrands are given as functions of y, let us transform the differentials $d\xi$ and dx to dy, and make an approximation for small angles β in the process. The nucleation energy becomes

$$\Delta G_{\text{NUCL}} = 2\mathscr{F}_{\text{DIS}} \int_{y_o}^{\hat{y}} \frac{\beta}{2}\,dy + 2\int_{y_o}^{\hat{y}} \frac{\Delta\mathscr{G}_{\text{DIS}}}{\beta}\,dy \qquad [51h']$$

Here, $\hat{y}$ is given by the condition that $\beta = 0$ (where the bulge reaches its maximum at $\Delta\mathscr{F}_{\text{DIS}} = 0$, see also sec. 24). Inserting the equilibrium value of β from eq. [51g'] gives the simple result

$$\boxed{\Delta G_{\text{NUCL}} = 2\mathscr{F}_{\text{DIS}} \cdot \int_{y_o}^{\hat{y}} \beta\,dy} \quad ; \qquad \beta(\hat{y}) = 0. \qquad [51i]$$

For an evaluation, one needs eqs. [51f], [51g'], and [51g''].

This model was first treated fully by DORN and RAJNAK (1964). Their result looks more complicated than ours only because they did not make a small-angle approximation—one which is obviously justified by eqs. [51c'] and [51g']. Furthermore, they did not use the equilibrium condition [51g] for the shape of the bulge, but instead determined it by a variational method applied to the general equation [51h] or [51h'], a procedure which is equivalent to rederiving the equilibrium conditions.

Application of eq. [51i] to the sinusoidal potential [51a], using eq. [51f] and the definition

$$Y \equiv \frac{y - y_o}{\lambda} = \frac{y}{\lambda} - \frac{1}{2\pi}\arcsin\frac{\sigma}{\hat{\tau}_{\text{P}}} \qquad [51j]$$

gives for the bulge nucleation energy

$$\Delta G_{\text{NUCL}} = 2\sqrt{2\mathscr{F}_{\text{DIS}} \cdot \hat{\tau}_{\text{P}} b\lambda} \cdot \lambda \cdot$$

$$\int_0^{\hat{Y}} \sqrt{\frac{1}{2\pi}\left\{\sqrt{1 - \left(\frac{\sigma}{\hat{\tau}_{\text{P}}}\right)^2} - \cos\left[2\pi Y + \arcsin\left(\frac{\sigma}{\hat{\tau}_{\text{P}}}\right)\right]\right\}} - \frac{\sigma}{\hat{\tau}_{\text{P}}}\,Y \cdot dY. \qquad [51j']$$

The integral was evaluated numerically; the resulting $\Delta G_{\text{NUCL}}(\sigma)$ relation is plotted in Fig. 51-4 (upper curve). It appears to be identical to that published by DORN and RAJNAK (1964) as it should. (The activation energy ΔG_{NUCL} is plotted horizontally: in this way, Fig. 51-4 may be interpreted as a flow-stress

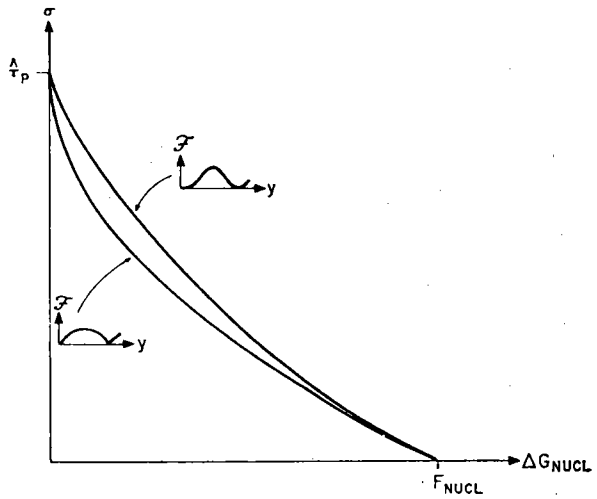

FIG. 51-4. Stress versus activation energy for bulge nucleation, from the sinusoidel potential (upper curve) and from the anti-parabolic potential (lower curve). (See Fig. 51-1b.)

versus temperature diagram at constant strain rate, for the case that bulge nucleation is in fact rate controlling.)

The shape of the anti-parabolic potential (eq. [51b]) traps the dislocation in a way which is unperturbed by small stresses. For this potential, then, $y_o = 0$,

$$Y = \frac{y}{\lambda} \qquad [51k]$$

and

$$\Delta G_{NUCL} = 2\sqrt{2\mathscr{F}_{DIS}\hat{\tau}_P b\lambda}\cdot\lambda \int_0^Y \sqrt{\left(1 - \frac{\sigma}{\hat{\tau}_P}\right)\cdot Y - Y^2}\, dY \qquad [51k']$$

which can be integrated in closed form and gives

$$\Delta G_{NUCL} = F_{NUCL}\cdot\left(1 - \frac{\sigma}{\hat{\tau}_P}\right)^2. \qquad [51k'']$$

This relation is plotted as the lower curve in Fig. 51-4. It is seen that the final results are not very dissimilar for the two drastically differing potentials. The total activation free energy, F_{NUCL}, for the anti-parabolic potential, is defined by eq. [51k']; it is

$$F_{NUCL} \equiv \Delta G_{NUCL}(\sigma = 0) = \frac{4}{\pi}\cdot\mu b^3\cdot\sqrt{\frac{\hat{\tau}_P}{\mu}}\cdot\left(\frac{\lambda}{b}\right)^{3/2} \quad (\textit{anti-parabolic pot.}) \qquad [51\ell]$$

For the sinusoidal potential the result (from eq. [51j']) is

$$F_{\text{NUCL}} \equiv \Delta G_{\text{NUCL}}(\sigma = 0) = \frac{4}{\pi^{3/2}} \cdot \mu b^3 \cdot \sqrt{\frac{\hat{\tau}_P}{\mu}} \cdot \left(\frac{\lambda}{b}\right)^{3/2} \quad (\textit{sinusoidal pot.}) \quad [51\ell']$$

These energies may be compared to the free energy [51e] of a full double kink in the elastic model: they are identical in form, but about one-third larger in magnitude.

This similarity is the more surprising when the critical geometry is examined.

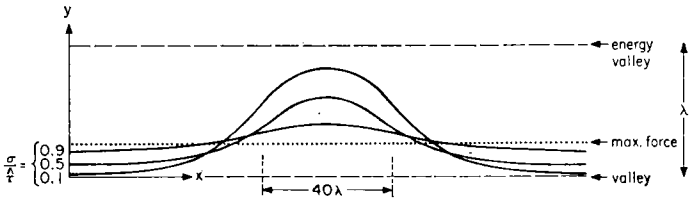

FIG. 51-5. Actual shape of bulges in sinusoidal potential for three stresses, using a constant line tension and a Peierls energy of 1/100 of the line tension. The y-scale is magnified 40 times with respect to the x-scale.

The gradual "kinks" of the bulge model are quite unlike the sharp steps of the kink model. Figure 51-5 shows the actual shapes of bulges over the sinusoidal potential, at 10%, 50%, and 90% of the Peierls stress, as derived from the relation $\beta(y)$, the integrand in eq. [51j'], using for the order of magnitude eq. [51c"]. Note that the y-axis is expanded by a factor 40 as compared to the x-axis. One can hardly call these shapes "double kinks", though in the limit of zero stress the shape does degenerate to two distinguishable kinks—smoothed though they are. (See also the construction in Fig. 24-4.) At any finite stress, the line tension makes the dislocation turn back before it has reached the next valley.

The application of the line tension approximation to changes on the atomic scale is obviously questionable. For this reason, the alternative double-kink model is developed further in the next subsection, where it is shown that in spite of geometric differences, the energetics of the kink and bulge models are very similar.

The Energy to Nucleate a Pair of Discrete Kinks

The *bulge* of Fig. 51-5 is sometimes called a "double-kink"—a confusing terminology because the individual kinks cannot be distinguished. There is an alternative model geometry that truly consists of a pair of (discrete) kinks, as illustrated in Fig. 51-6a. It is sometimes preferred as a basis for calculating the Peierls stress, because it does not presuppose the applicability of a line tension model on an atomic scale—indeed, it implies the breakdown of line tension concepts, since they always lead to kinks so shallow that their discreteness is lost.

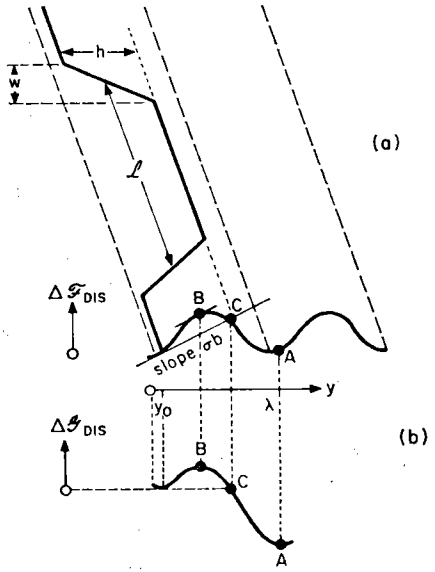

FIG. 51-6. (a) A pair of discrete kinks in a dislocation under the influence of a Peierls potential $\Delta\mathcal{F}_{DIS}$. Their spacing $\mathscr{L}$ and height h in equilibrium under an applied stress σ are derived, assuming $w \ll \mathscr{L}$; the value of h shown here already reflects the result. (b) The Peierls free enthalpy.

When, for atomistic reasons, kinks are narrow—that is, when the kink width w (Fig. 51-6a) is small compared to the kink spacing $\mathscr{L}$:

$$w \ll \mathscr{L} \qquad [51m]$$

—then the following model applies. The spacing $\mathscr{L}$ of a pair of kinks in the critical configuration can be derived by the method outlined below: it is 10λ or larger for all stresses (where λ is the period of the Peierls potential). Such a model, then, might realistically describe the behavior of covalently bonded crystals, in which kinks are likely to be narrow (i.e. w equal to a few atomic spacings at the most).

The parameters (Fig. 51-6a) of the double-kink model are the *kink spacing*, $\mathscr{L}$, and the *kink height*, h; w is considered to be constant. Previous treatments have assumed h to be either the full Peierls period λ, as in Fig. 51-2 or (more often) given by the assumption that the advance dislocation piece must be in an unstable equilibrium position on the Peierls potential; these two positions of the advanced dislocation are marked A and B, respectively, in Fig. 51-6. We shall show that they are limiting cases, asymptotically approached at low and high stresses respectively (although the point A is never beyond the next valley as it appears in the figure).

In general, $\mathscr{L}$ and h must be treated as internal parameters whose equilibrium values can be found by varying the free enthalpy at the given stress with respect to both. Let us call $\Delta G'_{NUCL}$ the free enthalpy associated with a kink

pair of arbitrary height h' and spacing $\mathscr{L}'$. (We shall use the unprimed symbols to describe the critical configuration.) Then $\Delta G'_{\text{NUCL}}$ is given by

$$\Delta G'_{\text{NUCL}} = \mathscr{L}' \cdot \{\Delta \mathscr{F}_{\text{DIS}}(y_o + h') - \Delta \mathscr{F}_{\text{DIS}}(y_o)\} - \sigma b h' \mathscr{L}' + 2F_{\text{KINK}}(h') - F^{\text{INT}}_{\text{KINKS}}(h', \mathscr{L}'). \quad [51n]$$

The first term is the difference in free energy of the piece of parallel dislocation in the ground state at $y_o(\sigma)$ and the (tentative) activated state advanced by h'; the second term is the work done by the external forces; and the last two together are the free energy of the kink pair. The kink interaction energy is frequently neglected; we shall comment on its influence below. Inserting its well-known dependence on h' and $\mathscr{L}'$, with an approximate proportionality factor, from eq. [24h], and inserting the Peierls free enthalpy $\Delta \mathscr{G}_{\text{DIS}}$ defined in eq. [51g″], eq. [51n] becomes

$$\Delta G'_{\text{NUCL}} = \mathscr{L}' \cdot \Delta \mathscr{G}_{\text{DIS}}(h', \sigma) + 2F_{\text{KINK}}(h') - \frac{\mu b^2}{10} \frac{(h')^2}{\mathscr{L}'}. \quad [51n']$$

This free enthalpy of a kink pair is plotted in Figs. 51-7a–c for three values of the applied stress, using the sinusoidal potential [51a] with $\hat{\tau}_P = \mu/100$, $\lambda = b$, and using a kink-self energy to be discussed below (eq. [51t]). In the figures, one can recognize the basic features of the Peierls potential: the general increase of free enthalpy in the h'-direction as the kinks grow in height

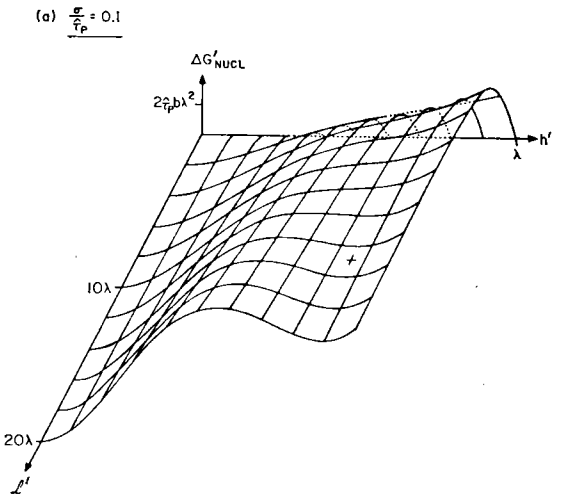

FIG. 51-7. The free enthalpy $\Delta G'_{\text{NUCL}}$, over that of a straight dislocation in equilibrium under a stress σ in a sinusoidal Peierls potential, of a piece of dislocation of arbitrary length $\mathscr{L}'$, that is advanced by an arbitrary distance h' and terminated by a pair of discrete kinks (eqs. [51a], [51g″], [51n′], [51s], [51t]). Figures a, b, c are for three ratios of the applied stress σ to the maximum element glide resistance $\hat{\tau}_P$ (the Peierls stress at $T = 0$ K).

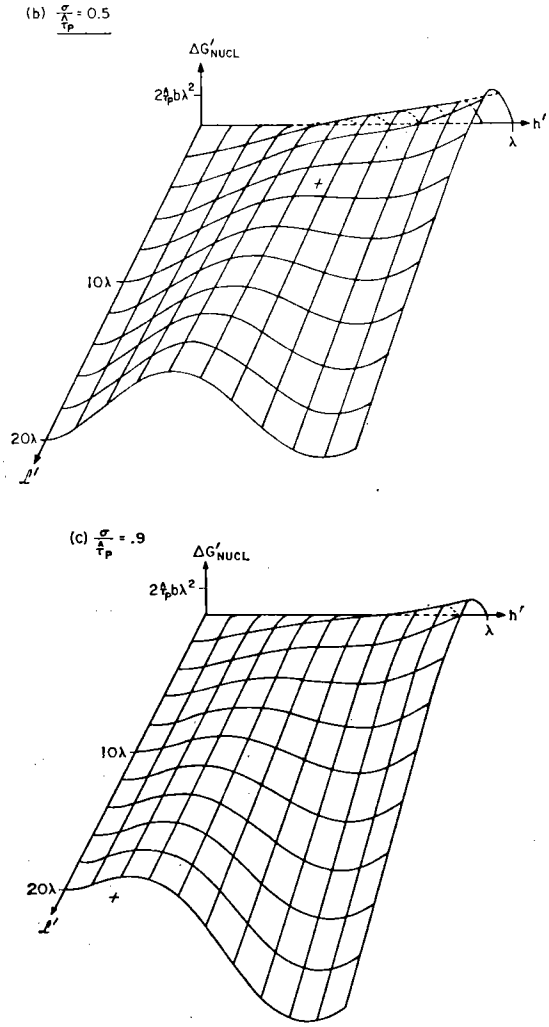

FIG. 51-7 (cont.)

(which vanishes as $\mathscr{L}' \to 0$ because of the kink–kink interaction); and the general lowering of free enthalpy due to external work as both $\mathscr{L}'$ and h' increase.

The *ground state* of the dislocation is at the origin of the figures. The *configuration after successful activation* must be in the valley as $h' \simeq \lambda$ at large values of $\mathscr{L}'$, which values increase as the kinks continue to move apart: there is no final stable equilibrium configuration. The *critical equilibrium configuration* (the "activated state") is between these; it is a position from which $\Delta G'_{NUCL}$ continuously decreases both towards the initial and the final states.

The critical configuration is marked by a cross in each figure. It was obtained by solving numerically the equilibrium conditions

$$\left.\begin{aligned} \frac{\partial \Delta G'_{\text{NUCL}}}{\partial \mathscr{L}'}\bigg|_{h',\sigma} &= 0 \\ \frac{\partial \Delta G'_{\text{NUCL}}}{\partial h'}\bigg|_{\mathscr{L}',\sigma} &= 0 \end{aligned}\right\} \quad \text{for } h' = h,\ \mathscr{L}' = \mathscr{L}. \qquad \begin{matrix}[51o] \\ [51o']\end{matrix}$$

For the small stress in Fig. 51-7a, the critical configuration is a true saddle point, the equilibrium being stable in the h'-direction and unstable in the $\mathscr{L}'$-direction. At the intermediate stress in Fig. 51-7b, the equilibrium is neutral in the h'-direction. Finally, at the highest stress, Fig. 51-7c, the critical configuration is in unstable equilibrium with respect to both h' and $\mathscr{L}'$ (but of course in stable equilibrium with respect to all other internal parameters). Thus, the phrase "saddle point" for the critical configuration may sometimes be misleading.

The result is especially simple when the kink interaction energy (the last term in eq. [51n']) is neglected. Then $\Delta G'_{\text{NUCL}}$ depends on $\mathscr{L}'$ only linearly through the first term. The differentiation according to [51o] requires that the Peierls free enthalpy of the advanced dislocation piece be zero: when the separation of the kinks is increased, the work done is just enough to provide the increased line energy of the advanced dislocation piece. The free enthalpy of nucleation ΔG_{NUCL} is then merely the energy of the two kinks:

$$\boxed{\begin{aligned} \Delta \mathscr{G}_{\text{DIS}} &= 0 \rightarrow h(\sigma) \\ \Delta G_{\text{NUCL}} &= 2F_{\text{KINK}}(h) \end{aligned}} \qquad \textit{(neglecting kink interaction).} \qquad \begin{matrix}[51p] \\ [51p']\end{matrix}$$

Equation [51p] specifies that the position of the advanced piece of dislocation is at C in Fig. 51-6a. This may, at first sight, seem surprising, since here this dislocation is not in equilibrium with respect to forward displacements (as it would be at A or B). But performing the differentiation [51o'] on eq. [51n'] shows that indeed there must be a forward force on the advanced dislocation to balance the "kink tension" at both ends:

$$\mathscr{L} b(\sigma - \tau_{\text{ELEM}}) = 2\left(\frac{\mathrm{d}F_{\text{KINK}}}{\mathrm{d}h}\right) \qquad [51q]$$

This equation determines the critical value of $\mathscr{L}$. It is large for both high and low stresses, and smallest for intermediate stresses, as may be seen in Figs. 51-7 for the sinusoidal potential. (Actually, in this figure, the kink interaction was not neglected, but its effect on $\mathscr{L}$ (as on ΔG_{NUCL}) is minor compared to that expressed in eq. [51q].)

Figure 51-8 shows the critical configurations derived for three stresses under the same conditions that were used to derive Figs. 51-7. The width of the kinks was arbitrarily set to $w = 5\lambda$. These shapes should be compared to the bulges

in Fig. 51-5 (although, for clarity, the scales are different). They have an important feature in common: the maximum excursion to where $\Delta\mathscr{G}_{\text{DIS}}=0$ is the same in the two figures. Clearly, the detailed assumptions concerning the line energy are not too important. In the kink model, the advanced piece of dislocation is treated as rigid, held back by the pull of the kinks at the ends; in the bulge model, it is treated as flexible, so that, to be in equilibrium, it must everywhere acquire a backward curvature; but these detailed differences apart—the two models lead to similar critical geometries.

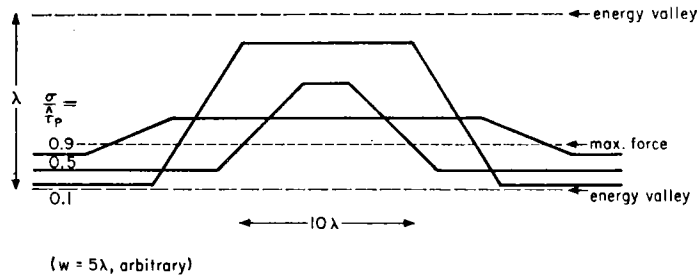

FIG. 51-8. Critical configurations in the discrete kink model (arbitrarily setting $w = 5\lambda$) for three stresses, using a sinusoidal Peierls potential (as for Fig. 51-7).

The height h of the kinks in the critical configuration follows from eq. [51p] —though, of course, it depends on the shape assumed for the Peierls potential. The anti-parabolic potential [51b] is especially easy mathematically, in part because $y_0 = 0$ at all stress. It follows immediately that

$$\frac{h}{\lambda} = 1 - \frac{\sigma}{\hat{\tau}_P}. \qquad [51r]$$

For the sinusoidal potential [51a], one must first determine $y_0(\sigma)$ from

$$b\sigma = b\tau_{\text{DIS}}(y_0) = \frac{\mathrm{d}\Delta\mathscr{F}_{\text{DIS}}}{\mathrm{d}y}. \qquad [51s]$$

Inserting this into [51g″] and applying [51p] gives for $h(\sigma)$ the transcendental equation

$$\frac{1}{2\pi}\left\{\sqrt{1-\left(\frac{\sigma}{\hat{\tau}_P}\right)^2} - \cos\left(2\pi\frac{h}{\lambda} + \arcsin\frac{\sigma}{\hat{\tau}_P}\right)\right\} - \frac{\sigma}{\hat{\tau}_P}\frac{h}{\lambda} = 0. \qquad [51s']$$

A numerical solution of this equation for h/λ differs, over the entire range, by less than 2% from the equation

$$\frac{h}{\lambda} = \sqrt{1-\sqrt{\frac{\sigma}{\hat{\tau}_P}}} \qquad [51s'']$$

which is an adequate approximation for further calculation.

The value of h from [51r] or [51s″] must now be inserted into the kink energy to obtain the activation energy for nucleation according to [51p′]. Here lies the major difficulty of the kink model: the dependence of F_{KINK} on h. We have seen in [51e] that a model based purely on the elastic interaction between kinks gives $F_{\text{KINK}} \propto h^{3/2}$, with a very crude assumption concerning the core energy, which contributes about half of the total energy in the case of kinks. More sophisticated calculations of the core term are based on the self-stress model (where a double kink is a bulge) and are inappropriate in the present treatment. If the core energy—which is presumably proportional to h—were known, one would have to add to it the elastic free energy, which is proportional to h^2 (as can be seen by integrating eq. [51d] between distance rather than stress limits).

Lacking anything better, we shall use, from eqs. [51e] and [51c″],

$$2F_{\text{KINK}} \simeq \frac{\mu b^3}{10}\left(\frac{h}{\lambda}\right)^{3/2}. \qquad [51t]$$

This leads to a kink pair nucleation energy of

$$\Delta G_{\text{NUCL}} = \frac{\mu b^3}{10}\left(1 - \frac{\sigma}{\hat{\tau}_{\text{P}}}\right)^{3/2} \qquad [51u]$$

for the anti-parabolic potential (eqs. [51b], [51r]), and

$$\Delta G_{\text{NUCL}} = \frac{\mu b^3}{10}\left[1 - \left(\frac{\sigma}{\hat{\tau}_{\text{P}}}\right)^{1/2}\right]^{3/4} \qquad [51u']$$

for the sinusoidal potential (eqs. [51a], [51s], [51s″]). These relations are plotted in Fig. 51-9 a and b, together with the previous results from the bulge model. It is seen that the differences are relatively minor. Whether the positive curvature of the solution for the sinusoidal potential near $\sigma \simeq \hat{\tau}$ is meaningful may be doubted in view of the uncertainties connected with eq. [51t].

Figure 51-9b contains one extra curve (dashed), which was calculated numerically by including the kink interaction energy in [51n′]. The difference is slight; and the behavior near $\sigma \simeq 0$ is as demanded by eq. [51d′]. The equation for the nucleation energy, in this complete model, is worth noting:

$$\boxed{\Delta G_{\text{NUCL}} = 2F_{\text{KINK}} - 2F^{\text{INT}}_{\text{KINKS}}.} \qquad [51p'']$$

It comes about because of the particular form of the interaction energy as shown in the last term of eq. [51n′]: the differentiation with respect to $\mathscr{L}'$ according to [51o] then gives

$$\Delta \mathscr{G}_{\text{DIS}} = -F^{\text{INT}}_{\text{KINKS}}$$

in place of [51p]. The critical position of the advance dislocation piece is somewhat to the right of C in Fig. 51-6, and the value of h is somewhat larger, than when the kink interaction was neglected.

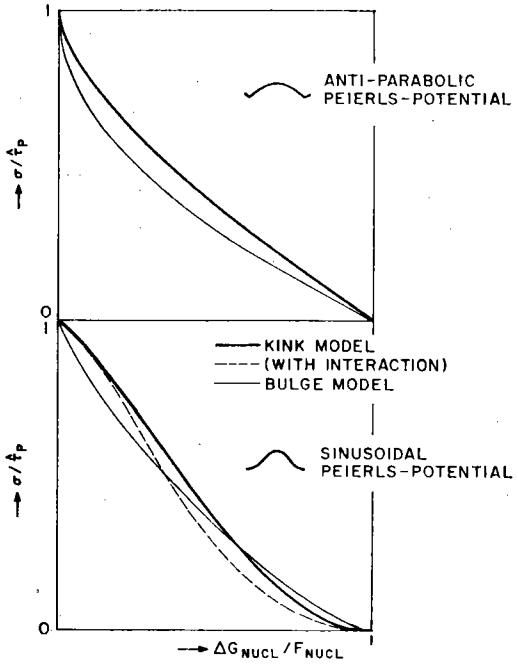

FIG. 51-9. Stress versus activation energy for (a) anti-parabolic, and (b) sinusoidal potential, in the kink (——) and bulge (——) models. The effect of elastic interaction between kinks is shown for the sinusoidal potential (- - -).

The Nucleation Rate

In the preceding sections, the activation energy ΔG_{NUCL} for nucleation over a linear barrier was derived in two different models for two different Peierls potentials that we consider to be limiting cases. Though based on different premises, the results were very similar: the stress dependence of ΔG_{NUCL}, for instance (Fig. 51-9 a and b), is similar in all cases. Figure 51-10 summarizes the range of reasonable relations as a shaded area. It also singles out a central curve that may be regarded as a good phenomenological description:

$$\Delta G_{\text{NUCL}} = F_{\text{NUCL}} \left[1 - \left(\frac{\sigma}{\hat{\tau}_P} \right)^{3/4} \right]^{4/3}. \qquad [51v]$$

For the upper and lower envelope of the shaded area, the same general relation (eq. [43w]) was used, with the inner exponent p and the outer exponent q being $\frac{3}{4}$ and 1, respectively, for the upper envelope, $\frac{2}{3}$ and $\frac{3}{2}$ for the lower envelope. (Only the relation [51k″] lies slightly outside the lower envelope at high stresses.) The total activation energy is in all cases (eqs. [51e],

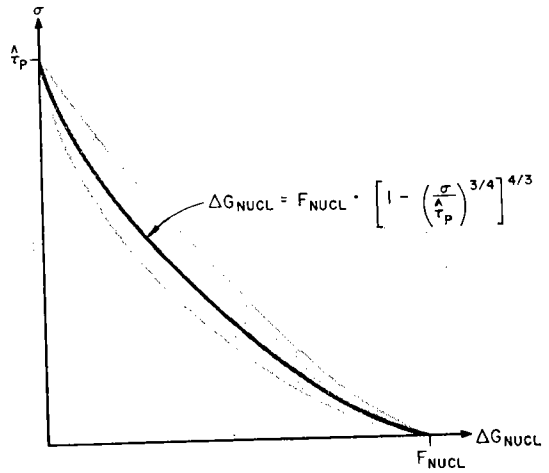

FIG. 51-10. The range of reasonable relations for the activation energy $\Delta G_{NUCL}(\sigma)$ of nucleation over a Peierls barrier, and a central phenomenological relation (eq. [51q]). With one exception, all published models (as reviewed by GUYOT and DORN, 1967) fall within the shaded band; the exception is that of SEEGER (1956), which lies off this diagram to the right.

[51ℓ], [51ℓ']) close to

$$F_{NUCL} \simeq \frac{\mu b^3}{2}\sqrt{\frac{\hat{\tau}_P}{\mu}}. \qquad [51v']$$

To calculate a nucleation *rate* one needs, in addition, a frequency factor. It may have one of two extreme forms: the first relates to the frequency ν_{NUCL} with which a straight dislocation "attempts" nucleation; the second is determined by a resistance to *motion* of the kinks across the (rather shallow) "saddle-point" area. The following paragraphs describe these two limiting cases in more detail, and discuss their dependence on stress, temperature, and structure.

First, consider the "attempt frequency", ν_{NUCL}, of a straight dislocation segment. In calculating the critical geometry, it was found that the length $\mathscr{L}$ of the critical segment was always large compared to the atom size ($\geq 10b$). So it is not unreasonable to use the vibration frequency of an infinitely long dislocation in front of a linear barrier, corrected for the possibility of coupled lateral translation rather than spreading of the resulting double kink, as it was derived in eq. [42v]:

$$\nu_{NUCL} = \frac{\omega_{ATOM}}{\pi\sqrt{2\pi}}\sqrt{\frac{2U_{KINK}}{kT}}\cdot\left[\frac{d(\tau_{ELEM}/\mu')}{d(y/b)}\right]_{y=y_0}. \qquad [51w]$$

For the internal energy $2U_{KINK}$ of the double kink (which enters because of

its mass) we may substitute its free energy $2F_{\text{KINK}}$ (which does not contain any configurational entropy terms). For a double kink of the correct height in the critical configuration (eq. [51p']), this is just $\Delta G_{\text{NUCL}}(\sigma)$.

The last factor in eq. [51w] is the normalized stiffness of the Peierls potential for the unactivated dislocation at $y = y_o$. For an order-of-magnitude estimate, we may set it equal to the initial stiffness in the sinusoidal potential, (eqs. [51a], [51f]), $(\hat{\tau}_p/\mu')\cdot(2\pi b/\lambda)$, which should be good up to $\sigma \simeq \hat{\tau}_p/2$. Then eq. [51w] becomes

$$\nu_{\text{NUCL}} \simeq \omega_{\text{ATOM}} \sqrt{\frac{\Delta G_{\text{NUCL}}}{kT}} \cdot \frac{\hat{\tau}_p}{\mu} \qquad [51w']$$

The activation energy ΔG_{NUCL} for kink nucleation under stress is of the general order of $30kT$ in the range where this nucleation is of interest for most macroscopic applications (eq. [51ii]). For Peierls stresses of the order of $\mu/100$, ν_{NUCL} is thus between 10^{10} and 10^{11} s^{-1}, approximately.

The frequency factor [51w] depends, in principle, on the instantaneous applied stress σ, because with increasing stress both the stiffness and the activation free enthalpy ΔG_{NUCL} become smaller. For the sinusoidal potential, the effect of both can be combined; the result of plotting this out is an approximately linear dependence of ν_{NUCL} on σ (eqs. [51a,] [51f,] and [51g] combined with eq. [51w']):

$$\nu_{\text{NUCL}} \simeq \omega_A \sqrt{\frac{\mu b^3}{kT}} \left(\frac{\hat{\tau}_p}{\mu}\right)^{5/4} \cdot \left(1 - \frac{\sigma}{\hat{\tau}_p}\right). \qquad [51w'']$$

If this frequency factor controls the activation kinetics, the rate of nucleation at any particular site becomes

$$P_t = \nu_{\text{NUCL}} \cdot \exp - \frac{\Delta G_{\text{NUCL}}}{kT}. \qquad [51x]$$

Note that a correction for "reverse jumps" is not applicable to this formula: there is no stable equilibrium configuration after nucleation, from which such a nucleation against the applied stress could take place. (See, for example, Fig. 51-7.)

When kinks move slowly, a different frequency becomes important. Reverse jumps of a sort may take place from the "saddle-point" area if the kink is not rapidly removed from there. This is particularly evident when there are subsidiary energy ripples over which moving kinks must propagate (Fig. 51-11): when the ripple spacing x is less than the width of the saddle point (which is of the order of the length $\mathscr{L}$ of the critical configuration) then these barriers to motion influence nucleation. Closely spaced (weak) solute atoms, will produce such an energy ripple; so, too, will a "second-order Peierls stress"—a periodic variation in the core energy of kinks. One must keep in

mind, however, that the finite width of kinks tends to average over variations of a smaller wavelength.

The net forward motion over small-scale variations such as the ripple shown in Fig. 51-11 can be described (in the manner of eq. [45j]) by an average kink velocity

$$v_{\text{KINK}} = x\nu_{\text{D}} \cdot \frac{\sigma b \lambda x}{kT} \cdot \exp - \frac{\Delta G_{\text{PROP}}}{kT} \qquad [51y]$$

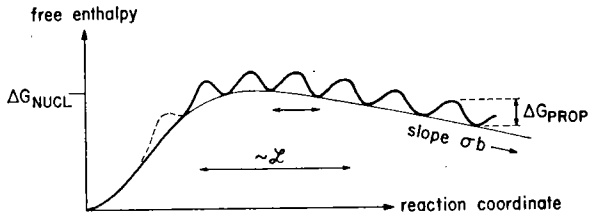

FIG. 51-11. Double kink nucleation when there are obstacles to kink propagation whose spacing x is smaller than the length $\mathscr{L}$ of the critical configuration.

where we have assumed that the attempt frequency for kink motion is the Debye frequency ν_{D}. The effective frequency factor for nucleation then becomes the reciprocal of the time it takes for the kink to traverse the "saddle-point area" at that velocity, in the picture used by GLASSTONE *et al.* (1941) in their derivation of "Absolute Rate Theory":

$$P_{\text{t}} = \frac{v_{\text{KINK}}}{\mathscr{L}} \exp - \frac{\Delta G_{\text{NUCL}}}{kT} \qquad [51z]$$

or, introducing a proportionality factor β of order 1,

$$P_{\text{t}} = \beta \frac{\sigma}{\mu} \cdot \frac{\mu b^3}{kT} \cdot \omega_{\text{A}} \exp - \frac{\Delta G_{\text{NUCL}} + \Delta G_{\text{PROP}}}{kT}. \qquad [51z']$$

This equation may formally apply even when $\Delta G_{\text{PROP}} = 0$ and the kink velocity is controlled by a drag mechanism linear in σ, such as phonon drag (eq. [31r]). In that case, one no longer has a succession of equilibrium states, and the derivation of eq. [51z'] is based on the diffusion theory of nucleation, or on the incorporation of the "Zeldovich factor" (HIRTH and LOTHE, 1968).

Equation [51z'] replaces eq. [51x] when it leads to a lower value of P_{t}. Comparison of eqs. [51z'] and [51w'] shows that this can happen for $\Delta G_{\text{PROP}} = 0$ only when $\sigma \lesssim \hat{\tau}_{\text{P}}/100$, in order of magnitude. But when ΔG_{PROP} is at least a few kT, eq. [51z'] should almost always be relevant.

Steady State of Free Slow Kinks

If a kink, once nucleated, is not impeded by any obstacles other than the drags or quasi-drags described above, it will ultimately collide with a second

kink of opposite sign. Assuming the inertial effects of sec. 31 are absent, the kinks annihilate each other. The mean free path of a kink, Λ, is then determined by a steady-state balance between nucleation time and travel time:

$$\frac{1}{(2\Lambda/b)P_t} = \frac{\Lambda}{v_{KINK}}. \qquad [51aa]$$

Here, the factor $2\Lambda/b$ on the left-hand side describes the number of sites for nucleation along a piece of dislocation of length 2Λ. (b appears in the denominator because the nucleation frequency was arbitrarily chosen in eq. [42v] to refer to a length b of dislocation).

Solution of eq. [51aa] for 2Λ, with [51z] for P_t gives

$$\Lambda \simeq b \exp \frac{\Delta G_{NUCL}}{2kT}. \qquad [51bb]$$

It is the steady-state spacing of individual kinks at the stress σ. For all interesting values of ΔG_{NUCL} ($\Delta G_{NUCL} > 15kT$) its magnitude is in excess of $10^4 b$. Most real materials contain structural obstacles (dislocations, precipitates, etc.) which are more closely spaced than this—so it is these obstacles, not the steady-state kink population, that determine the mean free path of a kink; this we treat in the next section. But in very "clean" materials, where 2Λ in eq. [51bb] might be smaller than the spacing of structural obstacles, the average dislocation velocity follows directly from eqs. [51y] and [51bb] ($\beta' \simeq 1$):

$$v_{DIS} = \frac{\lambda}{\Lambda} v_{KINK} = \beta' v_S \frac{\sigma b^3}{kT} \exp - \frac{\frac{1}{2}\Delta G_{NUCL} + \Delta G_{PROP}}{kT} \qquad [51cc]$$

—a typical drift velocity of individual kinks. It leads to velocities consistent with $v_{KINK} \lesssim 10^{-3} v_S$ (no inertial effects) only when ΔG_{PROP} is substantial.

For such quasi-viscous motion, the macroscopic strain rate follows by multiplying eq. [51cc] by b times the mobile dislocation density ρ_m. In the absence of other obstacles, ρ_m may be influenced by the elastic interaction between mobile dislocations as described in sec. 32. Under certain conditions, this can bring additional σ^2—dependence into the pre-exponential factor $\dot{\gamma}_o$.

Strong Obstacles to Kink Motion

We have pointed out that the mean free path of kinks on infinitely long dislocations is generally in excess of $10^4 b$. Yet free dislocation segments of such lengths are not usually available because of the presence of other obstacles that are too strong and too sparse to be smoothed out into a quasi-drag. The prototype of a strong obstacle to kink motion is a node in the dislocation network; but internal stresses, precipitates, or especially strong (interstitial) solute atoms could be equally effective.

A kink will be stopped at such an obstacle; the calculation of the dislocation velocity then becomes a problem in the superposition of two strengthening mechanisms (CELLI *et al.*, 1963; RYBIN and ORLOV, 1970). As further kinks sweep in from either side of the obstacle, a "kink pile-up" forms. As the number of kinks grows, the geometry of their distribution, as well as their stress field, become identical to the effects during the bowing-out of a smooth dislocation between the obstacles. Thus, the dislocation curvature stress must be subtracted from the applied stress in the activation energy for nucleation on such a segment. Conversely, when the double-headed kink pile-up exerts sufficient force on the obstacle—or, equivalently, when the cusp angle at the obstacle due to dislocation bow-out has reached the critical value given by the obstacle strength—the obstacle breaks and a large number of kinks of opposite sign can annihilate rapidly. The area swept out by the dislocation is then essentially that prescribed by the obstacle distribution.

The nucleation time for the first kinks (when the back stress is still small) is trivial compared to that for the last critical kink (when the back stress is a maximum). So one may write the macroscopic strain-rate in the form

$$\dot{\gamma} = b \cdot a_{\mathrm{OBS}} \cdot \dot{N}_{\mathrm{NUCL}} \qquad [51dd]$$

where $\dot{N}_{\mathrm{NUCL}}$, the nucleation rate per unit volume, is evaluated at $(\sigma - \tau^{\mathrm{OBS}}_{\mathrm{PLANE}})$, and a_{OBS} is the average slip plane area per obstacle. In addition to P_t, which was derived earlier, it contains the number of available sites for nucleation. This is equal to the number of mobile dislocation segments per unit volume, N_m, times the number of nucleation sites per segment, l/b (l = segment length). Thus we have

$$\dot{N}_{\mathrm{NUCL}} = N_m \cdot \frac{l}{b} \cdot P_t. \qquad [51ee]$$

The product of the mobile segment density N_m in eq. [51ee] and the area a_{OBS} in eq. [51dd] must together be equal to the reciprocal of the slip plane spacing d, for long-range slip (KOCKS, 1970b, see sec. 33). The slip plane spacing, in turn is proportional to l, when it is demanded that mobile dislocations on parallel slip planes can just pass each other at the flow stress (eq. [33cc]. Thus the various dependences on l in eq. [51dd] just cancel each other and we have, in order of magnitude,

$$\dot{\gamma} \simeq P_t \qquad [51ff]$$

as it was given in eq. [51x] or [51z′], with an "effective stress" $(\sigma - \tau^{\mathrm{OBS}}_{\mathrm{PLANE}})$ inserted instead of the applied stress σ.

This formula should hold even when the overcoming of the obstacles can also be aided by thermal fluctuations since, by virtue of the arguments presented in eqs. [44v] through [44y′], the waiting time in the critical configuration should be the same for both mechanisms (though the neglect of the bow-out time in eq. [51w] may be more serious here). Observation of the total

effective activation area as the obstacle density is varied, in a diagram of the kind shown in Fig. 44-13, would then help separate the two contributions.

In this model, we have assumed explicitly that the obstacles are far enough apart not to interfere with the nucleation mechanism. The length of the critical configuration can, however, be quite large both at very high stresses and at very low stresses. Then, the critical shape is influenced by the finite available length. The forward piece of dislocation may even advance as far as the next equivalent stable equilibrium position and then a second bulge may already be part of the critical configuration. This class of problems, discussed most recently by ONO and SOMMER (1970) will not be treated here.

Macroscopic Characteristics of a Lattice Resistance

We now summarize the model results in terms of the phenomenological Arrhenius relation

$$\dot{\gamma} = \dot{\gamma}_o \exp - \frac{\Delta G}{kT}.$$

Realistically, structural obstacles almost always limit the travel of a kink. (Only in the purest and most perfect crystals is the obstacle spacing greater than the mean free path of a kink.) Accordingly, we adopt eq. [51ff] with the nucleation rate given either by [51z′] or [51x] and [51w′]. In these cases, we have in order of magnitude

$$\dot{\gamma}_o \simeq \omega_A \cdot \frac{\hat{\tau}_P}{\mu} \quad \text{or} \quad \dot{\gamma}_o \simeq \omega_A \cdot \frac{\sigma b^3}{kT}. \qquad [51gg]$$

Either way, the preexponential factor has unusually large values for interesting stress ranges:

$$\dot{\gamma}_o \gtrsim 10^{10}\ \mathrm{s}^{-1} \qquad [51hh]$$

so that for a typical strain rate of $10^{-4}\ \mathrm{s}^{-1}$,

$$\boxed{\ln (\dot{\gamma}_o/\dot{\gamma}) \gtrsim 30.} \qquad [51ii]$$

Only in the case of slow free kinks, where eq. [51cc] holds, would $\dot{\gamma}_o$ be smaller; its order of magnitude would be as in [51gg], multiplied by $b^2\rho_m$. The term $\ln (\dot{\gamma}_o/\dot{\gamma})$ is then about 20 as in most other mechanisms.

If the activation energy is primarily determined by nucleation (eqs. [51ff] [51x], [51w′])—as it is when kink travel is obstacle limited—its value at zero stress is approximately (eq. [51v′])

$$\boxed{F_o = F_{NUCL} \simeq \frac{\mu b^3}{2} \sqrt{\frac{\hat{\tau}_P}{\mu}}.} \qquad [51jj]$$

To this may have to be added any total activation energy of motion (in case eq. [51z'] applies). For free slow kinks, F_o would be half the value in [51jj] but in that case, a substantial activation energy of motion must exist. We shall use eq. [51jj] for a general estimate of the lattice resistance mechanism. Since (eq. [51c]) the maximum Peierls stress must certainly be less than $\mu/20$, we have

$$F_o \lesssim \frac{\mu b^3}{10}. \qquad [51kk]$$

If one inserted, as a general average for metals (Table 2-I), $\mu b^3 \simeq 5$ eV, one would obtain, with eq. [51ii],

$$T_o \equiv \frac{F_o}{k \ln (\dot{\gamma}_o/\dot{\gamma})} \lesssim 200 \text{ K}. \qquad [51\ell\ell]$$

Furthermore, $\hat{\tau}_p$ is usually substantially less than $\mu/20$, so that, "in the average", the lattice resistance provides at best a very low-temperature mechanism.

On the other hand, the lattice resistance contributes in an important way to the flow stress of materials with highly covalent binding character. For these materials, $\hat{\tau}_P$ may approach $\mu/10$ and, in addition, μb^3 is often much larger (Table 2-I): for diamond, for example, $\mu b^3 \simeq 56$ eV and thus $T_o \simeq 3500$ K.

The *apparent activation area* for nucleation is plotted in Fig. 51-12, for our average phenomenological relation [51v] and for two extreme relations, including the rather unrealistic one of bulge nucleation over an anti-parabolic potential. It is not likely that they could be clearly distinguished experimentally. The general order of magnitude can be estimated by setting

$$\boxed{\Delta a' \equiv -\frac{\partial \Delta G}{b \partial \sigma} \approx \frac{F_o}{b\hat{\tau}_P} \simeq \frac{b^2}{2} \cdot \sqrt{\frac{\mu}{\hat{\tau}_P}}.} \qquad [51mm]$$

It is normally of order $10b^2$. The stress dependence of any activation energy of motion should be negligible by comparison.

The *relative* stress sensitivity of the nucleation energy is, when there are other obstacles (eq. [51ff]),

$$m_G \equiv \frac{b\Delta a'}{kT} \cdot (\sigma - \tau_{\text{PLANE}}^{\text{OBS}}). \qquad [51nn]$$

In a typical experiment, the temperature and the stress are not independently prescribed. Let us express the "effective stress" term above in terms of ΔG (eq. [51v], or more generally eq. [43w'']), which then relates to temperature and strain rate by the Arrhenius law. This gives

$$\boxed{m_G = p \cdot q \cdot \left[\left(\frac{T_o}{T}\right)^{1/q} - 1\right] \cdot \ln (\dot{\gamma}_o/\dot{\gamma}).} \qquad [51oo]$$

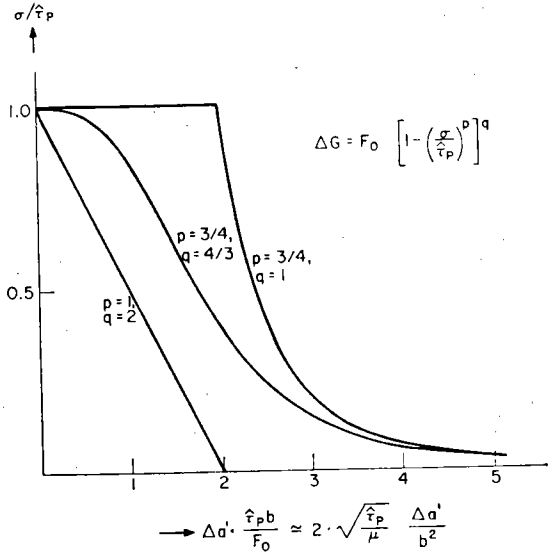

FIG. 51-12. Apparent activation area $\Delta a' \equiv -\partial \Delta G / b \partial \sigma$, against stress, suitably normalized, for "average" ($p = \frac{3}{4}$, $q = \frac{4}{3}$) and limiting forms of the activation energy $\Delta G(\sigma)$ of "double-kink" nucleation.

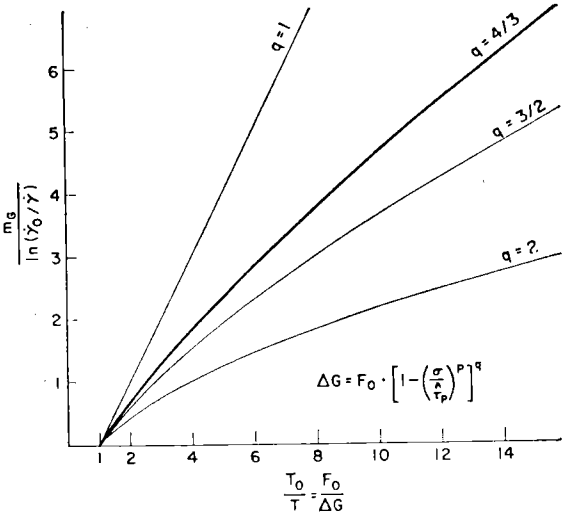

FIG. 51-13. The relative inverse rate sensitivity of the flow stress, m, at constant strain rate, as a function of reciprocal temperature. The values of q refer to the outer exponent in the phenomenological expression for $\Delta G(\sigma)$; the inner exponent p was chosen as 1/q. All curves for $q > 1$ may be mistaken for straight lines through the origin over a substantial range of temperatures.

This relation is plotted in Fig. 51-13, for various values of q and for $p = 1/q$. An interesting conclusion from this figure is that, over a substantial range of temperatures, the curves may be mistaken for straight lines through the origin—which, if it were exactly true, would imply a logarithmic dependence $\Delta G(\sigma)$. Such a dependence had been predicted in the least realistic of all Peierls stress theories (SEEGER, 1956; see, for example, GUYOT and DORN, 1967), and had been "confirmed" experimentally by PREKEL *et al.* (1968) (see KOCKS, 1970c). We see that such a plot is not a sensitive test of any particular theory.

With respect to the order of magnitude, we see that $m_G \gtrsim 10$ at $T \leqslant T_o$. In the higher temperature range, it becomes important to include any stress dependence from $\dot{\gamma}_o$. This appears when a (quasi-)drag acts on the motion of kinks, or when the density of mobile dislocations is only determined by their own interaction. All effects together can at most lead to a contribution of 3 to m from the preexponential. In terms of the curves in Fig. 51-13, this corresponds to any upward displacement by at most 0.1 (eq. [51ii]).

Summarizing, the characteristic orders of magnitude for a lattice resistance mechanism are: a low activation energy of about $\mu b^3/10$, an apparent activation area of order $10b^2$, an m-value of order 10, and possibly a high $\dot{\gamma}_o$-value (in excess of 10^{10} s^{-1}). None of the functional relations of these parameters on stress are characteristic enough to discriminate between different reasonable detail assumptions in the model—or, for that matter, to distinguish the lattice resistance from any other "short-range" flow stress mechanism.

52. PARTICLE RESISTANCE

As a prototype of discrete obstacles to dislocation motion, we treat here particles of a second phase coherently embedded into the lattice of an otherwise pure crystal. There are many physical mechanisms by which such precipitates resist the motion of dislocations. In many cases several mechanisms are operative simultaneously. A meaningful theory of precipitation hardening must, therefore, cope with the problem of superposition, which is non-trivial except in very special cases of "point" obstacles. The distinction between the element, line, and plane glide resistance introduced in Chapter 2 provides a sound basis for dealing with this problem.

Some mechanisms of interaction between precipitates and dislocations extend beyond the physical limits of the particle. At high concentrations, the precipitates may then interact with the dislocation cooperatively rather than individually; i.e. the obstacles are not truly "discrete". Such problems require dealing with more complex motions of a dislocation discussed briefly in sec. 25.

In order to demonstrate the method, we shall treat a specific case, using precipitates of an idealized geometry and with somewhat idealized interactions. In any real case, one must judge how closely these idealizations

correspond to reality, or modify the method outlined here to account for the differences.

The geometry to be considered consists of particles that intersect the slip plane in circles of diameter w. This diameter and all other properties as they are experienced *in the slip plane* are assumed to be identical for each particle. Particles whose *three-dimensional* properties are identical would, of course, exhibit a *spectrum* of properties in the slip plane. We idealize such a spectrum by a distribution of uniform "average" or "effective" particles. The remaining statistics would change the numerical constants of the results, but not their form (FRANK, 1968; FRANK *et al.*, 1968; FOREMAN and MAKIN, 1967; HIRTH, 1970; BROWN and HAM, 1971).

The spatial distribution of particles in the slip plane is assumed random: this is the only nonregular dispersion that has been described sufficiently well. We also neglect corrections necessary when the average spacing l is not large compared to the size w; they were given in sec. 25 for non-interacting particles.

For the interactions, we assume that macroscopic concepts such as line energy, interface energy, etc., are applicable even for rather small precipitates. In fact, at the end of this section, we shall discuss the common extrapolation of some of the precipitation hardening mechanisms to the interaction of dislocations with individual solute atoms in dilute solution. It is in this range of very small obstacles that the effects of thermal activation we derive become of special importance, but also where the use of macroscopic concepts is most questionable.

The treatment below follows the scheme proposed in Chapter 2. We will deal, in sequence, with the terms in the equation

$$\delta G = \delta F_{\text{ELEM}} + \delta F_{\text{DIS}} - \delta W.$$

First, we discuss the interaction energy δF_{ELEM} between particle and dislocation, then the changes δF_{DIS} in the free energy of the dislocation as it changes its shape and the work δW done by the external forces.

Mechanisms of Local Interaction

Among the many important interactions between dislocations and precipitates, we select a few that represent a variety of types: some are attractive, some repulsive, some energy-storing; some act throughout the particle, some only at the particle-matrix interface; some extend beyond the physical dimensions of the particle—but, in the range of concentrations in which the discreteness criterion is satisfied, we shall treat them all as if they were strictly localized.

Figure 52-1 illustrates the effect of a uniform element glide resistance inside the particle, and none outside. This could be due, for example, to a *friction stress*

$$\tau_{\text{ELEM}} = \hat{\tau}_{\text{FRIC}} \qquad [52a]$$

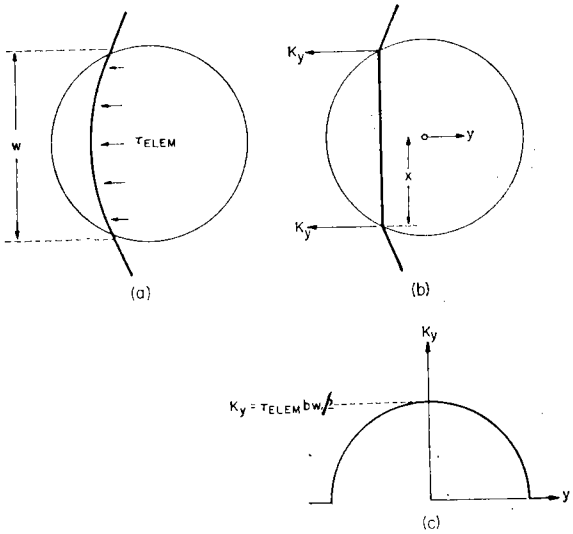

FIG. 52-1. Uniform resistance to dislocation glide inside the particle (a). It may be represented (b) by a force K_y at each interface, which is proportional to the length x (c). An example of such interactions is the generation of anti-phase boundary inside a precipitate where $\tau_{ELEM} = \chi_{APB}/b$.

or to the creation of *anti-phase boundary* (of specific free energy χ_{APB}) in an ordered precipitate:

$$\tau_{ELEM} b = \chi_{APB}. \qquad [52b]$$

The glide resistance on each element of dislocation in the particle can be integrated from the center to either side to give two equivalent point forces resisting motion in the y-direction (eq. [25a], Fig. 52-1b), each of magnitude

$$K_y = \bar{\tau}_{ELEM} b x. \qquad [52c]$$

It is plotted as a function of the forward displacement in Fig. 52-1c. In fact, the piece of dislocation inside the particle may be forced to be straight for physical reasons, so that the representation by a force K_y at each end (Fig. 52-1b) would be closer to the actual mechanism than the representation by a constant τ_{ELEM}.

Many coherent precipitates are surrounded by *misfit stresses*, which are proportional to the relative difference $|\epsilon|$ in lattice constants of matrix and precipitate in the unstrained condition. These internal stresses form an element glide resistance that varies rapidly both with forward displacement of the dislocation and also along the length of the dislocation at a particular position. Here we consider well-separated spherical precipitates with a volume misfit only. (The problem of overlap of their stress fields is discussed in sec. 25.) For such isolated precipitates, the element resistance is zero inside the particle and highest along the interface.

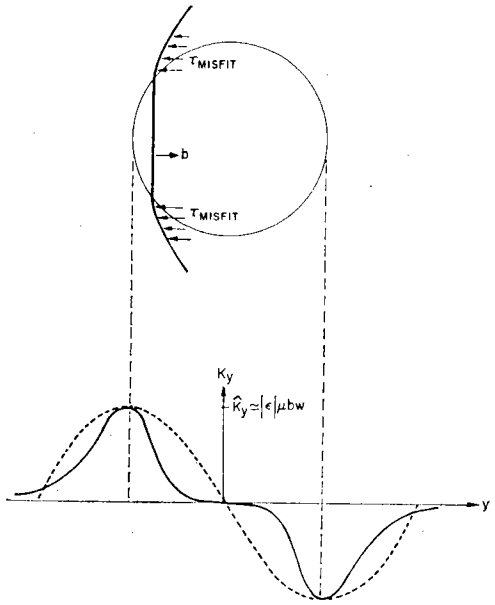

FIG. 52-2. The interaction of misfit stresses with an edge dislocation. The distributed glide resistance at either side of the precipitate may be represented by a point force K_y at each interface; but since the interaction begins before the dislocation has reached the particle, and extends beyond the point of exit, the precipitate must be thought of as having a larger effective diameter, e.g. $2w$. The force distance relation shown is qualitative and is schematically replaced by a sine curve (dotted) for future use.

One may again represent this distributed glide resistance by point forces K_y at each dislocation-interface intersection. For edge dislocations, their dependence on the forward displacement y must be qualitatively as shown in Fig. 52-2, except that for half the particles it will be attractive rather than repulsive as shown. (This depends on whether the particle center lies "above" or "below" the slip plane. The *magnitude* of K_y also depends critically on the spacing between particle center and slip plane.) Proper averaging over these "vertical" distances is a difficult problem (GEROLD and HABERKORN, 1966; BROWN and HAM, 1971). For the average maximum force one gets within a factor 2 or so:

$$\hat{K}_y \simeq |\epsilon|\mu bw \qquad (edge). \tag{52d}$$

It applies only to edge dislocations; the resistance to screw motion is less.

Next we consider a difference between the line energy of the dislocation inside and outside the precipitate. In the simplest case, this could be due to a change in *core energy*. In some instances, this is easily calculated. In a void or bubble, the core energy disappears completely, giving a maximum drop in energy of $w\mathcal{F}_{\text{CORE}}$ (where $\mathcal{F}_{\text{CORE}}$ is the specific free energy of the core). In general, the change of core energy reflects the different shapes of the *atomic*

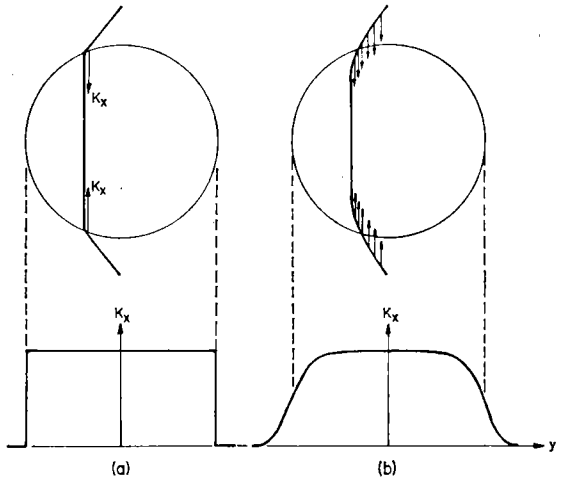

FIG. 52-3. A difference in dislocation line energy in particle and matrix: (a) due to a difference in core energies, (b) due to a difference in elastic constants (schematic). The force K_x describes only the line energy *difference*. The configuration shown corresponds to a higher line energy inside the particle.

force-distance curves for the atoms inside and outside the precipitate, and thus is related not only to the usual (2nd order) elastic constants, but to those of higher order also, since these describe the shape of the interatomic potential at the large displacements which exist in the core. An oxide, carbide or nitride particle, for instance, could have the same (2nd order) shear modulus as the metal matrix in which it was imbedded, yet possess higher order constants which differ completely from the matrix. This would lead to a very large change of core energy. For this reason, the passage of the dislocation through the precipitate is resisted.

Another reason for differences in line energy inside and outside the precipitate could be a *difference in stacking-fault energies*; the copper–cobalt system is an example.

The most important difference in line energy inside and outside the precipitate comes from a *difference in elastic constants* (of the usual "second order"). This is a nonlocal effect, since the strain energy of a dislocation is influenced by elastic heterogeneities even when it does not intersect them. Again, we idealize this effect to an abrupt change of line energy at the interface (RUSSELL and BROWN, 1972).

Figure 52-3a shows the geometry for all cases describable by such an abrupt change. One may express the effect by saying that there is a piece of dislocation of length $2x$ inside the particle whose free energy per unit length equals the *difference* $\Delta\mathscr{F}_{\text{DIS}}$ between that of the actual dislocation lying in the precipitate and one that would have matrix properties. When the dislocation is displaced forward by δy, its length changes by δx at each interface; the free

energy of the specimen thus changes by

$$\delta F = \Delta \mathscr{F}_{\text{DIS}}\, \delta x \qquad [52e]$$

at each interface. It is appropriate, then, to introduce a force

$$K_x = \Delta \mathscr{F}_{\text{DIS}} \qquad [52e']$$

acting on the dislocation at the interface in the direction along the dislocation in the particle (i.e. in the negative x-direction). This is in fact a "line tension" on this point. Obviously, it acts in a different direction than the retarding force K_y used before; nevertheless, it provides a resistance to forward motion, which we shall derive below.

In the core energy case, K_x is independent of how far the dislocation has advanced into the particle (Fig. 52-3a). When the difference in line energy is due to a difference in elastic constants, both the dislocation shape and the force–distance diagram vary more smoothly, which is qualitatively shown in Fig. 52-3b. The average, which we shall use, must be approximately given by

$$K_x \simeq \Delta\mu b^2 \frac{\ln(x/r_o)}{4\pi} \qquad [52e'']$$

for a screw dislocation. For an edge, differences in other elastic constants, including the compressibility, are equally important. The appropriate combination is the one that enters $\mathscr{F}_{\text{EDGE}}$.

The final mechanism we discuss is the creation of a step at the interface, also called *chemical hardening*. As a screw dislocation that cuts the particle advances by δy, the free energy increases at each interface by (Fig. 52-4a)

$$\delta F = \chi_{\text{INT}} b\, \delta y \qquad (\textit{screw}) \qquad [52f]$$

where χ_{INT} is the interfacial free energy. This gives rise to a constant interface force

$$K_y = \chi_{\text{INT}} b \qquad (\textit{screw}). \qquad [52f']$$

For an edge dislocation (Fig. 52-4b), the free energy change is proportional to the lateral displacement of the new surface generated:

$$\delta F = \chi_{\text{INT}} b \cdot |\delta x| \qquad (\textit{edge}). \qquad [52g]$$

Note that an interface step is created whether x increases or decreases as the dislocation moves forward. If the force K_x is defined to be always pointing inward (as in Fig. 52-3,), it is (Fig. 52-4b):

$$K_x = \chi_{\text{INT}}\, b \cdot \text{sign}\,(-y) \qquad (\textit{edge}). \qquad [52g']$$

(The origin of x and y was consistently chosen at the particle center, Fig. 52-1.)

In real materials, more complicated processes than those described here commonly occur; the simple interactions depicted in Figs. 52-1 through 52-4 may in practice

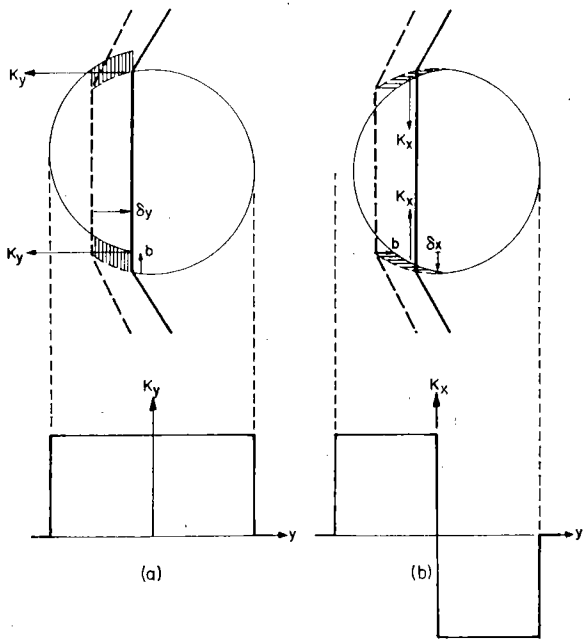

FIG. 52-4. Creation of an interface step by (a) a screw dislocation, (b) an edge dislocation. In (b), the difference between the shaded area $b\delta x$ and the actually created surface area is a second-order effect exaggerated in the figure. Note that K_x points outward in the second half where $\delta x < 0$; the change in free energy is always positive.

be oversimplifications. Internal disordering (Fig. 52-1) is partly avoided if dislocations move in groups of two or more, such that the net Burgers vector of the group does not disorder the particle; the details have been discussed by GLEITER and HORNBOGEN (1967), and by COPLEY and KEAR (1967). Change of stacking fault energy (Fig. 52-3a) can result in more complicated interactions, depending on the ratio of the particle size to the equilibrium separation of the partials (HIRSCH and KELLY, 1965). A misfit stress (Fig. 52-2) may cause a dislocation to undergo a complicated series of cross-slip maneuvers (GLEITER, 1967; DUESBERY and HIRSCH, 1969; HIRSCH and HUMPHREYS, 1970). In a particular size range, even more involved interactions may occur, whereby the glide dislocation permits the particle to lose complete coherency (BROWN and HAM, 1971; WOOLHOUSE, 1970).

Until now, we have only defined "forces" K_x and K_y as they seemed to be natural derivatives of the local free energy change.

$$\boxed{\delta F = K_x\,\delta x + K_y\,\delta y} \qquad [52g'']$$

We have not yet specified what components of those forces are relevant resisting forces to the motion of the dislocation. To do this, we must consider two successive equilibrium positions of the dislocation (Fig. 52-5, where the shape of the bowing free dislocation is, for now, irrelevant). As the dislocation

moves forward, *the cusp at the interface moves along the periphery of the particle*. Thus the relevant interface resistance (which led to the cusp in the first place) is the tangential force K_θ; the previously derived forces K_x and K_y are relevant only in their components tangential to the interface. With the sign convention used in Figs. 52-1 through 52-5:

$$K_\theta = K_y \cos\theta - K_x \sin\theta. \qquad [52h]$$

This equation immediately specifies a superposition law: while one may simply add the forces due to all mechanisms whose free energy storage rate is proportional to the same displacement (y or x here), the forces in different directions are added in their tangential components (eq. [52h]). Alternatively,

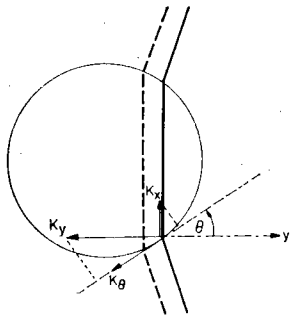

FIG. 52-5. The interface forces K_x and K_y act only in their components tangential to the interface, which add up to K_θ. The cusp in the dislocation is restricted to move along the interface.

one may add all forces *vectorially*, and then find the K_θ component of the resulting vector. For the mechanisms discussed here (eqs. [52c], [52e'], [52f'], [52g']), explicit expressions for the tangential force are

$$K_\theta^{\text{SCREW}} = \bar{\tau}_{\text{ELEM}} b \frac{w}{2} \cos^2\theta + \Delta\mathcal{F}_{\text{INT}} \sin\theta + \chi_{\text{INT}} b \cos\theta, \qquad [52h']$$

$$K_\theta^{\text{EDGE}} = \bar{\tau}_{\text{ELEM}} b \frac{w}{2} \cos^2\theta + \Delta\mathcal{F}_{\text{INT}} \sin\theta + \chi_{\text{INT}} b |\sin\theta|. \qquad [52h'']$$

Table 5-I summarizes the results for the various individual mechanisms for screws and edges, and gives orders of magnitude for the physical parameters. It also shows results for the maximum effective resisting force $\hat{K}$ and some thermal activation parameters to be derived below.

The Effective Resisting Force and the Plane Glide Resistance

Above we have discussed how all the effects of the particle on the dislocation can be considered as a pair of point forces along the particle boundaries.

Table 5-I. Individual Particle Resistance Mechanisms

Mechanism and order of magn.	Resistance to edge dislocation		Resistance to screw dislocation		Activation	
	K_x or K_y	$\hat{K}/2E \simeq$	K_x or K_y	$\hat{K}/2E$	p; q	F_o
Friction stress $\tau_{ELEM} \simeq \mu/100$	$K_y = \tau_{ELEM} b \frac{w}{2} \cos\theta$	$\tau_{ELEM}\, bw/2E$ (*) $(w/b)/100$	(same)	(same)	$1; \frac{3}{2}$	$\frac{\pi}{4} w^2 b \tau_{ELEM}$ $(w/b)^2/100$
Disordering $\chi_{APB} \simeq \mu b/100$	$K_y = \chi_{APB} \frac{w}{2} \cos\theta$	$\chi_{APB} w/2E$ (*) $(w/b)/100$	(same)	(same)	$1; \frac{3}{2}$	$\frac{\pi}{4} w^2 \chi_{APB}$ $(w/b)^2/100$
Misfit stresses $\lvert\epsilon\rvert \simeq 1/100$	$\hat{K}_y \simeq \lvert\epsilon\rvert \mu b w$	$\lvert\epsilon\rvert \mu b w/E$ $(w/b)/50$ or 100	(small)	(small)	$\frac{1}{2}; \frac{3}{2}$	$\simeq \mu b w^2 \lvert\epsilon\rvert$ $(w/b)^2/100$
Core energy diff. $\Delta\mathscr{F}_{DIS} \simeq \mathscr{F}_{DIS}/100$	$K_x = \Delta\mathscr{F}_{EDGE}$	$\sqrt{2\lvert\Delta\mathscr{F}\rvert/E}$ 0.2	$K_x = \Delta\mathscr{F}_{SCREW}$	$\sqrt{2\lvert\Delta\mathscr{F}\rvert/E}$ 0.1	$\frac{2}{3}; 2$	$w\lvert\Delta\mathscr{F}_{DIS}\rvert$ $(w/b)/200$
Modulus difference $\lvert\Delta\mu\rvert \simeq \mu/2$	$K_x \simeq \Delta\left(\frac{\mu}{1-\nu}\right) \cdot \frac{b^2}{5}$	$\sqrt{4\frac{\lvert\Delta\mu\rvert}{\mu} - \left(2\frac{\Delta\mu}{\mu}\right)^2}$ 1	$K_x \simeq \Delta\mu . b^2/5$	$\sqrt{2\frac{\lvert\Delta\mu\rvert}{\mu} - \left(\frac{\Delta\mu}{\mu}\right)^2}$ 0.7	$\frac{1}{2}; 2$	$\lvert\Delta\mu\rvert b^2 w$ $w/2b$
Interface step $\chi_{INT} \simeq \mu b/100$ $\chi_{VOID} \simeq \mu b/10$	$K_x = b\chi_{INT} . \text{sign}(-y)$	$\sqrt{2b\chi_{INT}/E}$ 0.3 0.8	$K_y = b\chi_{INT}$	$b\chi_{INT}/E$ 0.02 0.2	$\frac{2}{3}; 2$	$2bw\chi_{INT}$ $(w/b)/50$ $(w/b)/5$

* If $\hat{K}/2E \gtrsim \frac{1}{2}$, the dislocation bows around the particles at an effective force $\hat{K}/2E \simeq \frac{1}{2}$.

Now we discuss how the shape of the entire dislocation inside and outside the particle can be obtained by considering it as a dislocation of constant line tension subjected to these discrete forces. This, of course, would not account for the self stresses around the cusps.

The interactions between the neighboring dislocation branches are likely to be quite important in most cases of practical interest, where the particles are small. To take proper account of them, one must use computer relaxation methods, to obtain the correct line shape of a dislocation such that the total force on each element of the dislocation vanishes. The interaction force with the particle at its interface, which must be used in those calculations, is the force K_θ derived above. In order to avoid cusps, which may lead to problems in such calculations, one may substitute for the real interactions a distributed resistance τ_{ELEM} chosen such that it gives the correct value of K_θ when inserted into eqs. [52c] and [52h]. Note that, since only *differences* in line energy inside the particle were included in K_x, all dislocation elements inside the particle must be included in the relaxation and as self stress sources as if they had the same properties as the elements in the matrix.

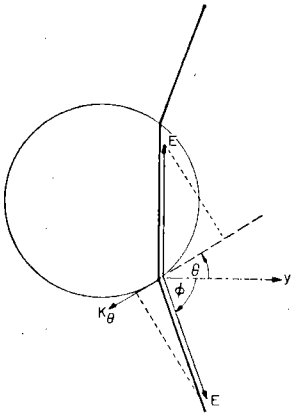

FIG. 52-6. The force on the particle, due both to line tension and applied stress, is the sum of the tangential (θ) components of both line tensions (E = matrix effective line tension—any *difference* of the particle line tension is contained in K_θ). This applied force must balance the resisting force K_θ in equilibrium. Note that again only *tangential* components matter: the three total forces shown in the figure are not and need not be in vector equilibrium.

When such numerical calculations do not exist, one may, in a first approximation, describe the effects of self stresses by considering the change in *length* of the dislocation between the two positions shown in Fig. 52-5. The associated free energy change, together with the work done in sweeping out the extra area, is properly accounted for in the "line tension construction" illustrated in Fig. 52-6, irrespective of the location of the next particle along the dislocation line (eq. [25o]). In terms of the cusp angle 2ϕ between neighboring dislocation branches on the same particle, the equilibrium condition is then

$$E \cos(\phi + \theta) + E \sin\theta = K_\theta. \qquad [52i]$$

In the same line tension approximation, one may define an *effective resisting force* of the particle on both branches of the dislocation by (eq. [25g'])

$$K = 2E \cos \phi \qquad [52j]$$

(where we have neglected the particle width with respect to the particle spacing). In a regular array of obstacles of spacing l along the dislocation, the flow stress would equal the line glide resistance and be given by

$$\tau_{\text{LINE}} = \frac{K}{bl} \qquad (\textit{regular array}). \qquad [52k]$$

In a random array, the effective resisting force or (exactly) the cusp angle 2ϕ at the particle, are also the determining factors, but the relation is no longer linear. As long as the obstacles are not too strong, i.e. $K \lesssim E$ (see Fig. 25-16), the "Friedel relation" gives

$$\tau_{\text{PLANE}} = (\cos \phi)^{3/2} \frac{2E}{bl} \qquad (\textit{random array}) \qquad [52\ell]$$

or, using eqs. [25g], [25v], [25ee], and [25ff],

$$\tau_{\text{PLANE}} = f^{3/2} \frac{b}{w} \mu \sqrt{c}. \qquad [52\ell']$$

Since $\cos \phi$ is thus the important parameter, let us express it in terms of the element force K_θ given from the physical mechanism [52h] by solving eq. [52i]:

$$f \equiv \cos \phi = \cos \theta \cdot \left(\frac{K_\theta}{E} - \sin \theta \right) + \sin \theta \cdot \sqrt{1 - \left(\frac{K_\theta}{E} - \sin \theta \right)^2} \qquad [52m]$$

(*line tension approximation*).

As can be seen from this equation and eq. [52h], the effective force K defined by eq. [52j] is *not* equal to $2K_y$ (from both sides of the particle), even when $K_x = 0$—unless $\theta = 0$, i.e. the particle–matrix interface is parallel to the direction of motion of the dislocation.

In the following figures, we shall present f as a function of $\sin \theta$ for the various interaction mechanisms *if they acted individually*, and present one case for two specific mechanisms acting simultaneously. These figures are diagrams of *effective* force (K) versus penetration depth. They show very marked differences, especially at the higher stresses, from the local or *element* force (K_x or K_y) diagrams shown in Figs. 52-1 through 52-4. Note, however, that they are not yet the diagrams of effective force versus *activation* distance needed for thermal activation; these will be obtained in the next subsection by considering the relation between penetration depth and activation distance.

For illustrative purposes, we start with the mechanism of creating an interface step by moving a screw dislocation (although this is one of the less

important contributions, see Table 5-I). In this case, the resisting force at the interface is in the direction opposite to the average direction of motion y of the dislocation, and is constant (eq. [52f']). But the *effective* resisting force K or, equivalently, the cosine of the cusp angle ϕ, is by no means constant (Fig. 52-7). At the entry side, it is raised to a value that corresponds to the limit up to which the dislocation must wrap around the particle before entry is more favorable. This maximum strength $\hat{K}$ can be obtained by setting the square-root in eq. [52m] equal to zero.

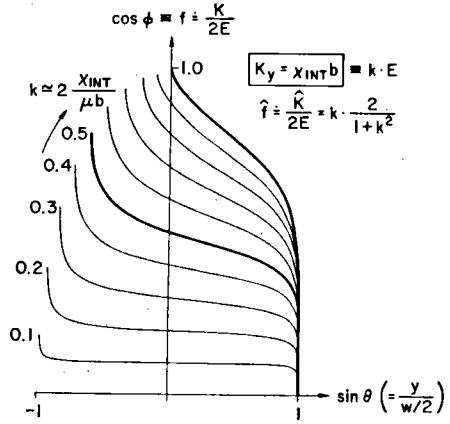

FIG. 52-7. Effective resisting force K as a function of interface inclination θ, for the generation of an interface step (specific interface energy χ_{INT}), by a screw dislocation (or for other mechanisms giving K_y = const., Fig. 52-4a). The locus of the maximum forces is the condition $\phi = -\theta$ up to which the dislocation wraps around the particle.

An interesting variation of this simple case is provided by the friction and misfit stress contributions (which are important contributions in practice). Here, the local interaction is still described by a K_y-force, but this force now depends on the penetration depth y (Figs. 52-1 and 52-2). Evaluation of eq. [52m] gives the curves shown in Figs. 52-8 and 52-9, respectively. While the friction stress is correctly described within the framework of the assumptions, the misfit stress is approximated by the dotted sin $(\pi y/w)$-dependence shown in Fig. 52-2; this should be good enough near the peak stresses, but obviously misrepresents the low-stress situation rather severely. One sees from Figs. 52-8 and 52-9a that the lower half of the strength range is altered only little by going from K_y to K; but in the upper half, the dislocation is again forced to wrap around the precipitate to some extent before entering, and the maximum effective strength is substantially higher. Figure 52-9b illustrates, in the same approximate way, the case of an *attractive* misfit stress (from a particle centered on the other side of the slip plane): *this case is qualitatively different from the repulsive one*. The effective resisting force remains similar to the local force K_y throughout, but is always somewhat *smaller*.

Next, we treat the case of a difference in line tension including, in an approximate fashion, that due to a difference in elastic constants. Here, the local force is in the lateral direction (Fig. 52-3) and must, therefore, give zero effective resistance for $y = 0$, where the interface is parallel to the direction of motion of the dislocation. Figure 52-10a shows the repulsive case (line energy *higher* inside the particle), Fig. 52-10b the attractive one (line energy *lower* inside the particle). The effective resistance is very considerable, even for small differences in line tension; since differences in elastic moduli in the order of 50% are not uncommon, this mechanism can be a major strengthening contribution (RUSSELL and BROWN, 1972).

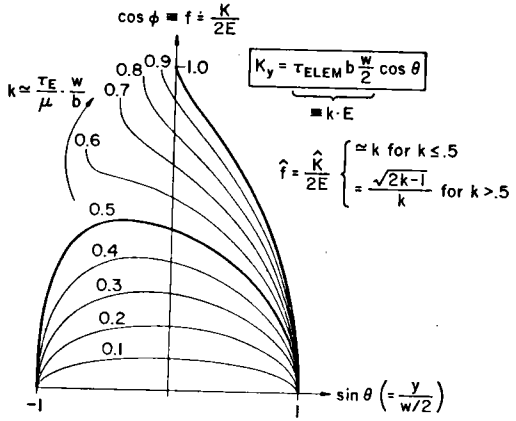

FIG. 52-8. Effective resisting force K as a function of penetration distance y for a circular obstacle (diameter w) when there is a constant additional element resistance ("friction stress") inside the particle. Internal disordering could fall in this class (Fig. 52-1).

Figures 52-10 a and b also give the effective resisting force for interface step generation, when it is accomplished by a moving *edge* dislocation (Fig. 52-7 gave it for a screw). Here, the resistance is positive both in the "entry" and in the "exit" half of the particle: it is the upper portion of Figs. 52-10 a and b put together (see Fig. 52-14a). The maximum resistance may significantly contribute to hardening by voids (where the interface energy is the free surface energy, and $k \simeq 0.2$, see COULOMB, 1957; WEEKS *et al.*, 1969). On the other hand, the strength is finite, not infinite as predicted by FRIEDEL (1969), who set $K = K_y = \tan\theta \cdot K_x$ without using the proper boundary conditions at the interface (Figs. 52-5 and 52-6, eqs. [52h], [52j], [52m]).

Finally, in one case, let us look at the superposition of two mechanisms: one in which K_x is specified and one in which K_y is specified. The first is taken to be a slightly higher line energy inside the precipitate, which by itself would give rise to the lowest curve in Fig. 52-10a; the second is assumed to be a friction stress of varying magnitude that by itself would have given the curves marked 0.1, 0.3, and 0.5 in Fig. 52-8. After superposing them in eq. [52h] and

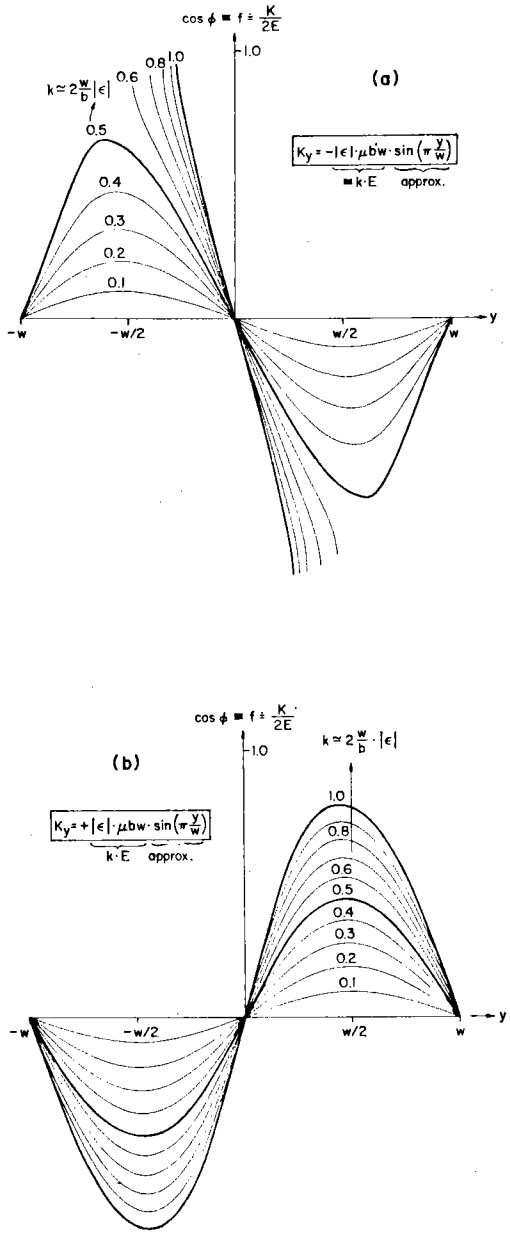

FIG. 52-9. Rough description of the effect of misfit stresses (Fig. 52-2, dotted curve), (a) in the repulsive, (b) in the attractive case. Note that they are not opposite to each other.

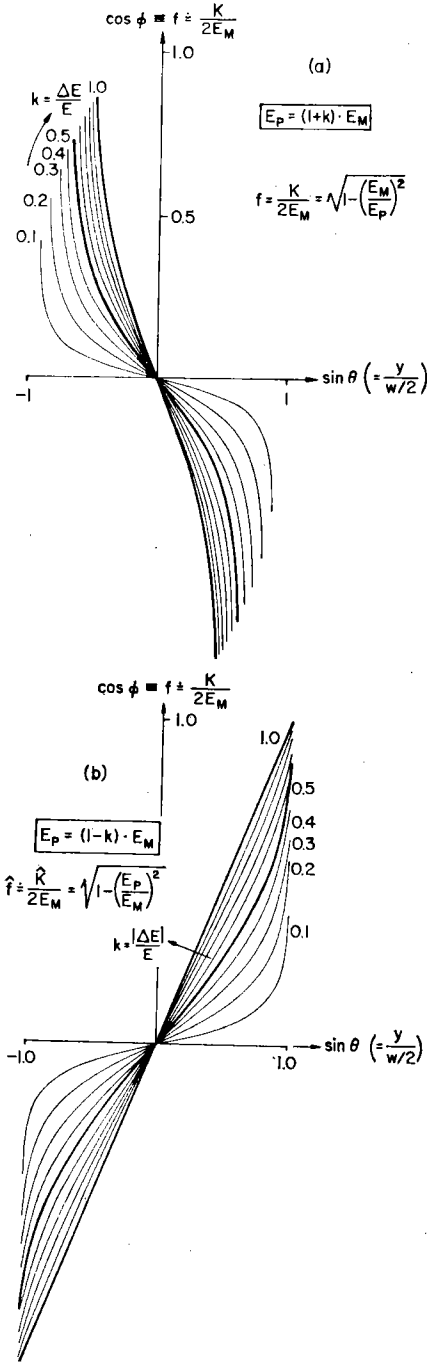

FIG. 52-10. Effective resisting force K as a function of interface inclination θ, for (a) an increased, (b) a decreased line energy inside the precipitate (Fig. 52-3). Line energy $\mathscr{F}$ and line tension E are assumed equal in the formulae, but the curves hold for any $|K_x| = k \cdot E$. The upper halves of both figures together give the case of an interface step creation by an edge dislocation ($k = \chi_{INT} b/E$, Fig. 52-4b).

inserting the resulting $K_\theta(\theta)$ into eq. [52m], evaluation gives the curves shown in Fig. 52-11. It is seen that the low value of the friction stress contributes virtually nothing to the strength, and the intermediate value contributes relatively the most. Mere addition of curves for the individual mechanisms (Figs. 52-8a and 52-10) would have given no change at all in the maximum strength, since the respective maxima are located precisely where the other mechanism has zero effective strength.

In Fig. 52-12 we have summarized the relations between the maximum effective strength $\hat{f}$ and the constant k in the local resisting force from Figs. 52-7, 52-8, and 52-10. Without use of the proper boundary conditions at the interface $\hat{f}$ and k would be the same; obviously, the deviations are substantial in many cases. Only distributed glide resistances, such as misfit stresses and a (dis)ordering resistance, are treated correctly by the conventional method (BROWN and HAM, 1971), and only if they are not too strong. The most severe deviations occur for K_x-mechanisms such as that due to a moduius difference; this was first realized by RUSSELL and BROWN (1972).

At this point, one must compare the particle strength associated with these cutting mechanisms in their actual combination, with the alternative of *Orowan bypassing*. In the line tension approximation, bypassing will occur when, by bowing, the dislocation is wrapped around the obstacle until $\theta = 0$, i.e. when the normalized obstacle strength exceeds 1. As was discussed in connection with Fig. 25-9, the line energy to be used for the local force is, however, only the line energy of a *dipole* of width w. Putting it another way, at a cusp angle ϕ as calculated on the line energy model, which is considerably greater than zero, the interactions between neighboring branches of the dislocation on either side of the particle cause the actual angle with which the dislocation leaves the particle to be zero and the Orowan stress to be reached (BACON *et al.*, 1973). The respective case for penetrable obstacles has not been solved; for that reason, it is at present unclear whether the interaction affects both processes equally, so that $\phi = 0$ is the correct criterion; or whether the formulas used here for cutting with a single line tension are approximately correct even in the presence of interactions, so that all the curves in Figs. 52-7 through 52-12 lose their significance for $f \gtrsim \frac{1}{2}$ (eq. [25y]).

Activation Distance and Activation Energy

In the preceding, we have derived the effective resisting force K of obstacles as a function of the distance y measured in the direction of the penetration of the dislocation into the particle (or, more generally, as a function of the angle θ between the particle interface and the direction of dislocation motion—which for circular particles are related by $y = w/2 \sin\theta$). For thermal activation analysis, we need know K as a function of the *activation* distance d, which is not the same as y.

Changes δd in the activation distance are defined (eq. [25g]) in such a manner that, with the chosen definition of K, one obtains

$$\delta F = K\,\delta d \qquad [52n]$$

for the change in free energy. Equivalently (eq. [44o]), it must be chosen so

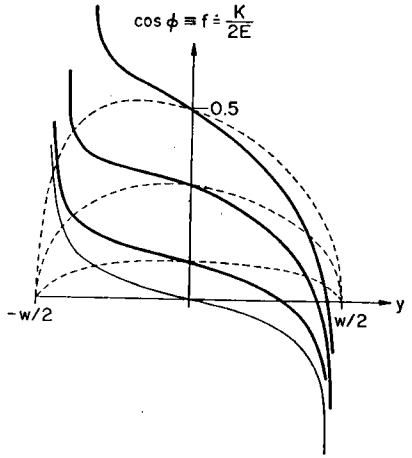

FIG. 52-11. Effective resisting force K as a function of penetration depth y, for two mechanisms acting simultaneously: a small positive difference in line energy (alone:——) and three levels of friction stress (alone: – – –). The superposition (——) is most effective at the intermediate level.

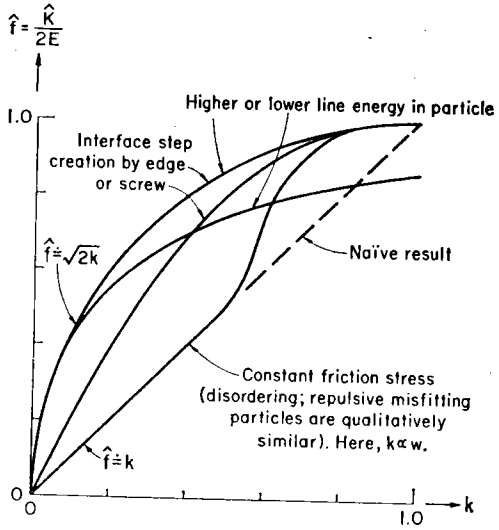

FIG. 52-12. Effective strength $\hat{f}$ (cosine of the breaking angle of the equivalent point obstacle) versus local strength parameter k, from Figs. 52-7, 52-8, and 52-10.

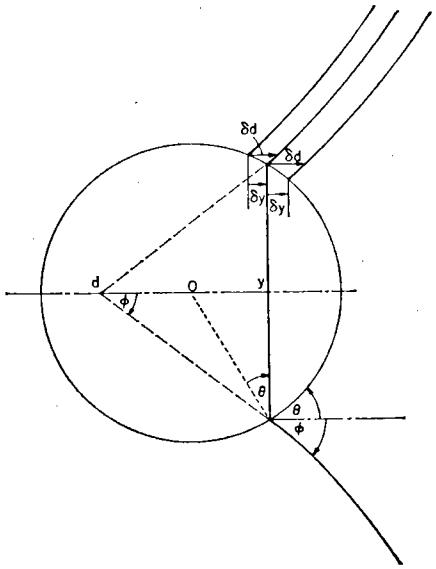

FIG. 52-13. Definition of the activation distance d. Together with the effective resisting force $K = 2E\cos\phi$, it defines an equivalent obstacle: a "ribbon" along the bisector of the two free dislocation branches. Note that the "ribbon" is generally longer than w: it extends beyond the particle on the "entry" side.

that the area swept by the dislocation of length l_e on either side of the particle between two equilibrium positions is

$$\delta a = l_e\,\delta d; \qquad [52n']$$

for then the applied stress K/bl_e in equilibrium with K does work $\delta W = \delta F$ during a virtual variation. Figure 52-13 shows the geometric definition of δd that fulfils these conditions, for three successive positions of the dislocation.

An integrated value of d, for convenient plotting of a K–d diagram, is (because of the overlap of δd's evident in Fig. 52-13) more easily obtained by extrapolating the free dislocation to the particle "axis" (i.e. the bisector of the two free dislocation branches). If we again neglect the particle dimensions with respect to the particle spacing, and therefore any dislocation curvature inside the particle, simple trigonometry shows that

$$d = y(1 - \cot\phi\cot\theta) \qquad [52o]$$

where $y = w/2\sin\theta$ and the origin of d was also chosen at the origin of y, for convenience (Fig. 52-12). Inserting $f \equiv \cos\phi = K/2E$, we obtain

$$\boxed{d = \frac{w}{2}\left(\sin\theta - \frac{f}{\sqrt{1-f^2}}\cos\theta\right)} \qquad [52o']$$

where f is itself a function of θ.

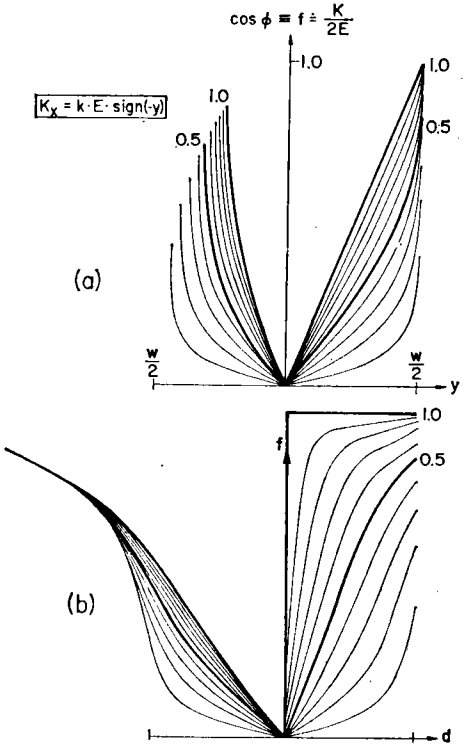

FIG. 52-14. The effective resisting force K (normalized by twice the line tension E) as a function of (a) the penetration depth y, (b) the activation distance d, for mechanisms in which K_x is prescribed: higher line energy inside the particle (left side); lower line energy (right); or interface step creation by an edge (both sides).

The meaning of the conjoint definitions of K (or f) and d can now be seen in a very plausible way: they correspond to a *mapping* of the particle-dislocation interaction onto an idealized, ribbon-like obstacle oriented symmetrically with respect to both branches (Fig. 25-1 for $w \ll l_c$). Included in this mapped "particle-dislocation interaction" are all changes in dislocation line length and shape called for by the varying orientation of the actual particle–matrix interface; but not included are changes in line length as a consequence of non-collinear arrangement of particles along the dislocation, as it would occur in a random array: they are represented, in such calculations, together with the applied stress, by the actual cusp angle 2ϕ at the "point obstacle".

The result [52o] is illustrated in Fig. 52-14b for interface step creation by an edge dislocation. It is seen that this K–d diagram deviates substantially from the corresponding K–y diagram in Fig. 52-14a. For example, the infinite slope at $\hat{K}$ in the K–y diagram has become finite in the K–d diagram Note also that the total area under the K–d curve for a specific value of $|K_x| = \chi_{INT} b$ is now equal on the left (or entry) side and on the right (or exit)

side of the particle, as it should: equal interface step area, and thus equal free energy, is created on either side. Figure 52-14b can also be used for the more important case of a difference in line energy (Figs. 52-4 and 52-10): the left half applies to the repulsive case, the right half to the attractive one.

The free enthalpy of activation at a given applied stress σ can now, in principle, be obtained by integration (eq. [44f]):

$$\Delta G = \int_{\sigma bl_\bullet}^{\hat{K}} \Delta d \, \mathrm{d}K \qquad [52p]$$

for each mechanism, or combination of mechanisms. The generally "pointed" shape of the K–d diagrams shows that thermal activation may have a considerable influence on the flow stress at least at low temperatures.

In order to proceed with a specific case, we assume that the result of such an integration comes close to one of the phenomenological relations for short-range obstacles introduced in eq. [44ℓ]:

$$\Delta G = F_0 \left[1 - \left(\frac{K}{\hat{K}}\right)^{p'}\right]^q. \qquad [52q]$$

Likely appropriate values for p′ and q, and thus for $p = \frac{2}{3}p'$ (eq. [44ℓ′]), can be gleaned from Fig. 43-7. For all mechanisms strictly limited to the confines of the obstacle, p′ should be equal to 1; for misfit stresses, which decrease with distance as $1/y^3$, $p' = \frac{2}{3}$ (eq. [43v] and following). The exponent q describes essentially the shape of the *top* of the K–d diagram (eq. [43v′], Fig. 43-7); Fig. 52-14b (and the equivalent K–d diagram for Fig. 52-7) show that for all interface mechanisms the top is pointed (q = 2), whereas for a distributed element resistance, if it is not too strong (Figs. 52-8, 52-9), the top is rounded (q = 3/2). We have inserted our best guesses for the various mechanisms into Table 5-I. As idealizations we may use

$$\Delta G = F_0 \cdot \left[1 - \left(\frac{\sigma}{\hat{\tau}}\right)^{2/3}\right]^2 \qquad [52q']$$

(a triangular K–d diagram for randomly distributed particles), or, for more smoothly varying interactions,

$$\boxed{\Delta G = F_0 \cdot \left[1 - \left(\frac{\sigma}{\hat{\tau}}\right)^{1/2}\right]^{3/2}.} \qquad [52q'']$$

The latter has the additional advantage that it provides a good fit to all reasonable relations for discrete obstacles, as was pointed out by ONO (1968).

Temperature Dependence and Age Hardening

A $\Delta G(\sigma)$ relationship such as that given in eq. [52q″] can be directly translated into a $\sigma(T)$ law at constant strain rate:

$$\frac{\sigma}{\hat{\tau}} = \left[1 - \left(\frac{T}{T_o}\right)^{2/3}\right]^2. \qquad [52r]$$

The temperature T_o at which the precipitates can be cut by thermal activation alone is given by

$$kT_o = F_o/\ln(\gamma_o \nu_G/\dot{\gamma}). \qquad [52r']$$

We must first derive an estimate for the logarithmic term.

It was shown in sec. 33 that the combination of parameters entering γ_o is, for discrete obstacles, primarily determined by the slip plane spacing, which in turn should be approximately equal to the average particle spacing l; thus (eq. [33z]),

$$\gamma_o \simeq \frac{b}{l} \simeq \frac{b}{w}\sqrt{c} \simeq 10^{-2} \text{ to } 10^{-3}. \qquad [52s]$$

The frequency factor ν_G was shown in sec. 42 to depend primarily on the normalized stiffness C of the particle. Figures 52-7 through 52-9 show that the force–distance relation rises quite rapidly for all repulsive obstacles, somewhat less rapidly for the attractive ones (acting at the exit side of the particle). As an order of magnitude, we have (eqs. [42g], [42h], [31g]) for $K/\mu b^2 \simeq \frac{1}{2}$,

$$\nu_G \simeq \frac{\omega_{ATOM}}{10} \cdot C \simeq \frac{\omega_A}{10} \cdot \frac{dK}{dd} \cdot \frac{1}{\mu b} \simeq 10^{11} \text{ to } 10^{12}\ s^{-1}. \qquad [52s']$$

With a typical strain rate $\dot{\gamma} \simeq 10^{-4}\ s^{-1}$, this gives the relatively high value

$$\boxed{\ln(\gamma_o \nu_G/\dot{\gamma}) \simeq 30.} \qquad [52s'']$$

The values of $\hat{\tau}$ and F_o to be used for our $\sigma(T)$ diagrams depend on the size of the particle. Inspection of Table 5-I shows that there are two classes of mechanisms:

Class A (friction stress, disordering, and misfit stresses). The free energy depends on the *square* of the particle diameter; for an order of magnitude description, we may write,

$$F_o = \frac{\mu b^3}{100}\left(\frac{w}{b}\right)^2. \qquad [52t]$$

The local force K_y, in turn, is *proportional* to the particle width. This proportionality does not exactly carry over into the effective resisting force K, and its maximum value $\hat{K}$, because of the nonlinear relation [52m] (see Fig. 52-12). Neglecting this subtlety for the present, or restricting ourselves to forces up to about half the limiting strength (Orowan strength), we may set, in order of magnitude,

$$\hat{K} = 2E \cdot \frac{1}{50} \cdot \frac{w}{b}. \qquad [52t']$$

With eq. [52ℓ′], this gives

$$\hat{\tau} = \frac{1}{50^{3/2}}\,\mu\cdot\sqrt{cw/b}. \qquad [52t'']$$

With this value and those of eqs. [52t] and [52s″], relation [52r] is plotted in Fig. 52-15 for various values of w/b. We postpone the discussion of this figure until we have introduced the other class of mechanisms from Table 5-I, and will have developed Fig. 52-16.

Class B (line energy difference, including modulus difference; all interface mechanisms). The constant-line-tension approximation leads to a free energy which varies *linearly* with the particle diameter w, and a force (local as well as effective) which is independent of w. But introducing a proper self stress, or approximating in some manner the branch–branch interaction, changes this: it leads to a w-dependent force, i.e. age hardening (RUSSELL and BROWN, 1972) which we neglect.

With typical numerical constants, then:

$$F_0 = \frac{\mu b^3}{10}\cdot\frac{w}{b} \qquad [52u]$$

and

$$\hat{\tau} = \frac{1}{2}\frac{b}{w}\,\mu\,\sqrt{c}. \qquad [52u']$$

The inverse width dependence of the flow stress stems from the change of particle spacing with particle diameter at constant volume fraction c. Insertion of these equations and [52s″] into eq. [52r] yields the curves in Fig. 52-16, for various values of w/b.

The diagrams in Fig. 52-15 and 52-16 show the expected qualitative behavior: the smaller particle sizes exhibit the stronger temperature dependence of the flow stress. This leads to a number of interesting effects. When the smallest particles give the highest mechanical threshold as in Class B (Fig. 52-16), the larger particles give a higher flow stress at high temperatures. This leads one to suspect that a "plateau"-like behavior at high temperatures may be the result of a *spectrum* of particle sizes (DIEHL *et al.*, 1965); we will not attempt to go into this further here. The temperature scale in the figures was chosen such that the range up to about half the melting temperature ($kT/\mu b^3 \simeq 0.01$) is covered.

For Class A mechanisms, the mechanical threshold *rises* with rising particle size; at a given volume fraction this can explain *age hardening*. At higher temperatures, as shown in Fig. 52-15, the effect gets accentuated. Putting it the other way around, at higher temperatures, the smallest particle sizes are already above their respective T_0 and thus give no strength; only after some aging has taken place, does the strength rise. Fig. 52-17 shows the resulting age-hardening curves for $T = 0$ K, $T \simeq T_M/4$, and $T \simeq T_M/2$. Such extra-

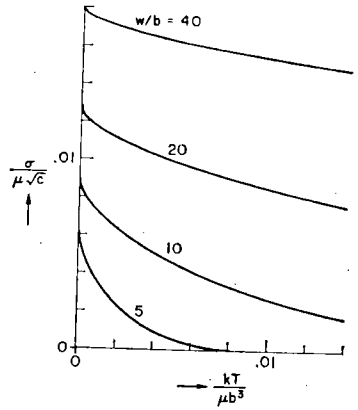

FIG. 52-15. Normalized flow stress vs. temperature diagrams for different particle sizes in an age-hardening material. For constants used, see eqs. [52r], [52s″], [52t′], [52t″]; the temperature scale covers the range up to about half the melting point.

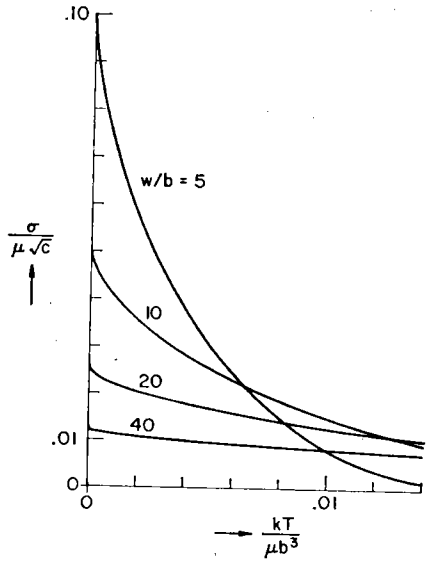

FIG. 52-16. Normalized flow stress vs. temperature diagram for different particle sizes, when the particle strength is independent of its size. At high temperatures, both age-hardening and age-softening may appear. For constants used, see eqs. [52r], [52s″], [52u], [52u′].

polation of the hardening curves to a finite particle size at zero strength has in fact been observed. In the upper strength range, the linear relation between K and w breaks down (Fig. 52-15), leading to a break-down of the Friedel relation, eq. [52ℓ]. Both effects have been incorporated semi-quantitatively into Fig. 52-17. As we have pointed out repeatedly, dislocation branch interaction may alter the behavior even more substantially.

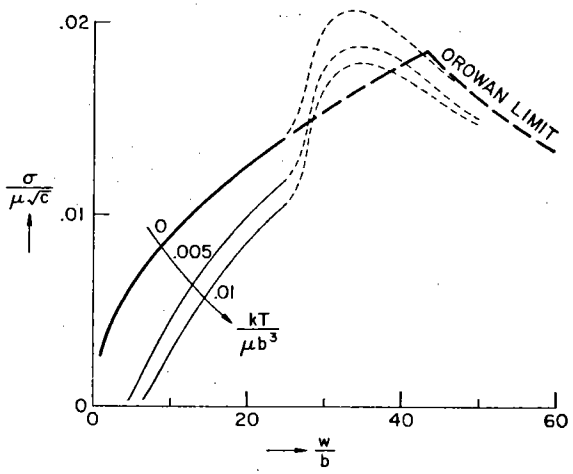

FIG. 52-17. Age-hardening curves at constant volume fraction, for different test temperatures, from Fig. 52-15. In the upper range, the thin dashed curves incorporate the effects from Figs. 52-12 and 52-14, in an approximate way. The solid dashed curve is the classical result.

If one knows which class of mechanisms is dominant in a particular material, one can make use of the known w-dependencies to obtain a universal curve characteristic of the obstacle profile. For age-hardening materials (Class A), the proper combination of variables is (eq. [52r], [52r'], [52t], and [52t"].

$$\left[\frac{\sigma}{\mu}\sqrt{\frac{b}{wc}}\right]^{1/2} \quad versus \quad \left[\frac{kT}{\mu b w^2}\ln(\dot{\gamma}_o/\dot{\gamma})\right]^{2/3} \qquad [52v]$$

and for materials of Class B (eqs. [52r], [52r'], [52u], [52u"])

$$\left[\frac{\sigma}{\mu}\frac{w}{b\sqrt{c}}\right]^{1/2} \quad versus \quad \left[\frac{kT}{\mu b^2 w}\ln(\dot{\gamma}_o/\dot{\gamma})\right]^{2/3}. \qquad [52v']$$

The overall exponents have been chosen such that a straight line would result if the phenomenological relation [52q"] in fact holds; but it is the point of plotting all data on these universal plots that the *actual* relation should thus be found. It would then be best to plot the σ-combination to the two-thirds power, which is proportional to K, versus the T-combination linearly, which is proportional to ΔG, in the manner of Fig. 44-5b.

The relative change of flow stress with temperature over the observable range is slight for the larger particles. Nevertheless, the $\sigma(T)$ dependence at very low temperatures is far from negligible for all particle sizes. Investiga-

tions in this range (BYRNE *et al.*, 1961; CHUN and BYRNE, 1969) should make it possible to obtain a meaningful value of the exponent q and, thus, qualitative information about the shape of the K–d diagram near the top.

To obtain meaningful results by this method, especially at higher temperatures where the effect of thermal activation is less pronounced, it is important that temperature dependencies of the physical properties have already been accounted for. As before, one hopes that use of the values of μ and b (also w) at the temperature of interest is sufficient. There may, however, be additional effects; e.g. when differences in stacking fault energy are important (which have no reason to depend on temperature as μb), or when the misfit stress depends on temperature because of differential thermal expansion (as has been shown to dominate the temperature dependence in Cu–Co alloys, PHILLIPS, 1965).

Strain-rate Effects

The relative inverse strain-rate sensitivity of the flow stress was defined (eqs. [34r], [45a], [45b]) as

$$\mathrm{m} \equiv \left.\frac{\partial \ln \dot{\gamma}}{\partial \ln \sigma}\right|_{T,r} = \mathrm{m_o} + \mathrm{m_G}. \qquad [52w]$$

The contribution $\mathrm{m_o}$ from the preexponential factors [52s] and [52s'] is zero; in general (sec. 33), it is no more than about 2. Since we shall see immediately that $\mathrm{m_G}$ is virtually always large in precipitation hardened alloys, the neglect of $\mathrm{m_o}$ is justified.

With various previous definitions (eqs. [43k], [44f'], [44h]) we have, for a random dispersion,

$$\mathrm{m_G} \equiv \frac{\Delta W'}{kT} = \frac{2}{3}\frac{K\Delta d}{kT} = \frac{2}{3}\frac{\mu b^3}{kT}\frac{K}{\mu b^2}\frac{\Delta d}{b} \qquad [52w']$$

Since $\mu b^3/kT \gtrsim 100$ below about half the melting temperature in most materials, and $\Delta d/b > 1$ in the meaningful range,

$$\mathrm{m} > 100 \cdot \frac{K}{\mu b^2} \qquad [52w'']$$

and m can be of order 10 or less only at very small stresses, i.e. for very small particles at very high temperatures.

The other common measure of strain-rate effects is the absolute strain rate sensitivity, or its inverse (eq. [43i])

$$\left.\frac{\partial \ln \dot{\gamma}}{\partial \sigma}\right|_{T,t} = \left.\frac{\partial \ln \dot{\gamma}_o}{\partial \sigma}\right|_{T,t} + \frac{b\Delta a'}{kT}. \qquad [52x]$$

If again we neglect the first term on physical grounds, the "operational activation area" is a measure of the "apparent activation area" $\Delta a'$. For our

randomly dispersed discrete obstacles, it is (see the development in sec. 44)

$$\Delta a' \equiv -\left.\frac{\partial \Delta G}{b\partial\sigma}\right|_{T,\dot{\varepsilon}} = -\left.\frac{\partial \Delta G}{\partial K}\right|_{T} \cdot \left.\frac{\partial K}{\partial \sigma}\right|_{l} \qquad [52x']$$

$$= \Delta d \cdot l \cdot \tfrac{2}{3}\sqrt{\frac{\mu b^2}{K}}.$$

First, we observe that $\Delta a'$ is proportional to the average particle spacing l and thus, at constant particle diameter,

$$\frac{\Delta\sigma}{\Delta \ln \dot{\gamma}} \propto \sqrt{c} \qquad [52x'']$$

just as the flow stress is. The method illustrated in Fig. 44-10 can, therefore, be used to test the discrete model and to separate out any additional contributions to the flow stress.

On the other hand, $\Delta a'$ is by no means proportional to the activation distance Δd, since the correction factor in eq. [52x'] depends on Δd through K; it expresses the dependence of the *effective* particle spacing on the obstacle strength. The easiest way to disentangle these two effects was proposed in sec. 44: it is to differentiate the $\ln \dot{\gamma}$-term with respect to $\sigma^{2/3}$, which is proportional to K, rather than with respect to σ itself. In the spirit of the universal plots introduced above, we may combine all variables and write, as follows directly from the preceding equations,

$$\boxed{\frac{\Delta d}{b} = \left(\frac{b^2 c}{w^2}\right)^{1/3} \frac{\mathrm{d}\left(\dfrac{kT}{\mu b^2}\ln\dot{\gamma}\right)}{\mathrm{d}(\sigma/\mu)^{2/3}}} \qquad [52y]$$

and, again,

$$\boxed{\frac{K}{\mu b^2} = \left(\frac{\sigma}{\mu}\frac{w}{b\sqrt{c}}\right)^{2/3}.} \qquad [52y']$$

This is a prescription for deriving the obstacle profile from macroscopic data.

Extension to Point Obstacle Resistance

The interaction of a dislocation with an individual solute atom (or other point defect) may, in some respects, be formally similar to that with a precipitate of atomic size. On this basis, FLEISCHER (1961, 1962, 1963, 1964) formulated a set of theories of solution hardening, primarily using the size and modulus misfit mechanisms. We have seen that these are just the mechanisms whose effect extends beyond the physical limits of the "particle", so that the

effective size of the "point defects" is larger than b. Thus, they can be treated as discrete obstacles only in rather dilute solutions.

FLEISCHER (1964) further noted that observations on the strength of such crystals can be grouped into two classes: those in which the strength contribution per point defect is small, and those for which it is large. Typically, substitutional solute atoms are weak, interstitial solutes strong.

Weak obstacles must, of course, be present in substantial concentrations in order to exert a noticeable influence on the flow stress. This substantial concentration poses a number of problems. First, the assumption of a random distribution of the obstacles may be far from true. Second, especially when the distribution is non-random but even when it is not, the ranges of interaction of various "obstacles" will severely overlap: at 10% concentration, even the *average* spacing of solutes in each slip plane is $\sim 3b$; smaller distances must frequently occur. A treatment in terms of discrete obstacles is then open to question: the dislocation may have to overcome many obstacles at a time. However, even when the discreteness criterion is not violated, we have seen (sec. 25, Fig. 25-16) that the combination of low obstacle strength and high concentration demands "Mott statistics" rather than the "Friedel statistics" used for precipitation hardened alloys: only *fluctuations* in the distribution of forward and backward forces on the dislocation contribute to the strength of the alloy. For all these reasons, we believe that the FLEISCHER theory for weak solutes (1961, 1963) must be abandoned; a theory based on the original work by MOTT and NABARRO (1948), with suitable modifications (RIDDHAGNI and ASIMOW, 1968; LABUSCH, 1970, 1972), seems more appropriate. Experiments, which initially favored the FLEISCHER theory (see, for example, HAASEN, 1970), now also point more in this direction. Since there is no detailed theory of thermal activation under Mott statistics, we shall not deal with this problem further here.

In dilute solutions of *strong solutes*, such as interstitial atoms, none of these problems exist. One may then apply the relevant concepts developed above for precipitation hardened alloys, in the manner proposed by FLEISCHER (1962, 1964) but including the influence of statistics according to Friedel.

Three separate interactions can be identified as being strong. First, the interaction force due to a different modulus, which was found to be strong and independent of particle size in precipitation hardening, should survive in the limit $w \to b$ (FLEISCHER, 1961). Of course, it is not the solute atom that has a different modulus, but its "bonds" to the matrix may well have different "spring constants". This effect can be described by an interaction force

$$\hat{K} \propto b^2 \frac{\mathrm{d}\mu}{\mathrm{d}c}. \qquad [52z]$$

In this section we have not discussed the differences between screw and edge dislocations. Often these differences can be quite important. In such cases, as well as when the anisotropy of the crystal is large, the appropriate combination of elastic constants describing the dislocation energy must be inserted into eq. [52z] instead of μ.

Second, not only can the "spring constants" of the solute-matrix bonds be different, but so can be the bond energies themselves. During the passage of a

dislocation the bonds must be "broken" and reformed, leading to an interaction force.

$$\hat{K} \simeq F_{\text{BOND}}/b. \qquad [52z']$$

It may be looked upon as a local difference in Peierls stress. This effect, which is a result of a changed ratio of bond strength to modulus may be quite important in all cases where a local covalent bond is formed (MOTT and NABARRO, 1940).

Finally, misfit stresses may exist around solute atoms. Their influence on the flow stress may, at first glance, seem negligible (Table 5-I, Fig. 52-12) inasmuch as it is proportional to $\sqrt{w}$. However, the misfit strain for individual solute atoms can be much larger than that for coherent precipitates (for which it is usually less than 4%). It is especially severe around interstitial atoms, where it is frequently "tetragonal" rather than merely dilational (FLEISCHER, 1962), and may typically be, say, 40%. The interaction force is

$$\hat{K} \simeq \mu b^2 |\epsilon|. \qquad [52z'']$$

Even in substitutional solutions, especially when the solute is larger than the host atom, $|\epsilon|$ may be substantial (FLEISCHER, 1963). When it is primarily dilational, it may be represented by (ESHELBY, 1957)

$$|\epsilon| = \frac{\mathrm{d} \ln b}{\mathrm{d}c}$$

which often exceeds 10%.

The three mechanisms discussed above, certainly in combination, can give rise to a mechanical threshold that is a substantial fraction of the Orowan limit ($\hat{K} \simeq \mu b^2$). On the other hand, the total activation energy F_0 is severely limited because of the small size of the obstacle (since it is being treated as discrete):

$$F_0 \simeq \frac{\hat{K}b}{2} \lesssim \frac{\mu b^3}{5}. \qquad [52aa]$$

Even this limit is of the order of the bond energy and can probably only be reached by the use of eq. [52z']. Even if we insert for $\ln(\dot{\gamma}_0/\dot{\gamma}) = 20$, the lowest reasonable value, we have

$$kT_0 = \frac{F_0}{\ln(\dot{\gamma}_0/\dot{\gamma})} < \frac{\mu b^3}{100} \simeq \frac{kT_{\text{MELT}}}{2}. \qquad [52bb]$$

The hardening by randomly distributed solutes can thus at best be explained on the basis of discrete-obstacle theories in the low-temperature regime and not near the high-temperature, concentration dependent "plateau" stress frequently observed. This conclusion is confirmed by looking at the strain-rate sensitivity (eqs. [52w"], [45b]): m must scan the entire spectrum from very high to very low values as the temperature is raised from 0 K to T_0; the high values observed in the "plateau" region are at variance with this.

53. Superposition of Effects Due to Different Obstacles

Rarely if ever is the glide resistance in a crystal the result of one type of obstacle. In deformed pure metals, for example, in addition to the lattice resistance there are attractive and repulsive forest dislocations acting as discrete obstacles, and dislocation dipoles, long sessile dislocations, as well as grain boundaries, etc., acting as linear barriers in the slip plane. In precipitation hardened and subsequently strained material there are, in addition to the obstacles listed above, penetrable and possibly also impenetrable particles as well as solute atoms remaining in solution and possibly antiphase boundaries. Thus, thermal analysis of a real material requires at least a rudimentary understanding of the superposition of some of these mechanisms.

On a local scale, the superposition principle is a simple one: *the element glide resistances add* at every point in the slip plane, since they describe the free energy change required at that point, due to any mechanism whatever, if the dislocation element is to move through it. However, the element resistance map of each of the individual sets of obstacles or barriers may be affected by the presence of the others; for example, the presence of solute atoms may affect the stacking fault energy and thereby change the lattice resistance as well as the strength of the dislocation forest; or the *distribution* of solute atoms or precipitates may be affected by the presence of dislocations or grain boundaries. In these cases, one says that the different strengthening mechanisms *interact*; unless the details of this interaction are known, it is then useless to compare the properties of the "mixture" with those of the "pure" states. In the following, we assume, that one knows the element resistance map for each set of obstacles if it existed alone, but *in the distribution and with the material constants as they actually exist in the mixed state.*

We have seen in sec. 23 that the element glide resistance may depend on the direction of motion of the dislocation; for example, it may be different for screws and edges. When one resistance mechanism that acts primarily on quasi-straight screw dislocations (e.g. the lattice resistance) or on quasi-straight edge dislocations (e.g. weak particle hardening) is added to one that requires substantial bow-outs (e.g. a hard particle resistance), the *line glide resistance* may be affected severely. Thus, even strengthening mechanisms that are non-interacting in the metallurgical sense used above may interact by way of the mobile dislocations. Furthermore, the values of effective line tensions to be used in the flow-stress formulae may depend on the degree of mixture through the same geometric effects. It seems unlikely that these complications can be dealt with in any quantitative way other than by computer simulation.

With these significant reservations in mind, we shall now compare the *plane glide resistance* due to the simultaneous presence of *two* sets of obstacles or barriers with that due to each set alone. Some simple cases lead us to suspect that upper and lower limits for the superposition law can be stated with some confidence. We shall address ourselves first to the value of the mechanical threshold, then to rate effects. Other recent discussions of the subject have

been given by KLAHN *et al.* (1970) and, for some special cases, by STANIEK and HORNBOGEN (1973).

The Superposition of Mechanical Thresholds

A useful approach in superposition of threshold mechanisms is to grade them according to increasing structural scale. Whenever the structural dimensions for constituent threshold mechanisms differ by an order of magnitude or more, the plane resistance of the one with the "finest" structure can be considered smooth and added to the one of next larger scale as a constant *friction stress*:

$$\hat{\tau}_{\text{PLANE}} = \hat{\tau}^{(1)}_{\text{PLANE}} + \hat{\tau}^{(2)}_{\text{PLANE}}. \qquad [53a]$$

(Here, the word "friction" is used without any implications regarding energy storage or susceptibility to thermal activation.)

One example of superposition was considered in sec. 51. It concerned the *lattice resistance*, for which the relevant structural dimensions are the spacing of the Peierls valleys (of order b) and the length of a critical nucleus (of order 10 to 100b). This lattice resistance may be regarded as a friction stress when it is added to the resistance due to *strong obstacles* such as nodes in the dislocation network or inclusions (whose spacing is typically 1000b). Conversely, the strong obstacles may be said to impose a curvature on all dislocations whose lattice resistance is being derived, and thus to provide an "*internal stress*" that must be subtracted from the applied stress (sec. 51).

Another example of linear superposition (eq. [53a]) was treated in sec. 24 (Fig. 24-6), where *widely spaced strong linear barriers* (e.g. grain boundaries) were supposed to exist in addition to a *small-scale glide resistance variation* throughout the slip plane. (The small-scale mechanism was there also described by a linear barrier such as a lattice resistance; however, the same result would apply if it were due to discrete obstacles such as small precipitates or forest dislocations.) Strong linear barriers of sufficient spacing permit the accumulation of dynamic pile-ups behind them; then the plane glide resistance due to them alone depends on the square root of the line resistance and the inverse spacing (second term in eq. [24n]). This *plane* resistance is *added* to that of the small-scale obstacles. Again, one may either regard the closely-spaced obstacles as providing a friction stress to be subtracted from the applied stress in the derivation of the equilibrium pile-up configuration (eq. [24k]); or one may regard the other dislocations in the pile-up as providing a back stress to be subtracted from the applied stress in the consideration of the interaction of each dislocation with the small-scale obstacles (eq. [24ℓ]). Either one of these mechanisms may be thermally activated or athermal.

A third example of linear superposition (eq. [53a]) was given in sec. 44 (Fig. 44-12), where two sets of discrete obstacles were assumed present: few strong ones and many weak ones. The duality between regarding one as a friction stress or the other as a back stress is evident here, too.

When the structural scales of the two sets of obstacles are not widely different, linear superposition does not generally hold. A simple, while rather artificial, example is the simultaneous presence of *two periodic linear barriers* of the energy-storing kind, which have the same spacing but may be "in phase" or "out of phase" with respect to each other: if they are "in phase", the mechanical thresholds obviously add; but if they are exactly 180° out of phase, only the larger of the two determines the strength:

$$\hat{\tau}_{\text{PLANE}} = \max\,(\hat{\tau}^{(1)}_{\text{PLANE}}, \hat{\tau}^{(2)}_{\text{PLANE}}). \qquad [53b]$$

For an arbitrary phase relation, the superposition law lies between these two extremes, i.e. between the curves marked a and b in Fig. 53-1.

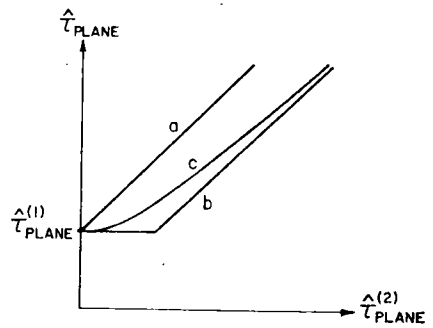

FIG. 53-1. Variation of the mechanical threshold $\hat{\tau}_{\text{PLANE}}$ with the contribution due to one set of obstacles (2) whose strength or spacing is varied, while the contribution $\hat{\tau}^{(1)}_{\text{PLANE}}$ from the other set is held constant. Curve a describes linear superposition (eq. [53a]), curve c addition of the squares (eq. [53c]), and curve b a sole contribution of the higher threshhold.

Another special case is that of *two sets of discrete obstacles of identical strengths*, but varying densities. For example, any two impenetrable obstacles would fall in this category; approximately, one might also treat "almost-impenetrable" obstacles in the same way, such as strong precipitates and forest dislocations. In this case, the obstacle *densities* simply add and thus, under Friedel statistics, the *squares* of the mechanical thresholds (KOPPENALL and KUHLMANN-WILSDORF, 1964):

$$\hat{\tau}_{\text{PLANE}} = \sqrt{(\hat{\tau}^{(1)}_{\text{PLANE}})^2 + (\hat{\tau}^{(2)}_{\text{PLANE}})^2}. \qquad [53c]$$

Note that this superposition law, although it is not linear, was derived under the explicit assumption that the two mechanisms do not interact.

Another case of considerable interest is that of *two sets of obstacles of the same density, but different strengths*; for example, misfitting solute atoms in the atomic plane just above, and just below, the slip plane; or, more generally, any spectrum of obstacle strengths. For the first case, LABUSCH (1970) using his statistical treatment (cf. eq. [25ww]) obtains

$$\hat{\tau}_{\text{PLANE}} = [(\hat{\tau}^{(1)}_{\text{PLANE}})^{3/2} + (\hat{\tau}^{(2)}_{\text{PLANE}})^{3/2}]^{2/3}. \qquad [53d]$$

The case of a continuous spectrum was treated by FOREMAN and MAKIN (1967) in their computer simulation method, unfortunately using a uniform distribution of breaking *angles* rather than strengths (thus emphasizing the stronger obstacles). Their results appear to fit eq. [53a] approximately; certainly, an averaging of the *plane* glide resistances gives a better fit than an averaging of the strengths (i.e. of the *line* glide resistances).

Figure 53-1 shows, in addition to the plots of eqs. [53a] and [53b], already introduced, one of eq. [53c] (curve c); eq. [53d] would obviously look qualitatively similar. It is seen that they lie between the limits of "linear superposition" and "only the stronger obstacle matters". We do not know whether this convenient rule has generality. In data analysis, an investigation of the right-hand side of Fig. 53-1 would be helpful; i.e. a variation of the concentration or strength of the *dominating* strengthening component: if it does not extrapolate back to zero, another mechanism is superposed *linearly*, but if at low total strength it does extrapolate back to zero, other mechanisms may nevertheless be important.

Rate Effects

When the kinetics of dislocation motion is considered, a number of additional "superposition" effects become possible that are not already described by a derivation of the combined element glide resistance diagram for the two sets of obstacles. Some of them are, in fact, not related to two *obstacles* at all and thus do not fall under the title of this section; we merely mention them in rough outline.

First, there is the superposition of a velocity-dependent drag on the glide resistance (whether this glide resistance be due to one or to many sets of obstacles). For applied stresses above the mechanical threshold, i.e. for continuous glide, this superposition was treated in some detail in sec. 32. It led to a quadratic superposition law in a special case (eq. [32i], Fig. 32-1):

$$\sigma^2 = \hat{\tau}^2 + \left(\frac{B\bar{v}}{b}\right)^2. \qquad [53e]$$

Below the mechanical threshold, the drag should influence the time spent by a dislocation segment between thermal release from one equilibrium configuration and arrest at the next including, for example, the time required for bow-out between discrete obstacles. This time must be added to the waiting time (eqs. [33r], [33s]) so that, in a rough way, the inverse strain rates are additive:

$$\frac{1}{\dot{\gamma}} = \frac{1}{\dot{\gamma}_1} + \frac{1}{\dot{\gamma}_2}. \qquad [53f]$$

At a prescribed total strain rate, the flow stress must then depend on both mechanisms. FROST and ASHBY (1971) have shown by a computer calculation that these drag effects are negligible everywhere except *very* near the mechanical threshold; e.g. in shock-loading experiments at room temperature. (Note that at low temperature, where the mechanical threshold can be approached under normal loading rates, the damping coefficient would be negligible, see Fig. 34-3.)

A more complicated case of a superposition between drag (or a quasi-drag due to

solute atoms) and a line glide resistance was that of the nucleation and propagation of kinks treated in sec. 51. Under some circumstances, the mean free path was governed by a balance between the rates of nucleation and propagation: thus, they were not "independent". If one were to define strain rates $\dot{\gamma}_1$ and $\dot{\gamma}_2$ for the two processes, one could derive from eqs. [51aa] and [51cc] a superposition law

$$\dot{\gamma} \propto \sqrt{\dot{\gamma}_1 \cdot \dot{\gamma}_2}, \qquad [53g]$$

i.e. a geometric mean.

In juxtaposition to the first case above, in which the dislocation had to progress through a set of states in *series* and the *times* spent for each displacement were to be added, there are cases in which *alternative* paths (a set of states in *parallel*) are available to the dislocation. So long as rate effects are not considered, one merely selects the easiest available path that yields macroscopic deformations; but when the rates are finite along two different paths, one must add the strain rates (presuming the processes are independent):

$$\dot{\gamma}(\sigma, T) = \dot{\gamma}_1(\sigma, T) + \dot{\gamma}_2(\sigma, T). \qquad [53h]$$

A special case of a possibility to achieve the macroscopic strain rate in different ways is by the movement of screw or of edge dislocations. They are not independent inasmuch as an advancing screw increases the length of the edge component of the same loop and vice versa. From these geometric effects, though they are transient, GILMAN (1969) derived a superposition law of the form [53g] for the two strain rates. We have seen that another dependence between different dislocations in the same slip plane is of prime importance: the back stresses from edge dislocations, for example, prevent the continued generation of screws, and vice versa. Thus, the sides of a dislocation loop with the higher velocity (e.g. the screws) will quickly arrive at the surface or other sinks; from then on, long range slip is determined by the dislocation with the smaller velocity (e.g. the edge):

$$\dot{\gamma} = \min(\dot{\gamma}_{\text{SCREW}}, \dot{\gamma}_{\text{EDGE}}). \qquad [53i]$$

Finally, let us return to our area of prime concern in this section, the superposition of the effects of *two sets of obstacles*, now at stresses below, rather than at, the mechanical threshold. The treatment of thermal activation is then trivial if it affects one of the obstacles only (set 2) and the other is "athermal" (set 1): one merely uses the superposition law for the mechanical thresholds (e.g. eqs. [53a], [53b], [53c], or [53d]), replacing $\hat{\tau}_{\text{PLANE}}$ by $\sigma(\dot{\gamma}, T)$ and $\hat{\tau}^{(2)}_{\text{PLANE}}$ by $\tau^{(2)}_{\text{PLANE}}(\dot{\gamma}, T)$, which now appears in the Arrhenius law

$$\dot{\gamma} = \dot{\gamma}_o \cdot \exp\left\{ -\frac{F_o}{kT} \cdot g\left(\frac{\tau^{(2)}_{\text{PLANE}}}{\hat{\tau}^{(2)}_{\text{PLANE}}} \right) \right\}. \qquad [53j]$$

For a linear superposition law (eq. [53a]), this is the familiar rate equation using "effective stresses"; but it holds for other superposition laws as well, under certain restrictions.

Some care is necessary if the thermal activation of one obstacle set changes its relative contribution to the total flow stress, compared to the contribution from the other set, in a qualitative way; for example, when the effective obstacle strengths of the two sets change from being similar to being grossly different. Then, the superposition law cannot retain any one of the simple limiting forms throughout the entire temperature range.

Two thermally activatable obstacle sets can also often be treated. This is especially so when the thresholds superpose linearly, e.g. *when the structural scale of the two sets is different in order of magnitude*, so that

$$\tau_{\text{PLANE}}(\dot{\gamma}, T) = \tau^{(1)}_{\text{PLANE}}(\dot{\gamma}, T) + \tau^{(2)}_{\text{PLANE}}(\dot{\gamma}, T). \qquad [53k]$$

We have discussed in detail the case of two sets of discrete obstacles, few strong and many weak ones (sec. 44, Fig. 44-12). The argument may be extended to other cases: it was that the macroscopic rate is determined by the configuration at which *the waiting times at both obstacles are equal*; at a given temperature, this means

$$\Delta G^{(1)} = \Delta G^{(2)} = kT \cdot \ln(\dot{\gamma}_o/\dot{\gamma}). \qquad [53\ell]$$

A very useful relation of the combined "effective activation area" $\Delta a'$ (eq. [43g]) in terms of those due to each set if it were alone, then follows directly from eqs. [53k] and [53ℓ] (eq. [44x]):

$$\frac{1}{\Delta a'} = \frac{1}{\Delta a'_1} + \frac{1}{\Delta a'_2}. \qquad [53m]$$

Note that the linear superposition law [53k] varies smoothly with temperature and becomes eq. [53a] at zero temperature. This feature was absent in the attempts by LI (1968) and by FROST and ASHBY (1971) to treat the "small-scale" glide resistance as a quasi-drag obeying a nonlinear *power-law* (without threshold). In such cases, in the same way as for the linear stress-velocity relation (see eq. [32ℓ]), the influence of the one threshold always vanishes when the other becomes dominant, while in eq. [53k] the constant contribution survives.

Obstacles of *similar strengths*, which obey the superposition law [53c] with respect to their mechanical thresholds, are much harder to treat when they are both subject to thermal activation: small differences in the shape of their profiles can then lead to varying dislocation paths as the temperature is raised. DIEHL *et al.* (1965) have discussed this problem for the general case of a *spectrum* of activatable obstacles.

6. DATA ANALYSIS

Summary

The last chapter described specific models that predicted certain macroscopic properties: properties that can be measured. So the model could be checked by experiment—provided, of course, that the property in question is a model-sensitive one; a model-*insensitive* property is consistent with a number of competing models, and cannot be used to check them. Many characteristics of crystal plasticity are, in fact, model-insensitive.

To avoid this problem, one might ask the question the other way around: what properties must a physical model have if it is to agree with the experiments? Or more specifically: what properties must the obstacles to dislocation motion have to cause a specific macroscopic observation? By answering this question, one may learn enough about the obstacles to be able to identify them. Examples of this inductive approach are given in this chapter.

If one wishes to derive properties of a theoretical model from experimental data, it is essential that the reduction of the data themselves is done without any implicit assumptions of the theoretical model. In other words, the experimentally derived parameters have to be operationally well defined. Section 61 deals with appropriate *operational parameters* and their relation to the parameters in model-inspired phenomenological laws such as the Arrhenius equation. The main result is a summary of ways in which the data can be plotted, and of the conditions under which a given plot is appropriate.

The activation analysis of macroscopic data, as outlined above, is taken up in secs. 62 and 63. It concerns itself with such questions as: are there two different hardening agencies (such as two different kinds of obstacles, or one obstacle and a lattice friction)?; are the obstacles strong or weak, few or many, big or small, long-range or short-range?; what is the mechanical threshold stress?; is the τ–Δa diagram flat or rounded or pointed near the mechanical threshold?; what can one say about the mobile dislocation density and its dependence on stress and temperature?, and so on. Experimental data are probably never sufficient to answer all of these questions at the same time. The technique is then to make simplifying assumptions about those aspects of the problem that do affect the result very much. For example, any changes in mobile dislocation density have little effect when the material is *rate insensitive* (sec. 62). On the other hand, any temperature dependence of the activation energy or of an "internal stress" has little effect when the material is *rate sensitive* (sec. 63).

Special problems arise when one actually tries to establish the experimental relation between the operational variables stress, strain rate, and temperature; for at a prescribed temperature and stress, for example, the strain rate is by no

means constant, but usually varies first rapidly in a transient sort of way and then slowly. Suitable extrapolation procedures must be prescribed to define the operational parameters for each type of application. This is taken up in section 64.

Many authors have been concerned with the problem of inferring microscopic information from macroscopic measurements. Among the more recent ones are:

deMEESTER, YIN, DONER, and CONRAD (1973), *Thermally Activated Deformation of Crystalline Solids;*
EVANS and RAWLINGS (1969), *The Thermally Activated Deformation of Crystalline Materials;*
GIBBS (1969), *Thermodynamic Analysis of Dislocation Glide Controlled by Dispersed Local Obstacles;*
KLAHN, MUKHERJEE, and DORN (1970), *Strain Rate Effects;*
LI (1968), *Kinetics and Dynamics in Dislocation Plasticity;*
SUREK, KUON, LUTON, and JONAS (1974), *Linear Elastic Obstacles: Analysis of Experimental Results in the Case of Stress Dependent Pre-Exponentials.*

61. Operational Parameters versus Model Parameters

In this section we shall deal with descriptions of rate processes in which structure parameters do not appear. This may be so because one describes "*instantaneous*" *changes*, in which the structure is assumed not to change; alternatively, one may describe the "asymptotic" or *steady-state* behavior after a change, which is characteristic of a structure that has adjusted itself in all possible ways to the new boundary conditions, and thus is again uniquely defined by external parameters.

In either case, the only variables of the problem are strain rate, stress, and temperature. In a more general description, pressure and other stresses must also be included (see sec. 43). Effects of $\dot{\sigma}$, as they were introduced in sec. 33, are also neglected here, but will be discussed where they could be important.

Operational parameters frequently used to describe the interrelation between the main variables are:

$$Q \equiv \left.\frac{\partial \ln \dot{\gamma}}{\partial (-1/kT)}\right|_{\sigma} = kT \left.\frac{\partial \ln \dot{\gamma}}{\partial \ln T}\right|_{\sigma} \qquad [61a]$$

and

$$\mathrm{m} \equiv \left.\frac{\partial \ln \dot{\gamma}}{\partial \ln \sigma}\right|_{T} . \qquad [61b]$$

From these definitions follows

$$\left.\frac{\partial \ln \sigma}{\partial \ln T}\right|_{\dot{\gamma}} = -\frac{Q}{\mathrm{m}kT} \qquad [61c]$$

if indeed there is a functional relation between the three variables $\dot{\gamma}$, T, σ only. We have encountered (eq. [43i]) one other phenomenological parameter, which we called the "operational activation area":

$$\frac{kT}{b}\frac{\partial \ln \dot{\gamma}}{\partial \sigma}\bigg|_T = \frac{\mathrm{m}kT}{b\sigma}. \qquad [61d]$$

The definitions of the operational parameters Q and m do not, of course, imply that they are constant; in general they depend on stress and temperature (or on any two of the three variables). The special cases that they are both *constants*, or that both depend on *stress only* are, however, of some interest and will be elaborated below.

The operational parameters Q and m are related to model parameters such as activation enthalpy ΔH and apparent activation area $\Delta a'$ in an Arrhenius type rate equation (eq. [43a]),

$$\dot{\gamma} = \dot{\gamma}_o(\sigma, T)\cdot\exp -\frac{\Delta G(\sigma, T)}{kT}. \qquad [61e]$$

While this equation is model inspired, it may be used as a purely phenomenological relation, if the two parameters

$$\boxed{\dot{\gamma}_o = \gamma_o \nu_G} \qquad [61e']$$

and ΔG are allowed to depend in an arbitrary way on stress and temperature. The operational parameters are then identified as follows (eqs. [41m] and [43k]):

$$\boxed{\begin{aligned} Q &= kT\frac{\partial \ln \dot{\gamma}_o}{\partial \ln T}\bigg|_\sigma + \Delta H, \qquad [61a'] \\ \mathrm{m}kT &= kT\frac{\partial \ln \dot{\gamma}_o}{\partial \ln \sigma}\bigg|_T + \Delta W' \qquad [61b'] \end{aligned}}$$

where $\Delta W' = \sigma b \Delta a'$ as before.

Operational activation analysis consists in finding ways to measure, in each equation, each of the terms on the right separately, or to prove some of them negligible and to measure the rest. For example, the temperature dependence of the preexponential (the first term on the right of eq. [61a']) is almost always negligible compared to ΔH; typically,

$$kT\frac{\partial \ln \dot{\gamma}_o}{\partial \ln T}\bigg|_\sigma \simeq -kT/2. \qquad [61a'']$$

(See the discussion of eq. [43o]).

We now consider the special cases mentioned earlier, for which Q and m are either constant, or for which at least one of them depends only on stress.

Q and m *are Constant*

A rate equation of the form

$$\dot{\gamma} = A\sigma^n \exp -\frac{U_o}{kT} \qquad [61f]$$

with no implicit stress or temperature dependence, leads to congruence between the model parameters n and U_o, with the operational parameters m and Q, respectively. The plots relating the various measurable quantities to each other must then have the form shown in Fig. 61-1a through Fig. 61-1c, and the parameters can be easily derived from them.

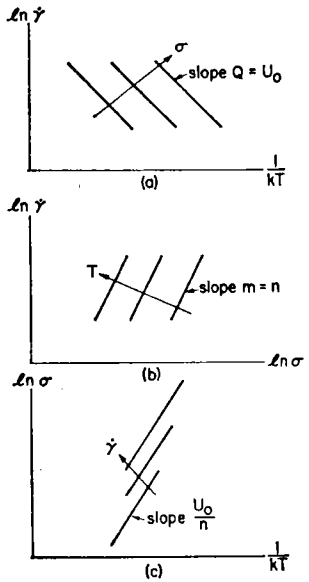

FIG. 61-1. The appropriate way to plot data when m and Q are constants. The data are then described by eq. [61f].

An "activation energy"

$$Q = U_o \qquad [61f']$$

independent of stress and temperature is a realistic approximation for some high-temperature applications. In these cases, the rate of reverse dislocation motion may not be negligible; it would (eq. [45j]) contribute a 1 to the exponent n. Other contributions to n may come from a dependence of the steady-state mobile dislocation density on stress (if asymptotic behavior is being discussed), and from a possible dependence of the frequency factor on stress (see sec. 42).

Equation (61f] is a sensible phenomenological relation only when n is not

too large; say, no larger than 5 or so. Whenever exponents much larger than this are encountered, the possibility of an exponential form of stress dependence must be investigated. (Some general rules about meaningful phenomenological relations were discussed in sec. 34.)

A minor modification of the rate eq. [61f] would be the incorporation of an additional known temperature dependence. For example, the reverse jumps quoted above would always imply an inverse temperature dependence of A. In such a case, one should replace $\dot{\gamma}$ on the left-hand side by $\dot{\gamma}T$, and the entire formalism can be applied in the same way as above.

JONAS and LUTON (1971b) have analyzed the empirical power law [61f] with *constant* parameters in more detail and compared it to the predictions of thermal activation analysis. In particular, they have shown that the assumption of a temperature independent n leads to peculiarities in the activation entropy. In the following, we shall always assume that the operational parameter m is trivially proportional to $1/T$ at constant stress—and that the product mkT may depend on stress.

Q and mkT *Depend on Stress but not on Temperature*

Another relatively simple case, which sometimes describes experiments adequately, is an Arrhenius equation with a *constant* preexponential and an activation enthalpy that depends on *stress* but not on temperature:

$$\dot{\gamma} = \dot{\gamma}_{\mathrm{H}} \cdot \exp - \frac{\Delta H(\sigma)}{kT}. \qquad [61g]$$

For reasons to be seen immediately, we have lumped the activation entropy ΔS in with the preexponential (eqs. [61e'], [42c])

$$\dot{\gamma}_{\mathrm{H}} \equiv \dot{\gamma}_{\mathrm{o}} \exp \frac{\Delta S}{k}. \qquad [61g']$$

Evidently, $Q = \Delta H$ depends on stress only. Furthermore,

$$\mathrm{m}kT = kT \left.\frac{\partial \ln \dot{\gamma}_{\mathrm{H}}}{\partial \ln \sigma}\right|_T - \left.\frac{\partial\, \Delta H(\sigma)}{\partial \ln \sigma}\right|_T \qquad [61h]$$

is independent of temperature, if the preexponential $\dot{\gamma}_{\mathrm{H}}$ is independent of stress as claimed in eq. [61g]. In part, this means (eq. [61g']) that the activation entropy must be independent of stress (as well as of temperature). We have seen in secs. 41 and 43 that this is possible to a good approximation over a large temperature range for certain kinds of glide resistance profiles (without "plateau"), even when ΔS itself is finite. In such a case, the activation *free* enthalpy ΔG would depend linearly on temperature; and for this reason, it was here more convenient to write the Arrhenius equation with ΔH as in eq. [61g].

For this special case ($\dot{\gamma}_H$ and thus ΔS independent of stress and temperature)

$$\mathrm{m}kT = -\left.\frac{\partial \Delta H}{\partial \ln \sigma}\right|_T \qquad [61i]$$

which implies that the operational activation area $\mathrm{m}kT/b\sigma$ is equal to the apparent activation area (eq. [43g]):

$$\frac{\mathrm{m}kT}{b\sigma} = \Delta a'. \qquad [61i']$$

The apparent obstacle profile (Fig. 61-2) is then particularly easy to determine experimentally.

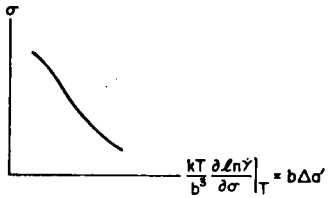

FIG. 61-2. The apparent obstacle profile derived from measurements of σ as a function of $\dot{\gamma}$ and T, in the special case that $\mathrm{m}kT$ and Q depend on stress but not on temperature.

Such an easy correspondence between operational and mechanistic parameters is very convenient. It depends primarily on the assumption of a constant preexponential in eq. [61g]—an assumption that must be verified. This can be done in a number of ways. First, if it were not true, $\mathrm{m}kT$ would have to depend on temperature at constant stress, according to eq. [61h]. Second, the straight lines in an Arrhenius plot (Fig. 61-3a), which are now no longer parallel as in Fig. 61-1a (eq. [61g]), must go through one point at infinite temperature—though, since the extrapolation is a long one, this can rarely be checked with much certainty. Finally, inversion of eq. [61g] gives:

$$\Delta H(\sigma) = kT \ln \frac{\dot{\gamma}_H}{\dot{\gamma}} \qquad [61g'']$$

so that, for this special case—and only this one—a plot of the measured activation enthalpy vs. temperature at constant strain rate gives straight lines through the origin up to the total activation energy U_o where the process begins to follow a form described by eq. [61f] (Fig. 61-3b).

When eq. [61g] describes the rate processes, $T \ln (\dot{\gamma}_H/\dot{\gamma})$ is the correct variable combining the effect of temperature and strain rate as was first recognized by MACGREGOR and FISHER (1946). If one plots the stress (or any function of stress) against this parameter for tests at many different strain rates, one must obtain a single curve provided one has chosen the right value of $\dot{\gamma}_H$ (SLEESWYK,

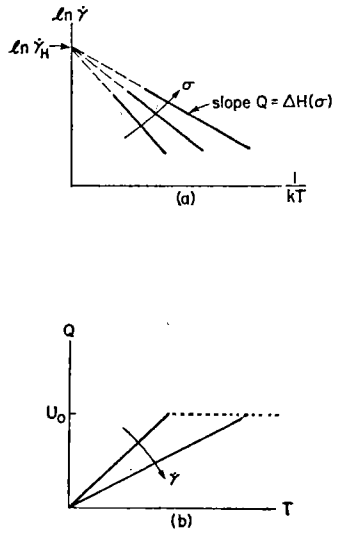

FIG. 61-3. Appropriate plots, and their characteristics, for the special case that Q and mkT depend on stress but not on temperature.

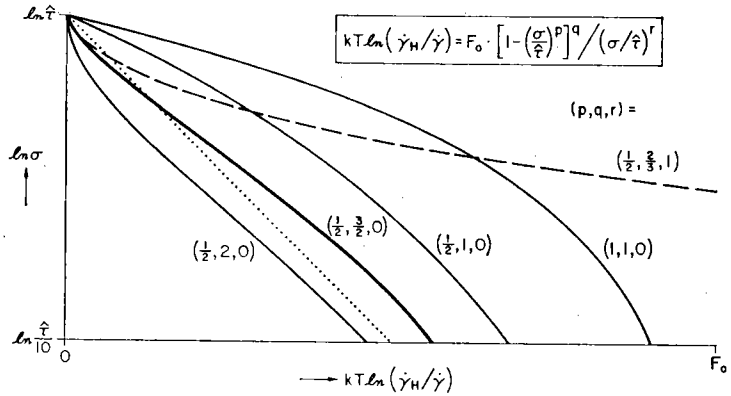

FIG. 61-4. The "Fisher plot" often used to display the temperature and strain rate dependence of the flow stress. The curves shown are for four "short-range mechanisms" (solid) and one "long-range mechanism" (dashed). The dotted line corresponds to m = $F_o/2kT$.

1970); this is, however, not a sensitive determination of $\dot{\gamma}_H$ (van DEN BEUKEL, 1970).

In Fig. 61-4, the *logarithm* of the stress is plotted versus this parameter. Diagrams of this type are widely encountered in the literature on creep of structural alloys and are sometimes called "Fisher plots". At any given temperature, Fig. 61-4 is a double-logarithmic strain-rate versus stress diagram like Fig. 61-1b, but with interchanged axes; only a small range along the

abscissa could in practice be tested at any one temperature. At a given strain rate, finally, Fig. 61-4 is a somewhat unconventional plot of the temperature dependence of the flow stress.

Figure 61-4 is useful for data analysis in terms of the kinds of mechanisms discussed in Chapters 4 and 5. This is because a straight line on this diagram (dotted) corresponds to a logarithmic dependence of the activation energy on stress, which is the borderline case between "short-range" and "long-range" mechanisms and corresponds to a power law with m $\propto 1/T$ but independent of σ; deviations from a straight line in Fig. 61-4 signal deviations from this power law stress–strain-rate relationship. We have plotted in Fig. 61-4 the calculated curves for various realistic phenomenological relationships between activation energy and stress. It is seen that the curvature is convex upward for all short-range mechanisms at stresses less than about half the 0 K flow stress, but remains convex downward for long-range mechanisms throughout the entire stress range. At very low temperatures, the curvature is convex downward even for short-range mechanisms, so long as the exponent $q > 1$ (i.e. the line glide resistance profile has a rounded or sharp top, not a flat one). It is also obvious from this figure, that a straight line may describe many experiments very well over a substantial range of the variables, even if the true material behavior is given by the typical short-range profile [43w″] (heavy line in Fig. 61-4). Thus, power-law relations between strain rate and stress do have phenomenological merit (despite CHRISTIAN, 1970); a typical value for the observed m would be about $F_o/2kT$.

Q Depends on Stress, m *Depends on Stress and Temperature*

When the tests for a constancy of the preexponential factor fail, but the lines in an Arrhenius plot are still straight, one may wish to assume a more general rate equation of the form

$$\dot{\gamma} = \dot{\gamma}_H(\sigma) \cdot \exp - \frac{\Delta H(\sigma)}{kT}. \qquad [61j]$$

The meaning of $Q = \Delta H$ is not changed, but the direct correspondence between the operational activation area

$$mkT/\sigma \quad \text{and} \quad - \left.\frac{\partial \Delta H}{\partial \sigma}\right|_T$$

is lost (eq. [61i′]). One must now determine

$$\left.\frac{\partial \Delta H}{\partial \sigma}\right|_T = \frac{dQ}{d\sigma} \qquad [61k]$$

from the stress dependence of the Arrhenius slopes. Information on the stress dependence of the preexponential can then be obtained from comparing the two measurements:

$$kT \cdot \frac{d \ln \dot{\gamma}_H}{d\sigma} = kT \frac{\partial \ln \dot{\gamma}}{\partial \sigma} + \frac{dQ}{d\sigma}. \qquad [61k']$$

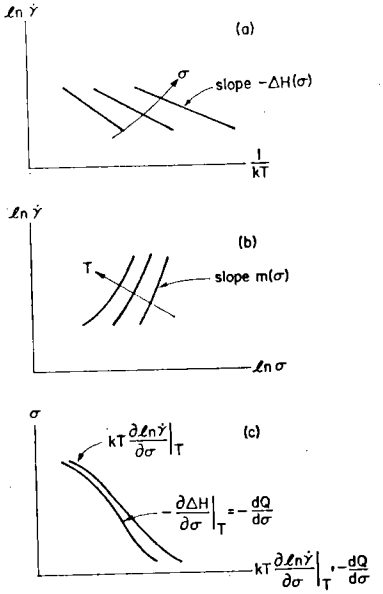

FIG. 61-5. Diagrams illustrating the experimental determination of the terms of eq. [61k']: (a) the determination of $(\partial \Delta H/\partial \sigma)_T$; (b) the determination of $(\partial \ln \dot{\gamma}/\partial \sigma)_T$; (c) evidence of the difference between them. The plots are appropriate when Q depends on stress but not on temperature.

Figure 61-5 illustrates the determination of a

$$\sigma \text{ vs. } kT \left.\frac{\partial \ln \dot{\gamma}}{\partial \sigma}\right|_T \qquad \text{and a} \qquad \sigma \text{ vs. } \left.\frac{\partial \Delta H}{\partial \sigma}\right|_T \qquad \text{diagram.}$$

The apparent activation area $\Delta a'$ cannot be obtained in this case, since the stress dependence of $\dot{\gamma}_H$ may contain one of ΔS: there is no operational way of separating the two.

In principle, the failure of the tests for a constancy of the preexponential according to Fig. 61-3 could have been due to a *temperature* dependence of $\dot{\gamma}_H$ rather than, or in addition to, the stress dependence assumed in eq. [61i]. Then, $Q = \Delta H$ would no longer be true and the straightness of the Arrhenius line would imply a temperature dependence of ΔH, which just compensates that of $\dot{\gamma}_H$. This seems unlikely. Note, however, that the test of a temperature independence of mkT at constant stress, according to eq. [61h], excludes the entire academic possibility.

Normalized Variables

If the Arrhenius plot (Fig. 61-1a or 61-2a) does not give straight-line plots, this may be due to a temperature dependence of the activation energy or of the preexponential with a simple origin. For example, many theoretical models

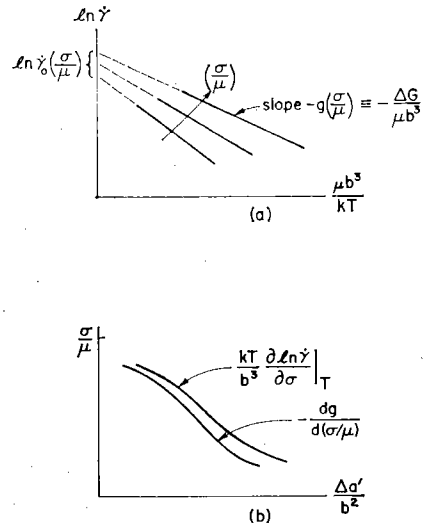

FIG. 61-6. (a) A modified Arrhenius plot according to eq. [61ℓ], illustrating the determination of $g(\sigma/\mu)$. (b) An apparent obstacle profile determined, first, from the stress vs. strain-rate relation and second, via Fig. 61-6a.

predict that these terms should depend on the shear modulus, or (less frequently) on other material properties such as an interfacial energy, whose temperature dependence is roughly equal to that of the shear modulus. In this case, one can properly introduce new variables σ/μ and $\mu b^3/kT$. This corresponds to a rate equation of the following kind:

$$\dot{\gamma} = \dot{\gamma}_o \left(\frac{\sigma}{\mu}\right) \cdot \exp\left(-\frac{\Delta G}{kT}\right); \qquad \Delta G = \mu b^3 \cdot g\left(\frac{\sigma}{\mu}\right). \qquad [61\ell]$$

If this form is obeyed, straight lines are obtained in the modified Arrhenius plot shown in Fig. 61-6a, from which one can read the functions $g(\sigma/\mu)$ and $\dot{\gamma}_o(\sigma/\mu)$. The apparent activation area follows directly from the stress dependence of the modified Arrhenius slopes (eq. [43g]):

$$\frac{\Delta a'}{b^2} = -\frac{dg(\sigma/\mu)}{d(\sigma/\mu)}. \qquad [61m]$$

Figure 61-6b schematically shows a normalized apparent obstacle profile that is obtainable in this way, and another one obtained directly from the stress vs. strain-rate relation as in Fig. 61-5. The two curves are different unless the preexponential term is constant.

Instead of using specialized plots, one could also obtain the activation free enthalpy ΔG, the apparent activation area $\Delta a'$ and the preexponential $\dot{\gamma}_G$ directly from the operational parameters Q and m defined by eqs. [61a] and [61b], according to the following formulae (see eq. [43t]):

$$\Delta G = \frac{Q + \mathrm{m}kT\dfrac{\mathrm{d}\ln\mu}{\mathrm{d}\ln T}}{1 - \dfrac{\mathrm{d}\ln(\mu b^3)}{\mathrm{d}\ln T}} \qquad [61\mathrm{n}]$$

$$\mathrm{b}\Delta a' = -\left.\frac{\partial\Delta G(Q,\mathrm{m})}{\partial\sigma}\right|_T \qquad [61\mathrm{o}]$$

$$\left.\frac{\partial\ln\dot\gamma_o}{\partial\ln\left(\dfrac{\sigma}{\mu}\right)}\right|_T = \mathrm{m} - \frac{\sigma b\Delta a'}{kT}. \qquad [61\mathrm{p}]$$

An equation resembling [61n] was derived by SCHOECK (1965), except that it contained non-operational parameters like $\dot\gamma/\dot\gamma_o$, which can be used only when $\dot\gamma_o$ has been *proved* to be constant (or is a *known* function of operational variables). Allowing *any* functional dependence of $\dot\gamma_o$ on σ/μ, we can derive eq. [61n] by expanding Q (eq. [61a]) in the independent parameters chosen here:

$$\frac{Q}{kT} \equiv \left.\frac{\partial\ln\dot\gamma}{\partial\ln T}\right|_\sigma = \left.\frac{\partial\ln\dot\gamma}{\partial\ln(kT/\mu b^3)}\right|_{(\sigma/\mu)} \cdot \frac{\mathrm{d}\ln(kT/\mu b^3)}{\mathrm{d}\ln T} + \left.\frac{\partial\ln\dot\gamma}{\partial\ln(\sigma/\mu)}\right|_T \cdot \left.\frac{\partial\ln(\sigma/\mu)}{\partial\ln T}\right|_\sigma.$$

Term-by-term identification, using eqs. [61b] and [61ℓ], gives

$$\frac{Q}{kT} = \frac{\Delta G}{kT}\cdot\left[1 - \frac{\mathrm{d}\ln(\mu b^3)}{\mathrm{d}\ln T}\right] + \mathrm{m}\cdot\left(-\frac{\mathrm{d}\ln\mu}{\mathrm{d}\ln T}\right)$$

which is the same as eq. [61n] (and similar to eq. [43t] derived previously). An equivalent relation (neglecting the temperature dependence of b) was derived by SUREK *et al.* (1974).

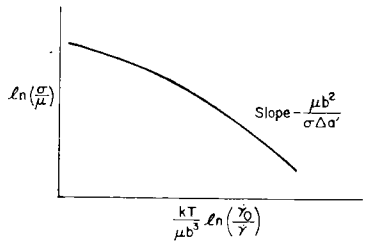

FIG. 61-7. The appropriate master plot when $\dot\gamma_o$, and its dependence on stress and temperature (if any) are known.

Sometimes, $\dot\gamma_o$ may in fact be found to be constant, or may be known (including weak dependences on stress and temperature) to sufficient accuracy. In that case, one would introduce $\dot\gamma/\dot\gamma_o$ as a new variable. As in Fig. 61-4, one could then plot all experimental results on a diagram (Fig. 61-7), in which all points should fall on a single curve, presuming the value of $\dot\gamma_o$ has been chosen correctly. One may, in this case, allow the free enthalpy ΔG to depend on stress and temperature in an arbitrary fashion, so that the rate equation reads

$$\ln\left(\frac{\dot\gamma}{\dot\gamma_o(\sigma,T)}\right) = -\frac{\Delta G(\sigma,T)}{kT}. \qquad [61\mathrm{q}]$$

One may then derive both the activation enthalpy ΔH and the activation free enthalpy ΔG by the procedure shown in Fig. 61-8, which was suggested by WOBSER and FRANK (1968). (The curvature of the plot in their figures was inverted, see sec. 41.) Note that, in principle, the value of $\dot{\gamma}_o$ can be obtained from the extrapolation of the low-temperature slopes of the curves (presuming the activation entropy goes sufficiently close to zero at the temperatures reached). In practice, however, the range of the plot that can be covered by experiments is too far away from the origin to make this procedure meaningful.

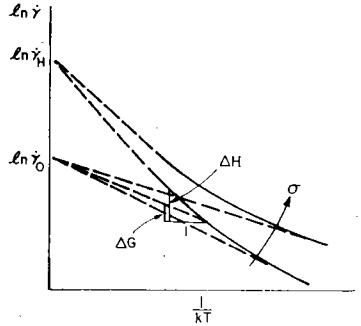

FIG. 61-8. The Arrhenius plot according to eq. [61q].

When the temperature dependence of ΔG is assumed to be known, conversely, one may allow any arbitrary dependence of $\dot{\gamma}_o$ on σ and T. This is possible by an iteration procedure suggested by SUREK *et al.* (1973a), who assumed the form of ΔG given in eq. [61ℓ], but an entirely general function $\dot{\gamma}_o(\sigma, T)$. One may then derive trial values of ΔH and $\Delta W'$ from eqs. [61a'] and [61b'], under the assumption of a trial form of $\dot{\gamma}_o(\sigma, T)$; these trial values are inserted into eq. [43t] to determine ΔG; when this is plotted, *at constant strain rate*, versus σ and T, a new dependence $\dot{\gamma}_o(\sigma, T)$ is found from eq. [61q], which is then used for the next iteration, and so on. SUREK *et al.* (1974) found, in fact, by this method that the form [61ℓ] is obeyed for a number of materials.

In summary, we have shown that four phenomenological equations [61f], [61g], [61j], [61ℓ] can be used to describe experiments with an equal degree of operational certainty, although the degree of physical sophistication does increase. The equation that has recently been used most often [61q] is of a somewhat different kind in that it requires fairly detailed knowledge of one of the parameters in the equation ($\dot{\gamma}_o$), in exchange for which the other one (ΔG) is then completely free.

Structure Variables

Any interpretation in terms of physical models will involve structural, or internal parameters in addition to the variables σ, T, and $\dot{\gamma}$ used here. The two most common ones are the glide resistance profile $\tau(\Delta a)$ (or at least its maximum value $\hat{\tau}$), and the mobile dislocation density ρ_m (see sec. 34). As pointed out in the beginning of this section, we have here assumed that they are either

constant (the "instantaneous change" assumption), or that they have steady-state values that are themselves unique functions of T and σ.

In practice, both may change as a function of strain and time, and no experimental observation of the operational parameters m and Q can be done "instantaneously" or without involving any plastic strain. It is then an important question how one should extrapolate the observations to either "instantaneous" or "steady-state" values; we shall deal with it in sec. 64. Another question is, which of these limiting cases is the property of interest? In the following sections, we shall deal with two simple cases: first, that changes in both obstacle structure and mobile dislocation density produce negligible effects in the operational parameters, which turns out to be the case when m is large; second, that changes in mobile dislocation density may produce important effects (m small), but the obstacle structure can be assumed constant. We do not treat in this article the case when changes in obstacle structure through work hardening and recovery must be considered.

The Approximate Magnitudes of the Terms of the Arrhenius Equation

It is useful at this point to set some reasonable limits on the magnitude of $\dot{\gamma}_o$ and ΔG, and on the way in which they vary with stress and temperature. One can do this only by invoking the models for thermally activated flow processes developed in Chapters 2 through 5; but the limits we list below are sufficiently wide that they include the entire range of variants that the models could reasonably adopt.

The preexponential term, $\dot{\gamma}_o$, has a value in the range between 10^5 and 10^{10} per second, that is

$$10^5 < \dot{\gamma}_o[s^{-1}] < 10^{10}. \qquad [61r]$$

This is arrived at by noting that

$$\dot{\gamma}_o = \nu_G \gamma_o$$

where ν_G is of the order 10^{11} (limits 10^{10} to 10^{12} s^{-1}: see sec. 42). It varies with stress through the obstacle stiffness (roughly linearly), but is effectively independent of temperature. In sec. 33, models for γ_o were discussed. Typically, γ_o has a value of about $10^{-4\pm1}$, varies with stress as $(\sigma/\mu)^{1\pm1}$, and is also practically independent of temperature except through $\mu(T)$. Assembling this information gives the limits for $\dot{\gamma}_o$ noted above. It typically varies with stress as $(\sigma/\mu)^{2\pm2}$, contributing a part $m_o = 2 \pm 2$ to the total stress dependence we have called m. And it varies only weakly with temperature.

Most laboratory mechanical tests are carried out in the strain-rate range 10^{-6} to 10^{-2} s^{-1}, since this is the range available on normal testing equipment and within the time range of most laboratory experiments. This sets limits to the value of $Q/kT \simeq \ln(\dot{\gamma}_o/\dot{\gamma})$ that are readily measurable:

$$\boxed{16 < \ln \dot{\gamma}_o/\dot{\gamma} < 35.} \qquad [61s]$$

For later use we take as a typical value

$$\ln \dot{\gamma}_o/\dot{\gamma} \approx 20. \qquad [61t]$$

This means that around room temperature, where $kT \approx \frac{1}{40}$ eV, only activation energies in the range

$$0.4 < Q[\text{eV}] < 0.9 \qquad [61u]$$

are accessible to normal experiments.

One might wish to include tests using special equipment, spanning a wider strain-rate range from 10^{-8} to 10^{2}/s. This widens the limits on $\ln \dot{\gamma}_o/\dot{\gamma}$ to

$$8 < \ln \dot{\gamma}_o/\dot{\gamma} < 40 \qquad [61s']$$

and, at room temperature, makes activation energies in the range 0.2 eV to 1 eV accessible. Note that even this is a rather limited range—if the activation energy of the rate-controlling step lies outside this range, the strain rate is either too slow or too fast to be measurable.

Using the result [61t], we can immediately assign an order of magnitude to readily measurable activation energies $\Delta G(\sigma,T)$ of roughly $20kT$. Their stress dependence was discussed in sec. 43, where it was shown that it can often be represented by (eq. [43w])

$$\Delta G(\sigma) = F_o \left(1 - \left(\frac{\sigma}{\hat{\tau}}\right)^p\right)^q$$

where $0 < p \lesssim 1$ and $1 \lesssim q \lesssim 2$ (eq. [43w']). For the most commonly encountered cases, this typically reduces to (eq. [43w"]).

$$\Delta G(\sigma) = F_o \left(1 - \left(\frac{\sigma}{\hat{\tau}}\right)^{1/2}\right)^{3/2}.$$

Its typical temperature dependence is more difficult to characterize; it depends, as discussed in secs. 43 and 61, on the way in which the physical constants that enter F_o and $\hat{\tau}$ vary with temperature. One common case is that which arises when the shear modulus is the only important contributor to a temperature dependence: then ΔG decreases slowly with increasing temperature, falling to roughly half its room temperature value at the melting point of the material.

62. Activation Analysis for Rate Insensitive Materials

The operational parameter describing the rate sensitivity of the flow stress (or rather the rate "insensitivity"), was defined in eq. [61b] as

$$m \equiv \left.\frac{\partial \ln \dot{\gamma}}{\partial \ln \sigma}\right|_T. \qquad [62a]$$

It is often found to be quite large: for example, in precipitation hardened or

pure fcc materials at room temperature, m is of order 100. In this case, a change in strain rate by a factor of 10 produces a change in flow stress of approximately 2%. Similarly, a 10% change in temperature produces approximately a 2% change in flow stress; this can be seen by inserting $Q/kT \simeq \ln \dot{\gamma}_o/\dot{\gamma} \simeq 20$ into eq. [61c]:

$$\left.\frac{\partial \ln \sigma}{\partial \ln T}\right|_{\dot{\gamma}} = -\frac{Q}{mkT} \simeq -\frac{20}{m}. \qquad [62b]$$

Of course, one cannot really speak of a rate-sensitive *material.* It is only in certain *ranges* of stress and temperature that a given material exhibits a large value of m—larger, say, than 20. For these ranges certain generalizations, which we now set out, can be made.

Data Reduction

In principle, contributions to m could arise from a stress dependence of the preexponential terms and from that of the activation energy (eq. [61b']). We pointed out at the end of sec. 61 that the preexponential contributes at most 4 to m. When the material is rate insensitive, as we have assumed here, with a total exponent $m > 20$ (and typically about 100), we may assume that *the stress dependence of the preexponential terms is negligible in comparison with that due to exponential terms*

$$m_o \equiv \left.\frac{\partial \ln \dot{\gamma}_o}{\partial \ln \sigma}\right|_T \ll m(\sigma, T) \qquad [62c]$$

or equivalently

$$\frac{m_o kT}{\sigma} \equiv kT \left.\frac{\partial \ln \dot{\gamma}_o}{\partial \sigma}\right|_T \ll b\Delta a' \qquad [62c']$$

so that

$$kT \left.\frac{\partial \ln \dot{\gamma}}{\partial \sigma}\right|_T \simeq b\Delta a'. \qquad [62d]$$

The last equation permits a very easy and direct quantitative determination of the glide resistance profile from strain-rate change tests at various temperatures.

To get the widest possible range of the glide resistance profile, one must test the strain-rate sensitivity at different temperatures. Any dependence of the profile itself on temperature (Fig. 43-3a) then becomes important.

We have seen in the last section (eq. [61q]) that the first-order effects are well accounted for by assuming the temperature dependences of the shear modulus and the Burgers vector to be the main effects. The appropriate variables are then σ/μ and $kT/\mu b^3$. The assumption can be tested by observing straight lines in the normalized Arrhenius plot (Fig. 61-6a).

The approximate constancy of $\dot{\gamma}_o$ can now be tested, and its value found, by plotting the normalized activation energy $g \equiv \Delta G/\mu b^3$, as it is obtained from the modified Arrhenius plot (Fig. 61-6a), versus temperature at constant strain rate, in the manner of Fig. 61-3: it should be a straight line through the origin.

To make the best use of the data, one should plot them all on a single diagram of σ/μ versus the combined parameter $(kT/\mu b^3) \ln (\dot{\gamma}_o/\dot{\gamma})$, as in Fig. 61-7. This is made possible by the assumption of a constant $\dot{\gamma}_o$; its approximate value can also be found by trial and error until all points fall on a single curve in this diagram.

Qualitative Separation of Mechanisms

Some important qualitative conclusions about the nature of the obstacles can, however, immediately be deduced from the fact that m is large. The meaning of the large value of m, in its mechanistic interpretation (62f), can be gauged by a slight expansion of that equation:

$$m \simeq \frac{\Delta W'}{\Delta G} \cdot \frac{\Delta G}{kT} = \frac{\Delta W'}{\Delta G} \ln \frac{\dot{\gamma}_o}{\dot{\gamma}}. \qquad [62e]$$

The logarithmic term is typically about 20 (eq. [61t]). Since m is supposed to be larger than 20, *the apparent activation work* $\Delta W' = \sigma b \Delta a'$ *must be larger than* ΔG. Figure 62-1 shows two ways in which this can happen.

First (Fig. 62-1a), the applied stress may be near the mechanical threshold. This must happen for all manner of mechanisms at very low temperatures. When the temperature of the experiments is not "very low", it may still be low compared to the temperature T_o that corresponds to the total activation energy of a *short-range* obstacle. (This temperature may be far in excess of the melting point; an example is provided by large precipitates.)

Second (Fig. 62-1b), the glide resistance mechanism may be *long-range* in nature (i.e. have infinite total activation energy); or it may consist of *two components* of which one is long range or even "athermal". In this case, the mechanical threshold may be considerably above the applied stress.

Figure 62-2 shows the normalized stress vs. temperature diagram for three typical mechanisms: (a) a short-range one with a high T_o (10 times the range shown on the abscissa); (b) a truly long-range mechanism; and (c) a short-range mechanism superimposed on an athermal plateau. The constants were chosen, within a reasonable range, to make the curves look similar. It is seen that the plateau in curve (c) can at best be distinguished in the top 20% of the temperature range.

A more characteristic behavior of a two-component mechanism is evident when m is plotted versus (inverse) temperature at constant strain rate (Fig. 62-3): as the athermal mechanism is approached, m must rise again. This effect should be seen even at about half the temperature where only the

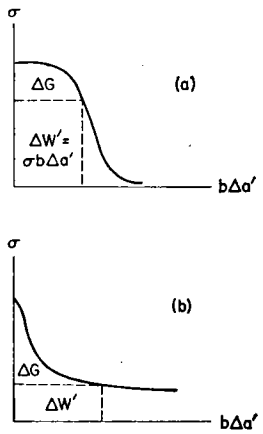

FIG. 62-1. Two examples [(a) and (b)] of obstacles for which $\Delta W' > \Delta G$, when m is large.

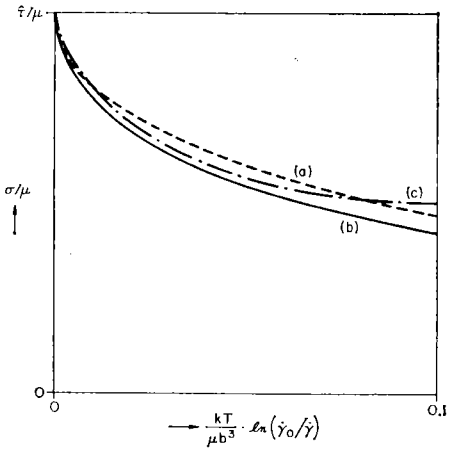

FIG. 62-2. A flow stress versus temperature diagram in proper normalization for rate insensitive materials. The three curves shown are:
(a—dotted line): for a "short-range" obstacle with a high total activation energy and a stress dependence

$$\Delta G = \mu b^3 \cdot \left[1 - \left(\frac{\sigma}{\hat{\tau}}\right)^{1/2}\right]^2.$$

(b—solid line): for a "long-range" mechanism such as unlocking of a continuously pinned dislocation, with an activation energy

$$\Delta G = \frac{\mu b^3}{5} \cdot \frac{[1-(\sigma/\hat{\tau})^{1/2}]^{3/2}}{\sigma/\hat{\tau}}.$$

(c—dash-dotted line): for a superposition of a short-range obstacle with an athermal mechanism characterized by $\hat{\tau}_\mu = \hat{\tau}/2$:

$$\Delta G = \frac{\mu b^3}{10} \cdot \left[1 - \left(\frac{\sigma - \tau_\mu}{\hat{\tau} - \tau_\mu}\right)^{1/2}\right]^{3/2}.$$

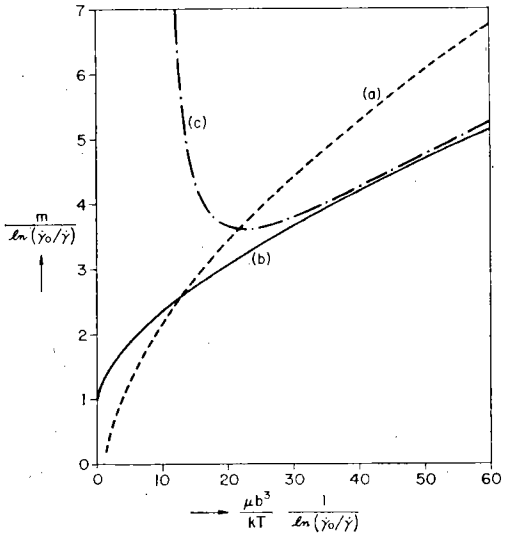

FIG. 62-3. The exponent m, the inverse relative strain-rate sensitivity of the flow stress, as measured at a given standard strain rate over a range of temperatures, for the three types of mechanism illustrated in Fig. 62-2. For a two-stage mechanism (c), m goes through a minimum at roughly half the temperature where the short-range mechanism ceases to contribute to the flow stress.

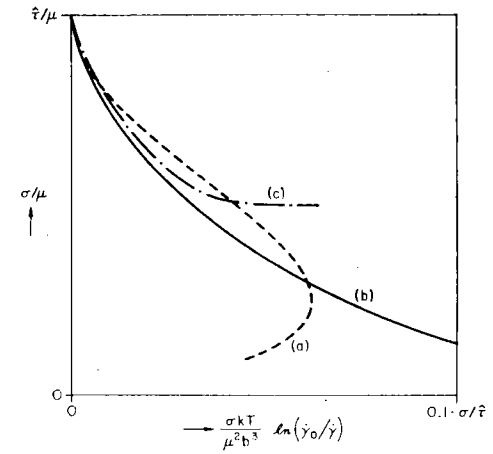

FIG. 62-4. A diagram designed to separate mechanisms with an infinite total activation energy (b) from those with merely a large one (a). The two-stage mechanism (c) also appears more abrupt than in Fig. 62-2. (The formulae introduced in Fig. 62-2 were used.)

athermal mechanism survives. The other two curves may not be experimentally distinguishable, although they exhibit a very characteristic difference in their extrapolation to high temperatures: in the short-range mechanism with the high T_o (curve a), m should continuously decrease to low values (it would reach zero at T_o); but in the long-range mechanism (curve b) m extrapolates to $\ln(\dot{\gamma}_o/\dot{\gamma})$ at infinite temperature: it always stays above 20. Only in the "limiting long-range mechanism", namely where $\Delta G \propto \ln(\hat{\tau}/\sigma)$, would one obtain an exactly straight line through the origin in this diagram.

A final diagram that may help separate the mechanisms discussed here is one of σ versus $\sigma \cdot T$, suitably normalized (Fig. 62-4). If the activation energy indeed has a $1/\sigma$-dependence, as it does for dislocation unlocking mechanisms (curves b in Figs. 62-3–62-4), then this dependence is eliminated in Fig. 62-4 and the remaining function is the dependence of the numerator on σ, which should be like that of any short-range mechanism (see Fig. 43-9). On the other hand, a short-range mechanism with a high T_o should show a characteristic reversal of curvature (curve a in Fig. 62-4), and the two-stage mechanism should show an accentuated plateau (curve c).

Determination of Mechanistic Parameters

Figure 62-4 already provided the final answer, if it indicated a dislocation unlocking mechanism or other very long-range interaction. In simple cases, one may obtain clearer evidence for a particular functional dependence of $\sigma\Delta G(\sigma)$ by raising the coordinates in Fig. 62-4 to various powers until the data fall on a straight line. However, the large value of m itself implies that the stress range accessible to experiments is not very wide. Most useful information about the binding potential can be obtained by going to low temperatures.

If the analysis of Figures 62-2 through 62-4 pointed towards short-range obstacles with a high T_o, it is probably a set of large, strong, widely spaced discrete obstacles such as precipitates, or possibly radiation damage or forest dislocations. The force vs. activation-distance diagram of the obstacle may then be obtained by plotting $(\sigma/\mu)^{2/3}$ vs. $(\Delta a'/b^2)(\sigma/\mu)^{1/3}$, as in Fig. 44-6, and phenomenological forms for it may be obtained by using the procedure prescribed in Fig. 44-7. However, as indicated in Fig. 62-2, the very rate insensitivity prevents one from getting the lower portion of this profile. Thus, the exponent p in the phenomenological description [43w″] of the activation energy cannot be obtained. One may set it to its maximum value $\frac{2}{3}$ for discrete obstacles (eq. [44ℓ′]) and write

$$\Delta G = \tilde{F}_o \cdot \left\{1 - \left(\frac{\sigma}{\hat{\tau}}\right)^{2/3}\right\}^q. \qquad [62f]$$

However, the constant F_o would be the total activation energy only if p were really $\frac{2}{3}$ for the entire obstacle profile; if p is lower than this maximum value, the obstacle has a "tail" at low stresses, and $\tilde{F}_o$ becomes a lower bound to the

real total activation energy:

$$\tilde{F}_o < F_o. \qquad [62g]$$

Finally, the analysis of Figs. 62-2 through 62-4 may have indicated the existence of a two-stage mechanism. We have emphasized before (sec. 43) that two mechanisms that relate to the *same* obstacle are, *in principle*, not separable by macroscopic measurements. However, if they relate to two different agencies, such a separation is possible if one can control the density or spacing of at least one of them.

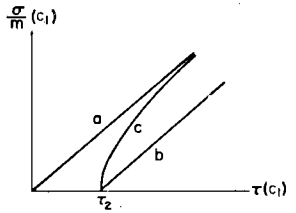

FIG. 62-5. The separation of two contributions to the flow stress by varying the density c_1 of one of them: (a) single profile; (b) two profiles, additive flow stresses; (c) two profiles, additive densities.

If at least part of the glide resistance profile is due to *discrete obstacles*, we can make use of the fact that their contribution to the flow stress varies inversely as their spacing, whereas their contribution to the activation area varies linearly with the spacing. This leads to a procedure, outlined in detail in sec. 44, of testing whether these obstacles are the only essential ones or, if they are not, of separating the various contributions.

If one can vary the area density of the discrete obstacles while measuring both flow stress and (apparent) activation area, one must plot $b^2/\Delta a' = b^2\sigma/kT\mathrm{m}$ (a measure of the reciprocal of the obstacle spacing) vs. τ, the flow stress at a standard temperature and strain rate, as this density is varied (Fig. 62-5): if a straight line through the origin is observed, the obstacles whoes density was varied provide the *only* contribution to both flow stress and activation area. If the points lie on a line, straight or not, that extrapolates to a positive intercept on the abscissa, there is at least one other contribution to the flow stress, which is less thermally activated (or not thermally activated at all). If the intercept is negative, another mechanism must be primarily responsible for the rate dependence. In Figs. 44-8 through 44-13, we have given the prescription for a separation of the respective contributions.

If by this procedure two separate contributions were found, the complete τ_1–Δa_1 diagram for the rate-controlling mechanism can be determined. One may do this by using a phenomenological relation of the kind (eq. [43w‴])

$$\Delta G = F_1 \cdot \left\{1 - \left(\frac{\sigma - \tau_2}{\hat{\tau} - \tau_2}\right)^{p_1}\right\}^q \qquad [62h]$$

where q essentially describes the shape of the top of the τ–Δa diagram

($q = 1$: flat; $q = \frac{3}{2}$: rounded; $q = 2$: pointed). This parameter should be easily found, now that the top part of the diagram is well known. Since, when τ_2 is known, the rate-controlling mechanism can be investigated in its entire stress range, p_1 can also be determined.

One may then proceed to get the force-distance diagram, if the rate-controlling mechanism is based on randomly dispersed discrete obstacles, by plotting

$$\left(\frac{\sigma-\tau_2}{\mu}\right)^{2/3} \text{ vs. } \frac{\Delta a'}{b^2}\cdot\left(\frac{\sigma-\tau_2}{\mu}\right)^{1/3}$$

which are proportional to K_1 and Δy_1, respectively (Fig. 44-6).

If activation energies are also measured, it must be remembered that this case of a two-stage profile (sec. 43) is the one in which there may be large discrepancies between $Q \simeq \Delta H$ and ΔG, and (near the plateau) between $-(\partial \Delta H/\partial \sigma)|_T$ (as determined from the stress dependence of the Arrhenius slopes) and $b\Delta a'$. Again, this could be avoided by using so-called "effective stresses" $\sigma-\tau_2$ (eq. [43r]) which, however, gives new information only if the activation entropy is *not* well described by the temperature dependence of shear modulus and Burgers vector.

63. Activation Analysis for Rate-Sensitive Materials

In contrast to the case discussed in the last section, we shall deal here with experiments in which the relative change in flow stress upon a change in strain rate or temperature is substantial so that, typically, $m < 10$. Again, m could in general depend on stress and temperature, so that we are not strictly dealing with a particular class of *materials*; we merely refer to materials that have a low value of m over at least part of the range of the experiments.

Qualitative Identification of Mechanisms

In the general framework of dislocation kinetics, we have encountered one region in which m may be low (Fig. 63-1): at stresses *above* the mechanical threshold, where phonon drag effects become important. This region can be further identified by two phenomenological observations (Fig. 63-1):

$$Q < 0; \qquad \left.\frac{\partial m}{\partial \sigma}\right|_T < 0. \qquad [63a]$$

This is a region of interest for the study of lattice drag, but it is irrelevant to macroscopic flow in steady state under normal test conditions.

When the conditions [63a] are *not* obeyed, thermal activation controls the strain rate, and we can use the identification [61b'] of m with model parameters. Since we have seen that the stress dependence of the preexponential factors m_o is typically 2 ± 2, this can no longer be considered a negligible contribution to the total m. But the fact that this reduces the contribution to m due to the activation work even further allows one to again draw important qualitative conclusions about the nature of the glide resistance profile.

Not surprisingly, these conclusions are the opposite ones from those arrived

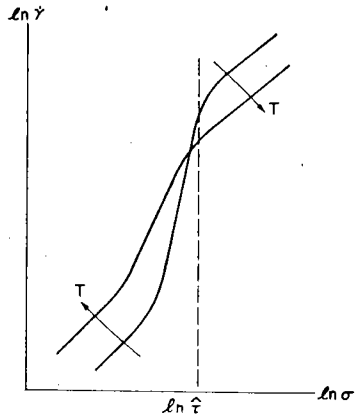

FIG. 63-1. Above the mechanical threshold $\hat{\tau}$, the flow stress is controlled by phonon and other drags and increases with increasing temperature. This leads to negative experimental activation energies.

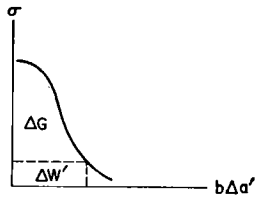

FIG. 63-2. Diagram illustrating the situation when $\Delta W' < \Delta G$, when m is small.

at for large m (Fig. 62-1): the apparent activation work $\Delta W'$ must now be *small* compared to ΔG (eq. [62c']). Thus, we must be concerned with the *lower portion of the glide resistance profile*, and it must necessarily be of the *short-range* kind (Fig. 63-2).

It is evident that in the temperature range where m is small, it is a reasonable aim to obtain the total activation energy F_o of the process and the shape of the "tail" of the profile, but *not* the maximum glide resistance and the shape of the "top". Of course, lowering the temperature would make the top of the obstacle accessible to measurement—although m would become large in the process and, since the obstacles now must be small, inertial effects could make measurements difficult.

Working in the lower range of the obstacle profile implies being near the temperature T_o (eq. [45o]). Thus, from eq. [61t], the order of magnitude of F_o is given by

$$F_o \approx kT \ln \frac{\dot{\gamma}_o}{\dot{\gamma}} \approx 20kT. \qquad [63b]$$

That is, about 0.5 eV at room temperature.

The average activation area must then be, in order of magnitude,

$$\frac{\overline{\Delta a}}{b^2} \approx \frac{F_o}{\hat{\tau} b^3} \approx 20 \frac{kT}{\mu b^3} \frac{\mu}{\hat{\tau}}. \qquad [63c]$$

At room temperature, this would be between about 5 and 200 for interesting values of $\hat{\tau}$.

Contribution from Glide Resistance Profile

When m is small, the stress dependence of the various preexponential terms is not negligible; in fact, it may be dominant. It is then hopeless to obtain a profile $\Delta a'(\sigma)$, even in its lower range, from m/σ, i.e. from strain-rate changes.

On the other hand, it is always possible to get

$$\left.\frac{\partial \Delta H}{\partial \sigma}\right|_T = \left.\frac{\partial Q}{\partial \sigma}\right|_T \qquad [63d]$$

so long as the *temperature* dependence of the preexponential terms is known or negligible (eqs. [61a'], [61a"]). Fortunately, we have seen that a small value of m implies a short-range obstacle, and that this, in turn, suggests that the stress dependence of the activation entropy may be negligible (eq. [43o]) which makes

$$b\Delta a' \simeq -\left.\frac{\partial \Delta H}{\partial \sigma}\right|_T = -\left.\frac{\partial Q}{\partial \sigma}\right|_T. \qquad [63d']$$

The obstacle profile may thus, in principle, be obtained from the stress

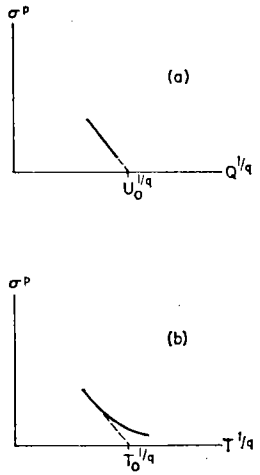

FIG. 63-3. (a) The appropriate way to extrapolate data for Q as a function of σ to zero σ, in order to obtain U_o. (b) This extrapolation is inappropriate because of the curvature of the plot at small σ.

dependence of the Arrhenius slopes. The very fact that m is small, however, makes $\Delta W' \ll \Delta G$ (eq. [62c']) so that the relative variation in Q with stress is bound to be small. It is, in fact, frequently neglected.

If it is, nevertheless, measurable, one should try to plot an appropriate power of σ against an appropriate power of Q such that the diagram becomes a straight line and can be extrapolated to zero stress to obtain U_o (Fig. 63-3a). This is better than plotting σ against T to find T_o (Fig. 63-3b), since $\dot{\gamma}_o$ can now not be assumed constant. For the special case that reverse jumps are important, we had seen in Fig. 45-4 that T_o would be virtually impossible to determine.

We have here neglected to account for the variation of elastic constants or Burgers vector with temperature. This is reasonable, because a small m implies a strong temperature dependence due to thermal activation alone (eq. [62b]). However, the appropriate corrections can easily be made, in which case Q is replaced by g and U_o by $F_o/\mu b^3$.

Contributions from Preexponential Terms

The total stress dependence of all preexponential terms is easily obtained from eqs. [61b'] and [63d']:

$$\left.\frac{\partial \ln \dot{\gamma}_o}{\partial \ln \sigma}\right|_T = \mathrm{m} - \frac{1}{kT}\left.\frac{\partial Q}{\partial \ln \sigma}\right|_T. \qquad [63e]$$

Since we found that T_o must be near the test temperature when m is small, reverse jumps may well be important (sec. 45). Then the preexponential term must be modified from eq. [61e'] according to eq. [45j] (presuming $\sigma \gg \tau_{\mathrm{STOR}}$):

$$\dot{\gamma}_o = \gamma_o \cdot \nu_G \cdot \frac{\sigma b a}{kT}. \qquad [63f]$$

The two main contributions to a stress dependence of $\dot{\gamma}_o$ are: the mobile dislocation density ρ_m; and the frequency factor ν_G through the normalized stiffness C of the obstacle (eqs. [42o], [42p], [42v]). Thus,

$$\left.\frac{\partial \ln \dot{\gamma}_o}{\partial \ln \sigma}\right|_T \simeq 1 + \frac{\mathrm{d} \ln \rho_m}{\mathrm{d} \ln \sigma} + \frac{\mathrm{d} \ln C}{\mathrm{d} \ln \sigma}. \qquad [63g]$$

One may be able to separate these contributions by the following mechanistic assumption: *the mobile dislocation density cannot change instantaneously*. This statement is almost self-evident, if the meaning of "mobile dislocation density" is as used in this treatise, viz. the pool of all dislocations that may potentially be activated to produce strain of the required kind during the experiment. Any change in the number of these dislocations requires both time and strain. As pointed out before, if the density of *moving* dislocations changes instantaneously, it is better treated by an activation term itself.

Assuming, then, that both an *instantaneous* change in stress upon a change in

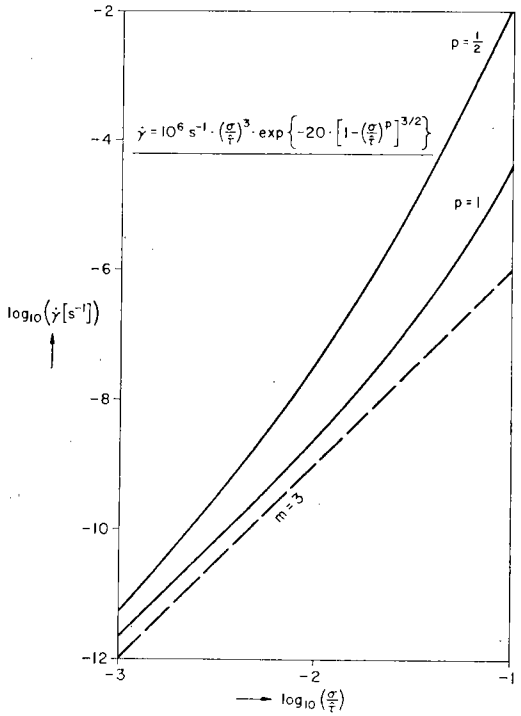

FIG. 63-4. Illustration of the gradual transition from "power-law creep" to "exponential creep" when the stress dependence of the activation energy is fully included.

strain rate (or any other of the operational derivatives) and an *asymptotic* change corresponding to the steady-state density of mobile dislocations can be measured, let us designate these by the superscripts i and a, respectively, on the derivatives. Our mechanistic assumption then amounts to saying that

$$\left.\frac{\partial \ln \rho_m}{\partial \ln \sigma}\right|^{i}_{T,\tau} = 0 \qquad [63h]$$

or

$$\left.\frac{\partial \ln \dot{\gamma}}{\partial \ln \sigma}\right|^{i}_{T,\tau} = \left.\frac{\partial \ln \dot{\gamma}}{\partial \ln \sigma}\right|_{T,\tau,\rho_m}. \qquad [63i]$$

If all other pre-exponential terms are instantaneously adjustable, this makes it possible to separate the effects of a change in mobile dislocation density from all others.

The stress dependence of the steady-state mobile dislocation density follows from

$$\left.\frac{\partial \ln \rho_m}{\partial \ln \sigma}\right|_{\tau} = \left.\frac{\partial \ln \dot{\gamma}}{\partial \ln \sigma}\right|^{a}_{\tau} - \left.\frac{\partial \ln \dot{\gamma}}{\partial \ln \sigma}\right|^{i}_{\tau}. \qquad [63j]$$

To be consistent with the general model presented here, the difference [63j] must be of order 2.

As pointed out in sec. 61, the stress dependence of $\dot{\gamma}_0$ contributes, typically, 2 ± 2 to m. The rate equation then becomes

$$\left.\begin{aligned} \dot{\gamma} &= A\sigma^{3\pm 2} \exp - \frac{\Delta G}{kT} \\ &= A'\sigma^{3\pm 2} \exp - \frac{\Delta H}{kT} \end{aligned}\right\} \qquad [63k]$$

where A and A' are constants. This is a form frequently encountered in measurements of high-temperature creep (see, for example, WEERTMAN, 1968; or MUKHERJEE *et al.*, 1969).

As was discussed in detail in sec. 45, the activation energy in eq. [63k] should still, in principle, be stress dependent—although this stress dependence matters less and less as the stress is decreased. To show the kind of effect to be expected, we have plotted in Fig. 63-4 a log $\dot{\gamma}$ versus log σ diagram for two typical relations $\Delta G(\sigma)$, in the low-stress range. For the very short-range obstacle (p = 1), the slope is very close to 3 over a significant range; for the longer-range one, m varies continuously from about 3 at $\sigma = 10^{-3}\hat{\tau}$ to about 6 at $\sigma = \hat{\tau}/10$.

64. Structure Changes and Extrapolation Procedures

We have, throughout this entire article, dealt with the constitutive relation of a material in a given state or at a given structure (equation 1a), and have deliberately excluded from treatment any changes of structure during the tests (eqs. [1b]). Thus, for example, we have assumed that any solid solution is stable and does not precipitate; that any precipitate or dispersion is stable and does not coarsen or dissolve; that solute atoms do not segregate to, or move with, moving dislocations; that the grain size does not change during the test; and so on. One kind of structure change, however, cannot be avoided in any tests of plastic properties: changes in the density and distribution of dislocations. Even if we do not wish to treat these processes in any detail, we must give an operational definition of what is meant by "tests at constant structure"; i.e. we must specify a test in which the structure does not change, or prescribe a back-extrapolation procedure by which the changes in structure are eliminated from the results.

We have, from section 22 on, used the dislocation glide rate $\dot{\gamma}$ as if it were the macroscopic strain rate $\dot{\epsilon}$ (except for a trivial orientation factor). In fact, $\dot{\gamma}$ is not an operational variable: for example, elastic and anelastic strain rates must be subtracted from the measured variable $\dot{\epsilon}$ to obtain the plastic strain rate. While, in principle, the plastic *strain* can be measured after unloading, there is no such easy prescription for the plastic strain *rate*. Another—and more important—reason for a discrepancy between a macroscopically measured strain rate $\dot{\epsilon}$ and a meaningful glide rate $\dot{\gamma}$ is the possible existence of macroscopic heterogeneities in deformation. While, again, we have excluded

a treatment of the many aspects of this problem from the present text, we shall outline below one particularly simple and important example: the steady-state propagation of a Lüders front.

Work Hardening

Figure 64-1 shows a typical stress–strain diagram obtained in a tensile test. Upon the first loading, it shows a rapid curvature, indicating the transition from elastic to plastic deformation. The slope of the stress–strain curve (Fig. 64-1) changes in this range by a factor of the order of 100. It is common (and correct) practice to obtain the "yield stress" of the material by back-extrapolating the stress strain curve to zero plastic strain.

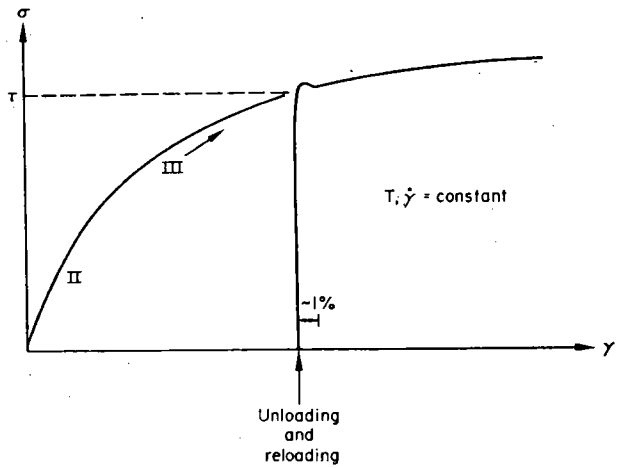

FIG. 64-1. Typical stress–strain diagram at constant temperature and strain rate, on a scale where the elastic slope appears to be infinite. When all (re)loading transients have been eliminated, the curve becomes a locus of the flow stress as a function of the prestrain.

If the specimen is unloaded after a certain amount of plastic strain and immediately reloaded, an initial transition region also occurs, often somewhat different in character; an example is shown in the Figure. The important observation is that, after this initial transition region (which may take fractions of a percent strain), the plastic curve follows precisely the forward extrapolation of the curve obtained before unloading. The back-extrapolated stress at zero plastic strain in the second test is called the current flow stress. A diagram looking very similar to Fig. 64-1 may thus be obtained that is a locus of the *flow* stress as a function of *pre*-strain: in principle obtained by a series of frequent unloadings and reloadings (allowing enough strain to take the material through the transient each time). This is the work-hardening diagram τ versus γ.

Work hardening is due to a change in the density (and possibly the arrange-

ment) of dislocations, through their effect on the glide resistance diagrams. It is a property of the dislocation structure that is retained in the unloaded state. This change in the "static" structure must be distinguished from the dislocation rearrangement occurring during loading and unloading: it is of a "dynamic" nature. For example, dislocations may become "mobilized" or generated, and they may multiply or form dynamic pile-ups. We have discussed some of these dynamic changes in sections 24, 32, and 33. Our concern with long-range slip has caused us to concentrate on a situation when these phases have reached their respective steady states. The adjustment of the dislocation structure while this steady state is being achieved is one cause of the transients observed after loading or reloading in Fig. 64-1. In earlier discussions, we have eliminated these effects by extrapolating through them (except in one case discussed in section 63).

The changes in the dynamic dislocation structure are different in principle from changes in the "static" structure due to work hardening: they occur in response to the change in the external boundary conditions on a specimen *whose initial state is entirely characterized by the "static" structure before the change*. Thus, dynamic structure parameters are not "parameters of state" and no macroscopically useful information can be derived by attempting to perform experiments at constant dynamic (as well as static) structure. Such experiments could, of course, help in the identification of mechanisms, but it is doubtful that there is any way of performing them with absolute confidence that no aspect of the structure has changed.

Abrupt Changes in Boundary Conditions

The kinetic laws we have discussed in earlier chapters are concerned with the relation between stress, temperature and strain rate. To measure such relations, at least one of these variables must be changed deliberately and the response measured. It is of no use, for this purpose, to obtain complete work-hardening diagrams of the kind shown in Fig. 64-1 for different strain rates or temperatures: the change in structure with strain may well depend on the strain rate or temperature itself. In fact, many work-hardening diagrams have a stage (labeled II in Fig. 64-1) whose slope is insensitive to strain rate and temperature (and approximately linear); in this stage, the difference between different continuous curves does allow at least approximate conclusions concerning the relation between flow stress, strain rate and temperature. On the other hand, in the following stage III, which exhibits a continuously decreasing slope, the work hardening curves and the corresponding structure changes are quite sensitive to strain rate and temperature. Here, one can derive relations between strain rate, stress and temperature "at a given structure" only by imposing an abrupt change in one of the variables.

As an example, Fig. 64-2 shows an abrupt change in strain rate and/or temperature at two places in a tensile test. The first is after a prestrain γ_1 in stage II of work hardening. Here, a transient of the same general character as

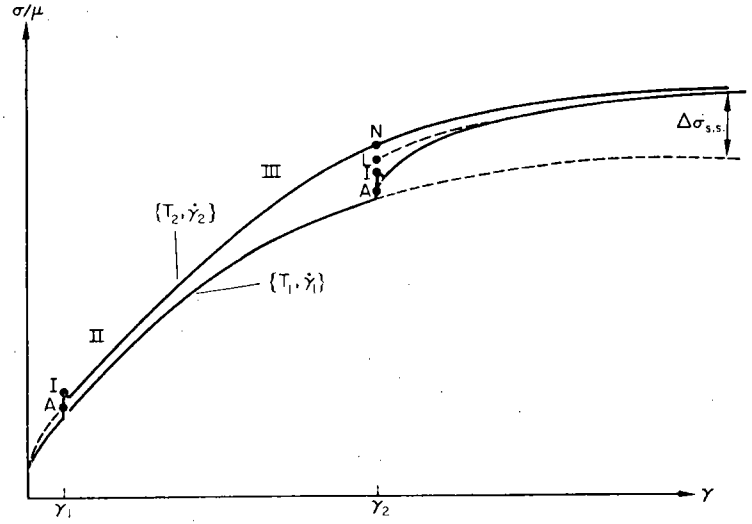

FIG. 64-2. Two stress–strain curves with an abrupt increase in strain or decrease in temperature: one after prestraining into stage II, the other into stage III of work hardening. Extrapolations of the curves at constant strain rate and temperature are shown dashed. Various methods of back-extrapolation to the amount of the abrupt change are indicated by capital letters.

upon unloading and reloading during a test is frequently observed; namely, a small overshoot and subsequent drop in the stress. There is no difficulty in extrapolating the "long-range" stress–strain curve back through the transient and thus obtaining the flow stress at A (see, for example, MAKIN 1958, HAASEN 1958, DIEHL and BERNER, 1960). Conversely, it is possible (although only with very hard machines and very good resolution of measurement, see MECKING and LÜCKE, 1966) to obtain the "instantaneous" stress change at point I before the dynamic changes leading to the transient become operative (see section 63).

The situation is much more complex after straining into stage III, at the pre-strain γ_2. An increase in strain rate (or a decrease in temperature) here leads to at least two transients: one of the same kind described before and another one that is much more gradual and may extend over several percent of subsequent strain. Its characteristic is an initial severe change in work-hardening rate from the one before the abrupt change, and a gradual approach of the work-hardening rate to the "normal" one corresponding to the new strain rate or temperature. Here, we have three possibilities of extrapolation: the "asymptotic flow stress" at A, the "instantaneous stress change" at I, and the "long-range extrapolation" at L. For completeness, we have also indicated in Fig. 64-2 the flow stress of a *continuous* stress–strain diagram at

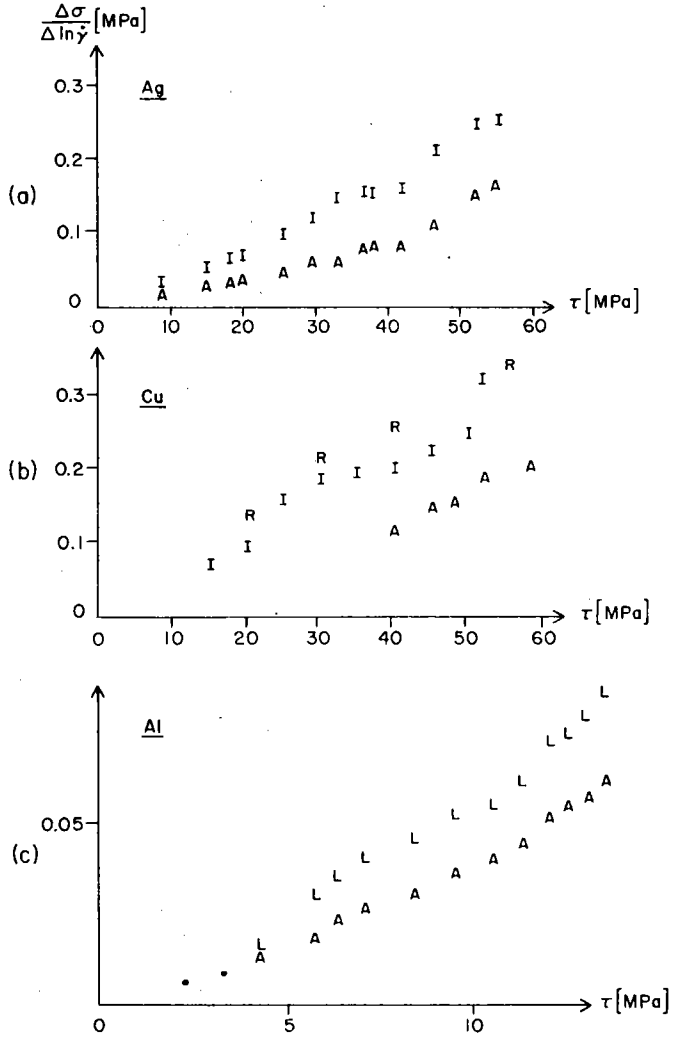

FIG. 64-3. The strain–rate sensitivity of the stress as defined by various measurement and evaluation methods, as a function of the flow stress attained before the change: (a) Silver (MECKING, 1967); (b) copper (C. Y. CHENG, unpublished results, summarized in CHENG and KOCKS, 1970); the symbol R refers to stress relaxation tests to be discussed later; (c) aluminum (H. S. CHEN, unpublished results, summarized in KOCKS *et al.*, 1968).

the new strain rate, taken to the same pre-strain γ_2, at point N. As we discussed above, this stress is of *no* relevance to the kinetic law at a given structure.

From the point of view of describing the flow stress for long-range slip, the extrapolation to A would be consistent with the previous treatment. This is hard to obtain in practice—primarily because the stress–strain diagram is rather strongly curved in the initial part of the long transient. Other

authors (e.g. COTTRELL and STOKES, 1955; BASINSKI, 1959; THORNTON *et al.*, 1962; MECKING and LÜCKE, 1966) have preferred the extrapolation I, or a use of the "upper yield stress" after the change (which depends on the hardness of the machine). In very few experiments has more than one method been used. Figure 64-3 shows three such cases, plotted as a function of the flow stress reached during the pre-straining. It is seen that, in all cases, one may claim a proportionality of the stress changes $\Delta\sigma$ obtained from the different methods of extrapolation; the absolute values differ by about a factor of 2.

It thus appears that the method of extrapolation chosen is not of critical importance in these cases—although it is not clear that this can always be relied upon.

Stress Relaxation

The stress relaxation test is a special case of an abrupt change in boundary conditions: the sudden arrest of the cross-head in a hard machine. Any further plastic strain in the specimen is now coupled, by interaction with the elastic strains in both the specimen and the machine, to a decrease in load. If one plots the logarithm of this negative slope in the resulting stress–time diagram versus the stress, one immediately has the kinetic diagram whose slope is related to the operational activation area; if, instead, the stress is also plotted logarithmically, the slope is the operational parameter m. To translate the *absolute magnitudes* on the logarithmic stress rate axis to logarithmic strain rates, it is easiest to make the back extrapolation to the point of unloading match the prescribed strain rate in the preceding tensile tests.

The continuous nature of the stress relaxation tests, once initiated, makes it especially attractive for a derivation of the stress versus strain rate relation. Moreover, an especially wide range of strain rates can be obtained (provided the experimental difficulty of keeping the temperature sufficiently constant has been solved). The chief advantage of the stress relaxation tests, however, as seen by its many recent proponents (e.g. FELTHAM, 1961; GUIU and PRATT, 1964; HULL and NOBLE, 1964; SARGENT, 1965; GUPTA and LI, 1970; CHENG and KOCKS, 1970; LEE and HART, 1971; YAMADA and LI, 1973) is that structural changes during this test are minimal or non-existent; for example, reloading after stress relaxation will, after a short transient, lead to a continuation of the previous work-hardening curve.

This very advantage may be a serious drawback in disguise. The absence of structural changes is a direct consequence of the small plastic strain accumulated during stress relaxation: it is usually of the same order as the elastic strain in the specimen. Dislocations would thus propagate only through the relatively easy regions in the slip plane (the "soft spots"), and the plane glide resistance may never be reached (section 44). The stress relaxation test, thus, corresponds more closely to the extrapolation marked I in the strain-rate-change tests (Fig. 62-2). In fact, it is probably a better test if one does attempt to measure properties at constant *dynamic* structure, rather than in long range slip.

Experiments where the activation parameters derived from stress relaxation tests were compared with those of strain-rate-change tests (HULL and NOBLE, 1964; CHENG and KOCKS, 1970) support this contention (Fig. 64-3b, letter R). They show that, again, the results of stress relaxation tests *correlate* with those on the asymptotic flow stress in this case, even though the absolute magnitude is different by approximately a factor of 2. *Once such a correlation has been established for a particular material,* the stress relaxation test is undoubtedly the easiest for a determination of the kinetic law for this material.

One additional difficulty arises in stress relaxation that does not occur for any of the other tests of the kinetic properties: that is that the *rate* of stress change is initially quite large, especially in the hard machines best suited for the test. We have seen in section 33 (eq. [33hh]) that this leads to additional terms in the rate equation. (For a more thorough discussion see KOCKS, 1966, 1970b, 1974b; LAW and BESHERS, 1972).

Lüders Front Propagation

Tensile tests of many materials in an annealed or strain-aged state show an initial drop in stress followed by a finite strain at essentially constant stress. Under various circumstances, this behavior can be the consequence of various causes, such as dislocation unlocking, solute dragging by dislocations, etc. The behavior is accompanied by more or less heterogeneous deformation: plastic deformation starts at one or more isolated places on the specimen and spreads through the volume by the propagation of one or more Lüders fronts. When more than one front is nucleated, the flow stress shows marked variations. (Other variations in flow stress may be caused by solute dragging.) All these effects were explicitly excluded from treatment in the earlier chapters. A particularly simple case, however, may serve as an illustration of the problems involved, and a possible avenue for their solution.

Consider a single Lüders band spreading from one end along a very long specimen, in steady state at a constant velocity v_L. When it has reached the other end of the specimen, homogeneous deformation ensues; the strain at the transition can be macroscopically measured and is called the Lüders strain ϵ_L. The macroscopic extension rate is then

$$\dot{L} = v_L \cdot \epsilon_L. \qquad [64a]$$

Since $\dot{L}$ and ϵ_L can be measured macroscopically no microscopy is necessary to determine the front velocity v_L (MOON and VREELAND, 1968); if it is separately measured and eq. [64a] found satisfied (VEREL and SLEESWYK, 1973), this confirms the existence of steady state.

What we are interested in for the determination of kinetic laws of this process is, however, not the front velocity but the local strain rate. For simplicity let us first assume that a width w can be defined in the neighborhood of the front, in which all the plastic deformation occurs. (For a more precise treatment, see below.) The macroscopic extension rate is then linked to

the strain rate in the front by

$$\dot{L} = \dot{\epsilon}_F \cdot w. \qquad [64b]$$

It is seen that information obtained by measuring the macroscopic extension rate $\dot{L}$ can furnish information about the local strain rate only if something is known about the width of the front. In principle, this could be measured metallographically (though it would have to be measured during the deformation, not after unloading); but here we have endeavored to use only *macroscopic* measurements for the determination of our operational parameters.

Of particular interest is the question of the stress changes associated with an imposed change in extension rate. In principle, they could be due either to a stress dependence of the strain rate or to a dependence of the front width on stress or strain rate. While we know of no argument that eliminates the latter possibility entirely, it would appear unlikely that a variation in extension rate by many orders of magnitude can be achieved by a variation of the front width only, for specimens of reasonable size. Furthermore, it seems self-evident that the front width cannot change instantaneously. If it tends to increase with increasing stress, a new yield point should be observed upon an increase in rate; if it tends to decrease with increasing stress, a rounded transient should be observed. In fact, what few experiments there are do not indicate a strong tendency towards either kind of transient: some recent authors obtained an increase of width with stress (DELWICHE and MOON, 1972), some a decrease (PREWO *et al.*, 1972) and some no noticeable change (VEREL and SLEESWYK, 1973).

The relation between strain rate and stress can thus be derived from the dependence of the extension rate on stress with a reasonable amount of confidence—the more so the more it is possible to back-extrapolate to instantaneous changes. However, the possibility of other changes cannot be eliminated with certainty. Experiments in the Lüders region and immediately past it have tended to confirm the equivalence—with one exception (NOBLE and HULL, 1964). These experiments, however, used stress relaxation which should not be expected to reflect *steady-state* Lüders band propagation.

We shall show below that the very existence of heterogeneous deformation can, without involving any rate *changes*, give some basic information on the strain-rate sensitivity of the material. This is based only on some very general principles the validity of which can, in addition, be macroscopically checked. The result makes it possible to determine the rate sensitivity co-efficient m from a mere measurement of the Lüders strain and the initial work-hardening rate. Conversely, a knowledge of the work-hardening rate and the strain-rate sensitivity of a material makes it possible to predict the amount of Lüders strain if any.

HART (1955b) has shown that force equilibrium along a specimen undergoing nonuniform uniaxial strain demands that

$$(\Theta - \sigma) \cdot \epsilon' + \frac{\partial \sigma}{\partial \dot{\epsilon}} \cdot \dot{\epsilon}' = 0 \qquad [64c]$$

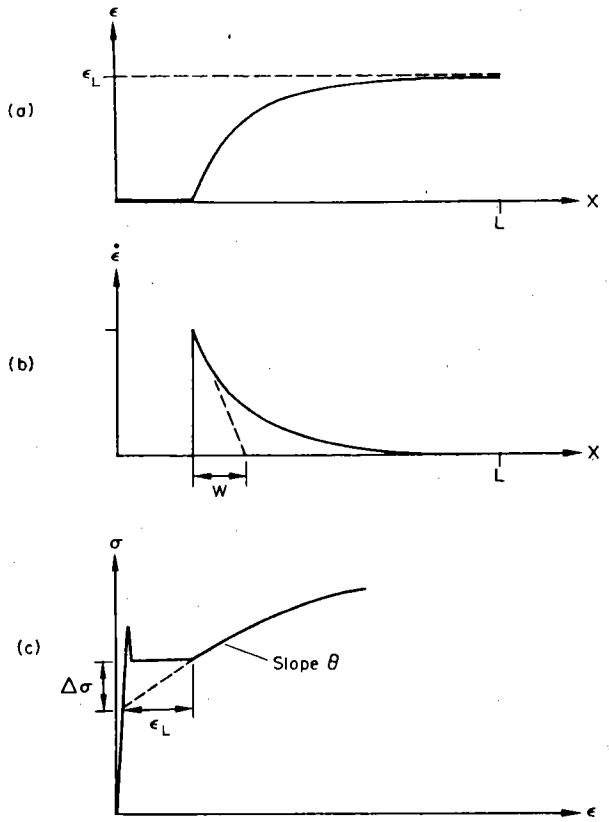

FIG. 64-4. Steady-state propagation of a Lüders front: (a) distribution of strain, (b) distribution of strain rate, along the length of a long specimen; (c) associated stress-strain diagram with various definitions.

within the deforming region, where Θ is the work-hardening rate $\left(\frac{\partial\sigma}{\partial\epsilon}\right)_{\dot{\epsilon}}$ and the prime means differentiation with respect to distance along the specimen. Steady state at every point demands

$$\dot{\epsilon} = v_L \cdot \epsilon'. \qquad [64d]$$

Inserting the derivative of [64d] into [64c] and remembering that the flow stress of most materials depends more closely on the *logarithm* of the rate (m/σ) rather than on the rate itself ($\partial\sigma/\partial\dot{\epsilon}$), we can write

$$-\frac{\epsilon''}{\epsilon'} = m \cdot \frac{\Theta - \sigma}{\sigma} \cdot \frac{\dot{\epsilon}}{v_L}. \qquad [64e]$$

Solution of this differential equation for constant Θ and m gives an exponential dependence of strain on distance (Fig. 64-4a). Metallographic observations have consistently indicated that there is substantial deformation behind the front, but none ahead of it, in agreement with this result.

If the initial strain rate gradient is used to define an effective width of the front w (Fig. 64-4b), eqs. [64a, b, and e] give the result

$$\frac{1}{m} = \frac{\Theta\epsilon_L}{\sigma} - \epsilon_L. \qquad [64f]\dagger$$

†See footnote next page!

This shows that the strain-rate sensitivity coefficient m can be derived from a macroscopic measurement of the Lüders strain and the work-hardening coefficient Θ. If Θ is indeed independent of strain rate over the range that occurs during Lüders extension (as we assumed by assuming it independent of distance), then it can also be measured immediately *after* the Lüders extension, as the initial slope of the work-hardening curve that follows (Fig. 64-4c). This assumption can be tested by comparing the initial work-hardening slopes in (continuous) tests at different strain rates. It is a very good assumption at lower temperatures where Θ is large (of order $\mu/100$), in stage II of work hardening. In this same region, $\Theta \gg \sigma$ for most materials so that the second term on the right-hand side of eq. [64f] can be neglected with respect to the first.

When the work-hardening rate immediately following the Lüders extension is a good measure of the value in the spreading front, then $\Theta \cdot \epsilon_L$ is the difference $\Delta\sigma$ between the lower-yield-point stress and the flow stress that would be obtained by back-extrapolation of the work-hardening region to zero strain (Fig. 64-4c), and thus

$$\frac{1}{m} = \frac{\Delta\sigma}{\sigma} - \epsilon_L. \qquad [64g]\ \dagger$$

Equations [64f and g] can also be read the other way around: when the strain dependence and the strain-rate dependence of the flow stress (in homogeneous deformation) are known, the length ϵ_L, and the height $\Delta\sigma$ above the continuous curve, of the Lüders extension region can be predicted. This is, of course, predicated upon the fact that the stress first rises above that necessary for homogeneous deformation; it is here that the difference between "generation stress" and "propagation stress" comes in, which has dominated discussions of heterogeneous deformation for so long. From the above discussion it would seem that the only requirement is:

$$\tau_{gen} - \tau_{prop} > \frac{\partial\sigma}{\partial \ln \dot{\epsilon}}. \qquad [64h]$$

In heavily work-hardened materials, where Θ may be a strong function of $\dot{\epsilon}$, eqs. [64g and h] no longer hold; the value of Θ at the front strain-rate must be inserted in eq. [64f].

---

† It was later shown that the integration of [64c] that led to [64f] and [64g] neglected the 'creep' deformation in the regime where the local strain rate is less than the applied one, $\bar{\dot{\epsilon}}$. A proper treatment leads to a form in which ϵ_L must divided by $\ln(\dot{\epsilon}_F/\bar{\dot{\epsilon}})$ in both eq.[64f] and [64g]. [U.F. Kocks, "Kinetics of nonuniform deformation": *Prog. Mater. Sci.* **Chalmers Anniversary Volume** (1981), p.219.]

7. CONCLUSIONS

AT THE time this study was undertaken, there had been intense discussions for a number of years, both in the literature and at conferences, of various problems in the theory of thermally activated motion of dislocations. We were, at that time, convinced that a fair number of these problems had been essentially solved, even though this may not have been generally accepted; we set out to delineate and summarize those areas. Our study revealed to us a number of additional problems that we deemed solvable; some of the solutions we arrived at were, in the same time span, proposed by other researchers. Finally, there were a few problems that appeared to stand out as worth solving which had not yet been solved. At this time, we would assess the status of some of these subproblems as follows.

Stress versus glide resistance. We consider it imperative that a clear distinction is maintained between the applied stress (an external variable and in general a tensor) and the resistance of the material to plastic deformation (a scalar material property, although possibly orientation dependent). The categorization of *internal stresses* in this scheme is, to some degree, a matter of taste; we consider them to be part of the glide resistance: this seems to us more logically consistent and better for an operational analysis of experiments without making any assumption about superposition laws. (Secs. 21, 22, 23.)

Superposition and the plane glide resistance. While the various forces on a straight element of dislocation due to applied stresses, internal stresses, self stresses, and various obstacle resistances superpose linearly, this is in general not true for the smoothed line glide resistance and the further smoothed plane glide resistance. The latter is all that can be measured in macroscopic experiments. Fairly detailed knowledge about the relative location of the various element resistance mechanisms, and about the statistics of their distribution, is necessary before meaningful statements on the superposition of strengthening mechanisms can be made. For the superposition of effects due to different types of obstacles, some simple rules have been established that describe limiting behavior. (Secs. 24, 44, 52, 53.)

Line tension and self stress. All theoretical models have, until now, used a line tension approximation. It is well known that substantial deviations from this assumption may exist, for example, because of the attraction between neighboring branches of a dislocation on either side of a discrete obstacle. These self stresses tend to lower the glide resistance from that derived from a

line tension model, more for smaller obstacles than for larger ones, and more for attractive ones than repulsive ones. Computer calculations and useful analytical approximations of these effects are needed and are in progress. (Secs. 23, 24, 52.)

Elastic anisotropy. The proper combination of elastic constants to be inserted into the flow stress formula according to any particular mechanism has almost always a value larger than that corresponding to the shear modulus that enters the line energy of a screw dislocation. In many cases, this may increase the predicted flow stress by a factor of 2 or more. However, the appropriate effective line tension that should be entered depends (especially for stronger obstacles) on the degree of bow-out and thus on the strength of the obstacle itself. Since the effective obstacle strength must be modified, as we have seen, by the effects of dislocation branch interactions, the solution of the anisotropic problem, while itself possible with present knowledge, must await the solution of the interaction problem. (Secs. 23, 25.)

Screws versus edges. One reason for the generally upward influence of elastic anisotropy on the flow stress is the fact that the flow stress must always be controlled by that kind of dislocation which is harder to move. This realization is a direct consequence of the notion that the plane glide resistance corresponds to the stress for long-range slip in each slip plane. The hardest dislocation to move will usually be either the pure screw or the pure edge, and different mechanisms make fairly straightforward predictions as to which it must be. A suggestion has been advanced that this distinction alone may be, at least in part, responsible for the important difference between planar and wavy glide habit. (Sec. 25.)

Attractive versus repulsive obstacles. While the positive part of the element glide resistance diagram may be identical for attractive and repulsive barriers, they may nevertheless lead to profoundly different macroscopic behavior. In the case of linear barriers, repulsive ones are overcome by the nucleation of a pair of kinks, exactly like periodic ones; but attractive barriers demand the nucleation of a high-energy dislocation loop and produce a very long-range line glide resistance diagram. In the case of discrete obstacles, as was pointed out above, attractive obstacles are more strongly influenced by the expected deviations from the line tension approximation. In all cases, attractive obstacles are more easily overcome by means of dislocation inertia than are repulsive ones. Finally, attractive point obstacles may significantly alter the statistical effects on the plane glide resistance (in the same way as substitutional solute atoms) and thereby lead to longer-range effects. (Secs. 24, 52, 21, 25.)

The mechanical threshold: jerky versus continuous glide. The maximum plane glide resistance, i.e. the applied stress above which equilibrium of dislocations

on the average slip plane is impossible, is the most important parameter describing the mechanical "state of the material". At applied stresses above this mechanical threshold, dislocations must move continuously, whereas below it, glide is always jerky and long-range slip is only possible with the help of thermal activation. At zero absolute temperature, the flow stress is equal to the mechanical threshold, in the absence of dislocation inertia and quantum effects. (Secs. 31, 32, 33, 41.)

The mobile dislocation density. The treatment of jerky glide as a quasi-continuous process controlled by average waiting times implies that the preexponential term contains all those dislocation segments actively "waiting" for thermal activation, in addition to the very small number actually running: the sum of both is the "mobile dislocation density". It is a structural parameter and can, in principle, not change instantaneously with changes in applied stress. If adjustments in the mobile dislocation density do occur in a time span smaller than that resolved in the observations, through interactions in the same slip plane and particularly through interactions between neighboring slip planes, the mobile dislocation density may be expected to depend on the first or second power of the applied stress. Since the stress dependence of the waiting time, i.e. the Boltzmann term, is usually considerably stronger, measurements of the stress dependence of the strain rate do furnish the apparent activation area quite well, in those cases. (Secs. 32, 33, 62, 63.)

Stress rate effects. In addition to the effects of stress and temperature, the strain rate may be influenced by the rate of stress change; for example, in stress relaxation experiments and during stress changes in creep tests. A general rate equation for jerky glide, incorporating this effect and those due to structure changes, has been proposed. (Secs. 33, 34, 64.)

Transients; small versus large strains. Throughout this discussion, we have emphasized the necessity for long-range slip through average slip planes. Experiments at very small strains, and experiments at very small times, may reveal transient effects that can be important tools in identifying structure parameters whose values eventually achieve a steady state dictated by the external parameters; the mobile dislocation density is a case in point. While the long-range-slip limit always has a well-defined meaning and obeys a relatively simple kinetic law with few structure parameters, it is by no means evident that the most "instantaneous" observation one can make provides any more basic or any more useful information. (Secs. 33, 34, 63, 64.)

Lüders front propagation. While the deformation was assumed to be homogeneous throughout most of this article, the special case of the steady-state propagation of a single Luders front was shown to be easily analyzable and useful for the determination of the rate sensitivity—even without changing the rate. (Sec. 64.)

Dislocation damping and inertia. The various mechanisms that have been proposed as controlling the velocity of dislocations under positive driving force all give similar answers around and above the Debye temperature; the behavior at low temperature is not well understood theoretically and not well established experimentally. The damping is generally high enough to keep the *average* dislocation velocity considerably below the speed of sound; however, the severe variations in glide resistance across a slip plane necessitate accelerations and decelerations of dislocations that are not always overdamped. As a result, one should expect inertial penetration of obstacles by dislocations and kinks in the interesting stress range, if the effective interaction range of the obstacle is not much more than an atomic dimension, or if the temperature is very low. (Sec. 31.)

The frequency factor and the activation entropy. For most problems of any interest, the frequency factor in a rate equation for plastic flow does not depend on the obstacle spacing but only on the obstacle stiffness. It is generally of the order of 10^{11} s^{-1}. This incorporates all entropy effects due to vibrations of the dislocation. In addition, there may be an entropy contribution from the obstacle-dislocation interaction; its average value over the range of the measurements should be about one or a few k, which produces an additional factor of 10 in the preexponential that is not operationally distinguishable from the attempt frequency or other preexponential factors. (Sec. 42.)

Activation enthalpy versus activation free enthalpy. In principle, the activation enthalpy ΔH is all that can be measured experimentally—and then only if other temperature dependences of the preexponential are negligible (as they usually are) or can be assumed to have a known form. If ΔH is measured over a wide temperature range, especially extending to low temperatures, one may be able to draw sufficient conclusions about the activation entropy for a complete analysis. If a value of ΔH that was measured over a certain temperature range is compared with predictions of a theoretical model, the material constants in the model, such as the shear modulus, must be those obtained by a straight-line extrapolation from the range of experimental temperatures to absolute zero. In practice, all that can be reasonably handled, and which is usually sufficient, are entropy effects due to the temperature dependence of the elastic constants (and of the lattice constants). These effects are completely accounted for by introducing the normalized variables σ/μ and $kT/\mu b^3$. The "activation energy" measured in such normalized variables is $\Delta G/\mu b^3$. In these expressions, μ and b are to be inserted *at temperature* in the analysis of the experiments and in the theoretical expressions. Use of the above normalized coordinates makes all the proposed equations for converting ΔH into ΔG unnecessary. (Secs. 41 through 44, and 61.)

The activation area: true and apparent. The true activation area is a geo-

metric quantity describing the area in the slip plane between the stable and unstable equilibrium positions of the dislocation at a given stress. It is a theoretical quantity of interest in the derivation of the activation free enthalpy ΔG. The negative derivative of ΔG with respect to the applied stress σ is *not* in general equal to this activation area; we have here called it "apparent activation area". The differences are due to a possible dependence of the true activation area on the applied stress as distinct from the glide resistance; for example, because of a dependence of the effective obstacle *spacing* in randomly distributed discrete obstacles upon the applied stress. In all cases we have investigated, the apparent and true activation areas are proportional to each other. We know of no way of measuring the true activation area; even the apparent activation area can only be measured if certain assumptions about the shear-stress dependences of the preexponential terms are satisfied. Thus, the common use of the *order of magnitude* of the activation area for purposes of identifying the kind of glide-resistance mechanism involved is generally acceptable; the use of the detailed stress dependence for a derivation of the obstacle profile is always subject to a number of provisos. (Secs. 41, 43, 62, 63.)

The low-stress limit. At very low stresses, the contribution to the "stress exponent" m (i.e. the inverse relative strain-rate sensitivity of the flow stress) from the activation energy becomes linear in the stress itself. Then, contributions from the preexponential terms become important. Reverse jumps of the dislocations are rarely of any importance because of the large difference between forward and backward activation areas. In the limit, it does give an additional preexponential factor which is *linear* in stress for all glide resistance profiles—except that the *average* of the element glide resistance over the entire slip plane, which is proportional to the rate of energy storage, must always be subtracted from the applied stress. (Sec. 45.)

Parameters describing a single set of obstacles. When low stresses are able to produce deformation, that is when the temperature T_0 at which thermal activation alone can effect the overcoming of an obstacle, is within the range of measurements, then a good estimate of the total free energy F_0 (or the total energy U_0) associated with overcoming the chief obstacle to glide can be obtained. It must be within a factor of about three either way of 1 eV for this to be possible. Together with the flow stress at zero temperature (obtained by extrapolation), this also gives the approximate magnitude of the average activation area, i.e. a combined measure of the size of the obstacles and their spacing if they are discrete. Only if the spacing can be varied can the strength and the effective size of the obstacles be determined. A further analysis of the details of the temperature dependence of the flow stress is not likely to produce much further information, since all mechanisms lead to similar macroscopic observations in this respect. Only the shape of the top of the obstacle profile may be determined with some degree of accuracy by measurements at very low temperatures, unless these are masked by inertial effects. When the temperature T_0 is outside the range of measurements, or when another high-

temperature mechanism affects the deformation significantly, a determination of the total activation energy F_0 becomes essentially meaningless because of the uncertainty about the correct extrapolation procedure. In this case, the maximum obstacle strength and the shape of the top of the obstacle is all that can be deduced from experimental data, at best. (Secs. 62, 63.)

Multiple glide resistance mechanisms. The possibility that two glide resistance mechanisms make important contributions to the flow stress cannot be asserted unless at least one of the contributions stems from discrete obstacles whose density can be varied. In this case, simultaneous measurement of flow stress and activation area may serve to separate the two contributions. Two mechanisms associated with the same obstacle cannot be distinguished in principle. However, the existence of an "athermal plateau", whether it is due to a separate contribution or merely a property of the obstacle profile, can be ascertained by the observation that the strain rate sensitivity parameter m must go through a minimum as a function of temperature at constant strain rate. (Secs. 44, 62.)

The lattice resistance. As an example of linear barriers, we have considered the lattice resistance to the motion of full dislocations. We agree with, and have further extended, the conclusion by previous workers that a wide variety of different models give very similar results for the stress dependence of the nucleation energy. With regard to the kinetics of kink motion and annihilation, we find the steady-state models unrealistic unless they are coupled with a fairly high activation energy for motion of the kinks, due to a second-order Peierls stress or due to point defects along the dislocation. Alternatively, one must rely on strong obstacles such as dislocation nodes to determine the mean free path of kinks; then, the strain rate is determined entirely by the nucleation rate. (Secs. 24, 51.)

Precipitation hardened alloys. As a specific example of discrete obstacles, we have studied the various mechanisms of particle resistance. A consistent application of the concepts of element, line, and plane glide resistance has shown that both the obstacle profiles for individual mechanisms and the methods of superposing various mechanisms had not always been described correctly. Effects of thermal activation, while not especially strong, are by no means negligible; together with the derived nonlinear relation between element and line glide resistance, they alter significantly the predictions about age hardening. (Sec. 52.)

Substitutional solid solutions. Thermal activation analysis as well as recent theoretical considerations show that the discrete obstacle concept is not applicable to this case. While a theoretical prediction of the mechanical threshold may be at hand, a consistent treatment of the effects of thermal activation has not as yet been given. (Secs. 25, 52.)

Above we have outlined our conclusions regarding the state of understanding of a number of specific problems. Looking at the thermodynamics and kinetics of slip as a whole, we find that an essentially complete and reliable theory has been established. It makes two kinds of predictions. On the one hand, the theory specifies ranges of the experimental variables in which accurate and comprehensive observations can be expected to yield further information on the underlying deformation mechanisms. On the other hand, the theory allows one to delineate broad bands of mechanical properties that are insensitive to the details of the microscopic behavior and for which constitutive relations can therefore be specified to a fair degree of accuracy with present knowledge.

The confidence we profess in the present state of theoretical understanding is limited to materials in any given "mechanical state", or having any given metallurgical "structure". The problems connected with changes of structure concurrent with the plastic deformation are more difficult and are much farther away from a satisfactory solution. This is the area, therefore, where we feel further theoretical work is most needed.

REFERENCES

ALDEN, T. H. (1972) *Phil. Mag.* **25,** 785. (*100*)
ALDEN, T. H. (1973) *Met. Trans.* **4,** 1047. (*100*)
ALEFELD, G. (1964) *Phys. Rev. Letters* **12,** 37a. (*124*)
ALERS, G. A. and THOMPSON, D. O. (1961) *J. Appl. Phys.* **32,** 283. (*74, 78*)
ALEXANDER, H. and HAASEN, P. (1968) *Solid State Physics* (SEITZ, F. *et al.*, eds.) **22,** 27. (*69, 92, 173, 175*)
ARGON, A. S. (1968) *Mater. Sci. Eng.* **3,** 24. (*86*)
ARGON, A. S. (1969) in *Physics of Strength and Plasticity* (ARGON, A. S., ed.), p. 217, M.I.T. Press. (*98*)
ARGON, A. S. (1970) *Scripta Met.* **4,** 1001. (*93*)
ARSENAULT, R. J. (1971) *Met. Trans.* **2,** 1472. (*117*)
ARSENAULT, R. J. and LI, J. C. M. (1967) *Phil. Mag.* **16,** 1307. (*86*)
ASHBY, M. F. (1966) *Acta Met.* **14,** 679. (*47*)
ASHBY, M. F. (1970) *Proc. Second Intl. Conf. Strength Metals Alloys*, p. 507, Amer. Soc. Metals. (*173*)
BACON, D. J. (1967) *Phys. Stat. Sol.* **23,** 527. (*27*)
BACON, D. J., KOCKS, U. F. and SCATTERGOOD, R. O. (1973) *Phil. Mag.* **28,** 1241. (*27, 52, 53, 210*)
BARNETT, D. M., ASARO, R. J., GAVAZZA, S. D., BACON, D. J. and SCATTERGOOD, R. O. (1972) *J. Phys.* F **2,** 854. (*27*)
BASINSKI, Z. S. (1959) *Phil. Mag.* **4,** 393. (*38, 112, 260*)
BASINSKI, Z. S., DUESBERY, M. S. and TAYLOR, R. (1971) *Can. J. Phys.* **49,** 2160. (*171*)
BECKER, R. (1925) *Phys. Zeitschr.* **26,** 919. (*1*)
BESHERS, D. N. (1971) *Scripta Met.* **5,** 469. (*22, 28*)
BRAILSFORD, A. D. (1972) *J. Appl. Phys.* **43,** 1380. (*73, 78*)
BROWN, L. M. (1964) *Phil. Mag.* **10,** 441. (*25*)
BROWN, L. M. (1973) *Acta Met.* **21,** 879. (*18*)
BROWN, L. M. and HAM, R. K. (1971) in *Strengthening Methods in Crystals* (KELLY, A. and NICHOLSON, R. B., eds.), p. 9, American Elsevier. (*50, 173, 197, 199, 202, 211*)
BURKE, J. (1965) *The Kinetics of Phase Transformations in Metals*, Pergamon Press, Oxford. (*112*)
BYRNE, J. G., FINE, M. E. and KELLY, A. (1961) *Phil. Mag.* **6,** 1119. (*220*)
CELLI, V., KABLER, M., NINOMIYA, T. and THOMSON, R. (1963) *Phys. Rev.* **131,** 58. (*127, 192*)
CHENG, C. Y. and KOCKS, U. F. (1970) *Second Intl. Conf. Strength of Metals and Alloys*, p. 199, Amer. Soc. Metals. (*156, 259, 260, 261*)
CHOU, Y. T. and ESHELBY, J. D. (1962) *J. Mech. Phys. Sol.* **10,** 27. (*25, 26*)
CHOU, Y. T. and SHA, G. T. (1971) *J. Appl. Phys.* **42,** 2625. (*25, 26*)
CHRISTIAN, J. W. (1970a) *Proc. Second Intl. Conf. Strength of Metals and Alloys*, p. 31, Amer. Soc. Metals. (*173*)
CHRISTIAN, J. W. (1970b) *Scripta Met.* **4,** 811. (*171, 237*)
CHRISTIAN, J. W. and MASTERS, B. C. (1964) *Proc. Roy. Soc.* A **281,** 240. (*112*)
CHUN, J. S. and BYRNE, J. G. (1969) *J. Mater. Sci.* **4,** 861. (*220*)
CLAREBROUGH, L. M., HUMBLE, P. and LORETTO, M. H. (1967) *Can. J. Phys.* **45,** 1135. (*66*)
COCKAYNE, D. J. H., JENKINS, M. L. and RAY, I. L. F. (1971) *Phil. Mag.* **24,** 1383. (*66*)
CONRAD, H. and WIEDERSICH, H. (1960) *Acta Met.* **8,** 128. (*141*)
COPLEY, S. M. and KEAR, B. H. (1967) *Trans. Met. Soc. AIME* **239,** 984. (*202*)
COTTRELL, A. H. (1953) *Dislocations and Plastic Flow in Crystals*, Claredon Press, Oxford. (*39*)

OROWAN, E. (1940) *Proc. Phys. Soc.* **52,** 8. (*1, 69, 79, 97*)
OROWAN, E. (1941) *Nature* **147,** 452. (*91, 99*)
OROWAN, E. (1948) in *Symposium on Internal Stresses in Metals and Alloys*, p. 451, Inst. Metals, London. (*47*)
OROWAN, E. (1954) in *Dislocations in Metals* (COHEN, M., ed.), p. 69, Amer. Inst. Min. Met. Engs. (*173*)
PEIERLS, R. E. (1940) *Proc. Phys. Soc.* **52,** 34. (*173*)
PETCH, N. J. (1958) *Phil. Mag.* **3,** 1089. (*38*)
PHILLIPS, V. A. (1965) *Phil. Mag.* **11,** 775. (*220*)
POLANYI, M. and WIGNER, E. (1928) *Z. Phys. Chem.* A **139,** 439. (*121, 126, 127*)
POPE, D. P. and VREELAND, T., JR. (1969) *Phil. Mag.* **20,** 1163. (*74, 76*)
PREKEL, H. L., LAWLEY, A. and CONRAD, H. (1968) *Acta Met.* **16,** 337. (*196*)
PREWO, K., LI, J. C. M. and GENSAMER, M. (1972) *Met. Trans.* **3,** 2261. (*262*)
RICE, J. R. (1970) *J. Appl. Mech.* **37,** 728. (*9, 69*)
RICE, J. R. (1971) *J. Mech. Phys. Sol.* **19,** 433. (*16*)
RICE, J. R. (1973) in *Metallurgical Effects at High Strain Rates* (ROHDE, R. W. *et al.*, eds. p. 93, Plenum Press. (*8*)
RIDDHAGNI, B. R. and ASIMOW, R. M. (1968) *J. Appl. Phys.* **39,** 4144, 5169. (*60, 222*)
ROSENFIELD, A. R., HAHN, G. T., BEMENT, A. L. and JAFFEE, R. T., eds. (1968) *Dislocation Dynamics*, McGraw-Hill. (*69*)
RUSSELL, K. C. and BROWN, L. M. (1972) *Acta Met.* **20,** 969. (*200, 208, 211, 217*)
RYBIN, V. V. and ORLOV, A. N. (1970) *Soviet Physics Solid State* **11,** 2635. (*192*)
SARGENT, G. A. (1965) *Acta Met.* **13,** 663. (*260*)
SCHOECK, G. (1965) *Phys. Stat. Sol.* **8,** 499. (*112, 114, 240*)
SCHOEK, G. (1974) in *Dislocation Theory: A Treatise* (NABARRO, F. R. N., ed.), Dekker, in press. (*64, 112, 124*)
SCHOECK, G. and SEEGER, A. (1955) *Report Bristol Conference on Defects in Crystalline Solids*, p. 340, London, Phys. Soc. (*144*)
SEEGER, A. (1954) *Z. Naturf.* **9a,** 758. (*1, 145*)
SEEGER, A. (1955a) in *Handbuch der Physik*, VII/1 (FLÜGGE, S., ed.), p. 383, Springer. (*7, 66, 121, 126*)
SEEGER, A. (1955b) *Phil. Mag.* **46,** 1194. (*62, 65*)
SEEGER, A. (1956) *Phil. Mag.* **1,** 651. (*144, 188, 196*)
SEEGER, A. (1957) in *Dislocations and Mechanical Properties of Crystals* (FISHER, J. C. *et al.*, eds.), p. 243, Wiley, New York. (*139*)
SEEGER, A. (1958) in *Handbuch der Physik* VII/2, (FLÜGGE, S., ed.), p. 115, Springer. (*112, 139*)
SEEGER, A. and ENGELKE, H. (1968) in *Dislocation Dynamics* (ROSENFIELD, A. R. *et al.*, eds.), p. 623, McGraw-Hill. (*77*)
SLATER, J. C. (1939) *Introduction to Chemical Physics*, McGraw-Hill. (*113*)
SLEESWYK, A. W. (1970) *Scripta Met.* **4,** 355. (*235*)
STANIEK, G. and HORNBOGEN, E. (1973) *Scripta Met.* **7,** 615. (*225*)
STERN, R. M. and GRANATO, A. V. (1962) *Acta Met.* **10,** 358. (*25*)
SUREK, T., LUTON, M. J. and JONAS, J. J. (1973a) *Phil. Mag.* **27,** 425; *Phys. Stat. Sol.* b **57,** 647. (*140, 241*)
SUREK, T., LUTON, M. J. and JONAS, J. J. (1973b) *Scripta Met.* **7,** 1131. (*150*)
SUREK, T., KUON, L. G., LUTON, M. J. and JONAS, J. J. (1974) in *Rate Processes in Plastic Deformation* (LI, J. C. M., ed.), Plenum Press. (*231, 240, 241*)
SUTTON, P. M. (1953) *Phys. Rev.* **91,** 816. (*118*)
SUZUKI, H. (1957) in *Dislocations and Mechanical Properties of Crystals* (FISHER, J. C. *et al.*, eds.), p. 361, Wiley. (*144*)
TEUTONICO, L. J., GRANATO, A. V. and LÜCKE, K. (1964) *J. Appl. Phys.* **35,** 220. (*144*)
THORNTON, P. R., MITCHELL, T. E. and HIRSCH, P. B. (1962) *Phil. Mag.* **7,** 337. (*260*)
TURNBULL, D. and FISHER, J. C. (1949) *J. Chem. Phys.* **17,** 71. (*113*)
TURNER, A. P. L. and VREELAND, T., JR. (1970) *Acta Met.* **18,** 1225. (*74*)
TURNER, A. P. L., VREELAND, T., JR. and POPE, D. P. (1968) *Acta Cryst.* A **24,** 452. (*74*)
VAN DEN BEUKEL, A. (1970) *Scripta Met.* **4,** 789. (*236*)
VEREL, D. J. and SLEESWYK, A. W. (1973) *Acta Met.* **21,** 1087. (*261, 262*)
VINEYARD, G. H. (1957) *Phys. Chem. Sol.* **3,** 121. (*112, 125, 126*)
VREELAND, T., JR. and JASSBY, K. M. (1971) *Mater. Sci. Eng.* **7,** 95. (*76*)

WEEKS, R. W., PATI, S. R., ASHBY, M. F. and BARRAND, P. (1969) *Acta Met.* **17,** 1403. (*208*)
WEERTMAN, J. (1961) in *Response of Metals to High Velocity Deformation* (SHEWMON and ZACKAY, eds.), Interscience. (*72*)
WEERTMAN, J. (1968) *Trans. Amer. Soc. Met.* **61,** 681. (*255*)
WOBSER, G. and FRANK, W. (1968) *Scripta Met.* **2,** 341. (*241*)
WOOLHOUSE, G. R. (1970) *Proc. Second Intl. Conf. on Strength of Metals and Alloys*, p. 573, Amer. Soc. Metals. (*202*)
YAMADA, H. and LI, C. Y. (1973) *Met. Trans.* **4,** 2133. (*260*)

AUTHOR INDEX

SUBJECT INDEX

Numbers in bold type refer to definition of terms

CONTENTS OF PREVIOUS VOLUMES IN THIS SERIES